Department of Molecular & Clinical Cancer Medicine
Institute of Translational Medicine

Investigating carbohydrate metabolism in head and neck cancer by analysing the roles of p53, TIGAR, and Hexokinase 2

Thesis submitted in accordance with the requirements of the University of Liverpool for the degree of Doctor in Medicine (MD)

by

Sundarraj Lakshmiah

March 2021

This thesis is dedicated to the memory of my late father, Dr G Lakshmiah, who always believed in my ability to be successful in the academic arena

TABLE OF CONTENTS

I Abstract

Cancer is a multistep complex genetic disease that typically results from the acquisition of gain-of-function mutations in oncogenes and loss-of-function mutations in tumour suppressor genes. There is increasing evidence that impaired cellular energy metabolism is the defining characteristic of nearly all tumours regardless of cellular or tissue origin. The purpose of this present study is to investigate the process of metabolic adaptations in squamous cell carcinoma of the head and neck (SCCHN), in particular, carbohydrate metabolism, by analysing three essential proteins; p53, TIGAR and HK-2.

The rationale for selecting these three proteins is based on the following observations; this study aimed to investigate the role of critical genes that alter cellular metabolism in SCCHN and because of the importance of p53 in SCCHN, and recent studies which have confirmed the importance of p53 in metabolic regulation, p53 was our initial focus. We have also examined TIGAR (*TP*53 induced glycolysis and apoptosis regulator), a major p53 regulated gene known to play essential roles in regulating metabolism, in part, by acting enzymatically as a Fructose 2,6, bisphosphatase. Moreover, it is clear from the literature that TIGAR also interacts with another critical metabolic enzyme: HK-2 (Hexokinase 2), and through this appears to also impact upon cellular metabolism by a mechanism that is independent of the phosphatase activity of TIGAR. Therefore, we decided that it would be important to include an investigation of the expression of HK-2 in SCCHN as part of our studies.

Various authors have already studied the metabolic roles of p53 and HK-2 in SCCHN. Still, to the best of our knowledge, there are no studies regarding TIGAR expression in SCCHN and any potential correlation with p53 and HK-2 in this disease. The primary aims were to analyse the expression pattern of p53, TIGAR and HK-2 in head and neck cancers. To accomplish this, we examined SCCHN cell lines with defined *TP53* genetic status to investigate whether any obvious connection might exist between p53, TIGAR and HK-2 steady-state expression. We also examined tumour biopsy samples from patients with SCCHN by immunohistochemistry (IHC). In addition, we aimed to investigate whether any

association could be detected between the expression of these proteins and various clinical variables such as anatomical sites, T stage, N stage, differentiation, nerve invasion, vascular invasion, extracapsular spread, and also patient outcomes (survival).

'University of Michigan - squamous cell carcinoma' (UM-SCC) cell lines, including isogenic lines expressing no p53, wild-type p53 or p53 mutants and also wild-type cells manipulated by RNAi to express lower levels of p53 were used to examine the expression of p53, TIGAR, and HK-2. For IHC analysis, we used two sets of Tissue microarrays (TMAs) constructed from SCCHN patient samples. The first TMA *(TMA set 1)* (previously constructed and used by a previous colleague) originally included samples from 102 patients, but due to one sample core missing, we analysed 101 samples, with most from the oral cavity (n=93) and fewer from the oropharynx (n=8). Due to the paucity of tissue available, we analysed the expression of p53 and TIGAR only in this TMA. The second TMA *(TMA set 2*) (newly constructed by the Liverpool University LBiH 'Tissue Bio-Bank') was used to analyse the expression of p53, TIGAR, and HK-2, with 161 samples of which were from the larynx (n=77), hypopharynx (n=22), and oropharynx (n=62). Each patient sample contains representative tissue from the tumour core, advancing front of the tumour, normal tissue, and lymph nodes if involved. As the numbers of hypopharynx were small, we have combined larynx and hypopharynx together for analysis.

We inferred that p53 was likely to be mutated in approximately 62% of samples from TMA set 1 and 65% and 50% of samples from the tumour core and advancing front samples of the larynx and hypopharynx cohort of TMA set 2, respectively. This is similar to the estimate of 84% for p53 mutation obtained by TCGA network analyses of 279 SCCHN cases. However, for oropharynx samples, the inferred p53 mutation rate was 72.6% and 50.00% for tumour core and advancing front samples, respectively. This seems surprisingly high since we might expect p53 in these samples to frequently be wild-type as a result of HPV infection in many of this cohort. Analysis of TIGAR protein detected expression in 73% of samples in TMA set 1, whereas in TMA set 2, we observed TIGAR expression in all of the samples. We observed 42.4% and 28.3% of strong HK-2 expression in the tumour core and advancing front samples of larynx and hypopharynx, respectively, in TMA set 2. Oropharynx samples displayed a strong HK-2 expression of 54.8% in the tumour

core and 38.7% in the advancing front samples. There was a significant positive association between inferred p53 mutant status and strong HK-2 expression in tumour core (P=0.003) and in the advancing front (P=0.047) samples from larynx and hypopharynx, which suggests patients with strong HK-2 are more likely to have inferred p53 mutant status.

Our results in cell lines suggest that that the highest levels of TIGAR expression are associated with wt-p53, whether expressed from a lentiviral vector in a p53 null line, or comparing RNAi-mediated knock-down in a p53 wild-type line, or even comparing two essentially isogenic cell lines from a single patient obtained at different times, with one harbouring wt-p53 and one possessing a p53 mutation (UM-SCC-11A and 11B respectively). This suggests that in SCCHN, the connection between TIGAR expression and retention of wt-p53 is potentially retained. Analysis of the IHC data did not reveal any significant association between inferred p53 mutant status and TIGAR expression in TMA set 1 (P=0.580). Unfortunately, it has not been possible to address this in the TMA set 2 samples because of the overall strong staining of TIGAR in all the slides.

This is the first study of TIGAR expression in SCCHN, and our data suggest that, unlike some other cancers, the link between p53 and TIGAR expression is retained, at least in cell lines. HK-2 is expressed in all cell lines, and the steady-state levels do vary much between cells with different p53 status. It is, therefore, perhaps surprising that we have detected some variability in HK-2 expression in tumour samples by IHC. Moreover, we have identified a strong association between HK-2 expression and p53-inferred mutant status in tumour cores (P=0.003) and in the advancing tumour front (P=0.047). This suggests that loss of p53 function, which would be expected to increase glycolysis, is associated with increased expression of a key glycolytic enzyme. This is not surprising, but it is the first time that this association has been identified in SCCHN.

Importantly, this may indicate that targeting HK-2, for example, with an inhibitor could prove particularly effective in p53 mutant tumours.

These studies include the first attempt to characterise TIGAR expression in SCCHN, and combined with analysis of HK-2 and using IHC to infer p53 status, has revealed some intriguing associations. Clearly, similar studies using genetic approaches to the

patient analysis of p53 status will be necessary. However, the studies of cell lines suggest that functional studies of HK-2 inhibitors such as Benserazide would be potentially informative. Ultimately, it is clear that cancer cell metabolism is a highly attractive target for therapy. Hopefully, these preliminary results shed some light and suggest some future directions for further investigations of metabolic processes in cancer cells.

II Acknowledgements

I would like to thank my supervisors Professors Mark Boyd and Terry Jones, and Dr Nikolina Vlatkovic, for their invaluable guidance and support throughout my MD studies. I am indebted to my supervisors for taking a chance by allowing a maxillofacial surgeon with no research background into their group and for their patience and guidance throughout the development of this project; had it not been for their encouragement, this study would never have begun.

I appreciate all the members who assisted or advised me during the study from the Department of Molecular and Clinical Cancer Medicine, especially Mark Wilkie, Tuoyo Okoturo and Emad Anaam, who helped me in the lab. Special thanks to Dr Helen Kalirai for her sincere advice and help in the Immunohistochemical analysis. Special mentions are due to Mr Trevor Cox, Mr Richard Jackson, and Dr Srinivasan for their invaluable help in the statistical analysis. I am also immensely grateful to Dr Katherine Brougham, Consultant Pathologist, for scoring the TMAs. I sincerely thank my brother Dr Ganapathyraman Lakshmiah (Pathologist, Dubai Hospitals), for sparing time in his busy schedule to score the TMAs. Sincere gratitude must also go to Dr Janet Risk for providing oral cavity TMAs and their data.

Finally, I would like to thank my wife, Dhana, and my children, Dhaya and Sadha, for their love and support while I completed this study.

III Declarations

This thesis is the result of my own work. The material contained in the thesis has not been presented, nor is currently being presented, either wholly or in part for any other degree or other qualification.

This thesis was written entirely by me under the valued guidance of my supervisors, Professors Mark Boyd and Terry Jones, and Dr Nikolina Vlatkovic.

Sundarraj Lakshmiah

March 2021

IV List of figures

Ⅴ List of tables

VI Abbreviations

^{18}FDG : 18F fluorodeoxyglucose

2DG : 2-deoxy-D-glucose

2-DG6P : 2-deoxyglucose-6-phosphate

3-BP : 3-bromopyruvate

ADP : Adenosine diphosphate

APS : Ammonium persulfate

ATP : Adenosine triphosphate

BCL-2 : B-cell Lymphoma-2

BSA : Bovine serum albumin

CNA : Copy number aberration

COX : Cyclooxygenase

CTL : Cytotoxic CD8+ T Lymphocytes

DAB : 3,3'-diaminobenzidine

DISC : Death inducing signaling complex

DMEM : Dulbecco's modified Eagle's medium

DMSO : Dimethyl sulfoxide

DNA : Deoxyribonucleic acid

ECS : Extracapsular spread

EDTA : Ethylenediaminetetraacetic acid

EGFR : Epidermal Growth Factor Receptor

EMT : Epithelial-mesenchymal transition

F-1,6-P_2 : Fructose-2,6-bisphosphate

FADD : Fas-associated protein with death domain

FBPase-2 : Fructose-2,6-bisphosphatase

FBS : Fetal bovine serum

FDG : Fluoro-deoxy-glucose

FFPE : Formalin-fixed paraffin-embedded

G6P : Glucose 6 phosphate

GLUT1 : Glucose transport-1

H&E : Hematoxylin and eosin

HIF : Hypoxia-inducible factor

HK-2 : Hexokinase-2

HLA : Human leukocyte antigen

HPV : Human Papillomavirus

HRP : Horseradish peroxidase

hTERT : Human telomerase reverse transcriptase

IARC : International Agency For Research On Cancer

IHC : Immunohistochemistry

IL-8 : Interleukin-8

ISH : In situ hybridisation

LDH : Lactate dehydrogenase

LOF : Loss of Function

LOH : Loss of heterozygosity

MCT : Monocarboxylate transporter

MDM2 : Murine double minute 2

MHC : Major histocompatibility complex

MHNORG : Mersey Head and Neck Oncology Research Group

MMPs : Matrix metalloproteinases

MPTP : Mitochondrial permeability transition pore

mTOR : Mammalian target of rapamycin

NADH : Nicotinamide adenine dinucleotide

NADPH : Nicotinamide adenine dinucleotide phosphate

NPC : Nasopharyngeal carcinoma

NSCLC : Non-small cell lung cancer

OPSCC : Oropharyngeal Squamous Cell Carcinoma

OXPHOS : Oxidative phosphorylation

PBS : Phosphate-buffered saline

PCR : Polymerase chain reaction

PD-1 : Programmed cell death protein-1

PD-L1 : programmed cell death ligand-1

PET : Positron Emission Tomography

PFK-1 : Phosphofructo kinase-1

PGM : Phosphoglycerate mutase

PI3K : Phosphatidylinositol 3-kinase

PMSF : Phenylmethylsulphonyl fluoride

PPP : Pentose phosphate pathway

PTEN : Phosphatase and tensin homolog

R5P : Ribose-5-phosphate

Rb : Retinoblastoma protein

RITA : Reactivation of p53 and induction of tumour cell apoptosis

RNA : Ribonucleic acid

ROS : Reactive oxygen species

RR : Relative Risk

SCCHN : Squamous Cell Carcinoma of Head and Nek

SCO2 : Synthesis of cytochrome c oxidase-2

SDS : Dodecyl sulphate

SDS-PAGE : Sodium dodecyl sulphate - polyacrylamide gel electrophoresis

SEM : Standard error of the mean

SLIP : Stuart Linn Immunoprecipitation

SMA : Smooth muscle actin

TAD : Transcriptional activation domain

TCA : Tricarboxylic acid

TCGA : The Cancer Genome Atlas

TEMED : Tetramethylethylenediamine

TERF2 : Telomeric Repeat Factor 2

TIGAR : TP53 induced glycolysis and apoptosis regulator

TKTL1 : Transketolase-like-1

TLR : Toll-like receptors

TMA : Tissue microarray

TNF : Tumour Necrosis Factor

UK : United Kingdom

UM-SCC : University of Michigan - Squamous cell carcinoma

VDAC : Voltage-dependent anion channel

VEGF : Vascular endothelial growth factor

1. Introduction

1.1 Squamous cell carcinoma of the head and neck

Head and neck cancer is a broad term that denotes tumours that arise in the oral cavity, nasopharynx, oropharynx, hypopharynx, larynx, and least frequently from the sinonasal tract (1, 2). Even though tumours at the different anatomical sites have variable histology, squamous cell carcinoma is the most common malignancy in the head and neck region (more than 90%), and that is the reason the terms "head and neck cancer" and "squamous cell carcinoma of the head and neck" (SCCHN) are often used interchangeably (3). Squamous cell carcinomas are the exclusive focus of our study, and we have described them either as 'head and neck tumour' or 'SCCHN' throughout this thesis.

SCCHN ranks sixth among the most common worldwide malignancies and accounts for approximately 6% of all cancer cases, responsible for an estimated 1%-2% of all cancer deaths (4). In the United Kingdom (UK), SCCHN ranks eighth among the common cancers in males and sixteenth in females (5).

The frequency of SCCHN is much higher in developing countries, accounting for up to 40% of all cancers in the Indian subcontinent, with increased rates of SCCHN also reported for parts of South America, Southeast Asia, the western pacific, France and eastern Europe (6, 7). The larynx is the common site for SCCHN in most geographical areas (5), whereas, in the Indian subcontinent, the oral cavity is the common site for head and neck cancer compared to other anatomical subsites (8).

Management of SCCHN is always a challenge as these tumours arise from important anatomical sites such as the oral cavity or larynx, which are essential for speech, swallowing, and taste. Treatment such as surgery and radiotherapy can cause functional impairment and further reduces the quality of life for head and neck cancer patients (9). Despite advances in surgery, radiotherapy and chemotherapy for patients with SCCHN, survival rates have not improved significantly in recent years, and the 5-year survival rate for SCCHN remains poor due to uncontrolled or recurrent tumours and lack of suitable markers for early detection (10)

The four major subsites of head and neck tumours (oral cavity, oropharynx, larynx, and hypopharynx), with their anatomical boundaries, are shown in figure 1.1.

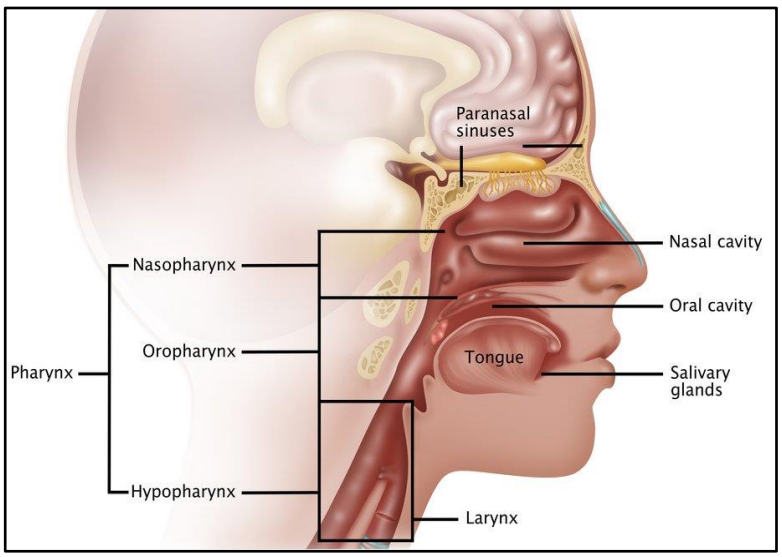

Figure 1:1 Anatomical regions of the head and neck. The oral cavity spans between the oral fissure anteriorly and the oropharyngeal isthmus posteriorly. The pharynx begins at the base of the skull and ends at the inferior border of the cricoid cartilage, and has three parts: nasopharynx, oropharynx, hypopharynx (also known as laryngopharynx). The larynx is located within the anterior aspect of the neck and is situated just below where the tract of the pharynx splits into the trachea and oesophagus. Paranasal sinuses are a group of air-filled spaces that surround the nasal cavity: the maxillary sinus, frontal sinus, ethmoid sinus, sphenoidal sinus. The salivary glands are exocrine glands that produce saliva. There are three paired major salivary glands (parotid, submandibular, and sublingual) as well as hundreds of minor salivary glands (11, 12).

The nasopharynx is also technically an SCCHN subsite, but nasopharyngeal carcinoma is generally considered as a separate clinicopathological entity given its distinct features such as silent growth in a hidden nasopharyngeal cavity, different histological arrangement (nasopharyngeal lumen is lined with transitional epithelium compared to the stratified squamous epithelium which gives rise to more than 90% of head and neck carcinomas), and increased chemo and radiosensitivity behaviour (13). Hence, nasopharyngeal carcinoma is not considered further in this thesis.

1.2 Risk factors and aetiology of head and neck cancer

The most significant risk factors for SCCHN in the UK, as in much of the developed world, are tobacco smoking, alcohol consumption and infection by oncogenic human papillomaviruses (HPV) (14, 15).

Smoking and alcohol appear to have a synergistic effect on mucosal surfaces (16). For head and neck cancer, smoking is an independent risk factor and smoking cessation for a short period (1-4 years) results in a head and neck cancer risk reduction compared with current smoking (OR 0.70, 95% CI 0.61-0.81) (17).

Alcohol is another major independent risk factor for head and neck cancer, and patients who continue to consume alcohol after head and neck cancer treatment have a worse quality of life and reduced survival compared to the patients who stopped drinking (18, 19). In a study of two hundred and sixty-four survivors of an early stage of head and neck cancer, history of alcohol before diagnosis dose-dependently increased the mortality risk to 4.9 (95% CI=1.5 – 16.3), and the risk has been further increased significantly when patients continued to drink in post-diagnosis period (RR continued drinking vs no drinking = 2.7, 95% CI, 1.2-6.1) (18).

Substantial evidence has accumulated in recent years, confirming that specific human papillomaviruses (HPV) are aetiologically involved in a subset of head and neck cancers: oropharyngeal squamous cell carcinomas (OPSCC) (20).

The developed world has experienced a significant rise in the incidence of OPSCC in recent years (21, 22). Sexual behaviour is a major risk factor for OPSCC, with a lifetime number of oral sex partners considered as the behavioural measure most strongly associated with OPSCC development (23).

Human papillomavirus is a member of the larger family of papilloma viridae, which are non-enveloped and contain a circular, double-stranded DNA genome (24). There are more than two hundred various HPV genotypes that have been identified (25), and the HPV types 16, 18, 31, 33, 35, 45, 52, and 58 are the high-risk types that have been linked to cervical cancers (26). Although all high-risk HPV types have been detected in the head and neck sites, most of the HPV infections in normal healthy individuals are cleared within 6-18 months, whereas infection due to HPV 16 type exhibits the lowest clearance rate with infection persisting up to 22 months (27). HPV types 16 and 18 contribute to 85% of HPV-associated head and neck cancer cases worldwide, while the remaining 15% of cases are caused by HPV types 33, 35, 52, 45, 39, 58, 31, 53, and 56 (28, 29). Following HPV infection, the oncogenes E6 and E7 integrate into the host chromosome, and persistent expression of these oncogenes interferes with the functioning of the cell cycle regulator (tumour suppressor) proteins (further discussed in section 1.5.4) (30).

Even though smoking, alcohol and HPV infections are considered to be the most significant risk factors for head and neck cancer in the developed world, it is interesting to note that in India, south-east Asia and some parts of China, betel quid

is known to be an independent aetiological agent (with or without tobacco) for oral cavity cancers (31-34) (see figure 1.2).

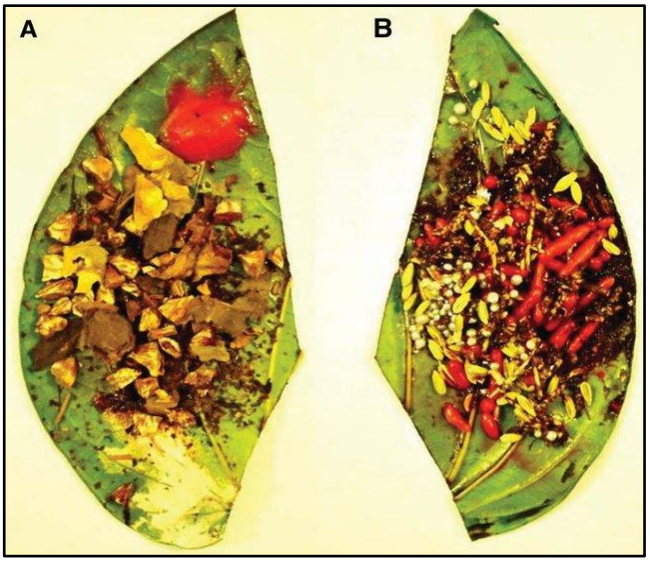

Figure 1:2 Betel leaf and quid with and without tobacco. [(A) Betel quid with tobacco (B) Betel quid without tobacco] A betel quid (synonymous with 'pan' or 'paan') is a mixture of ingredients, including betel nut (also called areca nut), slaked lime and may contain tobacco, wrapped in a betel leaf (35).

Betel quid with tobacco was first designated as a carcinogen by the IARC in 1985 (36), and betel quid without tobacco was also classified as a human carcinogen in 2004 (37).

The incidence patterns of SCCHN over time and by geography are intriguing, closely reflect the changing prevalence of the aforementioned major risk factors. In the UK, laryngeal cancer incidence has declined by 20% since 1990, but the rate has levelled off since 2005, reflecting the reduction in smoking over the preceding years (38). Despite the falling trends in smoking, the incidence of OPSCC has increased (38).

1.3 Hallmarks of head and cancer

To understand SCCHN, one needs to appreciate that it arises following a series of critical genetic alterations, which have been fairly well characterised (39). As with all cancers, the evolutionary process of a normal cell changing to a cancerous one is a complex mechanism, accompanied by multiple steps of genetic and epigenetic changes that confer selective advantages upon the altered cells (40). Hanahan and Weinberg originally proposed that the following six hallmarks of cancer are essential in the multiple stages of tumour progression: self-sufficiency in growth signals, insensitivity to anti-growth signals, evading apoptosis, limitless replicative potential, sustained angiogenesis, tissue invasion and metastasis (41).

In 2011, Hanahan and Weinberg updated their model and added two emerging hallmarks: reprogramming of energy metabolism and evading immune destruction (42). They also proposed two enabling characteristics which are not hallmarks but allow cancer cells to acquire the above hallmarks, and they are genome instability and tumour-promoting inflammation (43).

Figure 1.3 summarises the revised hallmarks of cancer and the molecular mechanisms known to be involved in SCCHN.

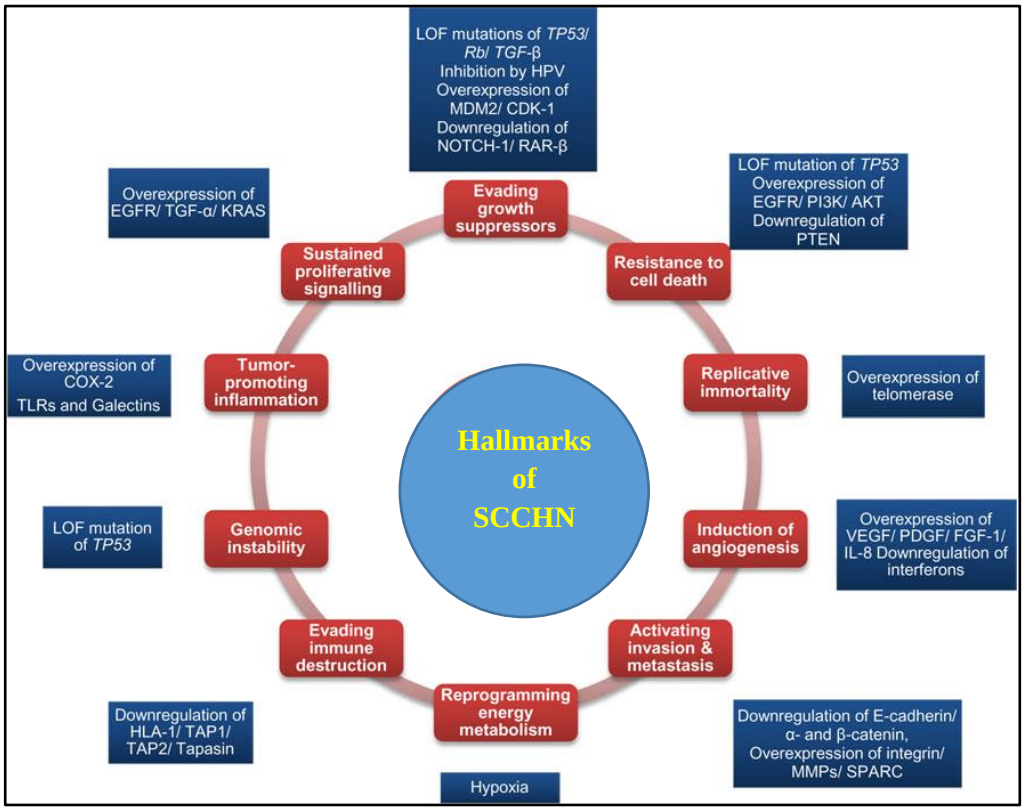

Figure 1:3 Hallmarks of cancer and examples from SCCHN. Hanahan and Weinberg proposed ten hallmarks of cancer (in red), and some examples of molecular mechanisms affecting each of the hallmarks that are known to be involved in SCCHN are shown in blue. (LOF – Loss of function). Only the most frequently implicated genes in SCCHN will be discussed further in this chapter since it is likely that these are the most critical pathways in SCCHN carcinogenesis (43).

1.3.1 Self – sufficiency in growth signals

Healthy cells receive growth-stimulatory signals from their surroundings, which are processed and integrated by complex circuits within the cell, which decide whether cell growth and division are appropriate or not (44). Cancer cells generate many of their own growth signals, thereby reducing their dependence on stimulation from their normal tissue microenvironment (41). Various families of growth factors and growth factor receptors have been implicated in the autonomous growth of tumour cells (45). A well-known example of such a signaling system is the epidermal growth factor receptor (EGFR) and the EGF- family of peptide growth factors, which play a central role in the tumorigenesis of various carcinoma types (46). The ErbB family of

receptor tyrosine kinases comprises four distinct receptors: EGFR (also known as ErbB-1/HER1), ErbB-2 (neu, HER2), ErbB-3 (HER3) and ErbB-4 (HER4) (45). Overexpression of EGFR is seen up to 90% in SCCHN, and the high expression of EGFR is associated with poor clinical outcomes (47-49). EGFR inhibitors such as Cetuximab have exhibited a significant anticancer effect in SCCHN and have improved locoregional control as well as survival (50). There is a significant survival benefit when combining external radiotherapy with Cetuximab for locally advanced SCCHN (51). Apart from EGFR, C-Met is another transmembrane tyrosine kinase receptor that is associated with the invasiveness and metastasis of squamous cell carcinoma of the tongue (52).

1.3.2 Insensitivity to Antigrowth signals

The evasion of anti-growth signaling is an essential hallmark of cancer cells, and in order to proliferate continuously, tumour cells must somehow uncouple themselves from many signals that exist to prevent cell growth (53). Examples of well-known anti-growth signaling pathways are those regulated by p53, phosphatase and tensin homolog (PTEN), retinoblastoma protein (Rb), and Notch (53).

p53 is the most important tumour suppressor protein (described in detail in section 1.5), known as the ‘guardian of the genome’ (54). p53 functions mainly as a transcription factor and can trigger many antiproliferative pathways by activating or repressing key effector genes (55). Cell-cycle checkpoints are essential to verify whether each phase of the cell cycle has been accurately completed before progression into the next phase and p53 plays a major role in cellular growth arrest at these checkpoints in response to various cellular stresses (55). In SCCHN, *TP*53 is the most commonly mutated gene (56) and deregulated p53 protein levels are

correlated with enhanced genetic instability in the preneoplastic epithelium, and it may exert a driving force for the increasing rate of accumulation of genetic events during head and neck tumorigenesis (57).

Retinoblastoma protein (Rb) is another crucial tumour suppressor protein, and Rb plays a role in the G1 phase of the cell cycle, where it suppresses the cell cycle progression by binding to and inhibiting the E2F transcription factors (58). One of the HPV oncoproteins, E7, is best known for its function to inactivate pRb, however functional loss of pRb is not fully accounted for the potency of E7 in causing SCCHN (59). It has been observed that pRb and p107 (one of the pocket proteins of pRb) act together to reduce the tumorigenesis in head and neck cancer, and degradation of these proteins by E7 leads to HPV-associated SCCHN (59). The other important HPV oncoprotein E6 binds p53 and targets it for degradation in about 20% of SCCHN (60), and *TP*53 is not mutated in HPV-associated SCCHN (43).

Phosphatase and tensin homolog (PTEN) acts as a tumour suppressor through negative feedback of the phosphatidylinositol 3-kinase/protein kinase B (PI3K)-AKT-mammalian target of rapamycin (mTOR) pathways, and it was observed in tongue cancer patients that loss of PTEN expression was associated with tumour progression and aggressive behaviour (61).

Evasion of growth suppression can also happen through mechanisms other than the loss of tumour suppressor gene function. Corruption of signaling pathways can repress growth, and a known example for that mechanism is NOTCH 1 signaling, which is down-regulated in SCCHN (43). NOTCH 1 is mutated in 10% to 15% of SCCHN, and these mutations are inactivating, which suggests that the NOTCH 1 gene is acting as a tumour suppressor in head and neck cancer (62).

1.3.3 Evading Apoptosis

Apoptosis is a process of programmed cell death, characterised by specific morphological characteristics such as cell shrinkage, pyknosis, and karyorrhexis and energy-dependent biochemical mechanisms (63). Apoptosis can occur either through the intrinsic (mitochondrial) pathway or the extrinsic (receptor-initiated death) pathway (64). The intrinsic pathway is chiefly regulated by the B-cell lymphoma-2 (BCL-2) protein family, which include pro-apoptotic effector proteins, proapoptotic BH3-only proteins, and antiapoptotic BCL-2 proteins (65).

The extrinsic pathway is activated by death signals mediated by death ligands (TNF, FASL/CD95L/TNFSF6, TRAIL/APO2L/TNFSF10) which bind to their respective receptors and recruit an adaptor protein called Fas-associated protein with death domain (FADD) (66). The adaptor protein (FADD) binds initiator procaspase to form a complex called the death-inducing signaling complex (DISC) (66). Both intrinsic and extrinsic pathways converge at the executioner caspases, a class of cysteine proteases (66).

In SCCHN, expression of Bcl-2 and Bax expression has a prognostic value, and it has been observed in an immunohistochemical analysis of the invasive front of oral squamous cell carcinomas that Bax expression had a better prognosis than those without Bax expression (67). The clinical significance of Bcl-2 overexpression is far from clear in some tumour types; for example, Bcl-2 overexpression in breast, colon, and lung is associated with better prognosis, whereas in cervix, melanoma, bladder, and prostate, Bcl-2 overexpression is correlated with poor prognosis (68). Considering the variation in the prognostic value of Bcl-2 expression, it has been observed that Bcl-2, although a marker of advanced disease, exhibited a favourable outcome in a small population (12.8%) of head and neck cancers (68).

1.3.4 Limitless replicative Potential

Normal cells have limited replicative potential, whereas most tumour cells can be distinguished from normal cells by a progressive acquisition of properties that includes immortality (69). Telomeres present at the linear ends of the chromosomes with a repeat sequence of TTAGGG and telomerase, a ribonucleoprotein enzyme that extends the 3' end of telomeres and maintains its length (41). Telomerase activity is transcriptionally regulated by human telomerase reverse transcriptase (hTERT), and overexpression of hTERT is associated with almost all human malignant tumours (70).

In the head and neck region, overexpression of hTERT has been observed in oral epithelial dysplasia and oral squamous cell carcinoma samples and correlated with aggressive nature (70). The telomerase activation has been observed in 78% of head and neck tumours, 85% of precancerous tissue, and 53% of adjacent normal tissues, and long telomeres and field change may be associated with poor disease-free survival (71). Increased expression of hTERT has been noticed as an early event in oral carcinogenesis, and hTERT could be used as a biomarker (72). By measuring the amount of cytoplasmic or nuclear expression of hTERT in SCCHN, it may be possible to predict the tumour progression, recurrence, and prognosis (72). TERF2 (Telomeric Repeat Factor 2) is a component of the shelterin complex, which interacts with the distal ends of chromosomes, and TERF2 overexpression has been observed as a predictor of poor prognosis in oral squamous cell carcinoma independent of tumour size (73).

1.3.5 Sustained Angiogenesis

Angiogenesis, which is the formation of new blood vessels, is important for the growth, invasion and metastasis of tumour cells (74, 75). For tumours less than or equal to 2 mm in diameter, distribution of nutrients to tumour cells occurs by diffusion, whereas larger tumours depend on a new vascular system to get the required nutrition; thus, angiogenesis is important not only for tumour progression but also for metastasis (76). Vascular endothelial growth factor (VEGF) and Interleukin-8 (IL-8) are important pro-angiogenic factors that facilitate angiogenesis by binding to the tyrosine kinase receptors (the VEGFRs) and G protein-coupled serpentine receptors respectively on endothelial cells, triggering their proliferation and migration (76). Increased levels of interleukin-8 (IL-8) and VEGF has been observed in SCCHN and correlated with high recurrence, shorter disease-free interval and a higher initial TNM staging (76). A large meta-analysis suggested that VEGF expression is a significant survival predictor in head and neck cancer (77). VEGF family members VEGF-A and VEGF-C were both correlated with lymph node metastasis in oral squamous cell carcinoma and, in addition, VEGF-C was associated with recurrence and poor 5-year survival (78). A large meta-analysis of 12 studies (n=1002 SCCHN patients) which evaluated the correlation between VEGF and 2-year overall survival identified that VEGF positivity was associated with poor overall survival in SCCHN patients (79).

1.3.6 Tissue invasion and metastasis

Invasion and metastasis are one of the important hallmarks of cancer cells which refer to the capability of individual tumour cells to detach from the primary tumour, invade the circulation and travel to a distant site, and form a secondary tumour (80). Metastatic cascade is a collective term used to represent the five steps of metastasis,

which are invasion and migration, intravasation, circulation, extravasation, and colonisation (80). In epithelial tumours, inter-cellular structures and cell to cell adhesion play a major role in maintaining a coherent primary tumour mass (81). One of the most potent regulators of adhesion is E-cadherin, which is a member of the cadherin family of proteins, plays a significant role in maintaining cell to cell adhesion (82).

A meta-analysis of nine studies identified that E-cadherin is a critical factor in the prognosis of oral squamous cell carcinoma patients, and reduced expression of E-cadherin correlated with poor overall survival (83).

Catenins (α-catenin and β-catenin) are a family of proteins found in complexes with cadherin cell adhesion molecules, and E-cadherin has been shown to be linked to the actin cytoskeleton via α-catenin and β-catenin (84). Expression of E-cadherin, α-catenin and β-catenin was observed to be low in cases of oral squamous cell carcinoma that develop regional metastasis suggesting the value of immunohistochemical investigation of these proteins for diagnosing the presence of metastasis (84).

Another important mechanism through which cancer cells invade the tissues and detach from the primary tumour is through matrix metalloproteinases (MMPs) which are secretory proteolytic enzymes that promote cancer cell migration and invasion into healthy surrounding tissues by degrading the extracellular matrix and modulating the tumour microenvironment (85). It has been observed that MMP-21 and VEGF-C expression were higher in lymph node metastatic foci in oral squamous cell carcinoma patients, and MMP-21 was a sensitive predictor of overall survival in oral cancer patients with lymph node metastasis (86). Epithelial-mesenchymal

transition (EMT) plays a major role in the invasion and metastasis of tumour cells, and EMT is a dynamic process by which epithelial cells can convert into a mesenchymal phenotype (87). Vimentin is a cytoskeletal protein, not expressed in epithelial cells, but expressed mainly in mesenchymal cells, that has been identified as a predictive marker in oral squamous cell carcinomas, and high vimentin expression was correlated with poor prognosis (88).

1.3.7 Genome instability and mutation

One of the characteristics of many cancers is a loss of replication fidelity leading to genomic instability. This contributes to the overall mutational processes in the cell, and it increases the mutation rate in the tumour cells. Cancer frequently develops from damage to various genes which are responsible for controlling the process of cell division and tumour suppressors.

It is generally accepted that SCCHN arises from normal cells after genetic and epigenetic changes caused by chronic exposure to any of the known carcinogens, which are primarily alcohol, smoking, viral infections, and inflammation (inflammation will be discussed in 1.3.8) (89). The genetic alterations include deletions, point mutations, promoter methylation, amplification of oncogenes and inactivation of tumour suppressor genes (90). In SCCHN, inactivation of tumour suppressor genes and activation of oncogenes occur in various frequencies due to loss of heterozygosity (LOH) and DNA copy number aberration (CAN) (91).

Loss of heterozygosity (LOH) on chromosomes 3p, 9p (inactivation of CDKN2A [commonly referred to as $p16^{INK4a}$ or p16] p16), and 17p (inactivation of p53) have been observed as the early genetic changes in head and neck cancer (92, 93); conversely, genetic changes on chromosomes 4q, 8p, 11q, and 13q are correlated

with the late-stage oral tumorigenesis (91, 94). A study on genome-wide loss of heterozygosity and DNA copy number aberration (CNA) identified a highly heterogeneous and complex genomic landscape of HPV-negative head and neck tumours and observed that the regions in 4q, 8p, 9p and 11q play a critical role in the disease-specific survival in SCCHN (95).

1.3.8 Tumour-promoting inflammation

Inflammatory responses play definite roles at various stages of tumorigenesis, such as initiation, promotion, malignant transformation, invasion, and metastasis (96). Prostaglandins generated from arachidonate by the action of cyclooxygenase (COX) isoenzymes are one of the important mediators of inflammation (97). COX-2 (cyclooxygenase-2) is one of the important isoforms of cyclooxygenase, upregulated in many cancers, including SCCHN (98, 99). COX-2 has been correlated with VEGF expression and tumour angiogenesis in SCCHN, and overexpression of COX-2 and high tumour angiogenesis were linked to shorter survival in head and neck cancer patients (98).

Various environmental risk factors of cancer are associated with some form of chronic inflammation, and a well-known example is a betel chewing with areca nut; and it has been reported that some of the inflammatory cytokines produced by areca nut can lead to increased cell proliferation, particularly IL-8 that was abundantly released in both T cells and monocytes (100). Another risk factor tobacco smoke, which initiates tumorigenesis due to its high carcinogen content but also promotes tumour growth due to its ability to trigger chronic inflammation (101). Alcohol is believed to trigger an inflammatory response with the increased production of pro-inflammatory cytokines and chemokines (102).

The relationship of SCCHN and inflammation is further evidenced by Toll-like receptors (TLR), which are a part of the ancient innate immune system, expressed by SCCHN (43). TLRs are normally expressed on guarding sites such as mucosal membranes and play an important role in host defence against pathogens. In contrast to the protective role against infections, TLRs have also been implicated in tumorigenesis when they are expressed on tumour cells (43, 103). TLRs may have some protective function, but It has been observed that TLR4 was functionally active on SCCHN cells and that TLR4 signalling modifies cancer behaviour and its resistance/sensitivity to immune and drug interventions, contribute to a better understanding of the role of TLR4 in cancer progression (103).

1.3.9 Evading Immune Destruction

The role of the immune system in suppressing carcinogenesis and the potential to target immune checkpoints is an area of considerable research activity. Recent work has demonstrated that many tumours, including SCCHNs, evade immune recognition by altering the expression of immune effectors such as regulatory cells ($CD4^+CD25^+$ $FOXP3^+$ regulatory T cells), antigen processing machinery (MHC 1 [major histocompatibility complex 1], and immune suppressive mediators (TGF-β) (104). In a majority of the cases, the immune response against tumours is dependent on an efficient CTL (cytotoxic $CD8^+$ T lymphocytes) response, and CTLs recognise antigenic peptides bound in the cleft of MHC class 1 molecule, which can be further stimulated to destroy cells expressing peptides for which they are specific (105). Deficiencies in antigen-presenting mechanisms are observed in cancer cells to evade the immune system, and loss of HLA (human leukocyte antigen) class 1 expression has been observed in SCCHN and correlated with tumorigenesis and lymph node

metastasis (105). Downregulation of interferon-inducible components of the antigen-presenting mechanisms, including TAP1, TAP2 and Tapasin, have been correlated with poor prognosis in SCCHN (106). The immune response to SCCHN is also impaired due to the apoptosis of $CD8^+$ T lymphocytes present at the tumour site, and it has been observed that rapid turnover of T lymphocytes and the loss of $CD8^+$ T cells might be contributing to tumour-related immunosuppression (107). One of the important cancer immunotherapy treatment is based on PD-1/PD-L1 (programmed cell death protein-1 / programmed cell death ligand 1) pathway, and evaluating this pathway is beneficial to our understanding of the biological behaviour of SCCHN (108). PD-1/PD-L1 axis modulates immune cells and other stromal cells, which has been proposed as a possible mechanism for creating an immunosuppressive microenvironment, further facilitating immune evasion and immune resistance (109). The expression of PD-1/PD-L1 has been observed to be a useful predictor for nodal metastasis and poor prognosis in SCCHN (108).

1.3.10 Reprogramming energy metabolism

It has been known for nearly 100 years that tumour cells display an altered metabolism compared to normal cells (110) but, this "Warburg" effect or phenotype has only relatively recently become a subject for intense investigation leading to novel ideas about how to therapeutically target tumour metabolism (including efforts by our own research group focussing on SCCHN) (111, 112). One of the critical changes observed is an increased dependency upon glycolysis, even in the presence of oxygen (112) and a concomitant reduction in the levels of oxidative phosphorylation. The reasons for these adaptations remain uncertain, but it has been speculated that tumour cells increase glycolysis to reduce the levels of ROS (reactive

oxygen species) and increase flux through the pentose phosphate pathway to support ribonucleotide biosynthesis and increased reducing capacity from the synthesis of glutathione and other reducing molecules (113).

Interestingly, this adaptation appears to be functionally dependent upon p53 activity, and loss of p53 function has been demonstrated to be a causative event promoting the "Warburg" tumour cell phenotype. Reprogramming energy metabolism will be discussed in detail in the following section 1.4.

1.4 Tumour metabolism

1.4.1 Warburg effect

As mentioned above (section 1.3.10), the Warburg effect, namely increased dependence upon aerobic glycolysis, is one of the most well-studied examples of reprogrammed tumour metabolism. As long ago as 1927, Otto Warburg identified that, compared to the healthy tissues, tumours would utilise more glucose and ferment most of the glucose into lactate, even in the presence of oxygen, and this altered metabolic pathway is now known as the 'Warburg effect (110). This metabolic phenotype is the basis for a tumour imaging technique called PET (Positron Emission Tomography) using labelled glucose analogues, and it will be explained in section 1.7.4.

Warburg proposed that the mechanism of oxidative phosphorylation (OXPHOS) is impaired or damaged in tumour cells when there are increased rates of aerobic glycolysis (110, 114). A majority of the healthy cells follow the "*Crabtree effect*", which defines that if an increased rate of glycolysis is maintained, then OXPHOS is reduced, whereas the tumour cells sustain increased rates of both glucose metabolism and OXPHOS to fulfil the high demand for their anabolic processes (115). However,

when the cancer cells in the tumour core become hypoxic during the growth of the tumour, the rates of OXPHOS are reduced while glycolysis is increased (116).

1.4.2 Reprogrammed metabolism in head and neck cancer

SCCHN is heterogeneous in nature, and this molecular heterogeneity hampers accurate prognostication, treatment planning, and identification of the causative tumour genes (117). However, it is clear that many of the most commonly mutated genes in SCCHN, such as *TP*53, NOTCH1, PTEN, PIK3CA and HRAS, play a crucial role in shifting the metabolic switch towards aerobic glycolysis (118). *TP*53 mutations are frequently seen in SCCHN, and the role of p53 in cancer metabolism is discussed in detail in section 1.5.3. NOTCH1 is the second most commonly mutated gene in SCCHN, and the hypoactive mutants of NOTCH have been observed to decrease the activity of the mitochondrial function and also further reduce p53 protein levels, causing a switch to increased glycolysis (119). PTEN is a tumour suppressor gene, and PTEN elevation has been identified to influence the metabolic switch by regulating PI3K pathways, and negatively impacted glutaminolysis and the Warburg effect (120).

PIK3CA plays an essential role in tumour cell growth, survival and metabolism, and activation of the PI3K pathway in SCCHN involves mutations in PI3K catalytic subunit, p110α (encoded by PIK3CA gene) (121). Increased Akt signaling due to mutations in PIK3CA induces Warburg phenotype and enhances the coupling of glycolysis to the Krebs cycle, which generates intermediates for biosynthetic pathway and NADH (reduced form of nicotinamide adenine dinucleotide) as the primary electron donor for oxidative phosphorylation (122).

Glucose transporter 1 (GLUT1) plays a major role in the transport of glucose in tumour cells, and increased expression of GLUT1 has been correlated with poor clinical prognosis in SCCHN (123, 124). GLUT-1 overexpression has been detected in preneoplastic and malignant tissue, suggesting that changes in GLUT-1 expression could be an early event during the development of SCCHN (125).

Tumour hypoxia plays an essential role in tumour metabolism, and hypoxia is another important factor associated with poor prognosis with advanced SCCHN (126). Hypoxia-inducible factor (HIF)-1α is one of the critical transcription factors mediating the cellular response to hypoxia, and it was identified that HIF-1α regulated the expression of GLUT-1 in oral squamous cell carcinoma, thus favouring enhanced glucose uptake (127). In addition, HIF-1α transcriptionally regulates hexokinases, lactate dehydrogenase A (LDH A), monocarboxylate transporter 4 (MCT4) and pyruvate dehydrogenase (PDK) (128, 129).

Lactate is generated from aerobic and anaerobic glycolysis, and increased tumour lactate concentrations have been correlated with the subsequent development of local or distant metastasis in SCCHN and thus, assessing tumour lactate might be useful for predicting the development of metastatic failure (130). It has been observed that elevated tumour lactate levels correlated with radioresistance in solid tumours (131).

Another evidence regarding the importance of metabolism in SCCHN is derived from studies of fluoro-deoxy-glucose (FDG) in PET imaging (discussed in section 1.7.4) for the diagnosis and staging of primary and recurrent disease (132). The FDG avidity works on the basis that there is a preferential uptake of a fluorinated glucose derivative into tumour cells, which will be converted into a non-metabolised intermediate (132). Since FDG is taken up preferentially by tumour cells, PET

imaging of FDG is used for diagnosing new SCCHN cases as well as the monitoring of response to therapy and post-treatment surveillance for recurrence and metastasis (133).

1.5 p53, a tumour suppressor protein

*TP*53 is the most frequently mutated gene in human cancers, and *TP*53 mutations occur in over 50% of all tumours (134). p53 protein is a transcription factor, and after activation in response to cellular stress signals, such as DNA damage or oncogenic stress, there is increased expression of p53 target genes, which are associated with cell-cycle arrest, senescence, DNA repair or apoptosis depending on the cellular damage (135). Apart from these well-known functions, it is now evident that the ability of p53 to influence gene expression has wide-reaching effects, and p53 has a distinct role in the regulation of glycolysis and autophagy, the repair of genotoxic damage, cell survival and regulation of oxidative stress, invasion and motility, angiogenesis, differentiation and bone remodelling (136, 137).

1.5.1 Structure of p53

p53 is encoded by the *TP*53 tumour suppressor gene located on the short arm of chromosome 17 (17p13.1), which contains 11 exons spanning 20 kilobases (138). The p53 protein is made up of 393 amino acids with functional domains, as indicated in figure 1.4 and is active as a tetramer (139).

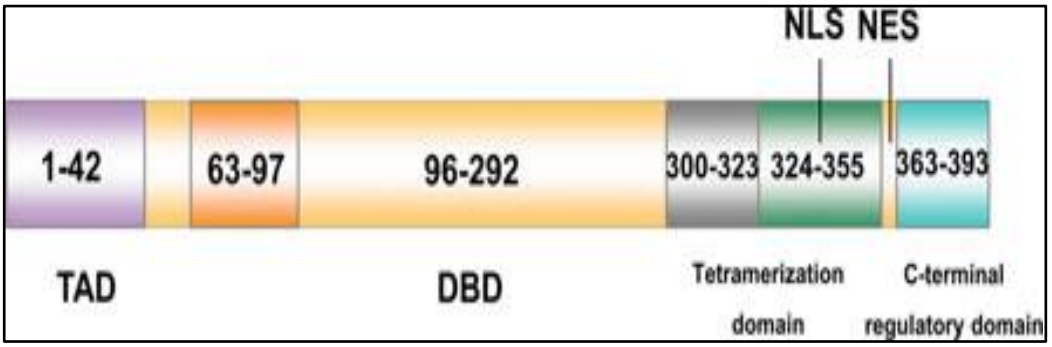

Figure 1:4 Basic structure of p53 protein.
p53 has 393 amino acids, encoded by 11 exons, and has three main functional domains: N-terminal (Transcriptional activation domain) (TAD), DNA binding domain (DBD), and C-terminal (Tetramerisation domain). The C-terminal domain is a multifunction domain that includes (1) signal sequences responsible for the nuclear export (NES) and nuclear localisation (NLS) of *TP*53, (2) an oligomerisation (or tetramerisation) domain for the formation of *TP*53 tetramers, and (3) the C-terminal regulatory domain (140)

The p53 protein has the following domains; an acidic N-terminus containing a transactivation domain (TAD) and a proline-rich region, a hydrophobic, central DNA binding core domain, and a basic C-terminus incorporating oligomerisation and regulatory domains (140)

The p53 monomer is structurally made up of two regions that are distinct in their characteristics; one that demonstrates a stable 3D conformation and one that is unfolded under normal physiological conditions (141). The central DNA-binding domain and the oligomerisation domains belong to the first group, where they have a stable 3D shape conformation, whereas the N-terminal and the C-terminal regions belong to the second group, where they are natively unfolded (141).

1.5.2 Regulation of p53 by MDM2

p53 is a short-lived protein with a reduced half-life ranging from five to thirty minutes (142), and p53 protein levels are maintained at low, often undetectable, levels in healthy cells by maintaining a short half-life under normal/unstressed conditions (143).

Tight regulation of p53 function is essential for normal cell growth and development, and one mechanism by which p53 function is controlled is via interaction with a cellular phosphoprotein called MDM2 protein (144). Human MDM2 has 491 amino acid residues and gets its name from the MDM2 gene (murine double minute 2), which was initially identified on double-minute chromosomes of spontaneously transformed mouse 3T3 fibroblasts (144, 145).

The wild-type p53 positively regulates MDM2 by activating MDM2 gene expression, and on the other hand, MDM2 inhibits the transactivating function of p53 and down-regulates the protein by forming an autoregulatory feedback loop (see figure 1.5) (146). p53 regulates the MDM2 gene at the level of transcription, and the MDM2 protein regulates p53 at the level of its activity and its stability (146).

Thus, the MDM2 protein is a negative regulator of p53 and functions as the E3 ligase, which ubiquitinates p53 and thus targets it for proteasomal degradation (147). The levels of MDM2 activity is crucial and depending upon its levels, MDM2 mono- or poly-ubiquitinates p53 (148). Low levels of MDM2 activity result in monoubiquitination and nuclear export of p53, whereas high levels of MDM2 promote polyubiquitination of p53 and nuclear degradation (148).

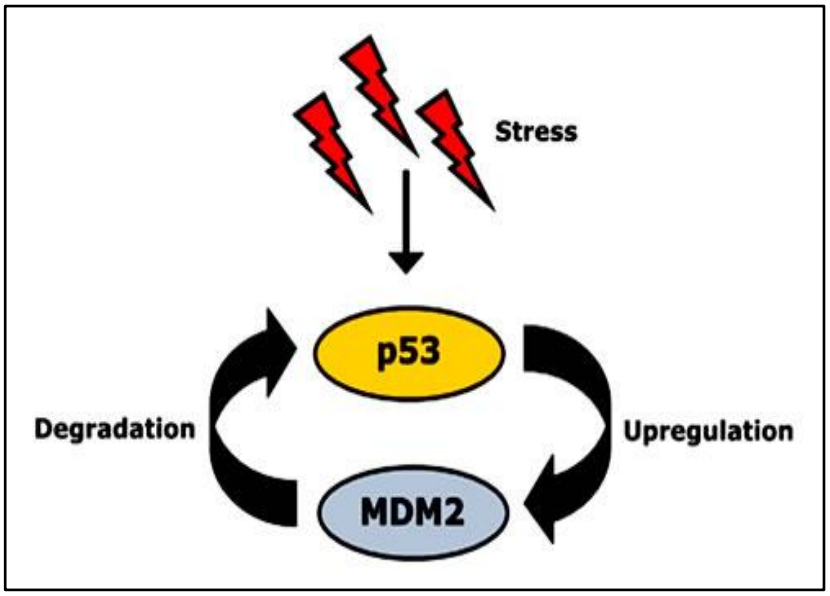

Figure 1:5 Auto regulatory loop between p53 and MDM2. Stress signals activate p53 which then upregulates MDM2 gene expression and increases MDM2 protein levels. As an E3 ligase, MDM2 binds to p53 and induces its degradation. By forming an auto-regulatory negative feedback loop, p53 and MDM2 regulate each other (149).

One of the characteristic features of this autoregulatory loop is that p53 and MDM2 levels oscillate, especially in response to stress (150). Stress signals such as gamma radiation can induce an immediate reduction of MDM2, and the resultant low levels of MDM2 increase the p53 protein levels, which can then transcriptionally induce MDM2 expression, and in turn, the induced MDM2 further decreases the levels of p53 (151).

1.5.3 Role of p53 in regulating glycolysis

p53 negatively regulates glycolysis by modulating glucose transporters and glycolytic enzymes (152) (see figure 1.6).

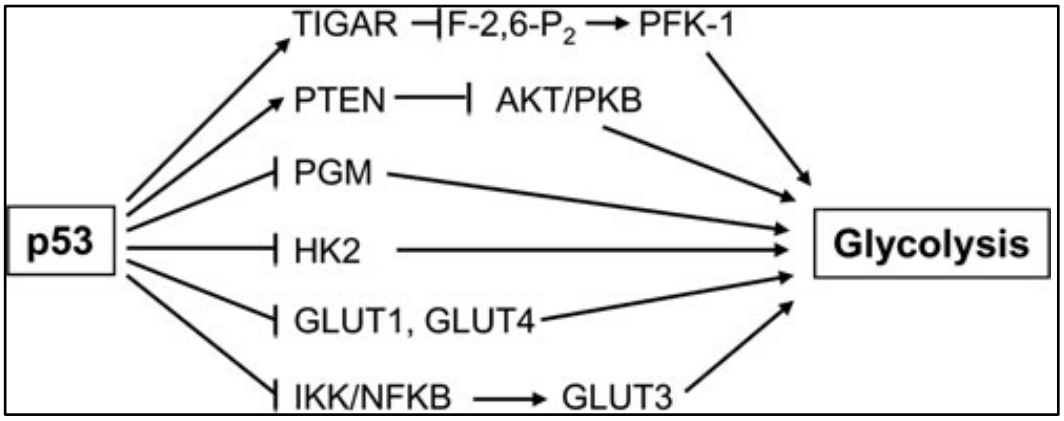

Figure 1:6 The negative regulation of glycolysis by p53. p53 inhibit glycolysis by reducing metabolic substrate availability via downregulation of glucose transporters and by modulating critical enzymes in the glycolytic pathway HK-2 (Hexokinase-2), PFK-1 (Phosphofructokinase-1), and PGM (Phosphoglycerate mutase) (153).

As the first line of defence, p53 prevents the uptake of glucose into the cell by repressing the expression of glucose transporters GLUT1 and GLUT4 (154). p53 further restricts glucose uptake by limiting the kinase activities of I_kB kinase alpha and beta (IKKα and IKKβ), leading to a reduction in NF-$_k$B activity and subsequently reduced expression of GLUT3 (155).

The glycolytic enzyme phosphoglycerate mutase (PGM) enhances glycolytic flux, and p53 represses PGM through increased ubiquitylation and proteasomal degradation (156). TIGAR (*TP*53 induced glycolysis and apoptosis regulator) is another p53-inducible protein that down-regulates glycolysis, and since it is a major focus of this study, it will be discussed in detail in section 1.6.

p53 can modulate glycolysis through its down-regulation of two central cell-growth pathways, the IGF/AKT-1 and mTOR pathways, that play an essential role in the regulation of cell proliferation, survival, and energy metabolism (157). During stress, p53 transcribes a group of negative regulators in these pathways, including IGF-BP3,

PTEN, TSC2, AMPK β1, and Sestrin 1/2, which reduce the activities of IGF/AKT-1 and mTOR pathways (157, 158).

HIF and p53 are likely to have opposing effects on glycolysis, which is promoted by HIF-1α and dampened by p53 (159). It is likely that mild hypoxia activates HIF whereas severe hypoxia induces p53, and these observations suggest that HIF response is designed to support cells survive mild hypoxia, whereas the p53 response is harnessed only under severe hypoxic conditions (160).

1.5.4 p53 mutations in head and neck cancer

*TP*53 mutation is the most frequently observed genetic alteration in SCCHN, and TCGA (The Cancer Genome Atlas) has reported a *TP*53 mutation frequency of over 80% in HPV negative head and neck cancer cases (39). The disruption of the p53 pathway not only occurs through typically missense mutations of the *TP53* gene but also happens through losses of heterozygosity or interaction with viral proteins such as E6 (161).

Tobacco carcinogens, one of the major risk factors of SCCHN, appear to target p53 mutation, and it has been observed that the frequency of somatic mutations in the p53 gene in smokers was twice as high as that of non-smokers (162). *TP53* mutations appeared to differ between smokers and non-smokers in lung cancer, and the transversion G:C > T:A was identified as a frequent base change among smokers who tend to cluster in hotspots, such as codons 157, 158, and 248 (163).

p53 mutations were identified 3.5 times more common among patients who both smoked cigarettes and drank alcohol than among patients who neither smoked nor drank (164).

On the contrary, p53 mutations are inversely associated with HPV infection in the oropharyngeal subset, which contains the most HPV-positive tumours (165). In a large series (202 cases) of oropharyngeal cancer, it was identified that HPV-positive oropharyngeal tumours were less likely to have p53 mutations than HPV-negative cases (166). Figure 1.7 highlighted the mutational distribution between HPV +ve and HPV -ve tumours in 279 SCCHN patients who were profiled by 'The Cancer Genome Atlas' (TCGA) (39).

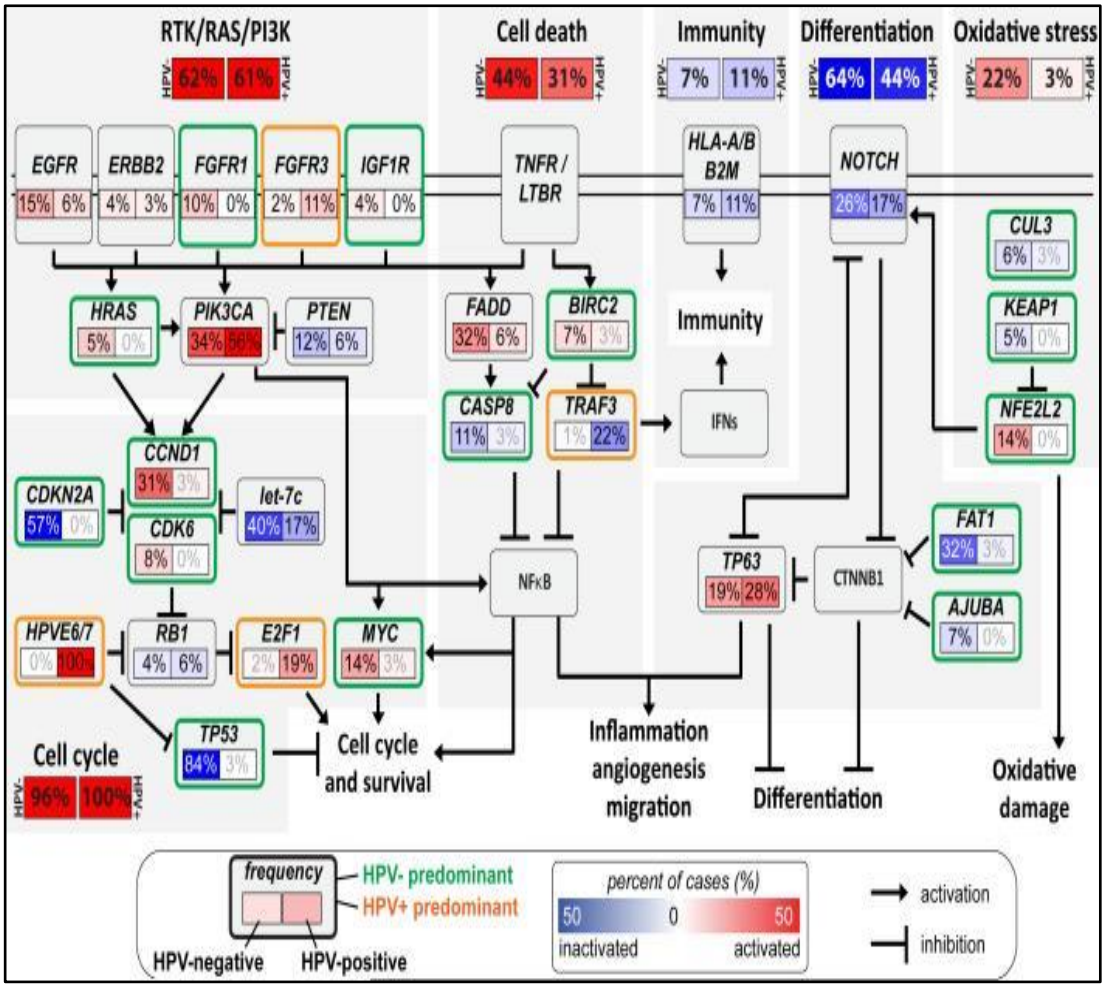

Figure 1:7 Mutational distributions between HPV +ve and -ve cases. Deregulation of signaling pathways and transcription factors are shown. The frequency (%) of genetic alterations for HPV (-) and HPV (+) tumours are shown separately within sub-panels and highlighted. N= 279. Those predominant in HPV -ve (green boxes) or HPV +ve (orange boxes) subsets are highlighted. Activated pathways / genes (red), inactivated pathways/genes (blue). (39)

The inverse relationship between HPV status and p53 mutations was further confirmed by results of 'updated TCGA analysis' (Broad Institute data) which demonstrated the lowest p53 mutation rate (28.6%) in oropharynx tumours compared to larynx and hypopharynx (83.5%) and tongue and oral cavity (75.6%) (167).

The mechanism of p53 inactivation is different in HPV infected OPSCC cases as HPV E6 viral oncoprotein promotes MDM2-independent degradation of p53, and it has been observed that inactivation of p53 by mutations induced by tobacco may not be functionally equivalent to its degradation by HPV E6 (168). In other words, E6 degradation of p53 protein is not functionally equivalent to a p53 mutation (169). In HPV infected cases, E6 oncoprotein binds to the cellular protein E6AP, and the E6/E6AP complex further induces ubiquitination and subsequent proteasomal degradation of p53 protein (170). The endogenous wild-type p53 in HPV infected cells can still activate some cellular target genes (171), and there is also an intact apoptotic response to radiation (172).

In a majority of human cancers, the loss of p53 function occurs mostly through mutations in p53 itself or perturbations in pathways signaling to p53 (173). Among p53 mutations, missense mutations are more frequent (73%), leading to amino acid substitution in the DNA binding domain (174). Other changes include frameshift insertions and deletions (9%), nonsense mutations (8%), silent mutations (4%), and splice-site mutations (2%) (174, 175).

In a small subset of SCCHN, HPV infection and p53 mutations sometimes occur together (176-178). It has been observed that p53 mutations seen in HPV positive cases were mostly of mutations that do not disrupt DNA binding (169). In a multicenter prospective study, among the selected SCCHN cases, both HPV 16 +ve

and HPV -ve cases harboured p53 mutations (25% versus 52%), but disruptive mutations were only identified in HPV -ve SCCHN cases (169).

p53 alterations appear at the early stages of head and neck tumorigenesis, and it has been observed that p53 mutations occurred in non-invasive lesions and increased in frequency with invasive carcinomas (179). No difference was observed in terms of p53 mutations when comparing primary tumour and nodal metastasis, and it has been suggested that p53 mutations develop in tumorigenesis before metastasis occurs and subsequently remain stable in the metastatic phase (180). Based on this observation, p53 may be considered as a clonal marker not susceptible to change during tumour metastasis (180). p53 mutations have been observed in all the stages of SCCHN tumorigenesis, but no mutations were identified in the normal mucosa that was never exposed to a carcinogen (181).

It is still a matter of debate when considering the prognostic value of p53 mutational status in patients with SCCHN (161, 182). The result of a large meta-analysis on p53 as a prognostic factor in patients with SCCHN was inconclusive as large heterogeneity was found across studies in study-level and patient-level characteristics, making it difficult to determine a clear picture (182). Overexpression of p53 has been related to poor prognosis in head and neck cancers (183, 184). Although this finding (p53 levels determined in the absence of p53 genetic information) is controversial and many studies did not find any relation between overexpression of p53 alone without mutations and clinical prognosis in SCCHN (185-188). Even though p53 overexpression in primary tumours is of limited clinical significance, p53 overexpression in the lymph nodes from supraglottic laryngeal cancers has been observed to be an independent predictor of regional failure and poor

prognosis (189). The status of p53 mutations is less controversial than p53 overexpression, and many studies have observed poor prognosis with p53 mutations in SCCHN (190-193). One of the most significant studies of p53 mutations and the associated prognosis was a prospective multi-centre study of 420 patients (from all head and neck sites) for p53 mutations (193). These were functionally classified as being either **disruptive** (*nonconservative mutation located inside the main DNA-binding domain (L2-L3 region plus nonsense mutations in any region*)) or **non-disruptive** (*conservative or non-conservative mutation outside the DNA binding domain)* (193). The study results identified an association between p53 mutations and survival, showing that p53 mutations were associated with reduced overall survival and disruptive p53 mutations have a stronger correlation with poor survival compared to non-disruptive p53 mutations (193).

1.6 TIGAR (*TP*53-induced glycolysis and apoptosis regulator)

1.6.1 TIGAR discovery

p53 regulates many genes, primarily through its function as a sequence-specific transcriptional regulator (137, 194), and a number of these appear to play an important role in the p53-mediated regulation of metabolism (112). However, it is probably correct to state that no p53-regulated gene has a stronger link with metabolic regulation than TIGAR (112, 195). Jen and Cheung identified genes that were regulated by p53 in response to ionising radiation by using computational and molecular techniques, including location analysis (ChIP-on-chip assay) (196). After examining 489 candidate genes that responded to ionising radiation, they found 38 genes that were p53 targets, some of which were already known to be regulated by p53 and others that were novel p53 target genes, including C12orf5 (196). Benasaad

et al. studied the structure and functions of the C12orf5 gene and discovered that it encodes a fructose-2,6-bisphosphatase and coined the name TIGAR in honour of its identified functions (197).

1.6.2 Structure of TIGAR

The TIGAR gene is located on chromosome 12p13-3 and has six potential coding exons and two p53 binding sites (see figure 1.8) (197). Among the two p53 binding sites, BS2 binds more efficiently with p53, and it has been identified as the functional p53-binding site (197).

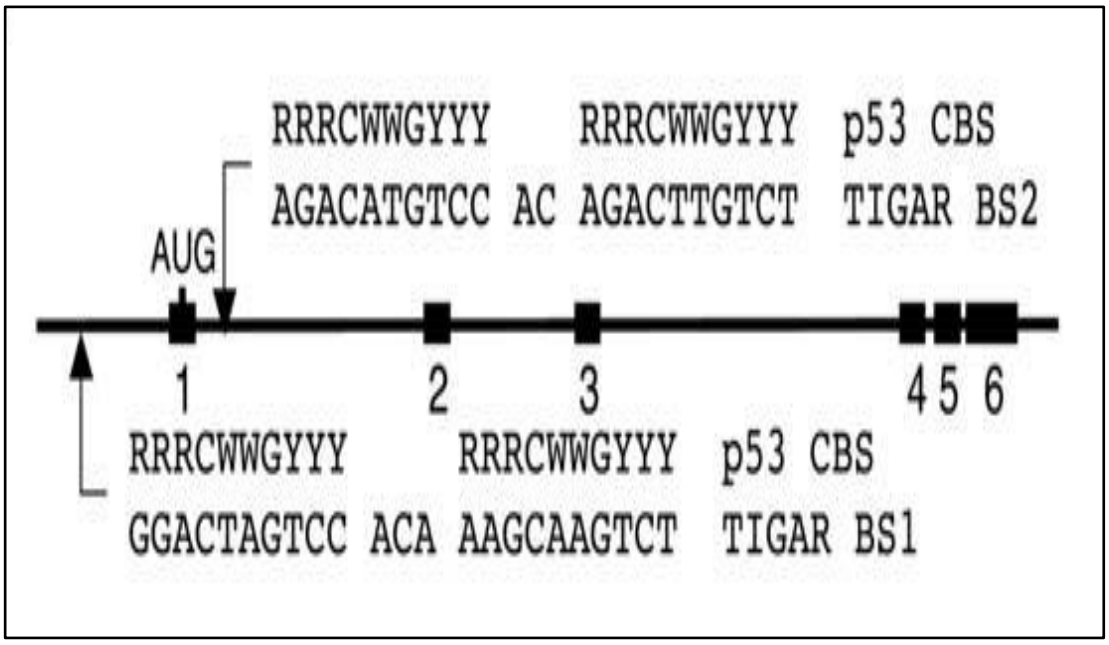

Figure 1:8 Genomic organisation of TIGAR showing the p53 binding sites. Exon/intron organisation of the genomic structure of human TIGAR, showing two possible sites for p53 binding; upstream of the first exon (TIGAR BS1) and within the first intron (TIGAR BS2) compared to the consensus p53 binding site (p53, CBS). R, purine; Y, pyrimidine; W, adenine, or thymine. The predicted initiation codon (AUG) is also indicated (197).

TIGAR protein consists of 270 amino acids (198). The structure of TIGAR forms a histidine phosphatase fold that is closely related to the bacterial broad specificity PhoE phosphatase (199).

1.6.3 Functions of TIGAR

1.6.3.1. TIGAR acts as a fructose-2,6-bisphosphatase

There are similarities between TIGAR and a glycolytic enzyme known as phosphofructokinase-2/fructose-2,6-bisphosphatase (PFK-2/FBPase-2), which is a bi-functional protein with kinase and bisphosphatase domains at the NH_2-terminus and at the COOH-terminus, respectively (200). Out of these two domains, TIGAR shares similarities only with the bisphosphatase domain of PFK-2/FBPase-2 and is able to function like fructose-2,6-bisphosphatase (FBPase-2) (197). Thus, TIGAR acts like a fructose-2,6-bisphosphatase and removes one phosphate from fructose-2,6- bisphosphate, thereby decreasing the levels of fructose-2,6- bisphosphate with the resultant enzymatic product of fructose 6 phosphate (200).

Fructose-2,6-bisphosphate (F-1,6-P_2) is a potent allosteric activator of phosphofructokinase-1 (PFK-1) which catalyses the conversion of fructose-6-phosphate (F-6-P) to fructose-1,6-bisphosphate (F-1,6-P_2), thus helping glycolysis to progress (figure 1.9) (200). Therefore, by reducing the levels of fructose-2,6-bisphosphate, TIGAR lowers the activity of PFK-1 and further inhibits glycolysis. Thus, TIGAR expression dampens the glycolytic pathway, and a number of consequences can be predicted after the activation of TIGAR, which are; the gluconeogenesis rate increases, surplus fructose-6-phosphate, is transformed back to glucose-6-phosphate, and excess glucose-6-phosphate enters into PPP (pentose phosphate pathway) and alters the production of ROS (200).

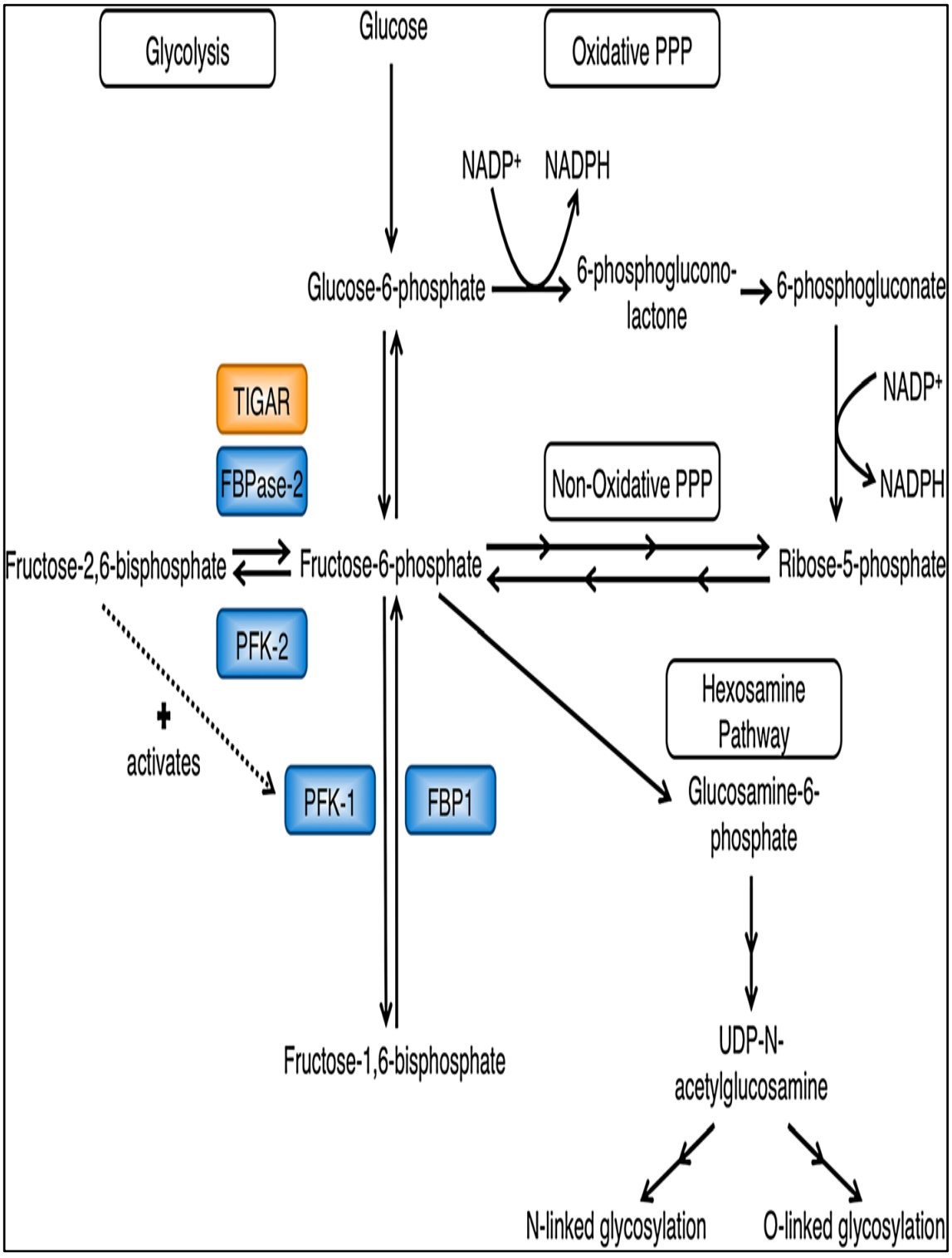

Figure 1:9 Inhibition of Glycolysis by TIGAR. TIGAR acts like FBPase-2 and reduces the levels of fructose-2,6-bisphosphate, which is a potent allosteric activator of phosphofructokinase-1 (PFK-1). PFK-1 catalyse the conversion of fructose-6-phosphate to fructose-1,6-bisphosphate and, in doing so, drives glycolysis. By lowering fructose-1,6-bisphosphate levels, TIGAR reduces the activity of PFK-1 and decreases glycolytic flux downstream of this point (200).

1.6.3.2 Antioxidant activities of TIGAR

Reactive oxygen species (ROS) are generated endogenously from the normal cell metabolism, in particular from the mitochondrial oxidative phosphorylation, or they may arise from interactions with exogenous sources such as xenobiotic compounds (201). ROS act as signaling molecules that are involved in various mechanisms regulating cell proliferation, senescence, apoptosis, necrosis and autophagy (202, 203).

TIGAR reduces the production of ROS through the pentose phosphate pathway in the following manner; when TIGAR inhibits glycolysis, the intermediate products of the metabolic reactions are diverted to alternate pathways like the hexosamine pathway to promote glycosylation and to the pentose phosphate pathway (both oxidative and non-oxidative pathways) (see figure 1.10) (200).

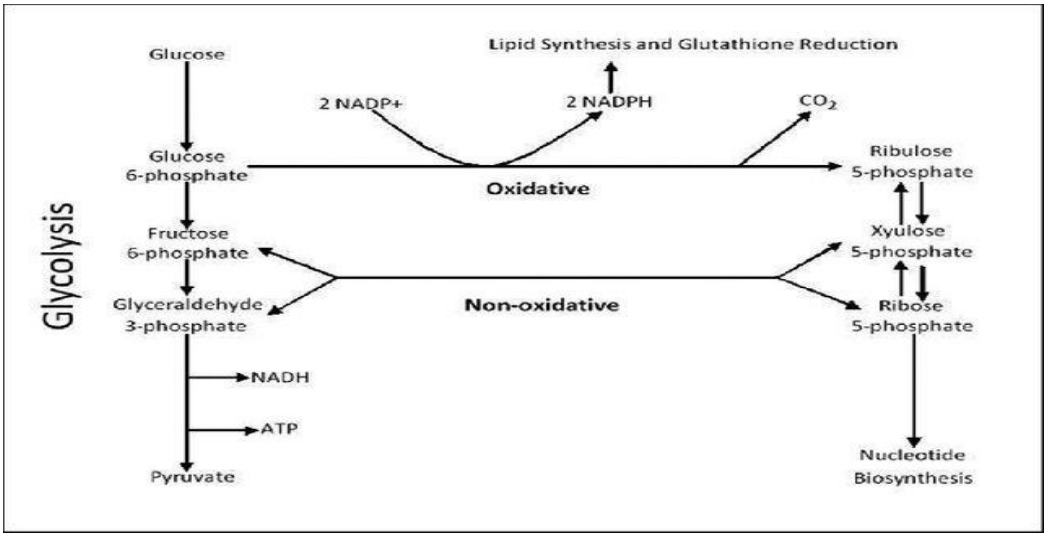

Figure 1:10 Pentose phosphate pathway (PPP). The oxidative and non-oxidative pathways of PPP produces reducing equivalents in the form of nicotinamide adenine dinucleotide phosphate (NADPH) and ribose-5-phosphate (R5P) (204).

In the oxidative arm of PPP, the enzyme G6PD (glucose-6-phosphate dehydrogenase) oxidises G6P (glucose 6-phosphate) and produces NADPH and ribose-5-phosphate (R5P) (204). In the non-oxidative arm, glyceraldehyde-3-phosphate and fructose-6-phosphate, which are the intermediates of glycolysis, are converted to R5P (204). As both pathways are reversible, whenever the cell needs more reducing power (in the form of NADPH), R5P can be converted back to fructose-6-phosphate and glyceraldehyde-3-phosphate by transketolase producing more NADPH (204). Thus NADPH is important, as it provides the reducing power that fuels the antioxidant mechanisms and recycles oxidised glutathione (205). NADPH reduces the oxidised form of glutathione to the sulfhydryl (reduced) form of glutathione. Thus, by increasing the production of NADPH, TIGAR contributes to the scavenging of ROS and lowers the sensitivity of cells to oxidative stress-associated apoptosis (197).

TIGAR, apart from contributing to anti-oxidant function via an intrinsic FBPase-2 activity, also contributes to reducing ROS as a result of an interaction with Hexokinase-2 (HK-2) as described below. During hypoxia, a fraction of TIGAR is transported to mitochondria where it binds to HK-2, and this results in increased HK-2 activity, which lowers mitochondrial membrane potential, leading to reduced oxphos, with a concomitant decrease in ROS (206). It has been observed that the translocation of TIGAR to the mitochondria and subsequent binding to HK-2 depends on the availability of glucose (206). Thus, TIGAR maintains cell survival via HK-2 during hypoxia.

1.6.3.3 Physiological functions of TIGAR

To study the effects of the role of TIGAR in various physiological functions, Cheung et al. developed and analysed Tigar deficient mice (207). Their study identified that TIGAR played an essential role in tissue regeneration and that lack of TIGAR resulted in a failure to repair damaged intestinal epithelium (207). After the whole-body radiation, the intestinal crypts of TIGAR knockout mice were acutely apoptotic and had difficulty in regenerating themselves compared with those of wild-type animals (207).

TIGAR plays a role in cardiac myocyte energy metabolism, and it has been observed that TIGAR was able to inhibit glycolysis and energy metabolism in hypoxic myocytes and inhibition of the p53/TIGAR system reduced hypoxia-induced apoptotic cell death (208).

Modulating p53 and TIGAR proteins may become a novel strategy for cardiac myocyte energy maintenance and a potential therapeutic approach for ischemic heart diseases (208). Maintenance of mitochondrial integrity by promoting mitophagy is essential for cardiac protection against ischemic injury, and it has been observed that p53-dependent upregulation of TIGAR attenuated cardiac myocytes mitophagy to cause accumulation of damaged mitochondria and further causing apoptosis (209). The damaging effects of cardiac myocytes were reversed by deletion of either TIGAR or p53 gene (209).

In contrary to TIGAR effects on cardiac myocytes (208, 209), upregulation of TIGAR exerts potent neuroprotection (210). TIGAR plays a protective role in ischemia/reperfusion-induced brain injury, and it was observed that there was a quick upregulation of TIGAR in response to ischemia/reperfusion damage, and TIGAR

expression was positively linked with the elevation of NADPH and negatively correlated with reactive oxygen species in the ischemic brain (210). TIGAR levels have been investigated in the mouse brain, and it was high in the embryonic stage, dropped at birth and partially recovered in the early postnatal period, and then continued to reduce to a lower level in early adult and aged mice (211). These results suggested that TIGAR expression changes during brain development and TIGAR expression levels might be correlated with the vulnerability of neurons to ischemic injury (211). It was observed that, upregulation of TIGAR in response to ischemia/reperfusion insult in the brain was not regulated by glucose but regulated by reactive oxygen species and hormones that regulate blood glucose such as adrenaline, glucagon, hydrocortisone, and insulin (212). In summary, TIGAR supports rapid proliferation in the adult intestinal epithelium, plays a neuroprotective role in brain ischemia and also exhibits a crucial role in cardiac myocyte energy maintenance by regulating glycolysis.

1.6.3.4 Role of TIGAR in autophagy

Apoptosis and autophagy are two self-destructive processes, where apoptosis can be described in simple terms as ‘self-killing’ and autophagy can be described as ‘self-eating’ (213). Autophagy is an intracellular catabolic process that happens under stressful situations like organelle damage, the presence of abnormal (misfolded) proteins, and nutrient deprivation (214). In many cancers, the modulation of autophagy plays dual roles in tumour promotion and also tumour suppression (see figure 1.11) (214). Elevation of autophagic activity is seen in most chemotherapeutic treatment, and cancer cells use this as a protective strategy to avoid being entirely

killed by chemotherapy drugs (215). This strategy provides tumour cells with a pro-survival ability and renders them resistant to anticancer drugs (216).

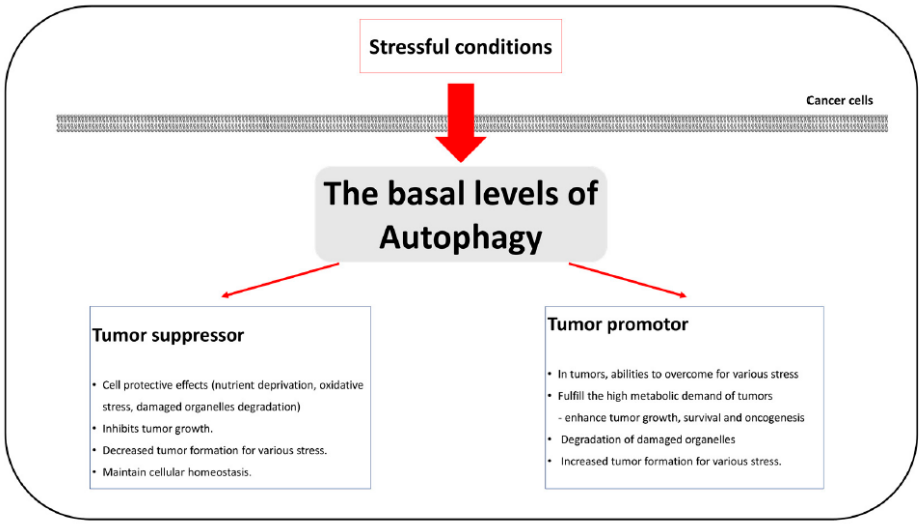

Figure 1:11 A schematic diagram of the dual roles of autophagy in cancer cells. Autophagy plays dual roles in tumour promotion and suppression and contributes to cancer-cell development and proliferation (214).

It has been observed that TIGAR could modulate ROS levels in response to nutrient starvation or metabolic stress, thereby inhibiting autophagy (217). This ability of modulating ROS exerts profound efforts on autophagy, and it has been demonstrated that the loss of TIGAR significantly increased the autophagy, even in otherwise unstressed cells (217). The mechanism of limiting autophagy through ROS regulation by TIGAR has been observed to be independent of p53 and mTOR pathways (217). To study the effects of TIGAR on autophagy, TIGAR silencing was induced in cancer cell lines (A549 [lung] and HepG2 [liver]) and tested with epirubicin (a DNA-damaging anticancer agent) (216). It has been observed that there was a slight increase in autophagic activity after TIGAR knockdown, but there was a noticeable increase in epirubicin-induced autophagy activation (216). This study also identified that the autophagy induced by TIGAR knockdown resulted in the elevation

of ROS and inhibition of mTOR and further proposed that TIGAR plays a dual role in cancer survival, with one favourable effect through ROS reduction and another unfavourable effect due to reduction of autophagic activity (216).

1.7 Hexokinase 2

One of the essential cancer hallmarks is the "deregulation of cellular energetics", with the 'Warburg effect' being a common adaptation (42). Our primary aim was to investigate the role of critical genes that are involved in cellular metabolism in SCCHN, and because of the important role of p53 in SCCHN, we investigated p53 in our studies. We included TIGAR in our analysis because TIGAR is a major p53 regulated gene known to play essential roles in metabolic regulation, in part, by acting enzymatically as a Fructose 2,6, bisphosphatase. There is good evidence from the literature that TIGAR also interacts with another critical metabolic enzyme: HK-2 (Hexokinase – 2), and though this appears to also impact cellular metabolism, by a mechanism that is independent of the phosphatase activity of TIGAR. We, therefore, decided that it would be important to include an investigation of the expression of HK-2 in SCCHN as part of our studies.

1.7.1 Isoforms of hexokinase

There are four isoforms of hexokinase, denoted as HK-1-4, and the type 4 isozyme is also known as 'glucokinase' (218). Primary sequence analysis revealed that each of the genes has arisen through duplication, and since three of them have two HK-4 like domains, it is most likely that one of them was duplicated both to a new location and then internally duplicated and that this copy with two "domains" was then further duplicated to two different locations resulting in all four alleles/isozymes (219, 220).

This explains the molecular mass of each hexokinase, which is closer to 100 kDa, whereas the molecular mass of glucokinase (HK-4) is approximately 50 kDa (221).

The HK-2 has a catalytic function in both of their N- and C-terminal halves, whereas HK-1 and HK-3 have the catalytic function mainly in the C-terminal half (see figure 1.12) (218).

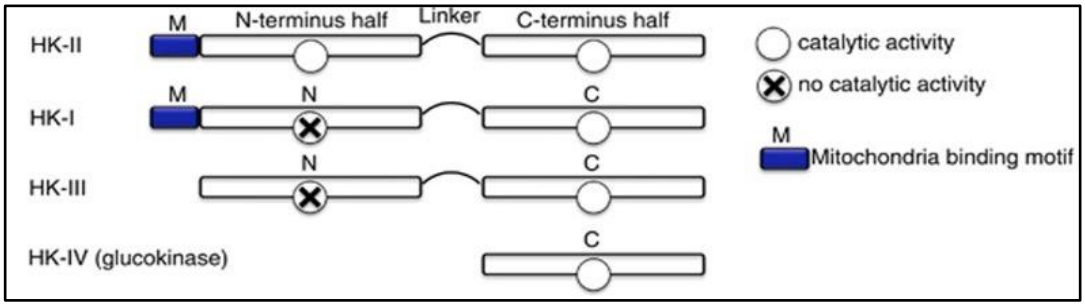

Figure 1:12 Hexokinase subtypes. As a result of a duplication event, HK-1, 2 and 3 have duplications of an ancestral kinase domain, but in the case of HK-1 and HK-3, only the carboxy-terminal domain has catalytic activity, whereas HK-2 has catalytic activity in both domains. HK-4 has only one domain (222).

HK-1, HK-2, and HK-3 are high-affinity isoforms (each has K_m values in the micromolar range), and one of the essential regulatory features of these hexokinases is the susceptibility to inhibition by its own product glucose-6-phosphate (G6P), providing a feedback inhibition mechanism (218). Glucokinase is a low-affinity isoform, and it is not inhibited by glucose-6-phosphate (223).

HK-1 is constitutively expressed in most mammalian adult tissues but predominantly expressed in the brain and kidney (223, 224). HK-2 is abundantly expressed in embryonic tissues; however, it is seen mainly in a limited number of adult tissues where they express more sensitivity to insulin such as adipose, cardiac and skeletal muscle (223, 225). HK-3 is expressed ubiquitously in all tissues but is usually expressed at low levels (224). Glucokinase, HK-4, is localised primarily to the liver

and pancreas (222, 226). There is a switch-over of expression from HK-4 to HK-2 during the tumour development in the liver, and this change is one of the original adaptations observed in the tumorigenesis in the liver and pancreatic tissues (227).

1.7.2 Role of hexokinases in metabolism

Hexokinases catalyse the initial step of glucose metabolism, phosphorylating glucose to glucose-6-phosphate (G6P) (228). Glucose-6-phosphate functions as a precursor for many metabolic pathways, including glycolysis (ATP), pentose phosphate pathway (NADPH and ribulose-5-P), glycogenesis (glycogen) and hexosamine biosynthetic pathway (UDP-GlcNAc) (218, 226, 229). Thus, hexokinases play an essential role in regulating anabolic and catabolic pathways (see figure 1.13) (222).

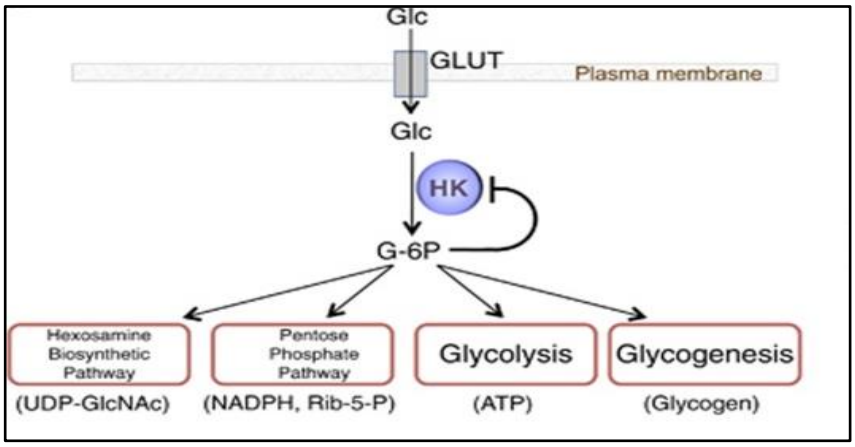

Figure 1:13 Metabolic role of hexokinase. Hexokinase has a diverse role on metabolism by producing more G6P, which serves as a precursor for glycolysis, PPP, glycogenesis and hexosamine biosynthetic pathway (222)

It has been observed that significant quantities of HK-1 and HK-2 were able to bind to the outer mitochondrial membrane via a mitochondrial binding motif in the hydrophobic N-terminus (230, 231). HK-2 binds to a voltage-dependent anion channel (VDAC), which is an outer mitochondrial membrane protein, forming a

contact between the inner and outer mitochondrial membranes (226, 232). The mitochondrial bound hexokinases facilitate the coupling between glycolysis and oxidative phosphorylation through preferential access to ATP produced by the mitochondria (233). The mitochondrial hexokinase catalytic activity generates ADP, which will be shuttled back into the mitochondria for rephosphorylation providing metabolic advantage (233).

HK-1 and HK-2 have overlapping tissue expression but different subcellular locations, as HK-1 is mainly associated with mitochondria and HK-2 associated with both mitochondria and cytoplasm (234). HK-1 ("the brain HK") is present ubiquitously in most tissues, especially in brain and red blood cells, whereas HK-2 ("the muscle HK") is found mainly in insulin-sensitive tissues such as adipocytes and adult skeletal and cardiac muscle (235, 236). It has been observed that HK-2 and its mitochondrial binding negatively regulate cardiac hypertrophy by reducing ROS production through mitochondrial permeability (237). In response to changes in the glucose levels, the subcellular translocation of HK-2 decides the metabolic fate of glucose and directs it between catabolic (glycolysis) and anabolic (glycogen synthesis and pentose phosphate shunt) uses, whereas HK-1 remains within the mitochondria to promote glycolysis (234).

1.7.3 Role of HK-2 in the Warburg effect

The Warburg effect describes a phenotype in cancers in which cancerous tissues and cells depend less on the mitochondrial electron transport chain than in normal cells and obtain as much as 50% of their ATP by metabolising glucose directly to lactic acid, even in the presence of oxygen. It has been suggested that HK-2 may be the most critical glycolytic enzyme involved in promoting the Warburg effect (229).

The functions of HK-2 rely on a number of cellular proteins, namely Glut transporters (glucose transporters which are located on the plasma membrane transport glucose into the cell), VDAC (voltage-dependent anion channel), ATP synthase, and the adenine nucleotide translocator (see figure 1.14) (227).

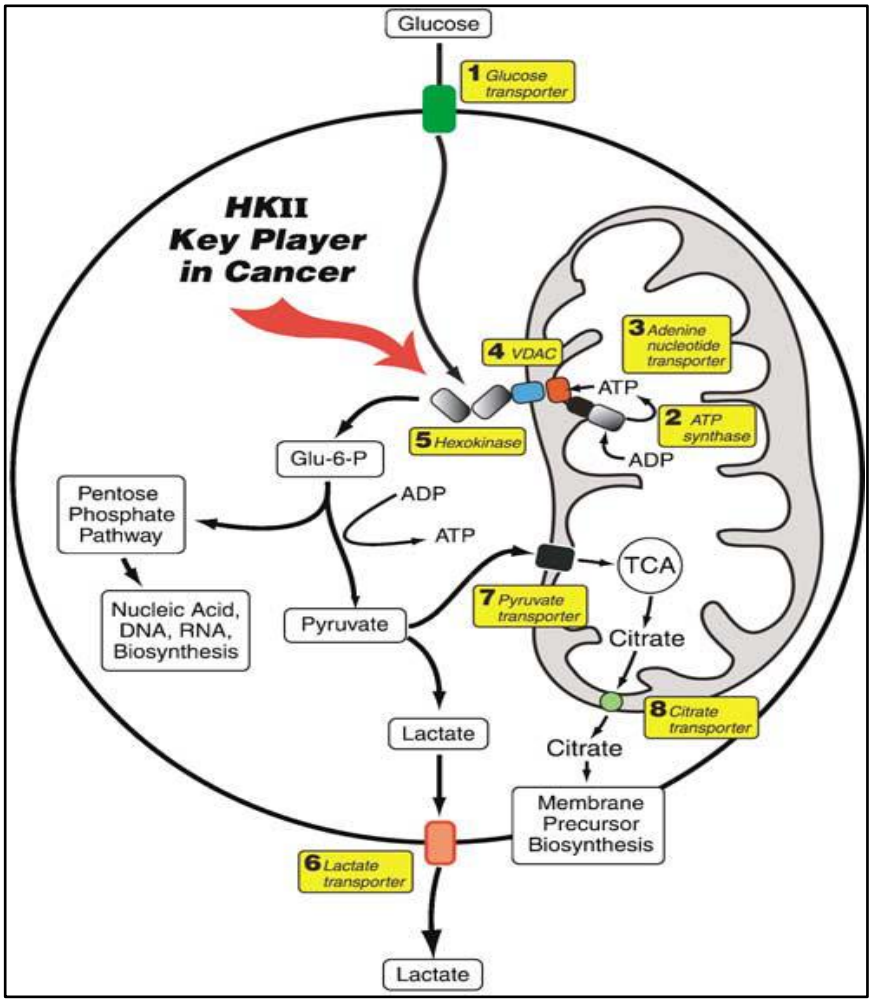

Figure 1:14 HK-2 and its main partners for cancer promotion. Glucose transporters (1) transport glucose across the plasma membrane, and glucose is quickly phosphorylated by HK-2 (5), which is bound to a voltage-dependent anion channel (VDAC) (4) located on the outer mitochondrial membrane. ATP synthase (2) generates ATP, which is then transported across the inner-mitochondrial membrane by the adenine nucleotide translocator (3). G6P is rapidly distributed across important metabolic routes like PPP or gets converted into pyruvate and lactic acid. Lactate transporters (6) transport lactic acid out of the cell, which will make the environment unfavourable for surrounding healthy cells. Some pyruvate is directed to mitochondria via the pyruvate transporter (7) to provide substrates for the TCA cycle. The generated Citrate exits the mitochondria via the citrate transporter (8) (227).

Glucose is the first substrate of HK-2, and HK-2 catalyses the phosphorylation of glucose into G6P (227). HK-2 binds to VDAC, which is present in the outer mitochondrial membrane (232). VDAC is responsible for regulating the routine metabolites exchange essential for mitochondrial function across the outer mitochondrial membrane and into the intermembrane space, where they are then accessible to the specific inner mitochondrial membrane transport mechanisms responsible for their uptake into the matrix (238). HK-2 is free from G6P inhibition because of its binding with mitochondria so that it can continue to produce G6P, which is important for the biosynthesis of many cellular building blocks (239). ATP synthase is an inner mitochondrial membrane protein and produces ATP, the second substrate of hexokinases, and the generated ATP has to be transported to the outer mitochondrial membrane and this transport is facilitated by an adenine nucleotide translocator (227) (see figure 1.14). The adenine nucleotide translocator carries the ATP across to the VDAC- HK-2 complex, and the outcome of the interactions among these groups of proteins is the efficient and increased generation of glucose-6-phosphate (221).

To maintain the high levels of glycolysis that occur in cancer cells and to keep up their proliferative potential, the glucose-6-phosphate quickly distributes across two metabolic pathways; (1) glucose-6-phosphate enters into PPP for the biosynthesis of nucleic acid precursors (2) conversion of the glucose-6-phosphate into pyruvate and lactic acid via glycolysis (221). Most of the pyruvic acid is reduced to lactic acid and carried out of the cancer cells via lactate transporters (in particular the monocarboxylate transporters such as MCT1 (240)), and some pyruvate is transported to mitochondria via the pyruvate transporter (227).

1.7.4 PET scanning is based on the 'Warburg effect'

The Warburg effect is a common phenotype of tumour cells, and a commonly used diagnostic tool known as positron emission tomography (PET) has been based on a key property of this phenotype (229).

PET imaging is based on the use of a radioactively traceable modified form of glucose (2-deoxy-D-glucose) (2DG), labelled with the positron emitter ^{18}F (^{18}FDG, 18F fluorodeoxyglucose, or 2-deoxy-2-[F-18]fluoroglucose) (229). The "deoxy" analogue of glucose can be phosphorylated by hexokinase to yield 2-deoxyglucose-6-phosphate (2-DG6P), but this cannot be metabolised further (241). ^{18}FDG, therefore, accumulates inside the cells and can be detected by PET (see figure 1.15) (221) (242). The tumour cells, which utilise more glucose than their normal cells of origin, are commonly called "PET-positive" (229).

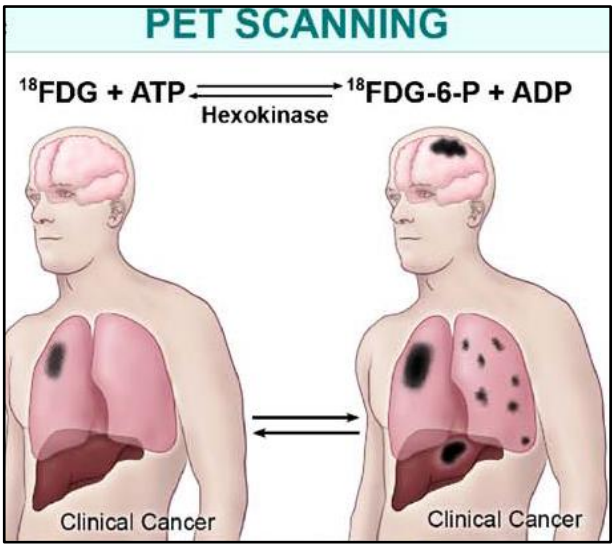

Figure 1:15 PET scanning based on radioactive glucose analogue uptake by tumour cells. Use of radiolabelled 2-deoxyglucose that is taken up by cancer cells and phosphorylated by HK-2 to give 2-deoxyglucose-6-phosphate (2-DG6P), which is not further metabolised (229)

PET scanning is used worldwide for diagnosis, staging, and follow-up of various malignancies (243).

1.7.5 Genetic and epigenetic events related to HK-2 in cancer promotion

The respective hexokinase isoforms and the associated transporter isoforms like HKs, Gluts, VDACs or adenine nucleotide transporters are implicated in the upregulation of glycolysis in malignant tumours, and they are all encoded at different chromosomal loci (227). None of the above-mentioned protein isoforms appears to result from alternative exon splicing events or chromosomal rearrangements/deletions, which suggest that genetic (e.g., gene duplication) and/or epigenetic (e.g., demethylation) events may play a role in activating these genes of interest, in particular, HK-2 that is 'switched-on during cancer development and progression (see figure 1.16) (227).

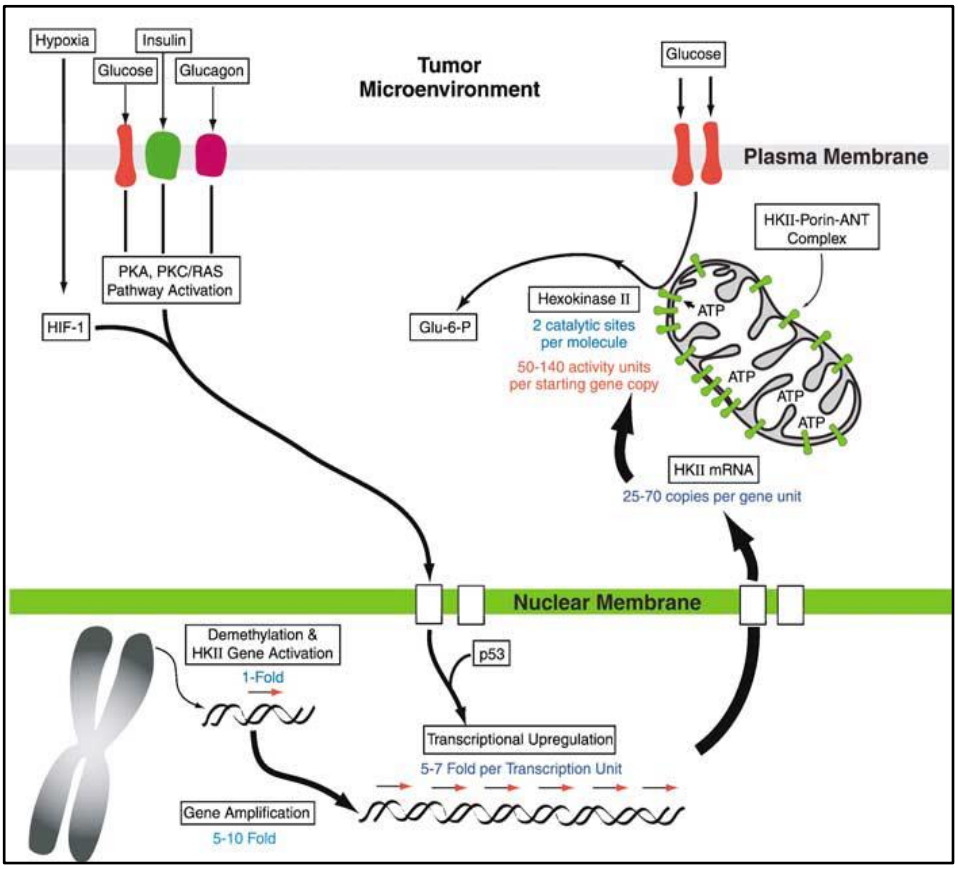

Figure 1:16 HK-2 in tumour promotion. During cancer development, where HK-2 is not present, the first demethylation may bring the gene out of its hibernation and amplify 5-10-fold. Following that amplification, the promoter of the gene, which is activated by HIF-1, p53, glucose, and by both insulin and glucagon, further supports the tumour's requirements by a continuous supply of the gene product (227)

1.7.6 Regulation of HK-2 by AKT/mTOR pathway

The correlation between AKT activity and HK-2 expression is supported by the fact that AKT transcriptionally regulates HK-2 (see figure 1.17) (222). This AKT mediated regulation of HK-2 is further evidenced by the inhibition of PI3K (an upstream kinase of AKT) and mTORC1, which decreases HK-2 expression during the insulin treatment, suggesting AKT /mTORC1 contribution for HK-2 activity (244, 245). Hypoxia-inducible factor 1α (HIF-1α) has also been linked to AKT/mTOR activation and HK-2 expression, and it has been observed that HK-2 promoter has a consensus motif for HIF-1α and therefore HK-2 expression is increased by hypoxia, providing cellular protection as well as a mechanism for increased glycolysis in tumours (246-248).

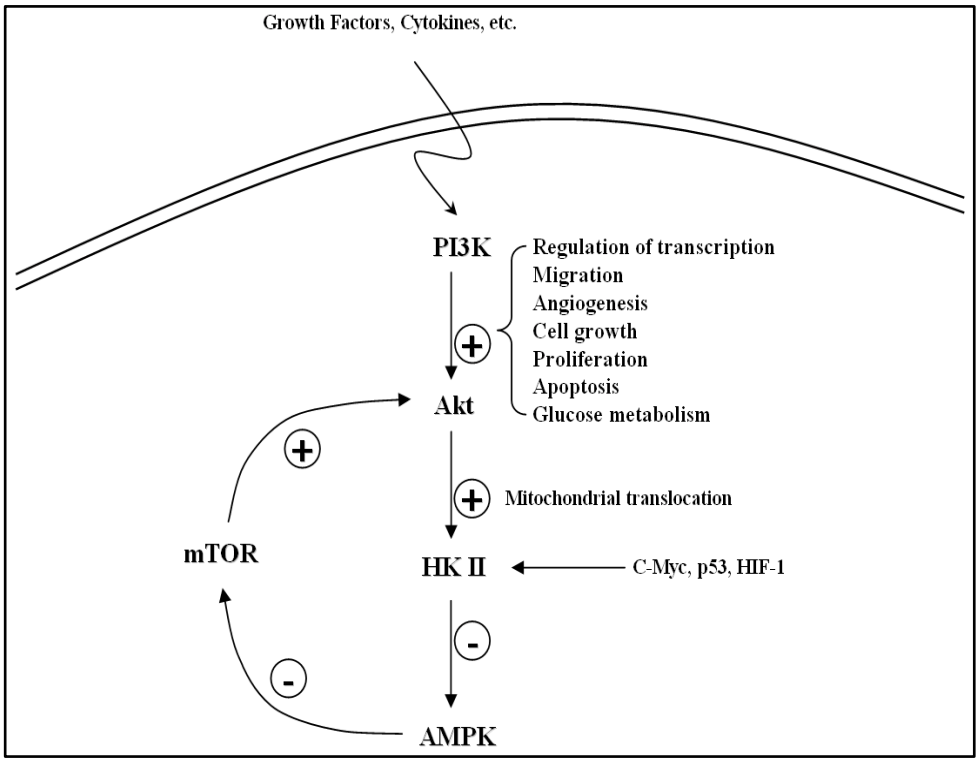

Figure 1:17 HK-2 on PI3K /AKT pathway. Activation of AKT by growth factors and PI3K leads to translocation of HK-2 to the mitochondrial outer membrane. Mitochondrial-bound HK-2 is crucial for energy supply as a form of ATP. Excessive ATP production inactivates AMPK, but AKT is activated through mTOR signalling. (+; Activation, -; Inactivation) (249)

1.7.7 Anti-apoptotic role of HK-2

Signaling by AKT contributes to cell survival in a number of ways. One of these is through promoting mitochondrial translocation of HK-2 so that it interacts with VDAC (227). In glucose metabolism, the translocation of cytosolic HK-2 to the outer membrane of the mitochondria is essential for effective anti-apoptotic activity (249).

AKT is well known to be a potent effector of antiapoptotic stimuli in tumours, which are modulated by two mechanisms; first, increasing the binding affinity of hexokinase-VDAC, which will further enhance the mitochondrial-bound HK fraction and the second one is the mobilisation of the antiapoptotic Bcl2 member Bcl-X_L to VDAC in the outer mitochondrial membrane (250, 251). By increasing the affinity of VDACs with HK-2 and by persistent channelling of adenine nucleotides, the opening of mitochondrial permeability transition pore complex (MPTP) is inhibited, which in turn inhibits access of VDACs to Bax and Bad and retains the cytochrome *c* in the intermembrane space, and in doing so inhibiting apoptosis (227).

1.7.8 HK-2 relative to other hexokinases (1,3,4) in cancers

It has been observed that in contrast to other hexokinase isoforms, HK-2 shows 100-fold amplification in tumorigenesis (227). However, in SCCHN, HK2 is not listed as a differentially expressed gene, nor is it listed as an amplified gene in a recent TCGA analysis (252). The possible reasons for why HK-2 is preferentially increased in tumorigenesis compared to other hexokinases are:

- HK-1 is constitutively expressed in most normal tissues, whereas HK-2 is the principal inducible isoform (226)

- HK-1 has a single catalytic domain in its carboxy-terminus, whereas HK-2 has two active catalytic domains in its amino and carboxy-terminals (223)
- HK-2 promoter's sequence analysis has identified well-defined *cis*-elements for transcription initiation (TATA box and CAAT elements) and *cis*-elements for activation by protein kinase-A (PKA) and protein kinase-C (PKC/RAS) pathways (253, 254). This promoter sequence is absent in HK-1, which explains the predominant expression of HK-2 in cancerous cells that displayed increased glycolytic phenotype (227). The main regulatory activity of HK-2 resides in the narrow segment (-281 to -35 bp) within the proximal region of its promoter (254).
- During tumorigenesis, the tissues that usually express HK-4 often display increased expression of HK-2 and also down-regulation of HK-4 (255). The switch from a lower affinity hexokinase subtype (HK-4) to a higher affinity subtype like HK-2 likely helps the increased energy demand in tumour cells and coincides with the onset of rapid proliferation and a switch to aerobic glycolysis of the tumour cells (222, 254).

In summary, the mitochondrial-bound HK-2 is now recognised as a key player not only for maintaining a high glycolytic rate in cancer, but also it has been shown to be crucial for tumour survival. TIGAR is one of the target genes of p53 and acts as a glycolytic inhibitor in a p53 dependent pathway. In tumorigenesis, loss of p53 function and elevation of TIGAR and HK-2 expression contributes to a pro-survival state of cancer cells.

2. Materials and methods

2.1 List of reagents

2.1.1 Tissue culture reagents

Reagent or product	Manufacturer
Dulbecco's modified Eagle's medium (high glucose) (DMEM)	Sigma-Aldrich
Dulbecco's phosphate-buffered Saline (PBS)	Sigma-Aldrich
Fetal bovine serum (FBS)	Sigma-Aldrich
L-glutamine solution 200mM	Sigma-Aldrich
Penicillin-streptomycin (P0781-100ML)	Sigma-Aldrich
Trypsin-EDTA solution (1×)	Sigma-Aldrich

2.1.2 Reagents used in IHC

Wash buffer (pH 7.6)	Agilent
Antibody diluent	Dako UK Ltd
Hydrogen peroxide block (Abcam kit)	Abcam
Peroxide blocking reagent (Dako kit)	Dako UK Ltd
Protein block (Abcam kit)	Abcam
Rabbit specific HRP conjugate	Abcam
Rabbit LINKER (GV80911-2)	Dako UK Ltd
DAB plus chromogen	Abcam
Mayer's Hematoxylin	VWR Chemicals
Acid alcohol	VWR Chemicals
Ammonia solution	VWR Chemicals
Xylene	VWR Chemicals

Aquatex™ aqueous mountant	Merck Chemicals Ltd, Nottingham, UK

2.1.3 Reagents used in western blot

(Unless otherwise indicated, all solutions were prepared using Milli-Q ≥18MΩcm^{-1} water)

Ammonium persulfate (APS)	Sigma-Aldrich
BSA solution, fatty acid-free (10%)	Sigma-Aldrich
Blotting grade blocker, non-fat dry milk	Bio-Rad
Ethanol, absolute	Sigma-Aldrich
Glycerol	Sigma-Aldrich
Glycine	Thermo Fischer Scientific
Methanol, analytical grade	Thermo Fischer Scientific
Phenylmethylsulfonyl fluoride (PMSF)	Sigma-Aldrich
Ponceau S 0.2% (w/v)	Sigma-AldrichSodium
dodecyl sulphate (SDS)	Thermo Fisher Scientific
Tetramethylethylenediamine (TEMED)	VWR
Tris base	Calbiochem
Tween-20	Sigma-Aldrich

2.1.4 Antibodies for western blotting

Primary antibodies

The following primary antibodies were diluted from stock in 5% blotting grade milk-PBS-Tween solution at the indicated concentrations:

For p53

OP43 – Anti-p53 (Ab-6) (Pantropic) mouse monoclonal antibody (DO-1) **Sigma-Aldrich**

(final concentration of 3 µg/ml)

(*Anti-p53 mouse monoclonal (DO-1) antibody (Calbiochem) was used in the initial experiments*)

For TIGAR

SC – 166290 TIGAR antibody (E-2) mouse monoclonal **Santa Cruz Biotech**

(final concentration of 3 µg/ml)

(T8828 - monoclonal anti-TIGAR antibody (Sigma-Aldrich) and AB10545 - purified rabbit polyclonal (Millipore UK Ltd) were used in the initial experiments)

For Hexokinase-2

Mouse monoclonal HK2 (B-8) **Santa Cruz Biotech**

(final concentration of 3 µg/ml)

For Actin

C-2 mouse monoclonal antibody **Santa Cruz Biotech**

(final concentration of 3 µg/ml)

For Vinculin

A-vinculin (V9131), mouse monoclonal antibody **Sigma-Aldrich**

(final dilution of 1:100 000)

Secondary antibodies

The following secondary antibodies were diluted from stock in 5% (w/v) blotting grade milk-PBS-Tween solution at the indicated concentrations:

RPN4201 – Sheep α-mouse antibody, used at a 1:2500 dilution (supplied by GE Healthcare)

NA934 – Donkey α-rabbit antibody, used at a 1:5000 dilution (supplied by GE Healthcare)

2.1.5 Antibodies for Immunohistochemistry

Primary antibodies

For p53

SC-47698 – p53 (DO-7) mouse monoclonal Antibody Santa Cruz Biotech

For TIGAR

AB10545 - purified rabbit polyclonal – 100 µg Millipore UK Ltd

(We tried monoclonal anti-TIGAR (T8828) antibody from Sigma-Aldrich for the initial optimisation staining)

For Hexokinase-2

NBP2-02272 – Mouse monoclonal HK - 2 antibody Novus Biologicals

(We tried 2867S - Rabbit monoclonal HK-2 (C64G5) antibody (Cell signalling) for the initial optimisation staining)

Secondary antibodies

For Mouse monoclonal – Horseradish peroxidase (HRP) (DAKO)

For Rabbit polyclonal – Rabbit specific HRP conjugate (Abcam)

2.2 Cell culture

2.2.1 Cell Lines

Immortalised cell lines derived from head and neck tumours are an invaluable tool for researchers investigating detailed molecular, biochemical, genetic, and immunological properties of SCCHN (256). Thomas E Carey and his team from the University of Michigan established hundreds of new SCCHN cell lines in the 1980s and subsequently, which were developed from patients with tumours of various sites in the head and neck region (257). We used a selection of these parental cell lines, which are named 'University of Michigan - squamous cell carcinoma (UM-SCC) cell lines, and which were kindly provided by Professor T. Carey (University of Michigan Medical School). Table 2.1 details the parental cell lines used in this study, including the details of SCCHN subsite of origin, type of lesion, and *TP53* status.

Table 2-1 Parental cell lines

CELL LINES	SEX	ANATOMICAL SITE OF ORIGIN	TYPE OF LESION	TNM STAGE	*TP*53 MUTATION	PRIMARY REFERENCE
UM-SCC-1	M	Floor of mouth	Primary	T2N0M0	Mutant: splice site (p53-null)	(256-258)
UM-SCC-5	M	Supraglottis	Primary	T2N1M0	Mutant: V157F	(256, 257, 259)
UM-SCC-10A	M	True vocal cord	Primary	T3N0M0	Mutant: G245C	(257-260)
UM-SCC-11A	M	Supraglottis	Primary	T2N2aM0	Wild-type	(257, 258, 261)
UM-SCC-11B	M	Supraglottis	Primary	T2N2aM0	Mutant: C242S	(256-258, 261)
UM-SCC-17A	F	Supraglottis	Primary	T1N0M0	Wild-type	(256-260)
UM-SCC-17as	F	Supraglottis	Primary	T1N0M0	Wild-type	(256, 257, 259, 260)
UM-SCC-81B	M	Tonsil	Metachronous primary	T2N0M0	Mutant: H193R	(256, 257, 259, 261, 262)

The secondary cell lines used were derived from UM-SCC-1 and UM-SCC-17A, obtained through collaboration with Professor J. Myers (University of Texas, MD Anderson Cancer Center, TX, USA). UM-SCC-1 cell lines were transduced with various *TP*53 mutations (R282W, C176F, R175H), wild-type *TP*53, and an empty vector to act as a reference (pBABE). UM-SCC-17A cells stably expressing short-hairpin RNA (shRNA) specific for p53 (shp53) from a lentiviral construct or empty vector control (lenti) were also obtained from Professor Myers.

Table 2.2 shows the secondary cell lines and their p53 status.

Table 2-2 Secondary cell lines

Secondary cell lines	p53 status
UM-SCC-1- pBABE	(p53-null) transduced with empty vector control (LOF)
UM-SCC-1-wtp53	p53 null parental cell line transduced with wild-type p53 (transduced with lentivirus expressing p53)
UM-SCC-1-R175H	mutant p53 (DNA, GOF)
UM-SCC-1-R282W	mutant p53 (DNA, GOF)
UM-SCC-1-C176F	mutant p53 (DNA, GOF)
UM-SCC-17A shp53	p53 wild-type parental line expressing a short hairpin RNA for p53 (shp53) such that p53 expression is reduced (knocked-down)
UM-SCC-17A lenti	wild-type p53 containing the same lentiviral backbone vector used to generate UM-SCC-17A shp53

(LOF=Loss Of Function; DNA=Dominant-Negative Activity; GOF=Gain Of Function)

All the cell lines were HPV negative.

2.2.2 Cell medium and growth environment

Cell lines were grown in Nunc^{TM} cell culture treated flasks (size – T75) with filter caps (Thermo Fisher Scientific) in a humidified cell incubator at 37^{o} C in an atmosphere containing 5% CO_2. All cell lines were maintained in Dulbecco's Modified Eagle's Medium (cDMEM) containing 10% (v/v) FBS, 1% (v/v) penicillin/streptomycin, 1% (w/v) L-glutamine, and non-essential amino acids (100X). The identity of all the cell lines was established using STR profiling performed as a service by staff in the Department of Molecular and Clinical Cancer Medicine. All the cell cultures were free of *Mycoplasma* species as determined by PCR, again provided as a service by staff in the Department and were maintained for no longer than 12 weeks after recovery from liquid nitrogen storage.

2.2.3 Cell subculture technique

Standard microbiological aseptic technique was performed at all times in order to avoid contamination, and tissue culture work was carried out in a class Ⅱ laminar flow tissue culture cabinet. All the cell lines grew as adherent monolayers on cell culture treated surfaces. If the cells reach maximum confluence in culture, then death can result from overcrowding and the related stress, so regular sub-culture or passage of cells was performed to ensure that the cells were maintained at sub-confluent densities.

When the cells reach 70-90% confluence, cells were passaged as follows;

1. Prior to passaging the cells, first, switch on the UV light in the class Ⅱ laminar flow tissue culture cabinet for 15 minutes. After the UV light has been turned off, remove the night door and clean the internal hood surfaces with ethanol

2. Aspirate the media from the T75 tissue culture flask, and the cell monolayer was washed once in 10 ml of PBS
3. Aspirate the PBS and add 3-5 ml of trypsin-EDTA to the monolayer and return the T75 flask to the cell incubator at 37ºC
4. Trypsinisation time varies depending on the cell lines but is typically between 5 to 15 minutes
5. The flask was agitated in order to facilitate the detachment of cells, which was regularly assessed by examination under a phase-contrast microscope
6. After adequate detachment of cells, the trypsin-EDTA was neutralised by the addition of an excess of complete media, (i.e. media containing FBS), the precise volume of which was dependent on the ratio of the cell split, which, in turn, was dependent on the growth characteristics of the individual cell line. Relatively slow-growing cell lines were typically split 1:10, and more quickly proliferating cell lines were typically split 1:20
7. The re-suspended cells with the media were aspirated, leaving the required volume of the trypsinized cells in the flask
8. Add 24 ml of fresh media to typically make 25 ml for a T75 flask and place it in the incubator

2.2.4 Storage of cells in Liquid Nitrogen (cryopreservation) and recovery

Cells were harvested by trypsinisation as described above (section 2.2.3) and pelleted by centrifugation at 300 x *g* for five minutes at 4ºC. The resulting supernatant was aspirated, and the remaining cell pellet was resuspended in 1-2 ml of freezing media (10% (v/v) DMSO in FBS) and then transferred to Nunk™ cryovials (Thermo Fisher Scientific). For gradual freezing of cells, the cryovials were placed in a pre-cooled

Styrofoam rack and stored at -80^{o}C, and after approximately 24-48 hours, the cryovials were transferred to liquid nitrogen for long-term storage.

In order to recover the cells from stocks stored in liquid nitrogen, cryovials were thawed expediently in a 37^{o}C water bath. The DMSO in the freezing media is toxic to cells at concentrations above 0.5%, and the cells were resuspended in a tissue flask containing at least 25 ml of fresh media that was pre-warmed to 37^{o}C. Once the cells had adhered to the surface of the flask, typically the following day, the media was changed.

2.3 Western blotting

2.3.1 Selection of cell lines

We used the University of Michigan - squamous cell carcinoma (UM-SCC) cell lines to evaluate the expression of p53, TIGAR and HK-2. The parental and the secondary cell lines which we used for the study were all HPV negative and have been discussed in section 2.2.1. The advantage of these cell lines is that some are isogenic, differing only in the expression of wild type p53, mutant p53 or being null or expressing low levels of down-regulated (knocked-down) wild-type p53, so that we can compare within the same genetic background, the effect of p53 status on cellular processes including levels of gene expression.

For the main experiment, we used two groups of cell lines; group 1 contained UM SCC 1 as the parental cell line and its secondary cell lines, and group 2 contained UM SCC 17A as the parental cell line and its secondary cell lines. Since we had only three cell lines in the second group, we added UM SCC 11 A and B to the second group. In this way, we could analyse six cell lines in each group.

Table 2.3 shows the two groups of cell lines that we used in our analysis.

Table 2-3 Cell lines analysed*

Group 1	**Group 2**	
Parental cell line – UM SCC 1	**Parental cell line – UM SCC 17A**	**Additional cell lines**
UM SCC - 1	UM SCC – 17A	UM SCC – 11A
UM SCC - 1 pBABE	UM SCC – 17A lenti	UM SCC – 11B
UM SCC - 1 WTp53	UM SCC – 17A shp53	
UM SCC – 1 R175H		
UM SCC – 1 C176F		
UM SCC – 1 R282W		

***Note that all of these cell lines are HPV negative**

Based on the approximate molecular weight of our proteins of interests (**p53** – actual mass is approximately 43.7 kDa but runs as an approximately 50 kDa molecule on SDS-PAGE, **TIGAR** – 30 kDa, and **HK-2** – 100 kDa), we selected two housekeeping proteins actin (42 kDa), and vinculin (124 kDa) to act as loading references. Accordingly, actin was chosen as a housekeeping protein to provide a loading reference for HK-2 and vinculin was similarly used for p53 and TIGAR.

We repeated each experiment three times, calibrated the densitometer readings, and took the mean value.

2.3.2 Principles of western blotting

Western blotting is one of the most important routine analytical techniques in cell and molecular biology, enabling researchers to identify specific proteins from a complex mixture of proteins extracted from cells and to determine the relative abundance of these between different samples in a semi-quantitative manner (263). There are three major elements in the western blot technique: (1) separation of the proteins by size, (2) transfer to a solid support, and (3) detection of specific target proteins using antibodies. Typically a primary antibody is used to detect a specific protein species, and then the signal is generated by using a secondary antibody that

recognises the species of the primary antibody (e.g. a rabbit antibody that recognises the primary murine IgG) employing some sort of detection chemistry [enhanced chemiluminescence] or physics [IR or fluorescent conjugate], to permit visualization (263).

Electrophoresis is used to separate proteins according to their electrophoretic mobility, and the commonly used gel electrophoresis is SDS-PAGE (Sodium dodecyl sulphate polyacrylamide gel electrophoresis) which separate proteins on the basis of their shape and size (264). The separated proteins are transferred from the gel to a membrane, typically nitrocellulose, and proteins bind to the membrane based on hydrophobic interaction (264). The membrane is then incubated with a blocking agent to suppress non-specific protein interactions of the antibodies, and then incubated with specific antibodies, and the antigen-antibody complexes that form on the blot in the region containing the protein can be visualised in a variety of ways, including electrochemiluminescence or colorimetric, radioactive or fluorescent detection (263).

2.3.3 Western blotting reagents

SLIP (Stuart Linn Immunoprecipitation) buffer:

50mM HEPES (pH 7.5)

Glycerol 10% (v/v)

Triton X-100

150mM NaCl

0.5mg/ml BSA

PBS / tween:

65mM $Na_2HPO_4 \cdot 2H_2O$

15mM $NaH_2PO_4 \cdot 2H_2O$

75mM NaCl

0.1% (v/v) Tween-20

Tris-glycine electrophoresis running buffer:

25mM Tris. HCl

250mM glycine 0.1% (w/v) SDS

Tris-glycine transfer buffer:

25mM Tris

192mM glycine

20% (v/v) methanol

4x protein sample loading buffer:

250mM Tris (pH 6.8)

8% (w/v) SDS

40% (v/v) glycerol

4mg/ml bromophenol blue

1% (v/v) β-mercaptoethanol

Diluted with water from a MilliQ system (>18MΩ (or mega ohm) resistance water) to make 2x and 1x sample buffer.

Ponceau S solution:

0.2% (w/v) Ponceau S

5% (v/v) acetic acid

2.3.4 Bradford assay

Proteins for analysis were extracted from the cells which were harvested by trypsinisation and pelleted by centrifugation at 300 x *g* for five minutes at 4ºC as described in section 2.2.3. The cell pellets were washed with 1ml of PBS, and the solution then transferred to Eppendorf 1.5ml microcentrifuge tubes. The cells were again pelleted by centrifugation, and the supernatant aspirated as before. The pellets were then stored at -80°C before further processing. On the day of sample processing, cell pellets were lysed by resuspension in lysis buffer (lysis buffer = SLIP buffer supplemented with the following protease inhibitors; aprotinin (2µg/ml), leupeptin (0.5µg/ml), pepstatin A (1µg/ml), a trypsin inhibitor from soybean (100µg/ml) and PMSF (1mM in 100% ethanol)). Samples were then incubated on ice for 10 minutes and then centrifuged for 10 minutes at 13,000 x *g* at 4°C. The supernatant from this centrifugation was transferred to a clean microcentrifuge tube. In the meantime, protein standards were prepared for the Bradford assay. Firstly, a solution of 20mg/ml BSA in lysis buffer was prepared and a serial dilution performed to produce six further standards of the following BSA concentrations: 10mg/ml, 5mg/ml, 2.5mg/ml, 1.25mg/ml, 0.625mg/ml, and 0.3125mg/ml.

2µl of each of the standards was then added to 1ml of Bradford protein assay dye reagent (diluted 1:5 with H2O) and vortexed for 10 seconds. 2µl of the SLIP buffer was also added to 1 ml of protein assay dye reagent and assigned as the blank. A standard curve was prepared on a BioPhotometer (Eppendorf AG, Hamburg, Germany) using the Bradford program, which measures absorbance at 595nm.

A coefficient of the variable of less than 5% was deemed an acceptable level for calibration. Following generation of the standard curve, 2µl of each of the protein

samples was added to 1ml of protein assay dye reagent in microcentrifuge tubes, and the protein concentrations determined based on the prepared standard curve using the BioPhotometer. Samples were then adjusted such that 50µg of total protein was made up in the sample loading buffer using indicated volumes of 1X, 2X and 4X (final concentration of the buffer 1X) to a total volume of 20µl. These samples were then stored at -80°C before gel electrophoresis.

2.3.5 SDS-Polyacrylamide gel electrophoresis

An SDS polyacrylamide gel was used to separate proteins according to their approximate mass by gel electrophoresis. The acrylamide percentage used in the separating gel was adjusted depending upon the size of proteins to be resolved. The higher the percentage of acrylamide, the smaller the pore size of the gel matrix. Therefore a higher percentage of gels are suited for low molecular weight proteins, and a low percentage of gel is useful for larger proteins. The separating gels are prepared as detailed in table 2.4.

Table 2-4 Preparation of different percentage of separating gel

	6 %	**7.5 %**	**10 %**	**12 %**	**15 %**
H_2O	5.8 ml	5.42 ml	4.8 ml	4.3 ml	3.55 ml
Acrylamide mix 40% (v/v)	1.5 ml	1.87 ml	2.5 ml	3 ml	3.75 ml
1.5 M Tris (pH 8.8)	2.5 ml	2.5 ml	2.5 ml	2.5 ml	2.5 ml
SDS 10 % (w/v)	100 µl	100 µl	100 µl	100 µl	100 µl
TEMED	8 µl	8 µl	8 µl	8 µl	8 µl
APS 10 % (w/v)	100 µl	100 µl	100 µl	100 µl	100 µl

To make 0.75 mm thick gels, glass slides were assembled, the separating gel poured into the gap, overlaid with H_20, and allowed to polymerise. After the gel had set (typically after one hour), the water on the top of the gel was poured off, and the

stacking gel was added. The preparation of the stacking gel is described in Table 2.5.

Table 2-5 Preparation of stacking gel

H_2O	7.225 ml
acrylamide mix 40% (v/v/)	1.275 ml
1 M Tris (pH 6.8)	1.25 ml
SDS 10 % (w/v)	100 µl
TEMED	10 µl
APS 10 % (w/v)	100 µl

After adding the stacking gel, a 10-well comb was inserted, and the gel left to polymerise (typically for at least 20 minutes). The comb was removed after the polymerisation, and the gel assemblies were placed in an electrophoresis tank filled with Tris-glycine electrophoresis running buffer.

The protein samples, which were already prepared, were retrieved from the -80°C freezer and were denatured by heating in a heat block at 100°C for five minutes, vortexed, and centrifuged at 13,000 x *g* at 4°C for two minutes. 20µl of each sample (containing 50 µg of total protein) was then loaded into the designated wells of the gel, alongside a blue broad-range prestained protein marker (Bio-Rad). SDS-polyacrylamide gel electrophoresis (PAGE) was performed using a two-gel Mini-PROTEAN^R Tetra cell (Bio-Rad) at 200V for one hour.

Note that for the later experiments, we used precast gels (10% mini-protean TGX precast protein gels, 10-well) from Bio-Rad.

2.3.6 Protein detection

After the gel electrophoresis, proteins were transferred onto a Hybond ECL nitrocellulose membrane (GE Healthcare) using a Mini Trans-Blot^R Electrophoretic

Transfer Cell (Bio-Rad). To create a transfer sandwich, the Hybond ECL nitrocellulose membrane was first pre-soaked together with two pieces of Whatman^{R} chromatography paper (Sigma-Aldrich) and two sponges in the transfer buffer and then the electrophoresis apparatus was dismantled. The gel was removed from between the glass plates, the stacking gel discarded, and the separating gel placed in between the nitrocellulose membrane and chromatography paper. Another piece of chromatography paper was placed on the opposing side of the nitrocellulose membrane, and two sponges were added onto the outside to complete the assembly. This was then placed in a transfer cassette, which was then placed in a tank in such a way that the membrane faced the positive electrode while the gel faced the negative electrode, thereby enabling the negatively charged proteins on the gel to migrate in the direction of the nitrocellulose membrane towards the cathode. The tank was filled with a transfer buffer and an ice pack to ensure cooling during transfer. The transfer was performed at 100 V for one hour using a two-gel Mini-PROTEAN^{R} Tetra cell.

For the last set of western blot experiments, we used the Trans-Blot Turbo transfer system (Bio-Rad) for protein detection. After the gel electrophoresis, the running apparatus was dismantled. Filter papers and the membrane used were provided in the Trans-Blot Turbo RTA Transfer kit (Bio-Rad). First filter papers were soaked in a transfer buffer and placed on the bottom tray of the transfer cassette. The nitrocellulose membrane was placed over the filter papers, and the gel was laid on top of the membrane. Five layers of filter papers were placed on top of the membrane, and the top of the transfer cassette was closed and locked securely. The apparatus was run for 13 minutes to permit the transfer of proteins. Subsequently, the transfer apparatus was dismantled, and the membrane stained briefly with Ponceau S and rinsed with H_2O to ensure the transfer of proteins had been successful. At this

point, the membrane was cut horizontally into strips based on the size of proteins to be probed. Figure 2.1 illustrates the protein ladder set with the molecular weight markers ranging from 10 – 250 kDa and one of the nitrocellulose membranes from our experiments which shows the visible protein ladder.

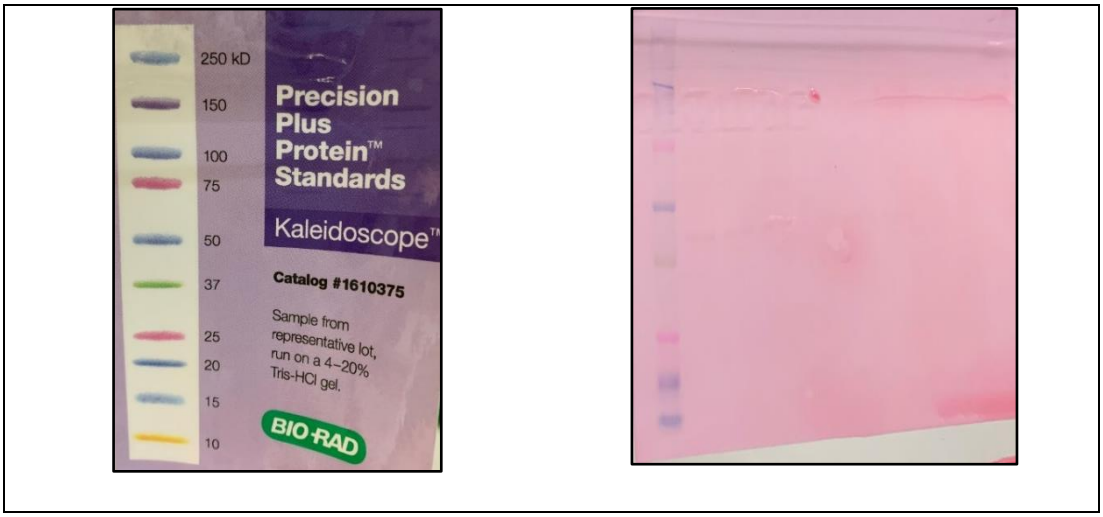

Figure 2:1 Left; Protein ladder from Bio-Rad, **Right;** Nitrocellulose membrane before cutting into strips based on the molecular weight of the proteins

Figure 2.2 shows the representation of cutting the membrane for p53, TIGAR, and HK-2 based on molecular weight.

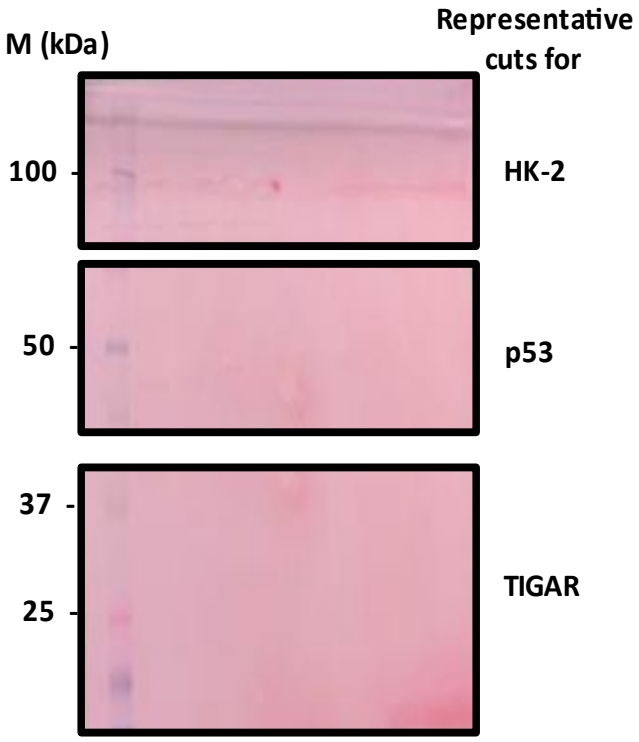

Figure 2:2 Process of cutting the Nitrocellulose membrane. Guiding molecular weight markers from the protein ladder are shown on the left, and this figure illustrates the process of cutting the membrane based on molecular weight for p53, TIGAR and HK-2

The membrane was then washed briefly in PBS/Tween to remove the Ponceau S stain and then cut into strips which were blocked in 5% (w/v) non-fat dry milk in PBS/Tween solution for 1 hour (to prevent non-specific binding of antibodies to the membrane). During blocking, the membranes were agitated on a shaker at room temperature. After one hour, the blocking milk was removed, and appropriate primary antibodies (section 2.1.4) were added and left on a shaker at 4°C overnight.

The following day, the membranes were then washed for 15 minutes in PBS/Tween three times, after which horseradish peroxidase (HRP)-conjugated secondary antibodies, raised to the relevant species (section 2.1.4) were applied and the membranes incubated for a further hour at room temperature. Next, the membranes were washed three times as previously before being transferred into dry trays.

Amersham ECL Prime detection reagent (GE Healthcare Life Sciences) was then applied (typically 1-2 ml per membrane) for five minutes, and the signal detected by chemiluminescence and recorded on a Kodak IM4000 image station using Carestream molecular imaging software (Carestream Health UK, Hemel Hempstead, UK). Further image processing was performed using CorelDRAW graphics suite X7. For the last set of experiments, we used a ChemiDoc^{TM} MP imaging system (Bio-Rad, Maxted Road, Hemel Hempstead, UK).

2.3.7 Densitometer analysis and data normalisation

Densitometer analysis was done with 'Image Lab' software from Bio-Rad (265). First, we selected the 16-bit raw image of the target protein and, with the help of the 'analysis tool', marked the individual lanes. Depending on the bandwidth, we resized the lanes individually and then detected the bands manually. The selected lanes were checked with the 'lane profile' tool, and with the help of the 'subtraction tool', we selected the maximum subtraction. The final analysis gave the adjusted volume with the required background subtraction.

Data normalisation is essential to accurately compare target protein expression across multiple samples in western blot analysis (266). To normalise the expression of the target protein, the intensity of the loading control protein of the first lane was divided by the corresponding loading control protein, then multiplied by the intensity of the target protein.

2.4 Immunohistochemistry (IHC)

2.4.1 Principles of IHC

Immunohistochemistry (IHC) is based on the detection of antigens in tissue sections by means of specific antibodies, and one of the main advantages of IHC over other

protein detection methods is the ability to correlate the presence of an antigen with its location in a tissue or cell (267). As its name indicates, IHC connects three important disciplines: immunology, histology, and chemistry (267).

The basic steps in IHC are fixation, antigen retrieval, blocking and antibody labelling and visualisation (268). Several methods exist to enable the visualisation of antigen-antibody interaction, and the most commonly used method employs a secondary antibody conjugated to an enzyme, such as peroxidase, that can catalyse a chromogenic reaction, but alternatives include conjugating the secondary antibody to a fluorophore, which might, for example, be fluorescein or rhodamine (269).

2.4.2 Selection of tissue microarrays (TMA)

We aimed to analyse the expression of p53, TIGAR and HK-2 in head and neck cancer samples by immunohistochemistry (IHC), taking advantage of previously constructed TMAs. We had access to two TMA sets potentially, both created at the University of Liverpool by members of the Mersey Head and Neck Oncology Research Group (MHNORG). One was created by Mr Paul Goodyar whilst a student registered in the research group. However, whilst this TMA had patient samples from the larynx, hypopharynx, and oropharynx tumours, there were no available sections that could be cut from the TMA block, and it was decided to make a new TMAs using new cores obtained from the same patient samples (this would become TMA set 2). Due to technical difficulties, there was a delay in constructing the new TMA, and so in the meantime, Dr Janet Risk (Senior Lecturer, Department of Molecular and Clinical Cancer Medicine, University of Liverpool) kindly provided access to another TMA with a different set of samples from head and neck cancer patients treated at University Hospital Aintree (TMA set 1). One of our proteins of interest is TIGAR, encoded by a relatively recently discovered p53 regulated gene. Since there

were no previous research papers related to IHC expression of TIGAR in SCCHN and sections of the TMA were limiting, we decided to analyse only p53, and TIGAR in TMA set 1. Later as the newly re-constructed TMA became available, we were able to prove that with p53, TIGAR and HK-2 antibodies (TMA set 2).

2.4.2.1 TMA set 1

TMA set 1 included samples from 102 patients who were treated at the University Hospital Aintree between June 2003 and June 2010. The results of the first study utilising this TMA were published by J Dhanda et al., who analysed the expression of SERPINE1 and SMA to determine whether this could predict extracapsular spread (ECS) in oral squamous cell carcinoma (270).

Ethical approval covering the generation and research use of the TMA was previously obtained (South Sefton EC 47.01 and REC No 10/H1002/53), and the inclusion criteria for selection were cases with a new histologically confirmed diagnosis of oral squamous cell carcinoma and treatment with primary surgery. All patients provided both snap-frozen and formalin-fixed paraffin-embedded (FFPE) samples. The following clinical parameters were available with the TMA data; anatomical sites, T stage, N stage, ECS (extracapsular spread), differentiation, and survival status. Out of 102, 95 patients were tested for HPV to clarify the underlying molecular aetiology of the tumour. Four cases were confirmed as HPV positive via RNA qPCR, the so-called “gold standard” test (271), and one of the cases was potentially overlapping the oropharynx (270). Unfortunately, we could not retrieve further information on the HPV results, and we were not able to trace the four HPV positive cases among the 95 samples.

TMA set 1 had three slides (A, B, and C), and they were constructed [source - Dhanda et al. (270)] using the cores selected from FFPE blocks of primary tumour samples, using a manual tissue arrayer (MTA-1, Beecher Instruments, Sun Prairie, WI, USA). An oral and maxillofacial pathologist identified the areas of the primary tumour and adjacent tumour-free mucosa and marked these areas on archival haematoxylin and eosin-stained (H&E) sections. Cores were cut from FFPE blocks in triplicate, to a 4-mm depth, from the pathologist-marked areas and transferred to a recipient array block using a randomised distribution, with each replicate located on a different array block.

For practical reasons, 0.6 mm diameter cores were obtained from the tumour centre and tumour-free mucosa. H&E sections of the TMAs were examined to confirm the accuracy of the tissue sampling (criteria for scoring the triplicate cores will be discussed in 2.4.5). Because the triplicate cores were distributed randomly in three blocks, there were three slides per TMA set. Table 2.6 provides a summary of the frequency distribution of cases in TMA set 1.

Table 2-6 Summary of TMA set-1

Total patients recruited	102
Sample missing (core from slide)	1
Total samples used for analysis	101
Anatomical sites	Oral cavity (tongue, floor of the mouth, alveolus, buccal mucosa, retromolar area, palate) (n=93 patients) and oropharynx (n=8 patients)
Number of TMA slides	3 slides TMA (A), TMA (B), TMA (C)
Proteins analysed	p53 and TIGAR

An overview of the TMA slides, which includes samples from TMA set 1, are shown in figures 2.3 and 2.4.

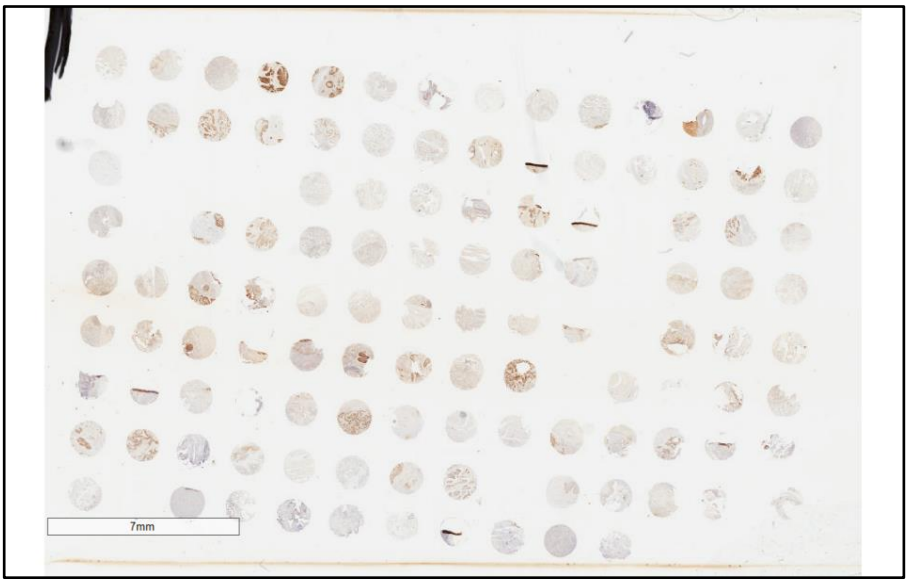

Figure 2:3 Immunohistochemical analysis of p53 expression in TMA set 1. A tissue microarray was stained using a mouse monoclonal antibody (DO-7) as described in section 2.4.3. This figure illustrates an overall distribution of the cores and also demonstrates variable staining of cores. Magnification is indicated by the scale bar in the figure.

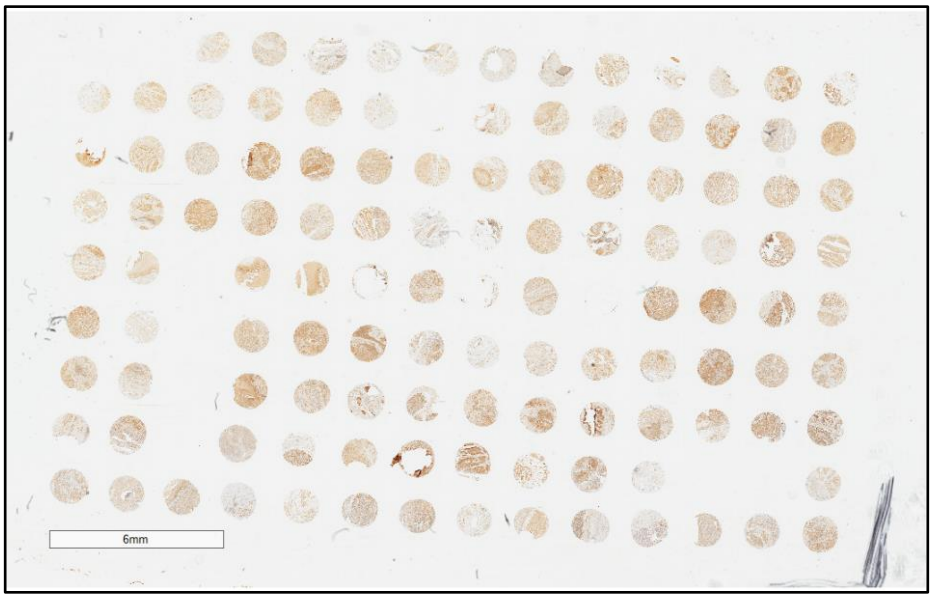

Figure 2:4 Immunohistochemical analysis of TIGAR expression TMA set 1. A tissue microarray (TMA) was stained using a rabbit polyclonal anti-TIGAR antibody (AB10545), as described in section 2.4.3. This figure illustrates an overall distribution of the cores and also demonstrates variable staining of cores. Magnification is indicated by the scale bar in the figure.

2.4.2.2 TMA set 2

The newly constructed TMA-2 had 163 patients' samples of primary squamous cell carcinoma of the head and neck (SCCHN) from the larynx (n=77), hypopharynx (n=22), and oropharynx (n=64). The TMA was constructed by the LBIH Biobank, University of Liverpool. The TMA set -2 was constructed using cores selected from formalin-fixed, paraffin-embedded (FFPE) blocks of primary tumours and from involved lymph nodes using a manual tissue-arrayer (MTA-1, Beecher Instruments). An oral and maxillofacial pathologist identified the areas of the primary tumour centre and invasive front of the tumour and adjacent tumour-free mucosa and marked these areas on archival haematoxylin and eosin-stained (H&E) sections. Cores were cut from FFPE blocks in triplicate, to a 4-mm depth, from the pathologist-marked areas and transferred to a recipient array block using a randomised distribution, with each replicate located on a different array block. For practical reasons, 0.6 mm diameter cores were obtained from the tumour centre and tumour-free mucosa whereas, 1 mm diameter cores were obtained from the invasive front of the tumour. H&E sections of the TMAs were examined to confirm the accuracy of the tissue sampling (criteria for scoring the triplicate cores will be discussed in 2.4.5).

The pathological details of the tumour and the clinical data were provided by the LBIH Biobank (they were originally collected by searching the archive of the pathology reports of University Hospital Aintree, Liverpool, from 1998 to 2008). Ethical approval was obtained by the previous researchers (Ref:07/MRE08/47/South Sefton Research Ethics Committee, EC.47.01-6; North West 5 Research Ethics Committee, EC.09.H1010.5).

As part of this process, it became clear that a considerable amount of work would be required to manage and curate the TMA data set, and I was involved mainly in

managing and reviewing the clinical data. I matched the old TMA location number with the new TMA location number for each individual patient sample so that accurate clinical details for each patient could be obtained. I was also involved in obtaining the data for the HPV status for the oropharynx patients and generated a revised and curated main data spreadsheet.

The old TMA was described by Upile et al., who analysed two hundred eighty-one cases of SCCHN using the HPV diagnostic testing algorithm and observed an incidence of 4% of HPV-driven cases across the subsites outside the oropharynx compared to 70% incidence in tumours of the oropharynx (272). Their numbers were high due to the inclusion of oral cavity cases, whereas our samples contain only the larynx, hypopharynx, and oropharynx.

Table 2-7 Frequency distribution of samples in TMA set 2

	Larynx	Hypopharynx	Oropharynx
Total patients (primaries)	77	22	64
Missing primary samples	0	0	2
Final primary samples	**77**	**22**	**62**
Lymph nodes	*19*	*12*	*29*

The new TMA had triplicate cores from adjacent normal mucosa, advancing front of the tumour and from the tumour cores. It also had triplicate cores from the neck lymph nodes in the case of patients with nodal metastasis. Table 2.7 summarises the overall number of cases in TMA set 2. The total number of patients in the larynx groups was 77. There were 21 lymph node samples from the larynx (2 nodal samples did not have primary tumour samples, so a total of 19). The total number of patients in the hypopharynx groups were 22. There were 13 lymph node samples from the hypopharynx (1 nodal sample did not have a primary tumour sample, so a total of 12). In the oropharynx group, there were 64 patients, but two patient samples were

missing in the block, so the total patient samples available were 62. We had 34 lymph node samples from the oropharynx (5 nodal samples did not have primary tumour samples, so a total of 29).

Since we had low numbers of hypopharynx samples, we combined larynx (77) and hypopharynx (22) together for statistical analysis. We analysed the oropharyngeal samples separately as the pathogenesis and clinical outcomes of oropharyngeal cancers are different from other head and neck cancers due to the involvement of HPV (discussed in section 1.2). The revised patient's cohort is summarised in Table 2.8.

Table 2-8 Revised frequency distribution of TMA set 2

	Larynx & hypopharynx	**Oropharynx**	**HPV status in the oropharynx (HPV status is missing -2)**	
			HPV +ve	HPV -ve
Primaries	99	62	45	15
Lymph nodes	31	29		

Two patients from the larynx and one patient from the hypopharynx group were HPV positive, and they were not included in statistical analysis. The oropharyngeal cases were previously analysed by Upile et al. for HPV involvement by doing p16 immunohistochemistry and high-risk HPV in situ hybridization. Samples that had positive results for both p16 IHC and HR-HPV ISH were assigned as HPV positive. If only HR-HPV ISH positive, they were scored as negative as chromogenic in situ hybridization (CISH) only highlights the presence of the HPV DNA but not viral transcription. If they were only p16 positive but CISH negative, then they were further tested for HPV 16 E6 DNA using qPCR (272).

Examples of the TMA set 2 slides were shown in figures 2.5 to 2.8. *(for the illustration purposes, the slides with TIGAR staining are shown as examples)*

Figure 2:5 Immunohistochemical analysis of TIGAR expression in larynx samples of TMA set 2. A tissue microarray (TMA) was stained using a rabbit polyclonal (AB10545) as described in section 2.4.3. This figure illustrates an overall distribution of the cores and also demonstrates variable staining of cores. Magnification is indicated by the scale bar in the figure.

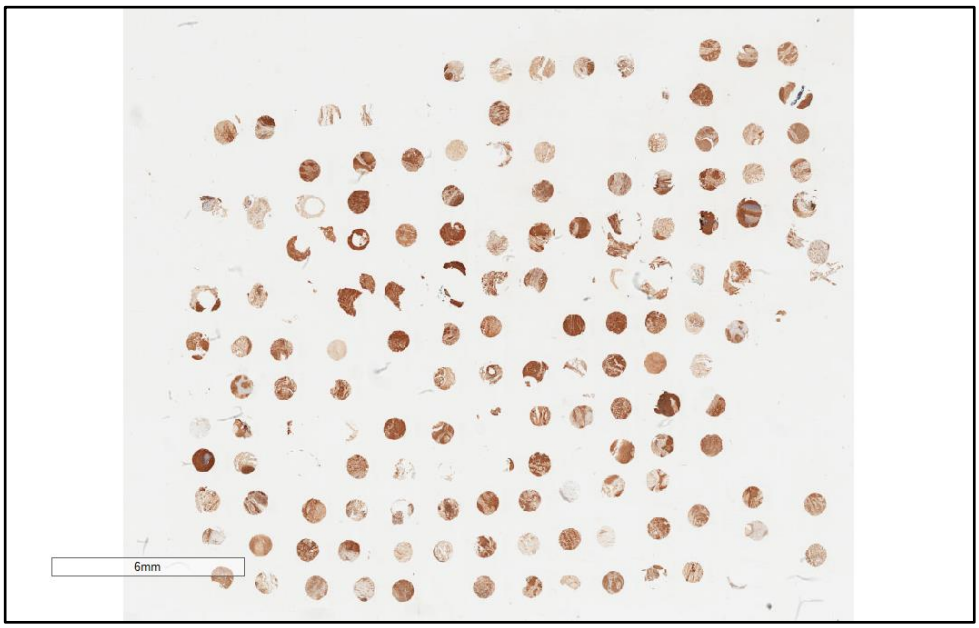

Figure 2:6 Immunohistochemical analysis of TIGAR expression in hypopharynx samples of TMA set 2. A tissue microarray (TMA) was stained using a rabbit polyclonal (AB10545) as described in section 2.4.3. This figure illustrates an overall distribution of the cores and also demonstrates variable staining of cores. Magnification is indicated by the scale bar in the figure.

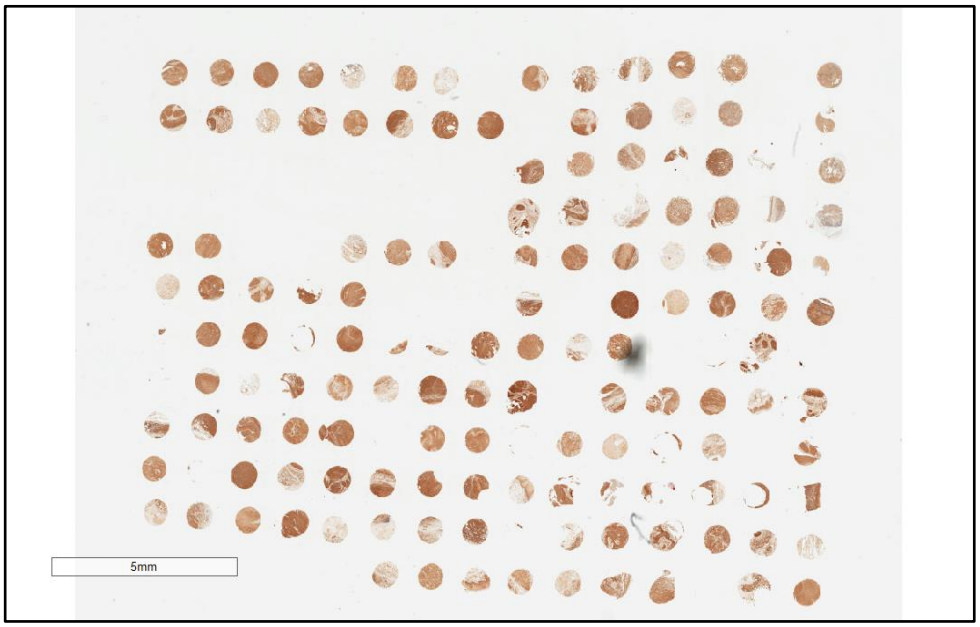

Figure 2:7 Immunohistochemical analysis of TIGAR expression in oropharynx samples of TMA set 2. A tissue microarray (TMA) was stained using a rabbit polyclonal (AB10545) as described in section 2.4.3. This figure illustrates an overall distribution of the cores and also demonstrates variable staining of cores. Magnification is indicated by the scale bar in the figure.

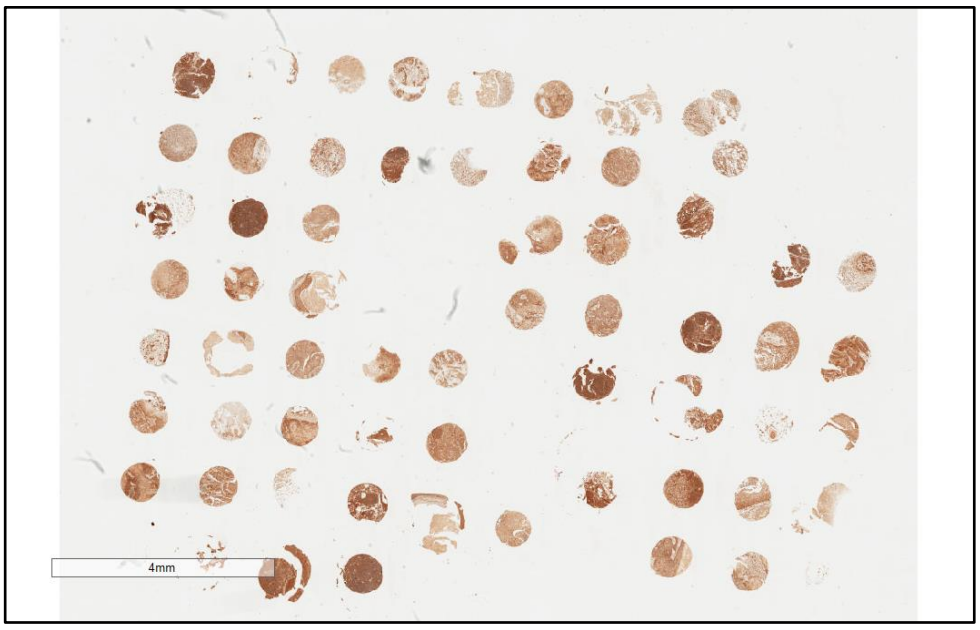

Figure 2:8 Immunohistochemical analysis of TIGAR expression in larynx lymph node samples of TMA set 2. A tissue microarray (TMA) was stained using a rabbit polyclonal (AB10545) as described in section 2.4.3. This figure illustrates an overall distribution of the cores and also demonstrates variable staining of cores. Magnification is indicated by the scale bar in the figure.

2.4.3 Immunohistochemical staining

2.4.3.1 Antigen retrieval

Antigen retrieval enables an antibody to access the epitope in the target protein within the tissue, and it can be done either by using enzymes to digest tissue components or by using heat treatment. We used a heat-induced epitope retrieval process on a PT-link machine (Dako UK Ltd, Cambridgeshire, UK). After preheating to 65^{o}C , the slides were incubated in a high-pH (pH 7.6) bath containing EnVision^{TM} FLEX target retrieval solution (Tris/EDTA buffer pH 9.0) (Agilent) at 96^{o}C for 20 minutes. The PT-link machine performs the deparaffinisation, rehydration and antigen retrieval steps as a single process.

2.4.3.2 Blocking

Blocking reduces the background signal in staining and false-positive scoring. For blocking and further staining procedures, we used two different kits according to the nature of the primary antibody. For mouse monoclonal antibody (p53 and HK-2), we used DAKO EnVisionTM FLEX/HRP detection system (Dako UK Ltd), and for rabbit polyclonal antibody (TIGAR), we used "Expose Rabbit specific HRP/DAB detection IHC kit" (Abcam) (273).

For TIGAR staining, the TMA slides were taken out from the PT-link machine and left for cooling before being washed with a FLEX wash buffer. The slides were first blocked with hydrogen peroxide to eliminate the endogenous peroxidase activity for 10 minutes, and then they were washed two times with a wash buffer. The protein block then applied and incubated for 10 minutes at room temperature to block nonspecific background staining. For p53 and HK-2 staining, after removal from the

PT-link machine, the slides were blocked with an EnVisionTM FLEX peroxidase block for 5 minutes.

2.4.3.3 Optimisation and selecting primary antibodies

Antibody optimization is essential as the quality of staining is influenced by the primary antibody concentration, the diluent used, the incubation time and temperature. Optimisation with different antibody concentrations was done for all three antibodies. As there were no reference articles for TIGAR staining in SCCHN, we performed initial optimisation experiments with samples of SCCHN tumours to evaluate TIGAR expression, including tonsils, tongue, soft palate, oropharynx, and lymph nodes. We tried two antibodies with different concentrations. The first one was a monoclonal anti-TIGAR (T8828) antibody from Sigma-Aldrich. The second one was purified rabbit polyclonal (AB10545) from Millipore UK ltd. We were satisfied with rabbit polyclonal antibody (Millipore) staining results and used rabbit polyclonal antibody in 1:50 concentration for the TMA set 1. We used the same concentration for the TMA set 2 and noticed very strong overall TIGAR staining. Further optimisation with the same antibody in 1:100 and 1:200 concentration done, and finally selected 1:200 antibody concentration for TMA set 2 (appendix 5.1 shows the examples from TIGAR optimization analysis).

For HK-2, we tried two antibodies, a rabbit monoclonal HK-2 (C64G5) antibody (New England Biolabs) and a mouse monoclonal HK - 2 antibody (Novus Biologicals). Finally, we selected a mouse monoclonal antibody from Novus for HK-2 and used it in 1:200 concentration (appendix 5.2 shows the initial optimisation results of HK-2 staining with two antibodies). For p53, we used standard DO-7 mouse monoclonal antibody in 1:250 concentration.

After blocking, the slides were washed, and appropriate primary antibodies were added and left for 30 minutes. For positive controls, we used a soft palate sample for p53, kidney for TIGAR and pancreas for HK-2. For negative controls, the primary antibody was omitted, and we added 'Dako antibody dilution' to the negative control slides for p53 and TIGAR, and we added IgG1 to the HK-2 negative control slide. The mouse monoclonal anti-HK-2 antibody is an IgG1 isotype; therefore, mouse IgG1 was used as a negative control as the same concentration as the HK2 antibody to rule out any non-specific binding of the immunoglobulins to Fc receptors on the surface of cells found in the tissue.

2.4.3.4 Adding secondary antibodies

The secondary antibody should be directed against the species in which the primary antibody was raised and can be either enzyme-labelled or biotinylated. We used an enzyme labelled secondary antibody, which is horseradish peroxidase (HRP). For rabbit polyclonal primary antibody, we applied rabbit specific HRP conjugate and incubated it for 15 minutes at room temperature. For monoclonal antibody, the slides were incubated with a rabbit linker (Agilent) for 15 minutes, and the bound antibody was then detected with HRP for 20 minutes.

2.4.3.5 Adding DAB

The chromogenic detection methods in IHC relies on enzymes that convert soluble substrates into insoluble, chromogenic products, and the most commonly used chromogen is DAB (3,3'-diaminobenzidine), which is used in combination with the HRP enzyme. After incubating with secondary antibody, the slides were washed, and DAB was applied (concentration, time etc.). The slides were then ready for counter-staining.

2.4.3.6 Counter-staining

After washing with a FLEX buffer and distilled water, the slides were placed in a slide rack and dipped quickly into Mayer's haematoxylin (VWR chemicals) for 30 seconds. The samples were washed in running tap water until the water ran clear. The slide rack was then dipped into an acid alcohol bath and immediately taken out and placed in running tap water until the slides were no longer showing pink staining.

After a thorough wash, the slide rack was placed in Scott's tap water/ ammonia water for 30 seconds. The samples were washed in running water for one minute and dehydrated through a series of ethanol solutions in a fume hood. This included 5 x IMS (Industrial Methylated Spirits) and 2 x Xylene. The slides were agitated for 10 seconds at each stage vigorously, and at the end, one drop of DPX mountant was added to the sample, and it was then covered with a coverslip, avoiding and, if necessary removing air bubbles. After adequate drying, the slides were ready for examination under the microscope.

2.4.4 The rationale for the scoring method and our scoring criteria

2.4.4.1 Scoring criteria for TIGAR staining

As we didn't have any previous reference staining protocol for TIGAR in head and neck cancer cells, we referred TIGAR-related articles and evaluated different scoring criteria for TIGAR expression (274-277).

Accordingly, in consultation with the pathologist, we determined an empirical scoring approach as follows: TIGAR cytoplasmic staining was scored according to the intensity as 1 (very weak), 2 (weak), 3 (moderate) and, 4 (strong). Because of the small numbers of 1 and 3 categories, we have combined 1 and 2 together and 3 and 4

in one group. The revised scoring criteria for TIGAR staining was 1 (weak) and 2 (strong).

2.4.4.2 Scoring criteria for p53 staining

p53 expression was typically detected as nuclear staining, and samples were scored according to the percentage of tumour cells with nuclear p53 expression. When >1% to <5% of tumour cells showed p53 expression, then they were considered as inferred wild-type p53 and allocated a score of 1. Tumour cells with >5% of p53 expression were considered as inferred mutant p53 and allocated a score of 2. This approach is based on one developed originally by the Lane research group, as described in Nenutil et al., 2005 (278), and on our research group's previously published studies. The method used for IHC detection of p53 and the antibody used is highly sensitive, so that the complete absence of staining often indicates the loss of p53 expression. For example, 80% of the IHC negative cases in the Nenutil et al. study harboured mutations resulting in loss of detectable p53 protein, often as a result of a nonsense mutation, though of course, this cannot be distinguished from any other cause of absence such as LOH (278). The anti-p53 antibody produced by hybridoma clone DO-7 was identified as the best available antibody for IHC by these authors, and we have used the same clone. Accordingly, we have scored complete absence of detectable p53 in tumour cells as indicative of a genetic alteration compromising p53 function, and these were therefore scored 2 and grouped with the other p53 inferred mutation samples.

2.4.4.3 Scoring criteria for Hexokinase-2 (HK-2) staining

We performed a literature search and evaluated different scoring criteria for immunohistochemical analysis of HK-2 expression (279-283). For HK-2 expression,

the samples were scored according to the intensity of cytoplasmic staining. The scoring scheme used for HK-2 was 1 (weak staining), 2 (moderate staining) and 3 (strong staining).

2.4.5 Evaluation of immunohistochemical staining

Immunohistochemistry-stained TMA slides were analysed and validated using a semi-quantitative method for scoring as described above. Two clinical pathologists, both blinded to previous diagnostic and clinical information, independently evaluated the slides. Scoring the triplicate scores was based on the following criteria: out of three cores, if two cores displayed the same value, we selected that score. If all three scores are different, or if one score is missing, we selected the maximum value. If two cores are missing, that will be discarded.

2.4.6 Distribution of cores in TMAs

In TMA set 1, we have three TMA slides (triplicate cores distributed in three TMA slides for 101 patients). Three patients had duplicate cores, and there was one blank core, so the total cores evaluated were 305.

In TMA set 2, for each patient, there were triplicate cores for normal tissue, tumour core and advancing front of tumour.

- For the larynx (77 primaries + 19 lymph nodes), we had 594 cores.
- For the hypopharynx (22 primaries + 12 lymph nodes), we had 175 cores.
- For the oropharynx (62 primaries + 29 lymph nodes), we had 509 cores.

The number of cores and the missing cores for each patient were given in the appendix (refer to appendix 5.3 for oropharynx, 5.4 for larynx, and 5.5 for hypopharynx).

2.4.7 Interobserver variability

The concordance between the two pathologists scoring (Inter-observer variability) is assessed by 'κ statistics', which provides a measurement of the observed agreements and the agreements expected by chance expressed as a fraction of the maximum possible difference (284). The level of agreement is normally categorised as almost perfect, substantial, moderate, fair, and slight when the κ value is >0.80, >0.60-0.80, >0.40-0.60, >0.20-0.40, and 0-0.20, respectively (284).

The discrepancies in the scoring between the two pathologists were further evaluated for inter-observer variability (see table 2.9, which provides a summary of the discordant scores by the two pathologists).

Table 2-9 Inter-observer variabilities (TMA set 1 and 2)

TMA	Staining/core number	Pathologist 1	Pathologist 2	3rd scoring by student and supervisor	4th scoring by Pathologist 3
TMA set 1 -1.A	p53 / A10	2	NT		2
TMA set 1 -1.A	p53 / A11	2	1	1	
TMA set 1 -1.A	p53 / E9	2	1	2	
TMA set 1 -1.A	p53 / E10	2	NT		NT
TMA set 1 -1.A	p53 / F3	NT	1		NT
TMA set 1 -1.A	p53 / G11	1	2	2	
TMA set 1 -1.B	p53 / A2	2	1	1	
TMA set 1 -1.B	p53 / E7	1	NT	NT	
TMA set 1 -1.C	p53 / A11	1	NT	NT	
TMA set 1 -1.C	p53 / C5	2	1	2	
TMA set 1 -1.C	p53/ E10	2	NT		NT
TMA set 1 -1.C	p53 / E12	1	2	2	
TMA set 1 -1.C	p53 / F8	1	2	2	
TMA set 1 -1.A	TIGAR / H10	1	2	2	
TMA set 1 -1.A	TIGAR / E8	NT	2		2
TMA set 1 -1.A	TIGAR / F11	2	NT	2	
TMA set 1 -1.A	TIGAR / F12	2	1	1	
TMA set 1 -1.B	TIGAR / H10	2	NT	NT	
TMA set 1 -1.B	TIGAR / F12	NT	2		2
TMA set 2 -HP	p53/A1	1	2	2	
TMA set 2 -HP	p53 / C5	1	NT	NT	
TMA set 2 -HP	p53 / C6	1	NT	NT	
TMA set 2 -HP	p53 / D3	1	2	2	
TMA set 2 -OP01	p53 / J5	NT	2	2	
TMA set 2 -OP02	p53 / K1	1	2	2	
TMA set 2 -OP03	p53 / D3	1	2	2	
TMA set 2 -OP - N	p53 / B4	NT	2	2	
TMA set 2 -HP	HK2 / C5	3	NT	NT	
TMA set 2 -LP 02	HK2 / A2	2	NT	NT	

(TMA=Tissue microarray; HP=Hypopharynx primary; OP=Oropharynx primary; LP= Larynx primary)

The variable scores between the two pathologists were further reviewed by myself and my supervisor to reach a consensus score. We could not make a consensus decision in six samples, and these were then sent to a third pathologist to try to resolve the situation and finalise the score. The revised data was then used for statistical analysis.

In our analysis, Cohen's Kappa κ was run to determine if there was a similarity (agreement) between two pathologists' scores on determining the levels of expression of p53, TIGAR, and HK-2 in both TMAs. The two pathologists' scores were similar for more than 90% of the samples. There was a very good agreement between the two pathologists' scores ($\kappa > 0.9$), and it is statistically significant in all categories ($P < 0.05$).

2.4.8 Statistical analysis

Since our sample set contained comparatively few hypopharyngeal cases, we combined the samples of larynx and hypopharynx for statistical analysis purposes. We analysed the oropharyngeal samples separately as the pathogenesis and clinical outcomes of oropharyngeal cancers are different from other head and neck cancers, and this is substantially, if not entirely, due to the involvement of HPV (discussed in 1.2). All statistical analyses (for TMA set 1 and TMA set 2) were performed using the SPSS statistical software package (version 25; SPSS Inc., Chicago, Ill). Immunohistochemistry results were provided in the form of summary statistics, and the Pearson Chi-square test was used to test associations between the expression of p53, TIGAR, and HK-2 to that of various known clinical variables, including T stage, N stage etc.

Survival curves were calculated using the Kaplan-Meier product-limit estimate, and the differences between survival times were analysed by the log-rank test method. Disease-specific survival analysis performed for up to 60 months. Deaths from causes other than head and neck tumours were not considered as treatment failures, and these patients were censored in all analyses that involved the length of survival.

A *P*- value <0.05 was considered statistically significant.

3. Results

As discussed in section 1.7 of the introduction, we were interested in understanding what happens to genes that play a critical role in regulating or contributing to altered tumour metabolism. In particular, we were focussing on *TP53*, *HK-2* and *TIGAR*, because there was good evidence that these genes may have important roles to play in carcinogenesis, and all three have connections with metabolic processes (206, 285, 286). Because of the evidence that *TP53*, in particular, is an important gene in SCCHN and regulates *TIGAR*, which interacts with HK-2, we have tried to examine all three in a substantial number of SCCHN patient samples using TMAs. We also performed limited analyses of the steady-state levels of the protein products in a panel of SCCHN cell lines, including several isogenic derivatives with defined altered *TP53* status.

We have grouped the results in two major sections: Section 3.1 describes western blot results for p53, TIGAR and HK-2 expression in parental and isogenic SCCHN cell lines, and sections 3.2 and 3.3 discuss the results of our immunohistochemical (IHC) analysis of p53, TIGAR and HK-2 expression in SCCHN samples. The overview of the results section is presented in figure 3.1.

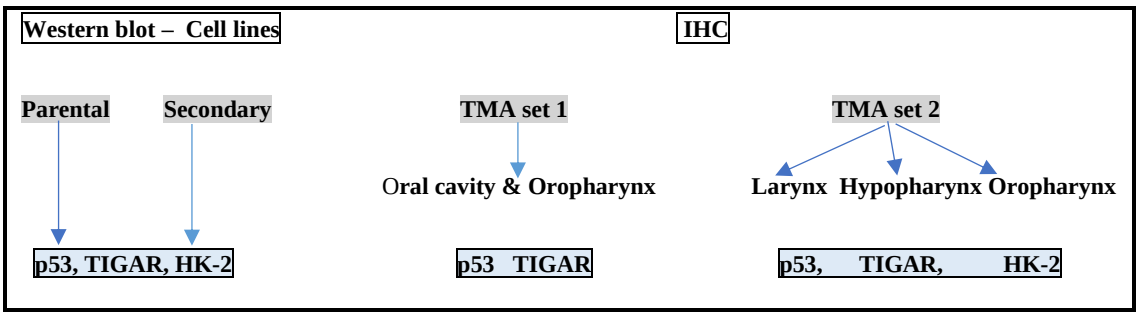

Figure 3:1 Overview of the results section. Systems used to examine three proteins, namely p53, TIGAR, and HK-2. Two major types of experiments were performed; western blot analysis (section 3.1), and IHC [performed in two sets of TMAs – TMA set 1 (section 3.2.1), and TMA set 2 (3.2.2)]

3.1. Western blot results

The rationale for measuring the steady-state levels of the selected proteins (p53, TIGAR, and HK-2) is as follows; the p53 protein is a transcriptional regulator of many genes, and TIGAR was originally identified because it is transcriptionally regulated by p53 (discussed in section 1.6). However, it is also well documented in tumour cells from some cancers that p53 and TIGAR expression become uncoupled. In addition, it has been discovered that one of the ways that TIGAR functions to alter cellular metabolism is mediated through an interaction with HK-2.

Accordingly, we set out to examine the relationship between p53 status and TIGAR and HK-2, taking advantage of existing isogenic cell lines that harbour defined altered *TP53* status (null, wild-type, and mutated) and also in isogenic cells that display altered levels of p53 expression as a result of RNAi mediated expression modulation.

Note that all cell lines have been recently STR profiled, and their identities confirmed as correct for the parental cell line. Individual isogenic lines match the expression profiles previously observed for p53 and display the expected sensitivity to an MDM2 antagonist- Nutlin 3 (287) *[and data not shown, generated by Mark Wilkie and Andrew Lau, in our laboratory]*.

The selection of cell lines has been discussed previously in section 2.3.1.

Each experiment has been repeated three times (Gel 1, Gel 2, and Gel 3), and densitometer values were obtained using Bio-Rad Image Lab 6.1 software (discussed in 2.3.7)

3.1.1 p53 and TIGAR expression in UM SCC-1 cell lines

Protein extracts were prepared from each cell line, harvested, and lysed as described in section 2.2.3. 20µg of protein was analysed in each lane. Primary antibodies (as mentioned in section 2.1.4) were used with appropriate secondary antibodies. Vinculin was used as a loading control. Figure 3.2 shows the p53 and TIGAR expression in UM SCC 1 isogenic cell lines.

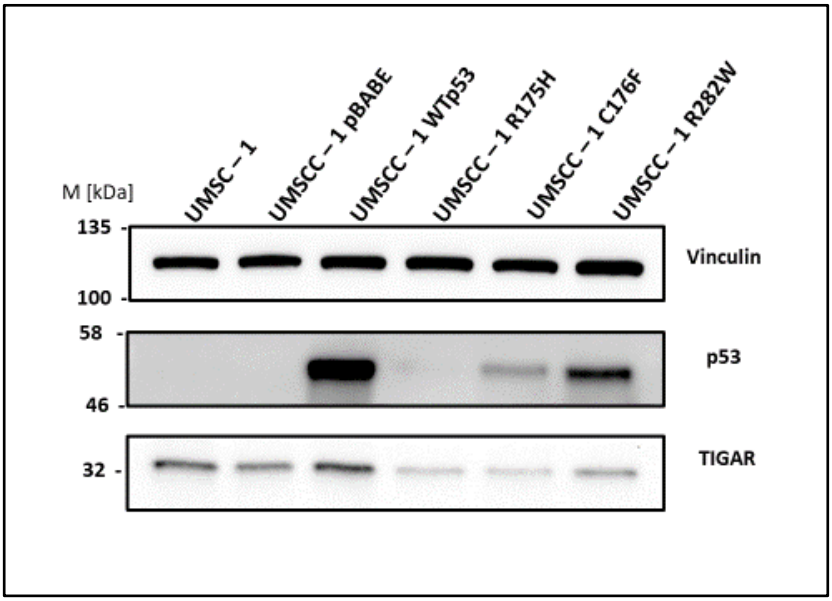

Figure 3:2 p53 and TIGAR expression in UM SCC 1 isogenic cell lines. Western blot showing protein expression levels of p53 and TIGAR in UM SCC 1 isogenic cell lines. Vinculin served as a protein loading control. The migration of protein standards of the indicated approximate molecular weight is shown in kDa. UM SCC -1 and UM SCC-1-pBabe (p53 null), UM SCC-1 WTp53 (wild type), UM-SCC-1 R175, UM-SCC-1 C176F, UM-SCC-1 R282W (p53 mutant). These data are representative of one experiment performed three times independently.

Images were analysed using Bio-Rad Image Lab 6.1 software, and the intensity of p53 and TIGAR expression was determined with background subtraction set as maximum and then normalised to the intensity of the loading control protein for each lane (as described in 2.3.7).

The normalised mean values of p53 expression relative to Vinculin in UM SCC 1 isogenic cell lines are given in Table 3.1 and are plotted in figure 3.3.

Table 3-1 The mean expression of p53 in UM SCC-1 isogenic cell lines

	Gel 1	Gel 2	Gel 3	Average	StDEV	SEM
UMSCC-1	3762	944	1596	2101	1475	852
UMSCC -1 pBABE	3594	8803	9605	7334	3264	1884
UMSCC - 1 WTp53	15690386	14763158	12814878	14422807	1467656	847352
UMSCC - 1 R175H	79811	2456	7330	29866	43323	25012
UMSCC - 1 C176F	776030	1149454	1141409	1022298	213312	123156
UMSCC - 1 R282W	3700902	4860217	6376710	4979277	1341871	774730

The mean value was calculated to find the standard deviation (StDEV) and standard error of the mean (SEM).

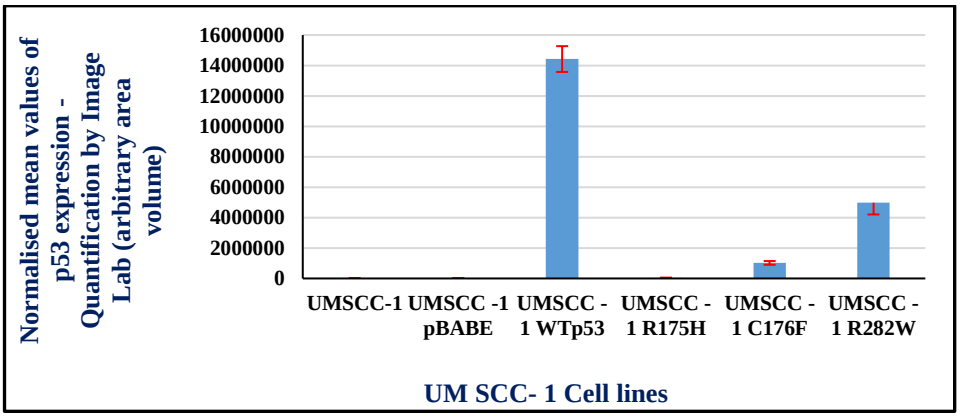

Figure 3:3 Representation of normalised mean values of p53 expression in UM SCC 1 cell lines. Expression of p53 was normalised to loading control bands of Vinculin using Bio-Rad Image Lab software. Error bars represent the standard error of the mean (SEM). [UM SCC -1 and UM SCC-1-pBabe (p53 null), UM SCC-1 WTp53 (wild type), UM-SCC-1 R175, UM-SCC-1 C176F, UM-SCC-1 R282W (p53 mutant)].

There was no p53 expression in the p53-null UM SCC-1 and UM-SCC-1-pBabe cell lines. In contrast, p53 expression was maximal in the UM SCC-1 WTp53 (wild-type) with varying expression in cells transfected with three mutated p53 constructs. Of these, p53 expression was lowest in R175H-expressing cell lines compared to cells transfected with C176F and R282W mutants.

The normalised mean values of TIGAR expression in UM SCC 1 isogenic cell lines are given in Table 3.2, and the representative bar graphs are plotted in figure 3.4.

Table 3-2 The mean expression of TIGAR in UM SCC-1 isogenic cell lines

	Gel 1	Gel 2	Gel 3	Average	StDEV	SEM
UMSCC-1	278802	405392	416448	366881	76478	44155
UMSCC -1 pBABE	310251	456590	254650	340497	104312	60225
UMSCC - 1 WTp53	537647	856419	580497	658188	173005	99885
UMSCC - 1 R175H	53775	120757	162569	112367	54880	31685
UMSCC - 1 C176F	76340	149459	80167	101989	41155	23761
UMSCC - 1 R282W	196882	362067	311295	290081	84611	48850

The mean value was calculated to find the standard deviation (StDEV) and standard error of the mean (SEM).

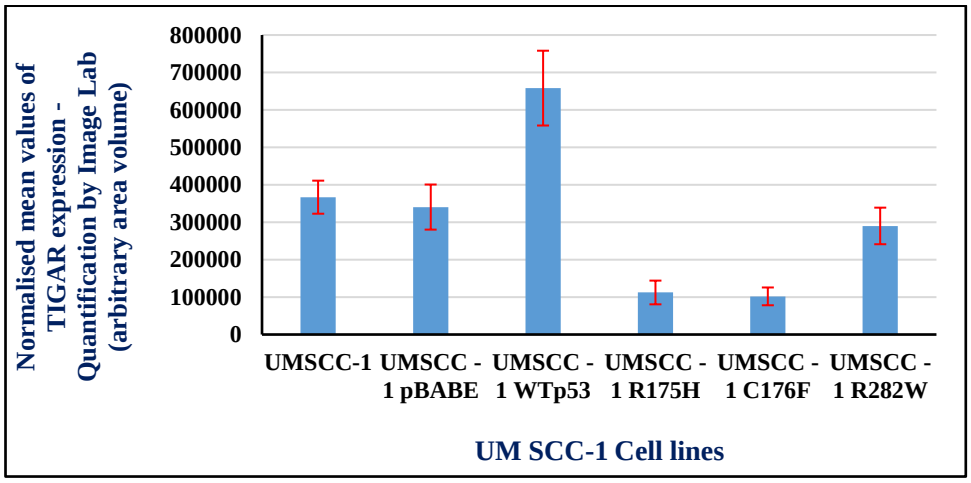

Figure 3:4 Representation of normalised mean values of TIGAR expression in UM SCC-1 cell lines. Expression of TIGAR was normalised to loading control bands of Vinculin using Bio-Rad Image Lab software. Error bars represent the standard error of the mean (SEM). [UM SCC -1 and UM SCC-1-pBabe (p53 null), UM SCC-1 WTp53 (wild type), UM-SCC-1 R175, UM-SCC-1 C176F, UM-SCC-1 R282W (p53 mutant)].

Higher TIGAR expression was seen in p53 null and wild-type cell lines compared to the mutant cell lines.

3.1.2 HK-2 expression in UM SCC-1 cell lines

Protein extracts were prepared from each cell line, harvested, and lysed as described in section 2.2.3. 20µg of protein was analysed in each lane. Primary antibodies (as mentioned in section 2.1.4) were used with appropriate secondary antibodies. Actin was used as a loading control. Figure 3.5 shows the HK-2 expression in UM- SCC 1 isogenic cell lines.

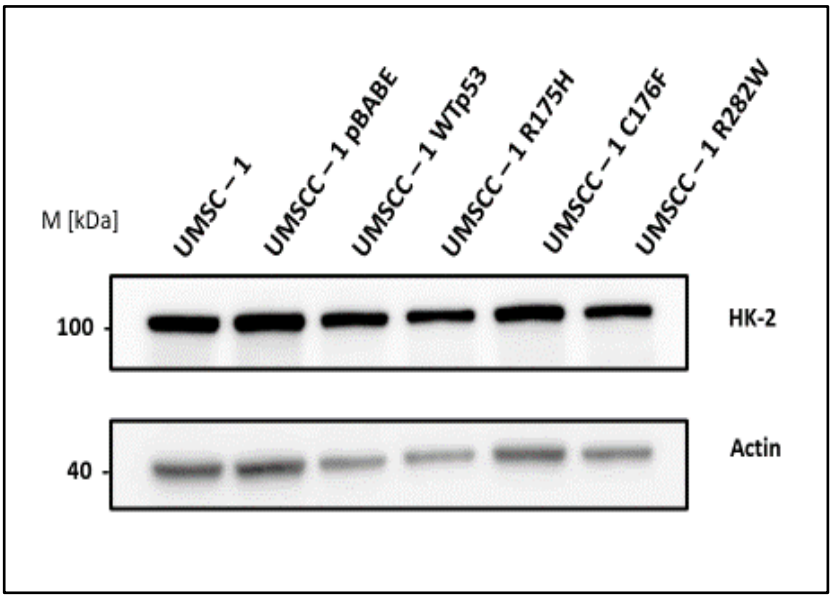

Figure 3:5 HK-2 expression in UM SCC 1 isogenic cell lines. Western blot showing protein expression levels of HK-2 in UM SCC 1 isogenic cell lines. Actin served as a protein loading control. The migration of protein standards of the indicated approximate molecular weight is shown in kDa. UM SCC -1 and UM SCC-1-pBabe (p53 null), UM SCC-1 WTp53 (wild type), UM-SCC-1 R175H, UM-SCC-1 C176F, UM-SCC-1 R282W (p53 mutant). These data are representative of one experiment performed three times independently.

Images were analysed using Bio-Rad Image Lab 6.1 software and the intensity of HK-2 expression was determined with background subtraction set as maximum and then normalised to the intensity of the loading control protein for each lane (as described in 2.3.7).

The normalised mean values of HK-2 expression in UM SCC 1 isogenic cell lines are given in Table 3.3, and the representative bar graphs are plotted in figure 3.6.

Table 3-3 The mean expression of HK-2 in UM SCC 1 isogenic cell lines

	Gel 1	Gel 2	Gel 3	Average	StDEV	SEM
UMSCC-1	27687690	27536940	31176650	28800427	2059250	1188908
UMSCC -1 pBABE	32345492	32958231	35983547	33762423	1947795	1124560
UMSCC - 1 WTp53	8212924	7755671	10319124	8762573	1367263	789390
UMSCC - 1 R175H	5296242	5081497	9073289	6483676	2245239	1296290
UMSCC - 1 C176F	20812113	21174416	9008234	16998254	6921932	3996379
UMSCC - 1 R282W	7896775	7964600	7478398	7779924	263322	152029

The mean value was calculated to find the standard deviation (StDEV) and standard error of the mean (SEM).

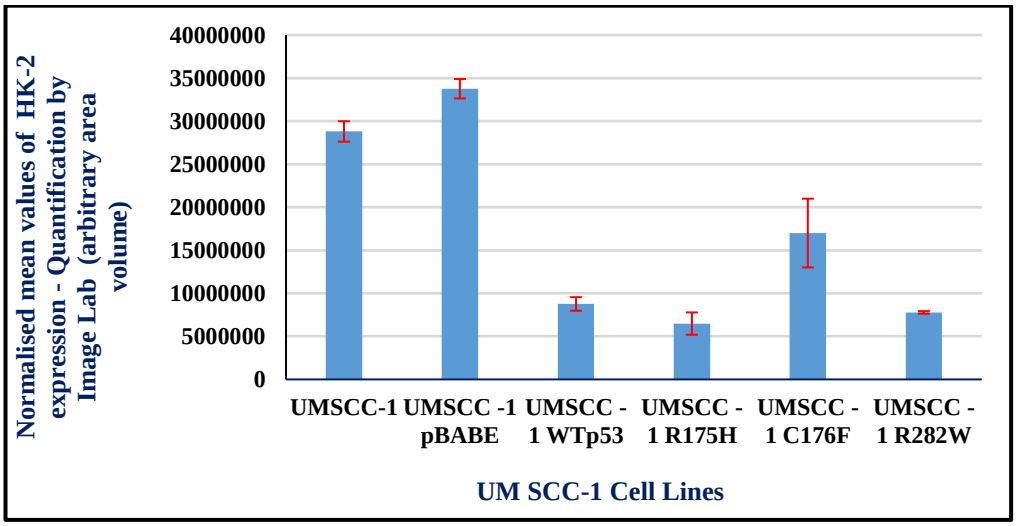

Figure 3:6 Representation of normalised mean values of HK-2 expression in UM SCC 1 cell lines. Expression of HK-2 was normalised to loading control bands of Actin using Bio-Rad Image Lab software. Error bars represent the standard error of the mean (SEM). [UM SCC -1 and UM SCC-1-pBabe (p53 null), UM SCC-1 WTp53 (wild type), UM-SCC-1 R175, UM-SCC-1 C176F, UM-SCC-1 R282W (p53 mutant)].

HK-2 expression was readily detectable in all the cell lines.

3.1.3 p53 and TIGAR expression in UM SCC-17A and UM SCC-11A & 11B cell lines

Protein extracts were prepared from each cell line, harvested, and lysed as described in section 2.2.3. 20µg of protein was analysed in each lane. Primary antibodies (as mentioned in section 2.1.4) were used with appropriate secondary antibodies. Vinculin was used as a loading control (see figure 3.7). Figure 3.7 shows the p53 and TIGAR expression in UM SCC-17A and UM SCC-11A & 11B cell lines.

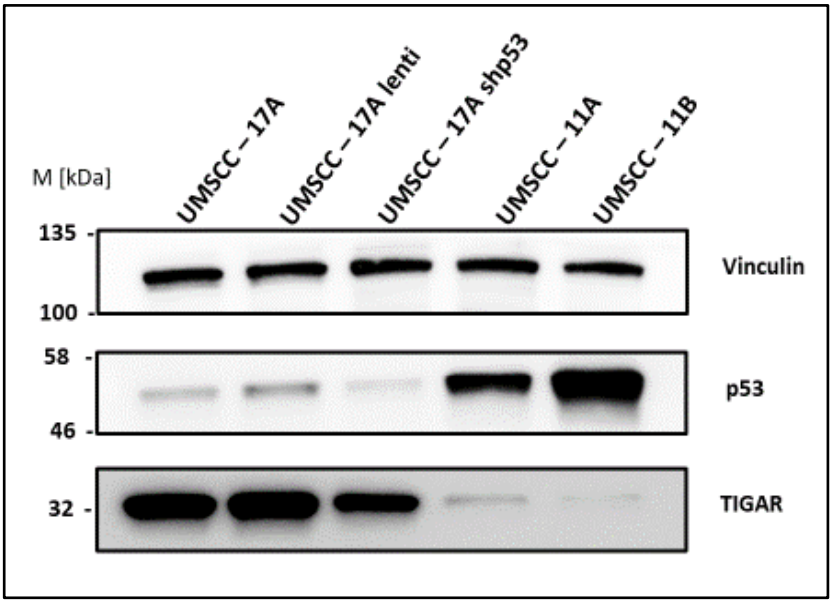

Figure 3:7 p53 and TIGAR expression in UM SCC-17A and UM SCC-11A & 11B cell lines. Western blot showing protein expression levels of p53 and TIGAR in UM SCC-17A and UM SCC-11A & 11B cell lines. Vinculin served as a protein loading control. The migration of protein standards of the indicated approximate molecular weight is shown in kDa. UM SCC -17A and UM SCC-17A lenti (p53 wild-type), UM SCC-17A shp53 (reduced expression of p53), UM SCC-11A (wild-type), UM SCC-11B (p53 mutant). These data are representative of one experiment performed three times independently.

Images were analysed using Bio-Rad Image Lab 6.1 software and the intensity of p53 and TIGAR expression was determined with background subtraction set as

maximum and then normalised to the intensity of the loading control protein for each lane (as described in 2.3.7).

The normalised mean values of p53 expression in UM SCC-17A and UM SCC-11A & 11B cell lines are given in Table 3.4, and the representative bar graphs are plotted in figure 3.8.

Table 3-4 The mean expression of p53 in UM SCC-17A and UM SCC-11A & 11B cell lines

	Gel 1	Gel 2	Gel 3	Average	StDEV	SEM
UMSCC-17A	1177385	833952	2579193	1530177	924561	533796
UMSCC 17A LENTI	1211823	1201699	2630009	1681177	821728	474425
UMSCC 17A sh p53	1549895	1216692	1392072	1386220	166679	96232
UMSCC 11A	9284129	11437607	7595329	9439022	1925816	1111870
UMSCC 11B	21419952	27603266	16185474	21736231	5715463	3299824

The mean value was calculated to find the standard deviation (StDEV) and standard error of the mean (SEM).

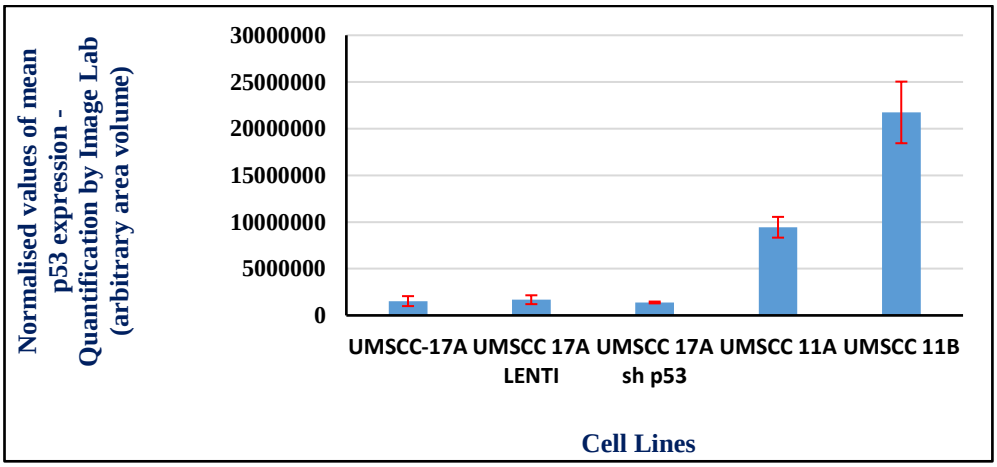

Figure 3:8 Representation of normalised mean values of p53 expression in UM SCC-17A and UM SCC 11A & 11B cell lines. Expression of p53 was normalised to loading control bands of Vinculin using Bio-Rad Image Lab software. Error bars represent the standard error of the mean (SEM). [UM SCC -17A and UM SCC-17A lenti (p53 wild-type), UM SCC-17A shp53 (reduced expression of p53), UM SCC-11A (wild-type), UM SCC-11B (p53 mutant)].

Increased p53 expression was seen in the UM SCC-11A and 11B cell lines. Slightly higher p53 expression seen in UM SCC-17A and UM SCC-17A lenti compared to the UM SCC-17A shp53.

The normalised mean values of TIGAR expression in UM SCC-17A and UM SCC-11A & 11B cell lines are given in Table 3.5, and the representative bar graphs are plotted in figure 3.9.

Table 3-5 The mean expression of TIGAR in UM SCC-17A and UM SCC-11A & 11B cell lines

	Gel 1	Gel 2	Gel 3	Average	StDEV	SEM
UMSCC-17A	3994112	3545984	7726180	5088759	2295038	1325041
UMSCC 17A LENTI	5028633	3877407	8330418	5745486	2311436	1334508
UMSCC 17A sh p53	2788624	3375052	3330750	3164808	326538	188527
UMSCC 11A	97607	63085	113670	91454	25847	14923
UMSCC 11B	121313	6657	17521	48497	63294	36543

The mean value was calculated to find the standard deviation (StDEV) and standard error of the mean (SEM).

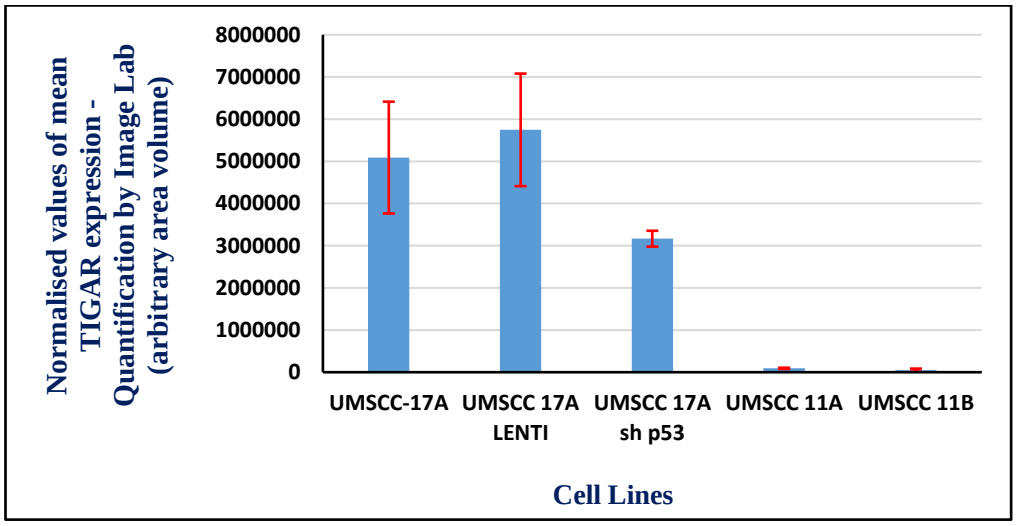

Figure 3:9 Representation of normalised mean values of TIGAR expression in UM SCC-17A and UM SCC 11A & 11B cell lines. Expression of TIGAR was normalised to loading control bands of Vinculin using Bio-Rad Image Lab software. Error bars represent the standard error of the mean (SEM). [UM SCC -17A and UM SCC-17A lenti (p53 wild-type), UM SCC-17A shp53 (reduced expression of p53), UM SCC-11A (wild-type), UM SCC-11B (p53 mutant)].

Higher TIGAR expression seen in UM SCC 17A, UM SCC 17A lenti and UM SCC 17A shp53 cell lines.

3.1.4 HK-2 expression in UM SCC-17A and UM SCC-11A & 11B cell lines

Protein extracts were prepared from each cell line, harvested, and lysed as described in section 2.2.3. 20µg of protein was analysed in each lane. Primary antibodies (as mentioned in section 2.1.4) were used with appropriate secondary antibodies. Actin was used as a loading control. Figure 3.10 shows the HK-2 expression in UM SCC-17A and UM SCC-11A & 11B cell lines.

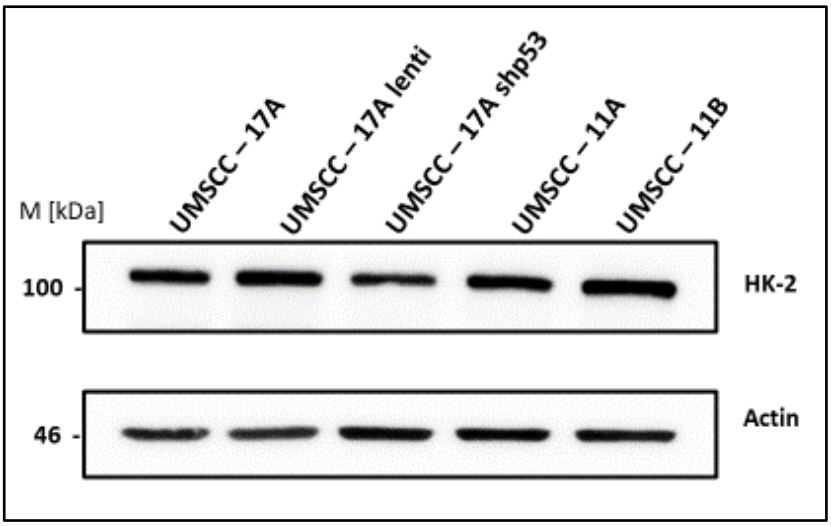

Figure 3:10 HK-2 expression in UM SCC-17A and UM SCC-11A & 11B cell lines. Western blot showing protein expression levels of HK-2 in UM SCC-17A and UM SCC-11A & 11B cell lines. Actin served as a protein loading control. The migration of protein standards of the indicated approximate molecular weight is shown in kDa. UM SCC -17A and UM SCC-17A lenti (p53 wild type), UM SCC-17A shp53 (reduced expression of p53), UM SCC-11A (wild type), UM SCC-11B (p53 mutant). These data are representative of one experiment performed three times independently.

Images were analysed using Bio-Rad Image Lab 6.1 software and the intensity of HK-2 expression was determined with background subtraction set as maximum and then normalised to the intensity of the loading control protein for each lane (as described in 2.3.7).

The normalised mean values of HK-2 expression in UM SCC-17A and UM SCC-11A & 11B cell lines are given in Table 3.6, and the representative bar graphs are plotted in figure 3.11.

Table 3-6 The mean expression of HK-2 in UM SCC-17A and UM SCC-11A & 11B cell lines

	Gel 1	Gel 2	Gel 3	Average	StDEV	SEM
UMSCC-17A	23674376	19967428	12895778	18845861	5476128	3161644
UMSCC 17A LENTI	19812792	18925853	16439003	18392549	1748977	1009773
UMSCC 17A sh p53	7876854	16969471	14615997	13154107	4719297	2724687
UMSCC 11A	11172803	23241677	21617014	18677164	6549539	3781378
UMSCC 11B	29097966	32975178	26776632	29616592	3131649	1808058

The mean value was calculated to find the standard deviation (StDEV) and standard error of the mean (SEM).

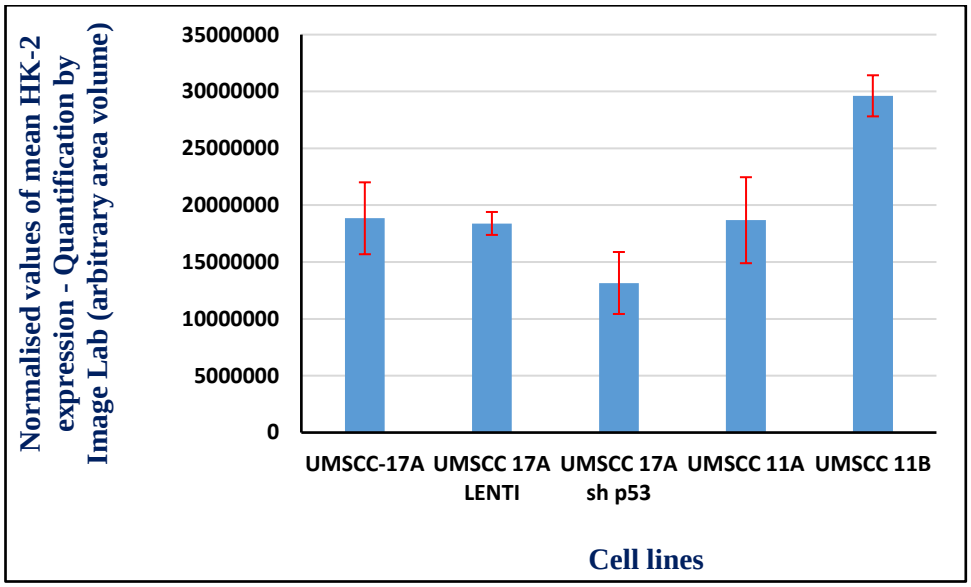

Figure 3:11 Representation of normalised mean values of HK-2 expression in UM SCC-17A and UM SCC 11A & 11B cell lines. Expression of HK-2 was normalised to loading control bands of Actin using Bio-Rad Image Lab software. Error bars represent the standard error of the mean (SEM). [UM SCC -17A and UM SCC-17A lenti (p53 wild-type), UM SCC-17A shp53 (reduced expression of p53), UM SCC-11A (wild-type), UM SCC-11B (p53 mutant)].

HK-2 expression was readily detectable in all the cell lines.

3.2 TMA set 1 -Immunohistochemistry analysis of p53 and TIGAR

The details of TMA set 1, including the selection of samples, construction of TMA, have been discussed in section 2.4.2.1. The scoring criteria for p53 and TIGAR expression were discussed in section 2.4.4. For every protein expression analysis, we have performed frequency distribution, Chi-square statistics, and survival analysis. The layout of the TMA set 1 results is shown in table 3.7.

Table 3-7 The results layout of TMA set 1

p53 expression in TMA set 1
Frequency distribution
Chi-square statistics
Survival analysis
TIGAR expression in TMA set 1
Frequency distribution
Chi-square statistics
Survival analysis
Association between p53 and TIGAR expression in TMA set 1 Chi-square statistics

3.2.1 p53 expression in TMA set 1

The pattern of p53 expression in TMA set 1 is shown in figure 3.12.

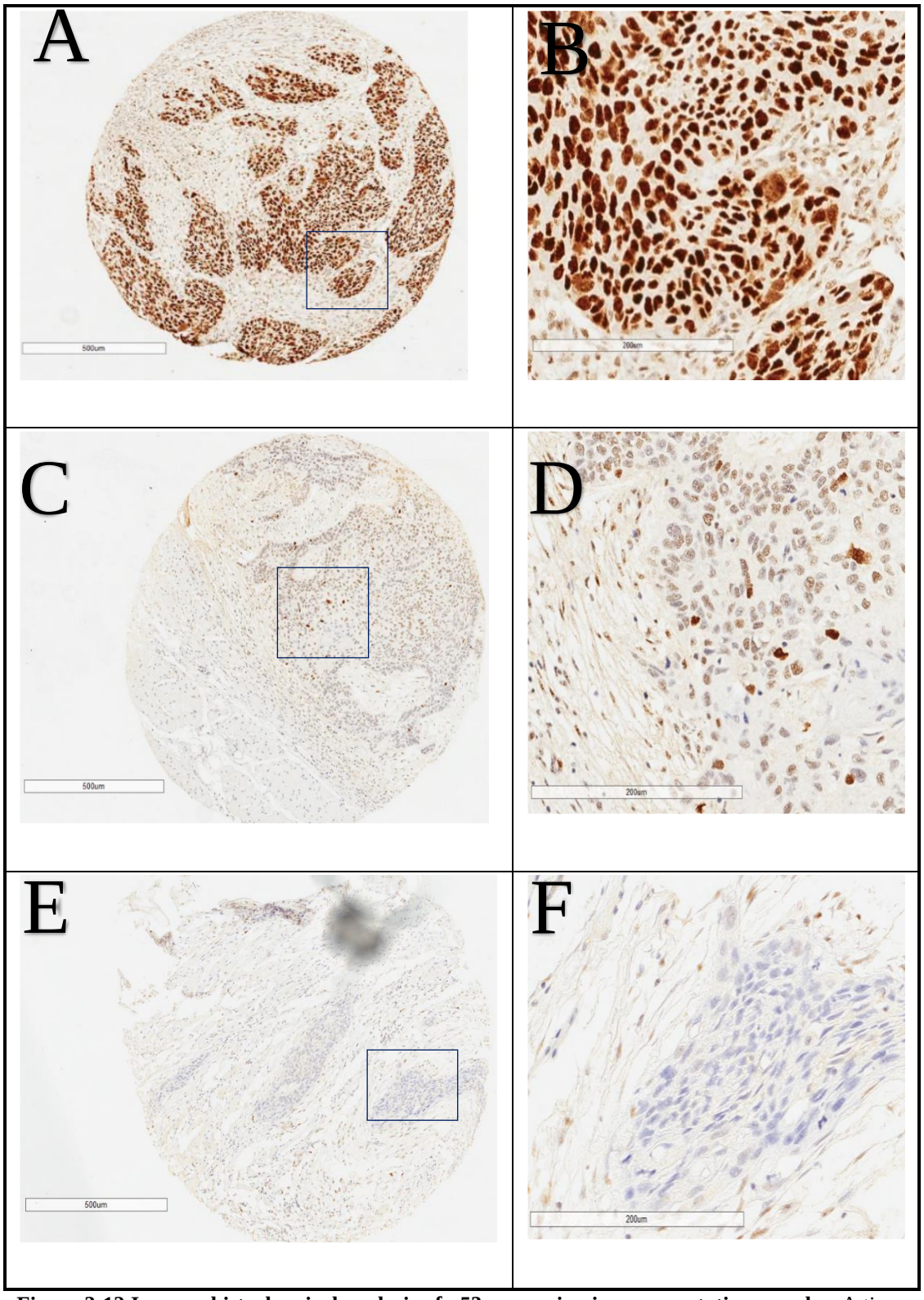

Figure 3:12 Immunohistochemical analysis of p53 expression in representative samples. A tissue microarray (TMA) was stained using a mouse monoclonal antibody (DO-7) as described in section 2.4.3. This figure illustrates the magnified views of representative cores from TMA set 1. Magnification is represented by the individual scale bar in the figure. (A) represents inferred p53 mutant (B) detailed image of the area indicated in blue in panel A (C) represents inferred wild-type p53 (D) detailed image of the area indicated in blue in panel C (E) represents the absence of p53 staining in tumour cells (F) detailed image of the area indicated in blue in panel E

3.2.1.1 Association of p53 expression with clinical variables in TMA set 1

We have observed 62.4% of 'inferred p53 mutation' in our immunohistochemical analysis of TMA set 1 (see table 3.8).

Table 3-8 Frequency distribution of p53 expression in TMA set 1

	Frequency	Percentage (%)
No tumour	19	18.8
Inferred wild-type	19	18.8
Inferred mutant	**63**	**62.4**
Total	101	100

We analysed whether any association present between p53 expression with other clinical variables like anatomical sites, T & N stage, differentiation, extracapsular spread (ECS), and death (see table 3.9).

Table 3-9 Association between p53 expression and clinical variables in TMA set 1 ('no tumour' samples excluded)

Clinical variables	p53 expression – TMA set 1		
	Inferred wild-type	Inferred mutant	*P*- value
Anatomical sites			
Oral cavity	17 (22.1)	60 (77.9)	0.357
Oropharynx	2 (40.0)	3 (60.0)	
T stage			
T 1	1 (25.0)	3 (75.0)	0.914
T 2	10 (21.7)	36 (78.3)	
T 3	1 (16.7)	5 (83.3)	
T 4	7 (28.0)	18 (72.0)	
N stage			
N 0	7 (25.0)	21 (75.0)	0.882
N 1	3 (18.8)	13 (81.3)	
N 2	9 (24.3)	28 (75.7)	
Differentiation			
Well	2 (22.2)	7 (77.8)	0.870
Moderate	16 (25.8)	46 (74.2)	
Poor	1 (16.7)	5 (83.3)	
ECS			
Yes	8 (22.9)	27 (77.1)	0.912
No	11 (23.9)	35 (76.1)	
Death			
Yes	6 (30.0)	14 (70.0)	0.463
No	12 (21.8)	43 (78.2)	

NOTE. Values are n (%). (ECS – extracapsular spread) P-value determined by Pearson Chi-Square test.

3.2.1.2 Disease-specific survival analysis of p53 expression in TMA set 1

Kaplan-Meier survival analysis was conducted as described in 2.4.8 to compare the survival period between two categories of p53 expression: inferred wild-type and inferred mutant type (see Table 3.10 for case processing summary) in TMA set 1.

Table 3-10 Case processing summary for survival analysis of p53 expression in TMA set1

p53 expression	Total No	No of deaths	No of censored	% of censored cases
inferred wild-type	18	6	12	66.7%
inferred mutant	57	14	43	75.4%
Overall	75	20	55	73.3%

A log-rank test was conducted to determine whether there were any differences in the survival distributions between inferred wild-type and inferred mutant categories (see figure 3.13).

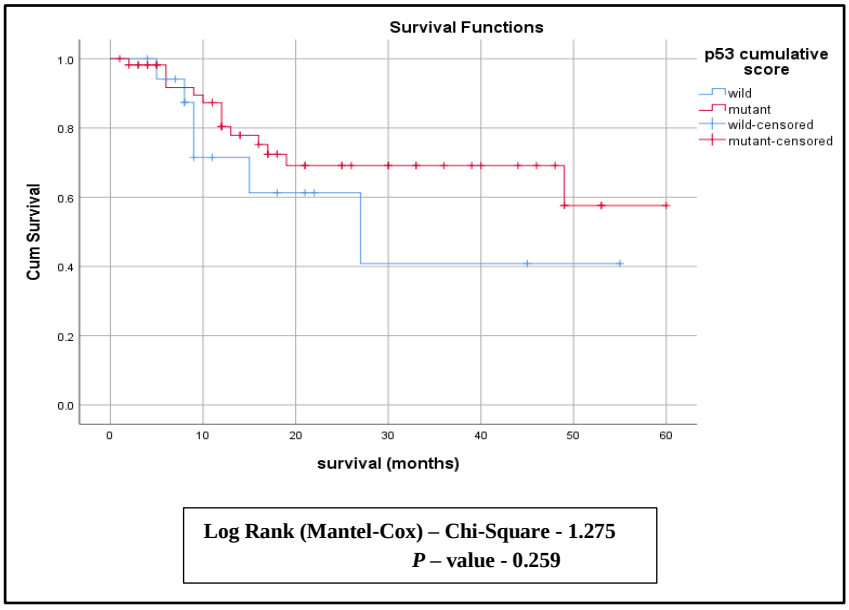

Figure 3:13 Disease-specific survival curve for inferred wild-type and inferred mutant samples in TMA set 1

Out of 101 samples, eight were from the oropharynx. To determine whether these samples influence the survival analysis, we excluded the oropharynx samples and then repeated the survival analysis (see table 3.11).

Table 3-11 Case processing summary for survival analysis of p53 expression in TMA set 1 – after excluding oropharynx samples

p53 expression	Total No	No of deaths	No of censored	% of censored cases
inferred wild-type	16	6	10	62.5%
inferred mutant	51	14	37	72.5%
Overall	67	20	47	70.1%

Following this, still, we found no association between the p53 status and survival analysis after excluding oropharynx cases (see figure 3.14).

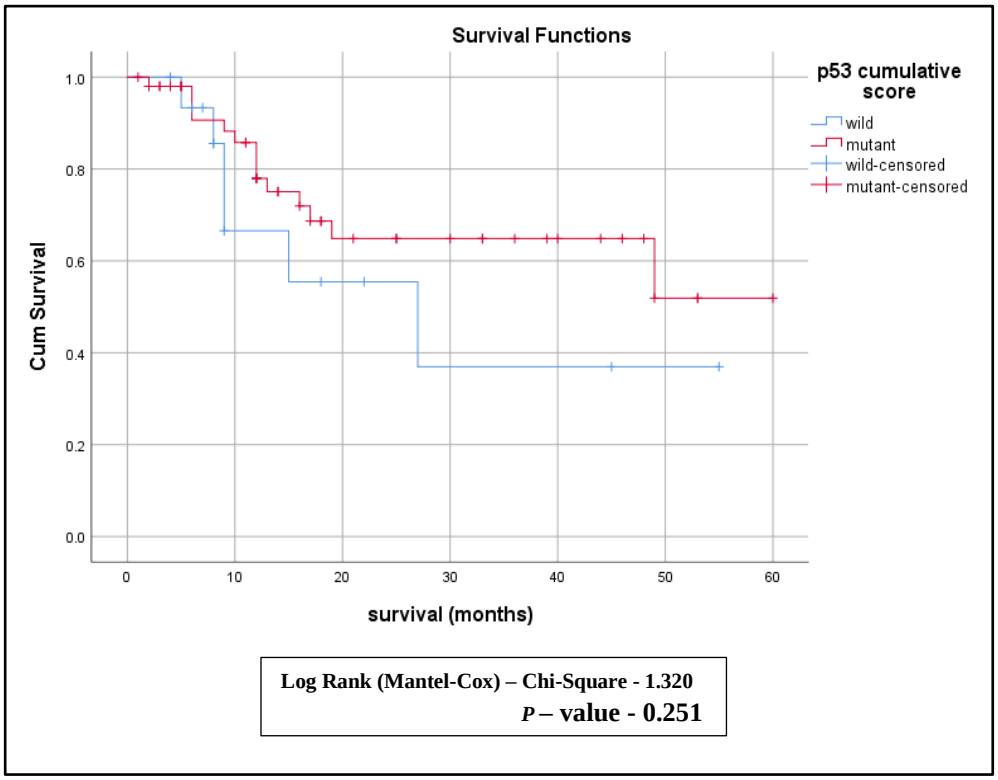

Figure 3:14 Disease-specific survival curve for p53 expression in TMA set 1 – after excluding oropharynx samples

3.2.2 TIGAR expression in TMA set 1

The pattern of TIGAR expression in TMA set 1 is shown in figure 3.15.

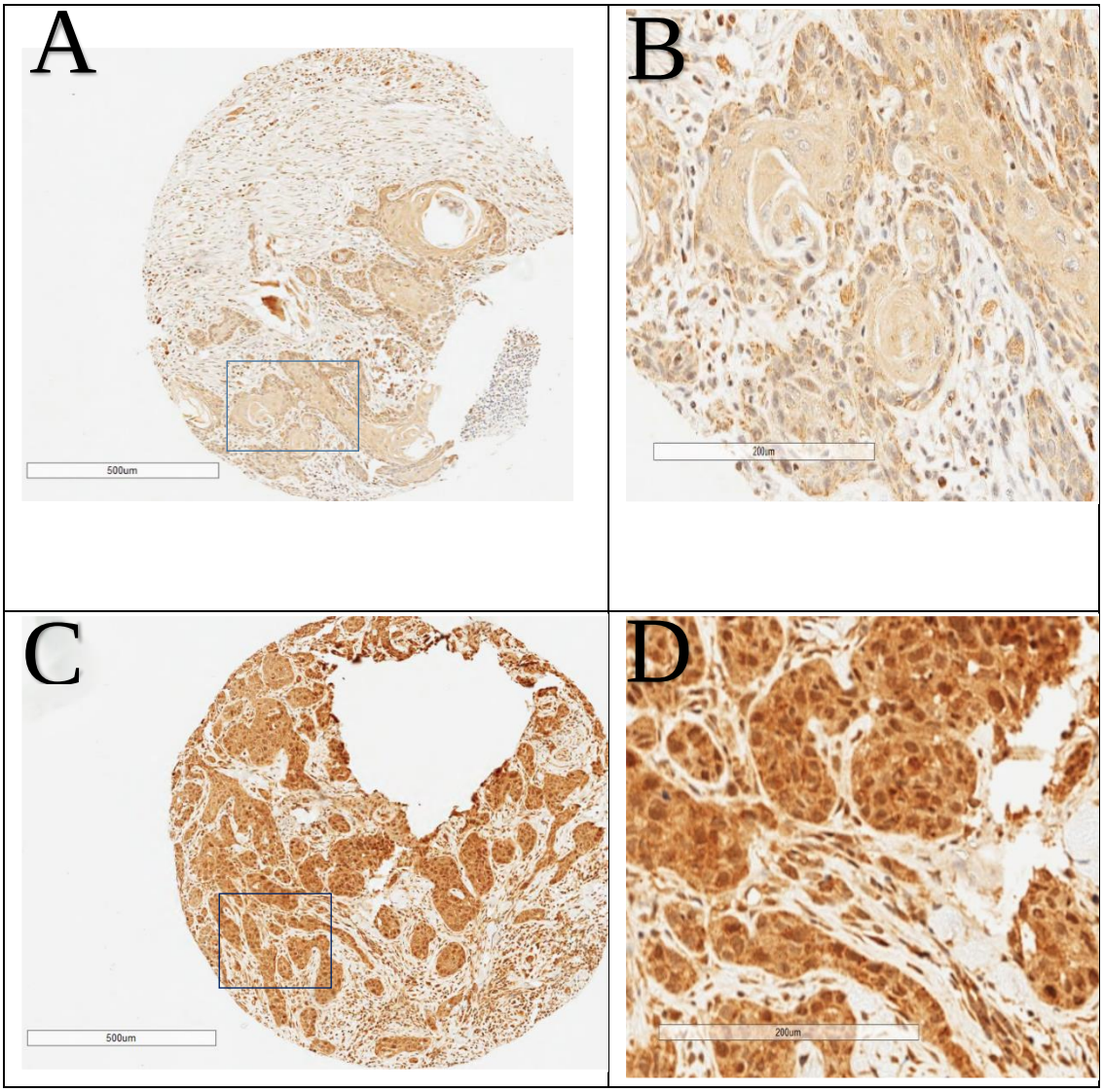

Figure 3:15 Immunohistochemical analysis of TIGAR expression in representative samples. A tissue microarray (TMA) was stained using a rabbit polyclonal anti-TIGAR antibody (AB10545) as described in section 2.4.3. This figure illustrates the magnified views of representative cores from TMA set 1. Magnification is represented by the scale bar in the figure. (A) represents weak TIGAR staining (B) detailed image of the area indicated in blue in panel A (C) represents strong TIGAR staining (D) detailed image of the area indicated in blue in panel C

3.2.2.1 Association of TIGAR expression with clinical variables in TMA set 1

We have observed 73.3% of strong TIGAR expression in our TMA set 1 sample (see table 3.12).

Table 3-12 Frequency distribution of TIGAR expression in TMA set 1

	Frequency	Percentage (%)
No tumour	21	20.8
Weak staining	6	5.9
Strong staining	**74**	**73.3**
Total	101	100

We analysed whether any association present between TIGAR expression with other clinical variables like anatomical sites, T & N stage, differentiation, extracapsular spread (ECS), and death (see table 3.13).

Table 3-13 Association between TIGAR expression and clinical variables in TMA set 1 ('no tumour' samples excluded)

	TIGAR expression – TMA set 1		
	Weak staining	**Strong staining**	***P*- value**
Anatomical sites			
Oral cavity	6 (8.0)	69 (92.0)	0.511
Oropharynx	0 (0.0)	5 (100.0)	
T stage			
T 1	1 (25.0)	3 (75.0)	0.076
T 2	1 (2.2)	45 (97.8)	
T 3	0 (0.0)	5 (100.0)	
T 4	4 (16.7)	20 (83.3)	
N stage			
N 0	3 (11.1)	24 (88.9)	0.694
N 1	1 (6.3)	15 (93.8)	
N 2	2 (5.6)	34 (94.4)	
Differentiation			
Well	2 (22.2)	7 (77.8)	0.214
Moderate	4 (6.6)	57 (93.4)	
Poor	0 (0.0)	5 (100.0)	
ECS			
Yes	3 (8.3)	33 (91.7)	0.821
No	3 (7.0)	40 (93.0)	
Death			
Yes	1 (5.0)	19 (95.0)	0.701
No	4 (7.5)	49 (92.5)	

NOTE. Values are n(%). (ECS – extracapsular spread) P-value determined by Pearson Chi-Square test.

3.2.2.2 Disease-specific survival analysis of TIGAR expression in TMA set 1

Kaplan-Meier survival analysis was conducted as described in 2.4.8 to compare the survival period between two categories of TIGAR expression; weak and strong (see Table 3.14 for case processing summary) in TMA set 1.

Table 3-14 Case processing summary for survival analysis of TIGAR expression in TMA set1

TIGAR expression	Total No	No of deaths	No of censored	% of censored cases
Weak	5	1	4	80.0%
Strong	68	19	49	72.1%
Overall	73	20	53	72.6%

A log-rank test was conducted to determine whether there were any differences in the survival distributions between weak and strong types of TIGAR expression (see figure 3.16).

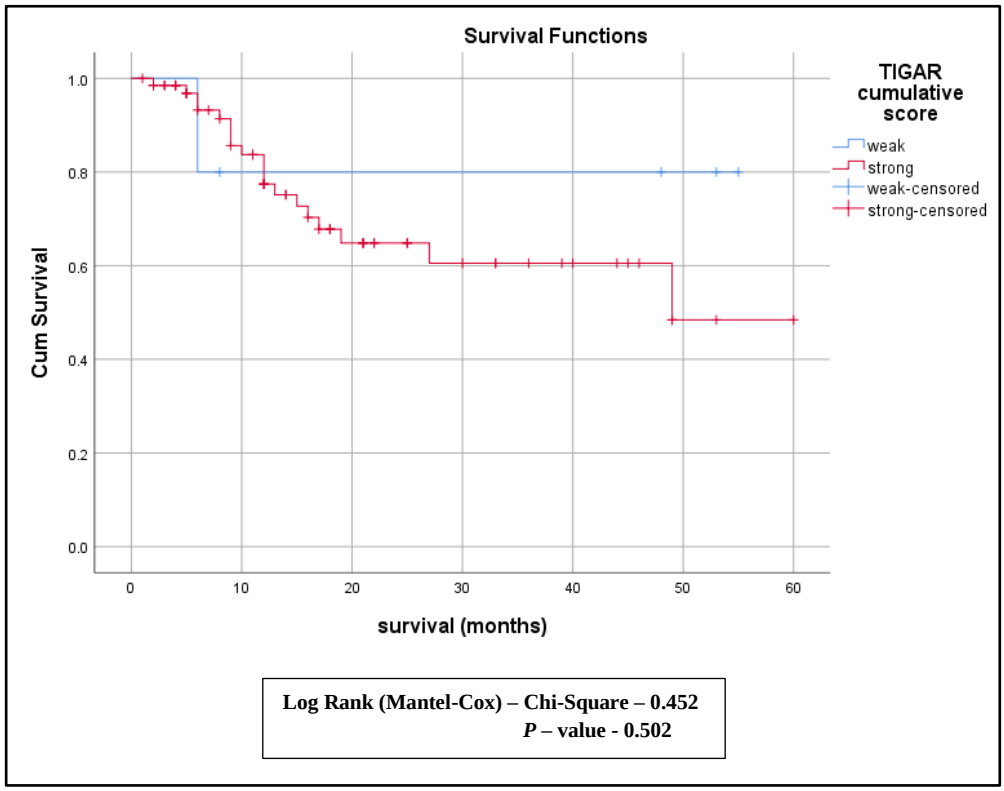

Figure 3:16 Disease-specific survival curve for weak and strong TIGAR expression in TMA set 1

3.2.3 Correlation between p53 and TIGAR expression in TMA set 1

We analysed whether there is an association between p53 and TIGAR expression in the samples of TMA set 1, and we found that there was no significant association between p53 and TIGAR expression (see table 3.15).

Table 3-15 Correlation between p53 and TIGAR expression in TMA set 1

		p53 expression		
		Inferred wild-type	**Inferred mutant**	
TIGAR expression	**Weak**	2	4	*P*-value 0.580
	Strong	17	56	

3.3 TMA set 2 - Immunohistochemistry analysis of p53, TIGAR and HK-2

The details of TMA set 2, including the selection of samples and TMA construction have been discussed in section 2.4.2.2. The scoring criteria for p53, TIGAR, and HK-2 expression has been discussed in section 2.4.4. For every protein expression analysis, we have performed frequency distribution, Chi-square statistics, and survival analysis. The layout of the TMA set 2 results given in table 3.16.

Table 3-16 Layout of TMA set 2 IHC results

p53 expression in larynx and hypopharynx		
Tumour core	Advancing front	Lymph node
Frequency distribution	Frequency distribution	Frequency distribution
Chi-square statistics	Chi-square statistics	Chi-square statistics
Survival analysis	Survival analysis	Survival analysis

p53 expression in the oropharynx		
Tumour core	Advancing front	Lymph node
Frequency distribution	Frequency distribution	Frequency distribution
Chi-square statistics	Chi-square statistics	Chi-square statistics
Survival analysis	Survival analysis	Survival analysis
p53 expression in the oropharynx in relation to HPV status		
Tumour core & advancing front		
Frequency distribution	Survival analysis	

HK-2 expression in larynx and hypopharynx		
Tumour core	Advancing front	Lymph node
Frequency distribution	Frequency distribution	Frequency distribution
Chi-square statistics	Chi-square statistics	Chi-square statistics
Survival analysis	Survival analysis	Survival analysis

Association between p53 and HK-2 expression in larynx and hypopharynx – Chi-square statistics

HK-2 expression in the oropharynx		
Tumour core	Advancing front	Lymph node
Frequency distribution	Frequency distribution	Frequency distribution
Chi-square statistics	Chi-square statistics	Chi-square statistics
Survival analysis	Survival analysis	Survival analysis

Association between p53 and HK-2 expression in the oropharynx – Chi-square statistics

3.3.1 p53 expression in larynx and hypopharynx primaries

The pattern of p53 expression in larynx and hypopharynx primaries is shown in figures 3.17 to 3.20.

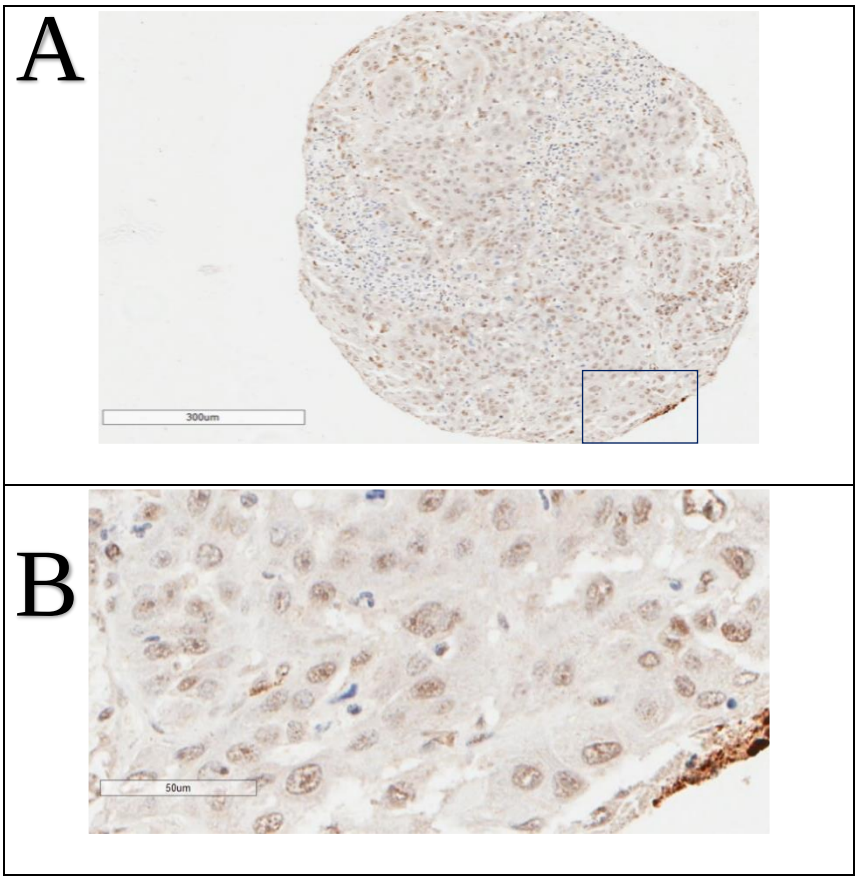

Figure 3:17 Immunohistochemical analysis of p53 expression in larynx samples. A tissue microarray (TMA) was stained using a mouse monoclonal antibody (DO-7) as described in section 2.4.3. This figure illustrates the magnified views of representative cores from TMA set 2. Magnification is represented by the individual scale bar in the figure. (A) represents inferred wild-type p53 (B) detailed image of the area indicated in blue in panel A

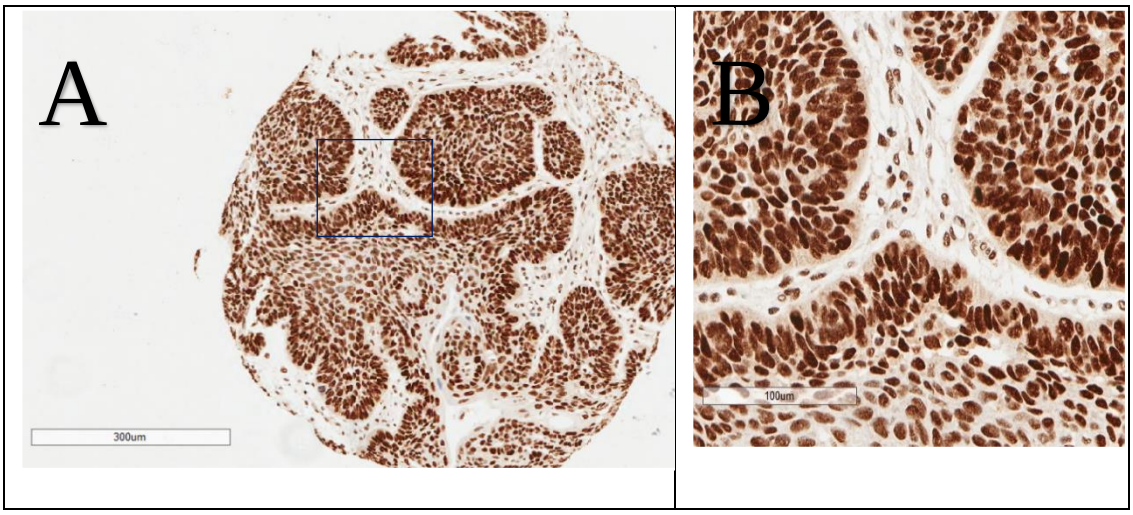

Figure 3:18 Immunohistochemical analysis of p53 expression in larynx samples. A tissue microarray (TMA) was stained using a mouse monoclonal antibody (DO-7) as described in section 2.4.3. This figure illustrates the magnified views of representative cores from TMA set 2. Magnification is represented by the individual scale bar in the figure. (A) represents inferred mutant p53 (B) detailed image of the area indicated in blue in panel A

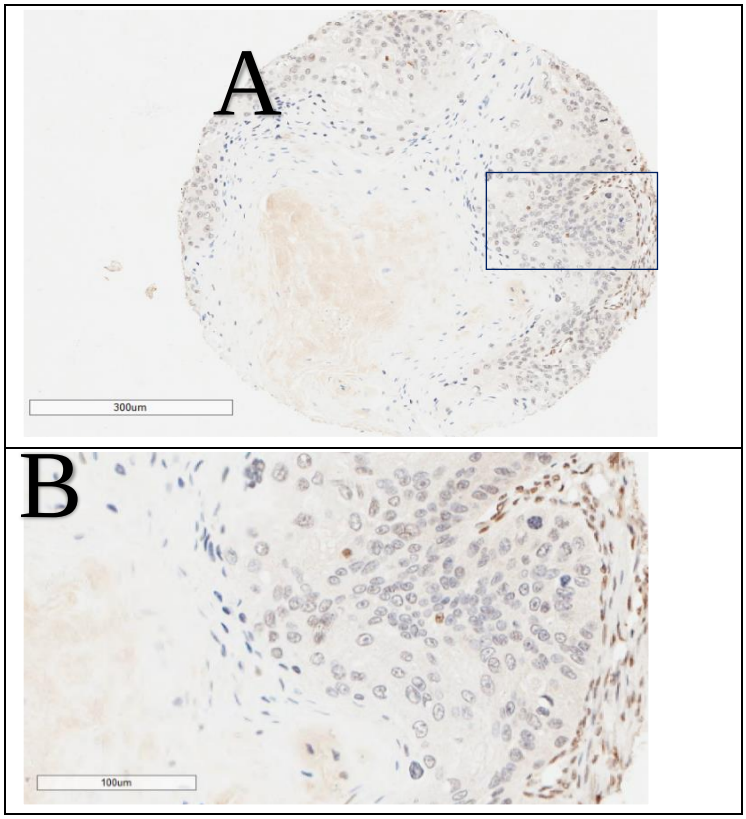

Figure 3:19 Immunohistochemical analysis of p53 expression in hypopharynx samples. A tissue microarray (TMA) was stained using a mouse monoclonal antibody (DO-7) as described in section 2.4.3. This figure illustrates the magnified views of representative cores from TMA set 2. Magnification is represented by the individual scale bar in the figure. (A) represents inferred wild-type p53 (B) detailed image of the area indicated in blue in panel A

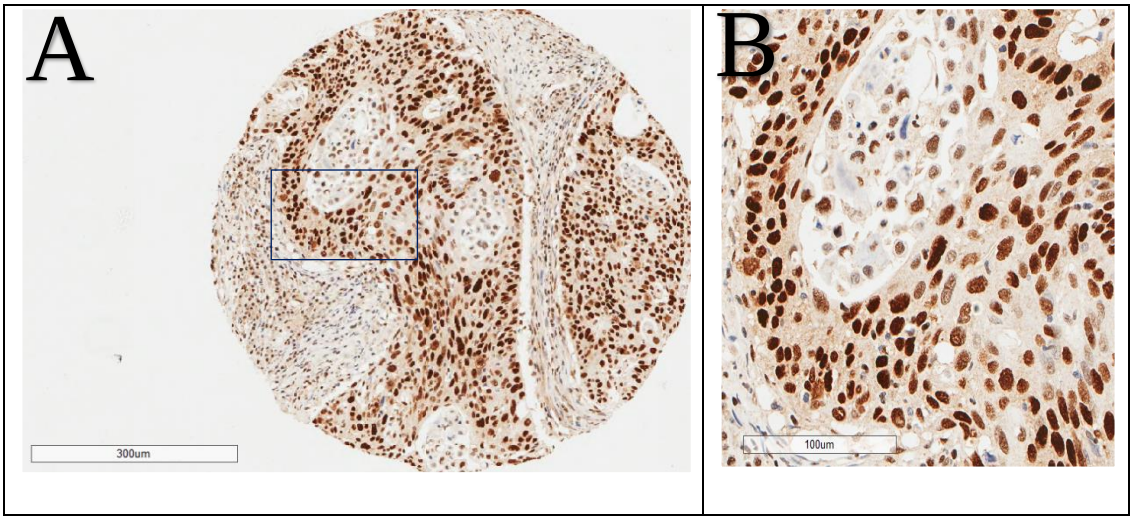

Figure 3:20 Immunohistochemical analysis of p53 expression in hypopharynx samples. A tissue microarray (TMA) was stained using a mouse monoclonal antibody (DO-7) as described in section 2.4.3. This figure illustrates the magnified views of representative cores from TMA set 2. Magnification is represented by the individual scale bar in the figure. (A) represents inferred mutant p53 (B) detailed image of the area indicated in blue in panel A

3.3.1.1 Association of p53 expression with clinical variables in tumour core samples of larynx and hypopharynx

We have observed 64.6% of 'inferred p53 mutation' in tumour core samples of larynx and hypopharynx primaries in TMA set 2 (see table 3.17).

Table 3-17 Frequency distribution of p53 expression in tumour core samples of larynx and hypopharynx

	Frequency	Percentage (%)
No tumour	4	4.0
Inferred wild-type	24	24.2
Inferred mutant	**64**	**64.6**
Missing	7	7.1
Total	99	100

We analysed whether any association between p53 expression in tumour core samples of larynx and hypopharynx with known clinical variables (see table 3.18).

Table 3-18 Association between p53 expression in tumour core and clinicopathological variables in larynx and hypopharynx ('no tumour' samples excluded)

	p53 expression – tumour core		
	Inferred wild-type	**Inferred mutant**	***P*- value**
Anatomical sites			
Larynx	21 (31.3)	46 (68.7)	0.139
Hypopharynx	2 (13.3)	13 (86.7)	
Larynx and Hypopharynx combined	0 (0.0)	5 (100.0)	
T stage			
T 1	1 (16.7)	5 (83.3)	0.653
T 2	3 (16.7)	15 (83.3)	
T 3	10 (30.3)	23 (69.7)	
T 4	9 (30.0)	21 (70.0)	
N stage			
N 0	13 (31.0)	29 (69.0)	0.754
N 1	2 (22.2)	7 (77.8)	
N 2	9 (24.3)	28 (75.7)	
Differentiation			
Well	5 (35.7)	9 (64.3)	0.396
Moderate	10 (21.3)	37 (78.7)	
Poor	9 (33.3)	18 (66.7)	
Invasive front			
Cohesive	6 (27.3)	16 (72.7)	0.918
Non-cohesive	17 (26.2)	48 (73.8)	
Vascular invasion			
Yes	4 (14.3)	24 (85.7)	0.062
No	20 (33.3)	40 (66.7)	
Nerve invasion			
Yes	6 (21.4)	22 (78.6)	0.376
No	18 (30.5)	41 (69.5)	
ECS			
Yes	7 (25.9)	20 (74.1)	0.703
No	4 (21.1)	15 (78.9)	
Death			
Yes	11 (33.3)	22 (66.7)	0.254
No	12 (22.2)	42 (77.8)	

NOTE. Values are n(%). (ECS – extracapsular spread) P-value determined by Pearson Chi-Square test.

3.3.1.2 Association of p53 expression with clinical variables in advancing front samples of larynx and hypopharynx

We have observed 49.5% of 'inferred p53 mutation' in advancing front samples from larynx and hypopharynx primaries in TMA set 2 (see table 3.19).

Table 3-19 Frequency distribution of p53 expression in advancing front of larynx and hypopharynx

	Frequency	Percentage (%)
No tumour	19	19.2
Inferred wild-type	27	27.3
Inferred mutant	**49**	**49.5**
Missing	4	4.0
Total	99	100

We analysed whether any association between p53 expression in advancing front samples of larynx and hypopharynx with known clinical variables (see table 3.20).

Table 3-20 Association between p53 expression in advancing front and clinicopathological variables in larynx and hypopharynx ('no tumour' samples excluded)

	p53 expression – advancing front		
	Inferred wild-type	**Inferred mutant**	***P*- value**
Anatomical sites			
Larynx	22 (40.0)	33 (60.0)	0.471
Hypopharynx	4 (26.7)	11 (73.3)	
Larynx and Hypopharynx combined	1 (20.0)	4 (80.0)	
T stage			
T 1	1 (33.3)	2 66.7)	0.307
T 2	2 (14.3)	12 (85.7)	
T 3	11 (40.7)	16 (59.3)	
T 4	13 (41.9)	18 (58.1)	
N stage			
N 0	12 (40.0)	18 (60.0)	0.478
N 1	5 (45.5)	6 (54.5)	
N 2	10 (28.6)	25 (71.4)	
Differentiation			
Well	5 (41.7)	7 (58.3)	0.570
Moderate	12 (30.0)	28 (70.0)	
Poor	10 (41.7)	14 (58.3)	
Invasive front			
Cohesive	5 (31.3)	11 (68.8)	0.655
Non-cohesive	22 (37.3)	37 (62.7)	
Vascular invasion			
Yes	7 (25.0)	21 (75.0)	0.143
No	20 (41.7)	28 (58.3)	
Nerve invasion			
Yes	12 (52.2)	11 (47.8)	0.060
No	15 (29.4)	36 (70.6)	
ECS			
Yes	6 (23.1)	20 (76.9)	0.088
No	9 (47.4)	10 (52.6)	
Death			
Yes	15 (45.5)	18 (54.5)	0.082
No	11 (26.2)	31 (73.8)	

NOTE. Values are n(%). (ECS – extracapsular spread) P-value determined by Pearson Chi-Square test.

3.3.1.3 Disease-specific survival analysis of p53 expression in tumour core samples of larynx and hypopharynx

Kaplan-Meier survival analysis was conducted as described in 2.4.8 to compare the survival period between two categories of p53 expression in tumour core samples of larynx and hypopharynx; inferred mutant and inferred wild-type (see Table 3.21 for case processing summary) in TMA set 2.

Table 3-21 Case processing summary for survival analysis of p53 expression in tumour core samples of larynx and hypopharynx samples

p53 expression	Total No	No of deaths	No of censored	Percentage
inferred wild-type	14	10	4	28.6%
inferred mutant	33	22	11	33.3%
Overall	47	32	15	31.9%

A log-rank test was conducted to determine whether there were any differences in the survival distributions between inferred wild-type and inferred mutant types (see figure 3.21).

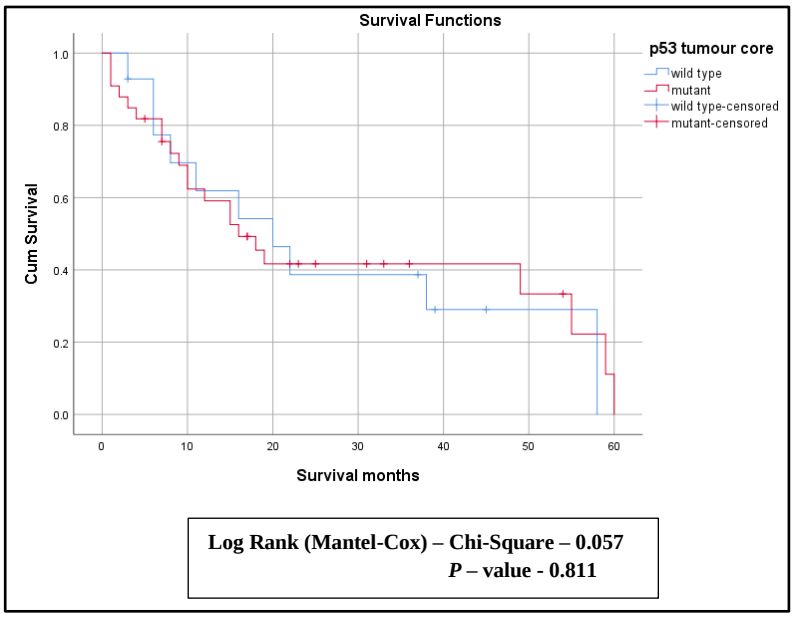

Figure 3:21 Disease-specific survival curve for inferred wild-type and inferred mutant categories in tumour core samples of larynx and hypopharynx

3.3.1.4 Disease-specific survival analysis of p53 expression in the advancing front samples from larynx and hypopharynx

Kaplan-Meier survival analysis was conducted as described in 2.4.8 to compare the survival period between two categories of p53 expression in advancing front samples of larynx and hypopharynx; inferred mutant and inferred wild-type (see Table 3.22 for case processing summary) in TMA set 2.

Table 3-22 Case processing summary for survival analysis of p53 expression in advancing front samples of larynx and hypopharynx samples

p53 expression	Total No	No of deaths	No of censored	% of censored cases
inferred wild-type	16	14	2	12.5%
inferred mutant	29	18	11	37.9%
Overall	45	32	13	28.9%

A log-rank test was conducted to determine whether there were any differences in the survival distributions between inferred wild-type and inferred mutant types (see figure 3.22).

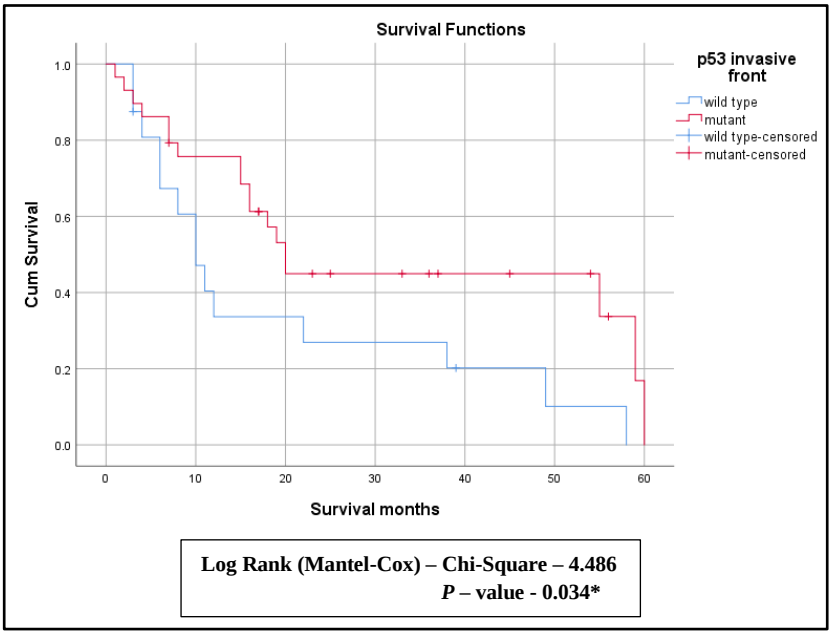

Figure 3:22 Disease-specific survival curve for inferred wild-type and inferred mutant categories in advancing front samples of larynx and hypopharynx **(* statistically significant at 5%)**

3.3.2 p53 expression in larynx and hypopharynx lymph nodes

Out of 99 larynx and hypopharynx samples, 31 samples were lymph node-positive. The pattern of p53 expression in lymph node samples of larynx and hypopharynx was represented in figures 3.23 and 3.24, respectively.

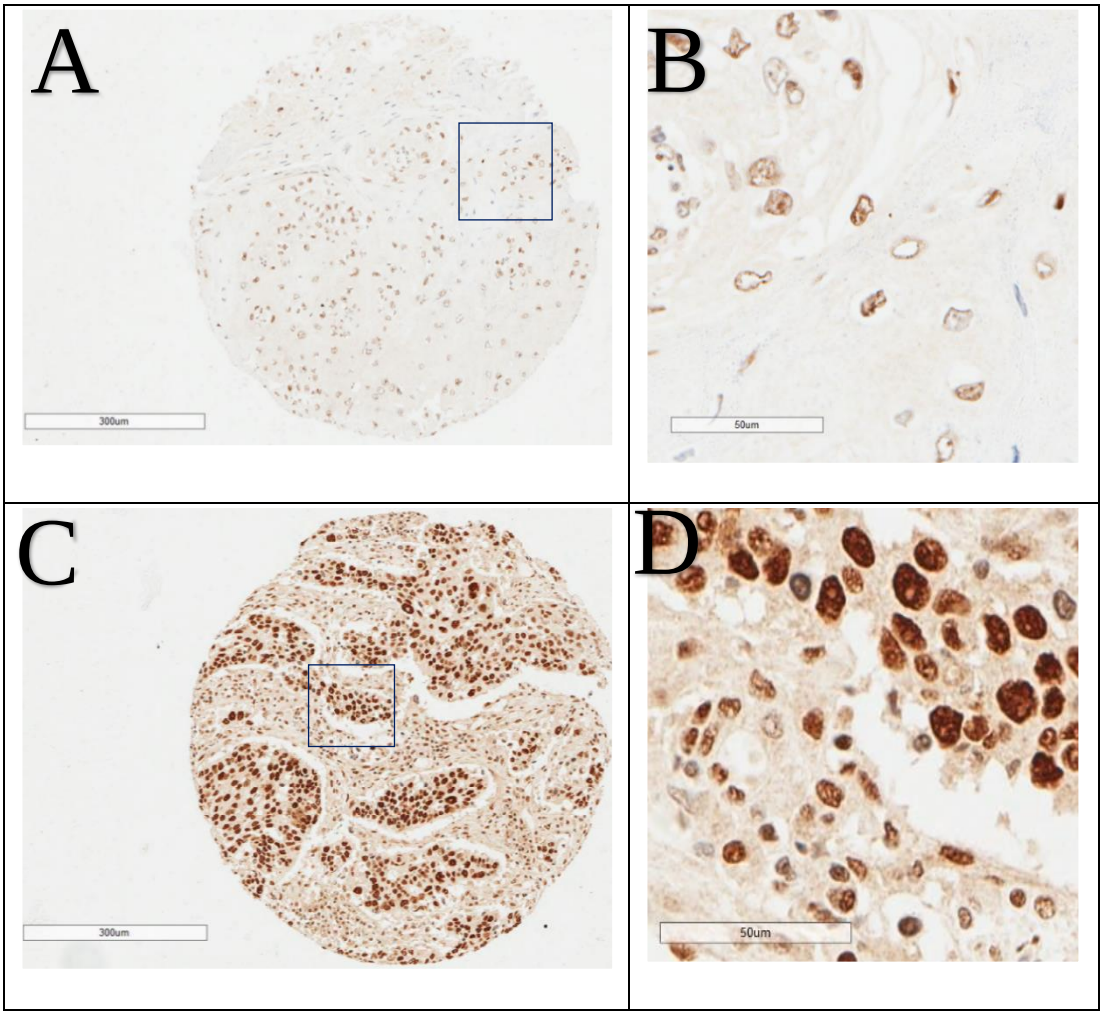

Figure 3:23 Immunohistochemical analysis of p53 expression in larynx lymph nodes. A tissue microarray (TMA) was stained using a mouse monoclonal antibody (DO-7) as described in section 2.4.3. This figure illustrates the magnified views of representative cores from TMA set 2. Magnification is represented by the individual scale bar in the figure. (A) represents inferred wild-type p53 (B) detailed image of the area indicated in blue in panel A (C) represents inferred mutant p53 (D) detailed image of the area indicated in blue in panel C

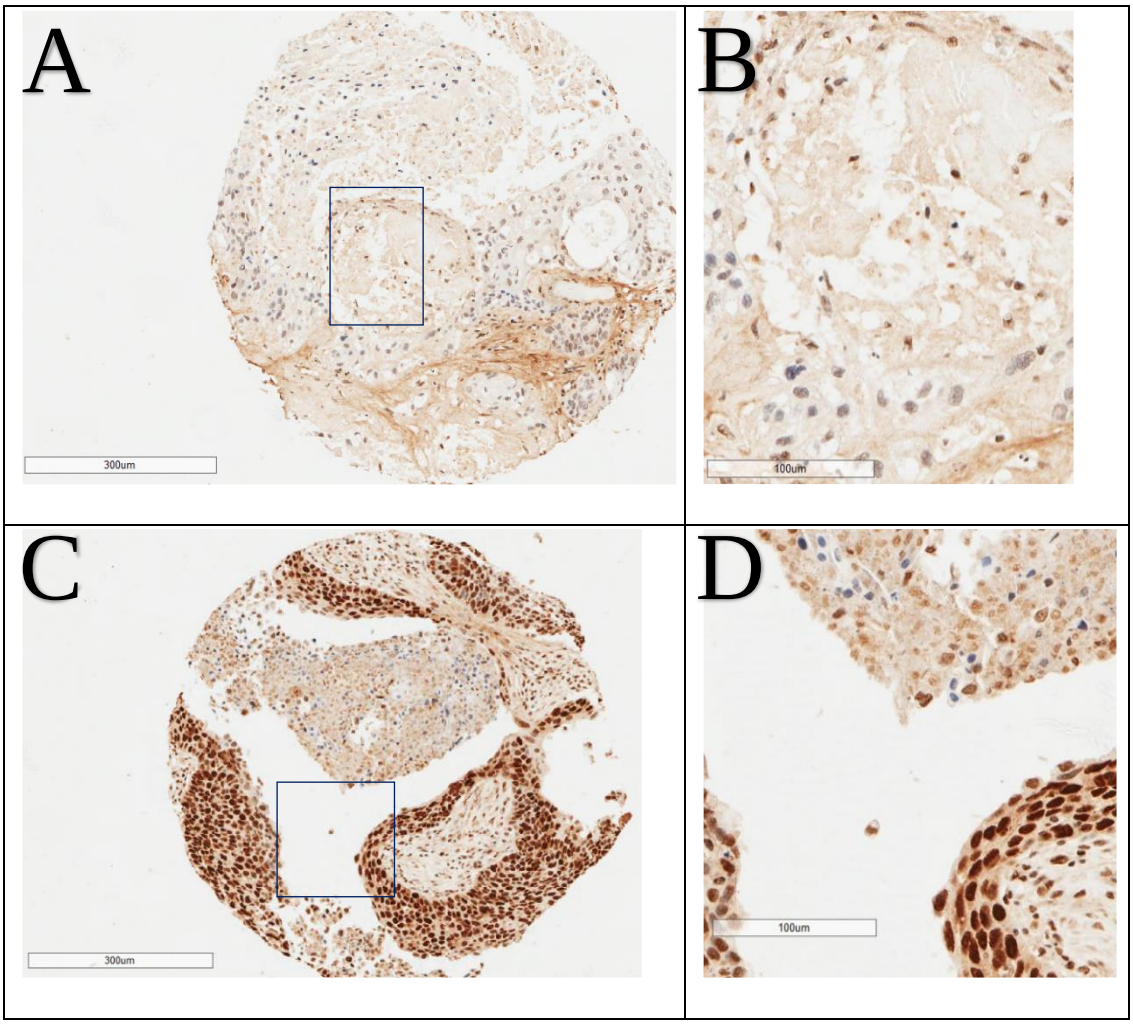

Figure 3:24 Immunohistochemical analysis of p53 expression in hypopharynx lymph nodes. A tissue microarray (TMA) was stained using a mouse monoclonal antibody (DO-7) as described in section 2.4.3. This figure illustrates the magnified views of representative cores from TMA set 2. Magnification is represented by the individual scale bar in the figure. (A) represents inferred wild-type p53 (B) detailed image of the area indicated in blue in panel A (C) represents inferred mutant p53 (D) detailed image of the area indicated in blue in panel C

3.3.2.1 Association of p53 expression with clinical variables in lymph nodes samples of larynx and hypopharynx

We have observed 83.9% of 'inferred p53 mutation' in the larynx, and hypopharynx lymph nodes in TMA set 2 (see table 3.23).

Table 3-23 Frequency distribution of p53 expression in lymph nodes of larynx and hypopharynx

	Frequency	Percentage (%)
No tumour	3	9.7
Inferred wild-type	2	6.5
Inferred mutant	**26**	**83.9**
Total	31	100

We analysed whether any association present between p53 expression in lymph node samples of larynx and hypopharynx with known clinical variables (see table 3.24).

Table 3-24 Association between p53 expression in lymph nodes of larynx and hypopharynx and clinicopathological variables ('no tumour' samples excluded)

	p53 expression – lymph nodes		
	Inferred wild-type	**Inferred mutant**	***P*- value**
Anatomical sites			
Larynx	0 (0.0)	16 (100.0)	0.144
Hypopharynx	2 (20.0)	8 (80.0)	
Larynx and Hypopharynx combined	0 (0.0)	2 (100.0)	
T stage			
T 1	0 (0.0)	1 (100.0)	0.442
T 2	1 (25.0)	3 (75.0)	
T 3	0 (0.0)	9 (100.0)	
T 4	1 (7.1)	13 (92.9)	
N stage			
N 1	0 (0.0)	5 (100.0)	0.494
N 2	2 (8.7)	21 (91.3)	
Differentiation			
Well	0 (0.0)	0 (0.0)	1.000
Moderate	1 (7.1)	13 (92.9)	
Poor	1 (7.1)	13 (92.9)	
Invasive front			
Cohesive	0 (0.0)	6 (100.0)	0.586
Non-cohesive	1 (4.8)	20 (95.2)	
Vascular invasion			
Yes	0 (0.0)	13 (100.0)	0.172
No	2 (13.3)	13 (86.7)	
Nerve invasion			
Yes	1 (10.0)	9 (90.0)	0.693
No	1 (5.9)	16 (94.1)	
ECS			
Yes	2 (13.3)	13 (86.7)	0.189
No	0 (0.0)	12 (100.0)	
Death			
Yes	1 (6.3)	15 (93.8)	0.832
No	1 (8.3)	11 (91.7)	

NOTE. Values are n(%). (ECS – extracapsular spread) P-value determined by Pearson Chi-Square test.

3.3.2.2 Disease-specific survival analysis of p53 expression in larynx and hypopharynx lymph nodes

Kaplan-Meier survival analysis was conducted as described in 2.4.8 to compare the survival period between two categories of p53 expression in lymph nodes samples in larynx and hypopharynx; inferred mutant and inferred wild-type (see Table 3.25) for case processing summary in TMA set 2.

Table 3-25 Case processing summary for survival analysis of p53 expression in lymph nodes samples of larynx and hypopharynx

p53 expression	Total No	No of deaths	No of censored	% of censored cases
inferred wild-type	1	1	0	0.0%
inferred wild-type	22	15	7	31.8%
Overall	23	16	7	30.4%

A log-rank test was conducted to determine whether there were any differences in the survival distributions between inferred wild-type and inferred mutant types in lymph nodes samples (see figure 3.25).

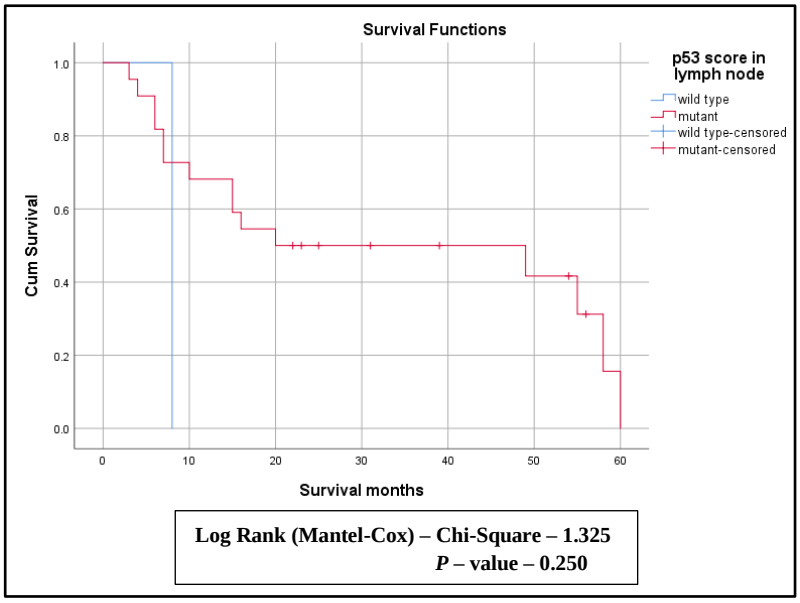

Figure 3:25 Disease-specific survival curve for inferred wild-type and inferred mutant samples from lymph nodes of larynx and hypopharynx

3.3.3 p53 expression in oropharynx primaries

The pattern of p53 expression in oropharynx primaries was represented in figures 3.26.

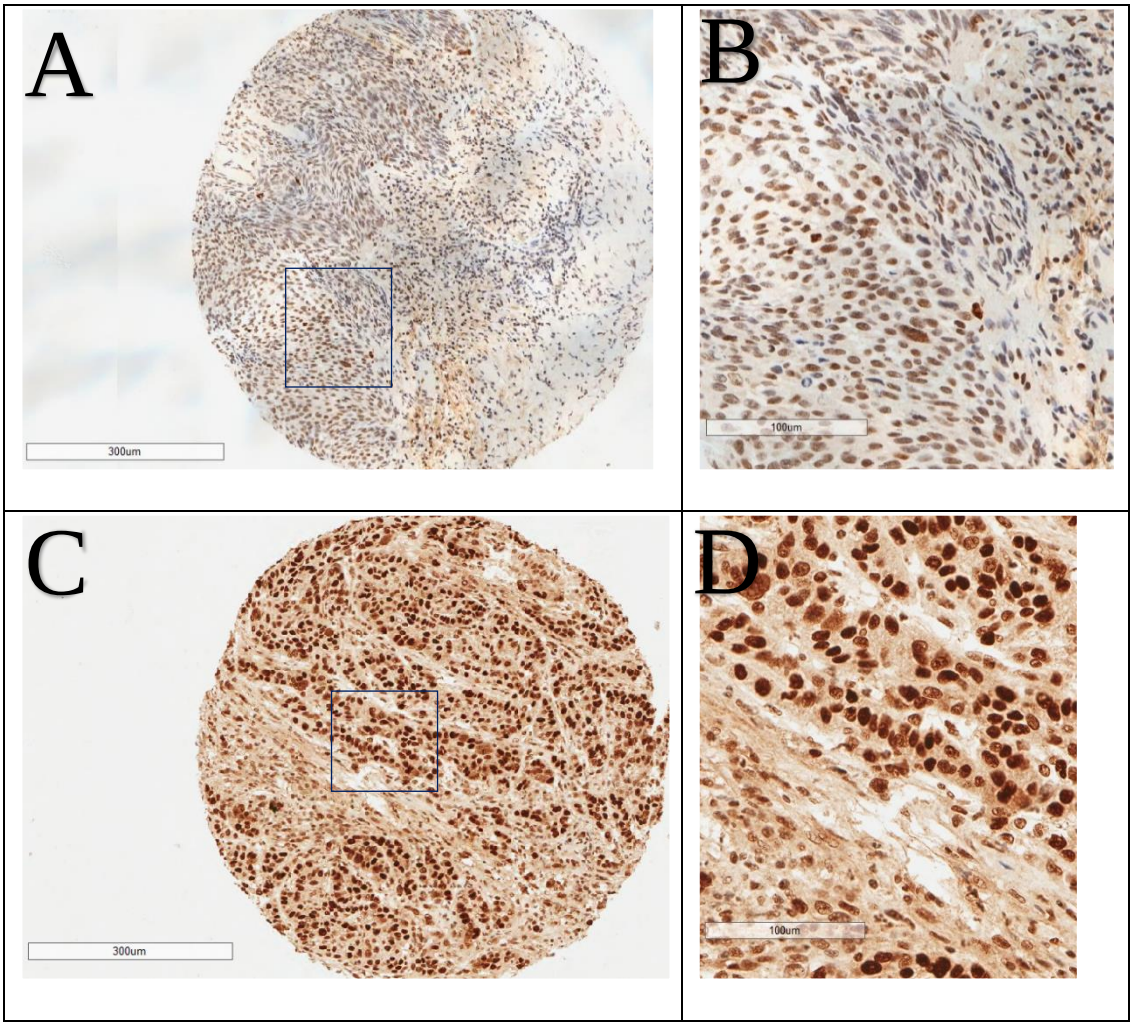

Figure 3:26 Immunohistochemical analysis of p53 expression in oropharynx primaries. A tissue microarray (TMA) was stained using a mouse monoclonal antibody (DO-7) as described in section 2.4.3. This figure illustrates the magnified views of representative cores from TMA set 2. Magnification is represented by the individual scale bar in the figure. (A) represents inferred wild-type p53 (B) detailed image of the area indicated in blue in panel A (C) represents inferred mutant p53 (D) detailed image of the area indicated in blue in panel C

3.3.3.1 Association of p53 expression with clinical variables in tumour core samples of the oropharynx

We have observed 72.6% of 'inferred p53 mutation' in tumour core samples of oropharynx primaries in TMA set 2 (see table 3.26).

Table 3-26 Frequency distribution of p53 expression in tumour core samples of the oropharynx

	Frequency	Percentage (%)
No tumour	1	1.6
Inferred wild-type	14	22.6
Inferred mutant	**45**	**72.6**
Missing	2	3.2
Total	62	100

We analysed whether any association present between p53 expression in tumour core samples of oropharynx primaries with known clinical variables (see table 3.27).

Table 3-27 Association between p53 expression in tumour core samples and clinicopathological variables in the oropharynx ('no tumour' samples excluded)

	p53 expression– tumour core		
	Inferred wild-type	**Inferred mutant**	***P*- value**
Anatomical sites			
Tonsil	5 (14.7)	29 (85.3)	0.011*
Tongue base	4 (22.2)	14 (77.8)	
Palate	4 (80.0)	1 (20.0)	
Posterior pharyngeal wall	1 (50.0)	1 (50.0)	
T stage			
T 1	1 (11.1)	8 (88.9)	0.399
T 2	8 (23.5)	26 (76.5)	
T 3	5 (35.7)	9 (64.3)	
N stage			
N 0	2 (28.6)	5 (71.4)	0.692
N 1	3 (33.3)	6 (66.7)	
N 2	9 (20.9)	34 (79.1)	
Differentiation			
Well	1 (33.3)	2 (66.7)	0.734
Moderate	4 (30.8)	9 (69.2)	
Poor	9 (21.4)	33 (78.6)	
Invasive front			
Cohesive	5 (21.7)	18 (78.3)	0.729
Non-cohesive	9 (25.7)	26 (74.3)	
Vascular invasion			
Yes	4 (25.0)	12 (75.0)	0.889
No	10 (23.3)	33 (76.7)	
Nerve invasion			
Yes	2 (22.2)	7 (77.8)	0.908
No	12 (24.0)	38 (76.0)	
ECS			
Yes	6 (25.0)	18 (75.0)	0.761
No	6 (21.4)	22 (78.6)	
Death			
Yes	6 (50.0)	6 (50.0)	0.017*
No	8 (17.0)	39 (83.0)	

NOTE. Values are n (%). (ECS – extracapsular spread) P-value determined by Pearson Chi-Square test. (*statistically significant at 5%)

3.3.3.2 Association of p53 expression with clinical variables in the advancing front samples of the oropharynx

We have observed 50.0% of 'inferred p53 mutation' in oropharynx primaries in TMA set 2 (see table 3.28).

Table 3-28 Frequency distribution of p53 in advancing front of the oropharynx

	Frequency	Percentage (%)
No tumour	13	21.0
Inferred wild-type	14	22.6
Inferred mutant	**31**	**50.0**
Missing	4	6.5
Total	62	100

We analysed whether any association present between p53 expression in samples from the advancing front of the oropharynx with known clinical variables (see table 3.29).

Table 3-29 Association between p53 expression in the advancing front samples of the oropharynx and clinicopathological variables ('no tumour' samples excluded)

	p53 – advancing front		
	Inferred wild-type	**Inferred mutant**	***P*- value**
Anatomical sites			
Tonsil	4 (16.7)	20 (83.3)	0.015*
Tongue base	5 (33.3)	10 (66.7)	
Palate	3 (75.0)	1 (25.0)	
Posterior pharyngeal wall	2 (100.0)	0 (0.0)	
T stage			
T 1	1 (14.3)	6 (85.7)	0.529
T 2	9 (36.0)	16 (64.0)	
T 3	4 (36.4)	7 (63.6)	
N stage			
N 0	2 (50.0)	2 (50.0)	0.150
N 1	4 (57.1)	3 (42.9)	
N 2	8 (23.5)	26 (76.5)	
Differentiation			
Well	0 (0.0)	2 (100.0)	0.596
Moderate	4 (30.8)	9 (69.2)	
Poor	10 (34.5)	19 (65.5)	
Invasive front			
Cohesive	4 (22.2)	14 (77.8)	0.256
Non-cohesive	10 (38.5)	16 (61.5)	
Vascular invasion			
Yes	2 (16.7)	10 (83.3)	0.207
No	12 (36.4)	21 (63.6)	
Nerve invasion			
Yes	3 (50.0)	3 (50.0)	0.283
No	11 (28.2)	28 (71.8)	
ECS			
Yes	6 (31.6)	13 (68.4)	0.763
No	6 (27.3)	16 (72.7)	
Death			
Yes	4 (40.0)	6 (60.0)	0.491
No	10 (28.6)	25 (71.4)	

NOTE. Values are n (%). (ECS – extracapsular spread) P-value determined by Pearson Chi-Square test. (* represents statistically significant value)

3.3.3.3 Disease-specific survival analysis of p53 expression in tumour core samples of the oropharynx

Kaplan-Meier survival analysis was conducted as described in 2.4.8 to compare the survival period between two categories of p53 expression in tumour core samples of oropharynx, namely, inferred wild-type and inferred mutant (see Table 3.30 for case processing summary) in TMA set 2.

Table 3-30 Case processing summary for survival analysis of p53 expression in tumour core samples of the oropharynx

p53 expression	Total No	No of deaths	No of censored	% of censored cases
inferred wild-type	12	4	8	66.7%
inferred mutant	45	6	39	86.7%
Overall	57	10	47	82.5%

A log-rank test was conducted to determine whether there were any differences in the survival distributions between inferred wild-type and inferred mutant types (see figure 3.27).

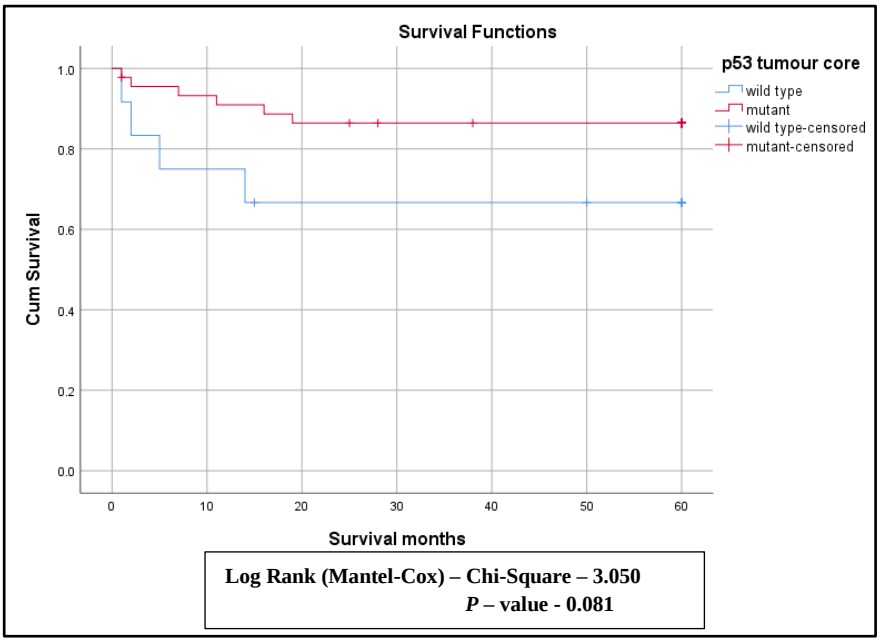

Figure 3:27 Disease-specific survival curve for inferred wild-type and inferred mutant categories in the tumour core samples of oropharynx

3.3.3.4 Disease-specific survival analysis of p53 expression in advancing front samples from the oropharynx

Kaplan-Meier survival analysis was conducted as described in 2.4.5 to compare the survival period between two categories of p53 expression in advancing front samples of oropharynx, namely, inferred wild-type and inferred mutant (see Table 3.31 for case processing summary) in TMA set 2.

Table 3-31 Case processing summary for survival analysis of p53 expression in advancing front samples of the oropharynx

p53 expression	Total No	No of deaths	No of censored	% of censored cases
inferred wild-type	14	4	10	71.4%
inferred mutant	30	5	25	83.3%
Overall	44	9	35	79.5%

A log-rank test was conducted to determine whether there were any differences in the survival distributions between inferred wild-type and inferred mutant types (see figure 3.28).

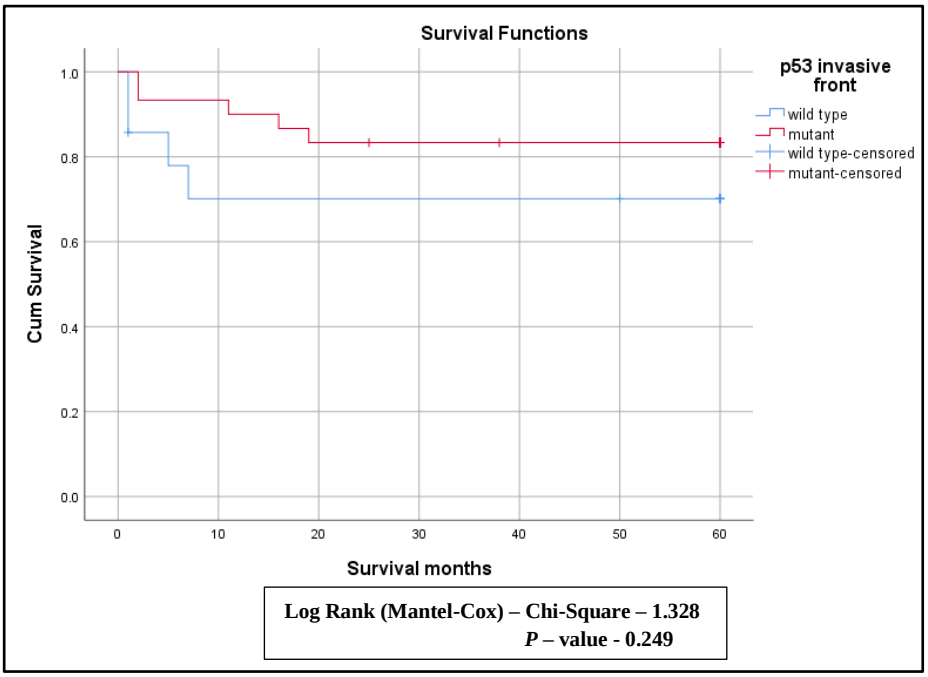

Figure 3:28 Disease-specific survival curve for inferred wild-type and inferred mutant in the advancing front samples from oropharynx

3.3.4 p53 expression in oropharynx lymph nodes

The pattern of p53 expression in lymph node samples in the oropharynx was represented in figures 3.29.

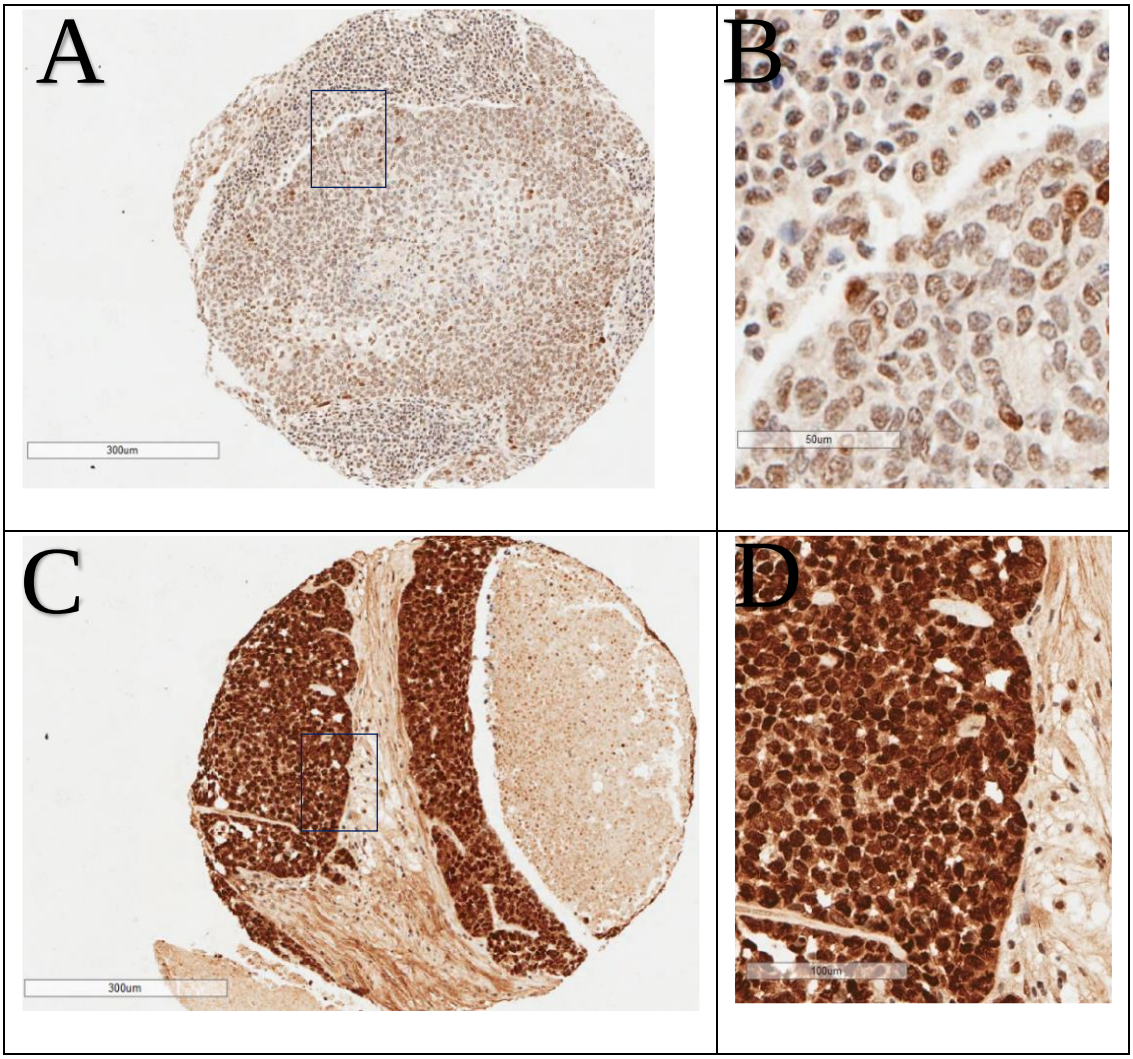

Figure 3:29 Immunohistochemical analysis of p53 expression in oropharynx lymph nodes. A tissue microarray (TMA) was stained using a mouse monoclonal antibody (DO-7) as described in section 2.4.3. This figure illustrates the magnified views of representative cores from TMA set 2. Magnification is represented by the individual scale bar in the figure. (A) represents inferred wild-type p53 (B) detailed image of the area indicated in blue in panel A (C) represents inferred mutant p53 (D) detailed image of the area indicated in blue in panel C

3.3.4.1 Association of p53 expression with clinical variables in oropharynx lymph nodes

We have observed 79.3% of 'inferred p53 mutation' in lymph nodes samples from the oropharynx in TMA set 2 (see table 3.32).

Table 3-32 Frequency distribution of p53 expression in lymph nodes of the oropharynx

	Frequency	Percentage (%)
No tumour	1	3.4
Inferred wild-type	5	17.2
Inferred mutant	23	79.3
Total	**29**	**100**

We analysed whether any association present between p53 expression in the lymph nodes samples from the oropharynx with known clinical variables (see table 3.33).

Table 3-33 Association between p53 expression in lymph nodes and clinicopathological variables in the oropharynx ('no tumour' samples excluded)

	p53 expression – lymph nodes		
	Inferred wild-type	**Inferred mutant**	***P*- value**
Anatomical sites			
Tonsil	3 (20.0)	12 (80.0)	0.786
Tongue base	2 (18.2)	9 (81.8)	
Palate	0 (0.0)	0 (0.0)	
Posterior pharyngeal wall	0 (0.0)	2 (100.0)	
T stage			
T 1	1 (20.0)	4 (80.0)	0.989
T 2	3 (18.8)	13 (81.3)	
T 3	1 (16.7)	5 (83.3)	
N stage			
N 1	0 (0.0)	5 (100.0)	0.250
N 2	5 (21.7)	18 (78.3)	
Differentiation			
Well	1 (100.0)	0 (0.0)	0.058
Moderate	0 (0.0)	5 (100.0)	
Poor	4 (18.2)	18 (81.8)	
Invasive front			
Cohesive	2 (16.7)	10 (83.3)	0.887
Non-cohesive	3 (18.8)	13 (81.3)	
Vascular invasion			
Yes	2 (20.0)	8 (80.0)	0.825
No	3 (16.7)	15 (83.3)	
Nerve invasion			
Yes	1 (16.7)	5 (83.3)	0.932
No	4 (18.2)	18 (81.8)	
ECS			
Yes	2 (15.4)	11 (84.6)	0.750
No	3 (20.0)	12 (80.0)	
Death			
Yes	1 (14.3)	6 (85.7)	0.776
No	4 (19.0)	17 (81.0)	

NOTE. Values are n (%). (ECS – extracapsular spread) P-value determined by Pearson Chi-Square test.

3.3.4.2 Disease-specific survival analysis of p53 expression in oropharynx lymph nodes

Kaplan-Meier survival analysis was conducted as described in 2.4.8 to compare the survival period between two categories of p53 expression in lymph nodes samples of oropharynx, namely, inferred mutant and inferred wild-type (see Table 3.34 for case processing summary) in TMA set 2.

Table 3-34 Case processing summary for survival analysis of p53 expression in lymph nodes samples of the oropharynx

p53 expression	Total No	No of deaths	No of censored	% of censored cases
inferred wild-type	4	0	4	100.0%
inferred mutant	23	6	17	73.9%
Overall	27	6	21	77.8%

A log-rank test was conducted to determine whether there were any differences in the survival distributions between inferred wild-type and inferred mutant types (see figure 3.30).

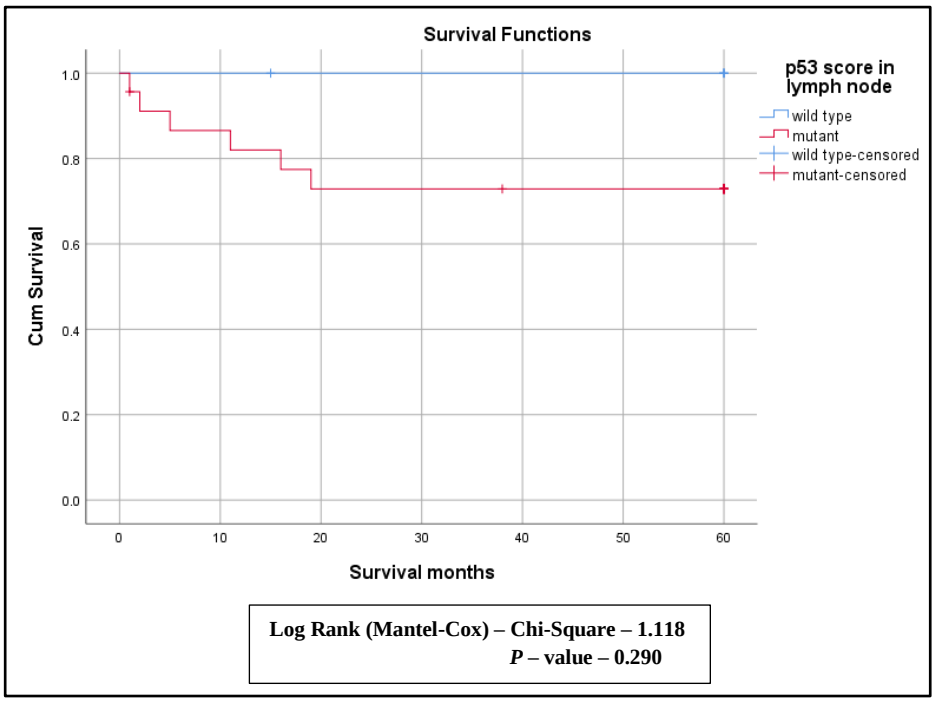

Figure 3:30 Disease-specific survival curve for inferred wild-type and inferred mutants in lymph nodes samples of oropharynx

3.3.5 p53 expression in relation to HPV status in oropharynx primaries

Out of 62 oropharynx samples in TMA set 2, forty-five cases were HPV +ve, and fifteen cases were HPV -ve (missing 2 cases).

3.3.5.1 Frequency distribution of p53 expression in HPV positive oropharynx primaries (tumour core and advancing front samples)

We have noticed 80% of 'inferred p53 mutant' levels in the tumour core samples of HPV positive cases (see table 3.35).

Table 3-35 p53 Frequency distribution of tumour core samples in relation to HPV status (missing – 3)

	HPV negative	HPV positive	Total
No tumour	0 (0.0%)	1 (100.0%)	1
Wild type	6 (46.2%)	7 (53.8%)	13
Mutant	9 (20.0%)	36 (80.0%)	45
Total	15 (25.4%)	44 (74.6%)	59 (100.0%

We have noticed 83.9% of 'inferred p53 mutant' levels in the advancing front samples of HPV positive cases (see table 3.36).

Table 3-36 Frequency distribution of advancing front samples in relation to HPV status (missing – 5)

	HPV negative	HPV positive	Total
No tumour	4 (33.3%)	8 (66.7%)	12
Wild type	6 (42.9%)	8 (57.1%)	14
Mutant	5 (16.1%)	26 (83.9%)	31
Total	15 (26.3%)	42 (73.7%)	57 (100.0%)

3.3.5.2 Disease-specific survival analysis between HPV positive and negative cases in the oropharynx

Kaplan-Meier survival analysis was conducted as described in 2.4.8 to compare the survival period between HPV positive and HPV negative cases in oropharynx samples (see Table 3.37 for case processing summary) in TMA set 2.

Table 3-37 Case processing summary – HPV status in oropharynx samples

HPV status	Total No	No of deaths	No of censored	% of censored cases
Negative	14	7	7	50.0%
Positive	44	3	41	93.2%
Overall	58	10	48	82.8%

A log-rank test was conducted to determine whether there were any differences in the survival distributions between HPV positive and HPV negative cases (see figure 3.31).

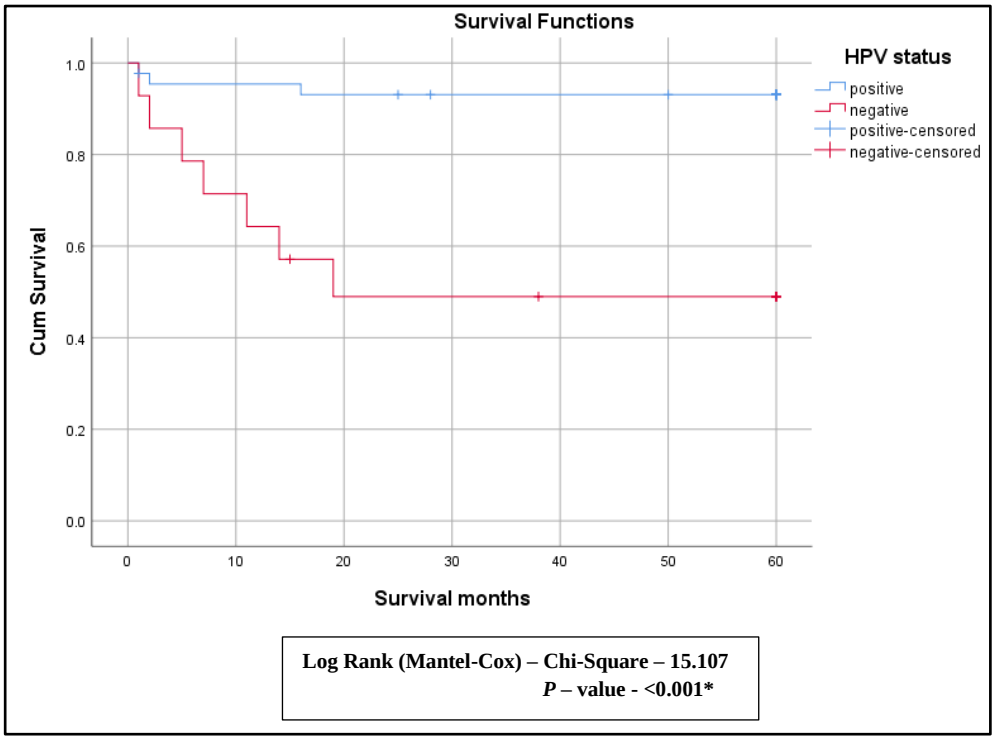

Figure 3:31 Disease-specific survival curve for HPV positive and HPV negative cases in oropharynx samples **(* statistically significant at 5%)**

3.3.6 TIGAR expression in TMA set 2

The immunohistochemical method for TIGAR staining was discussed in section 2.4.3. Examples of TMA slides with TIGAR staining were shown in section 2.4.2.2.

We observed 'strong' TIGAR expression in most of the tumour samples (99% in the advancing front of the tumours, 99% in the tumour core samples, and 100% in the neck nodes).

Since nearly all samples display high levels of TIGAR expression, it is not possible to compare strong and weak expressors, and TIGAR expression was not considered for further statistical analysis.

The following figure 3.32 shows the examples of strong TIGAR staining in the larynx, hypopharynx, and oropharynx samples.

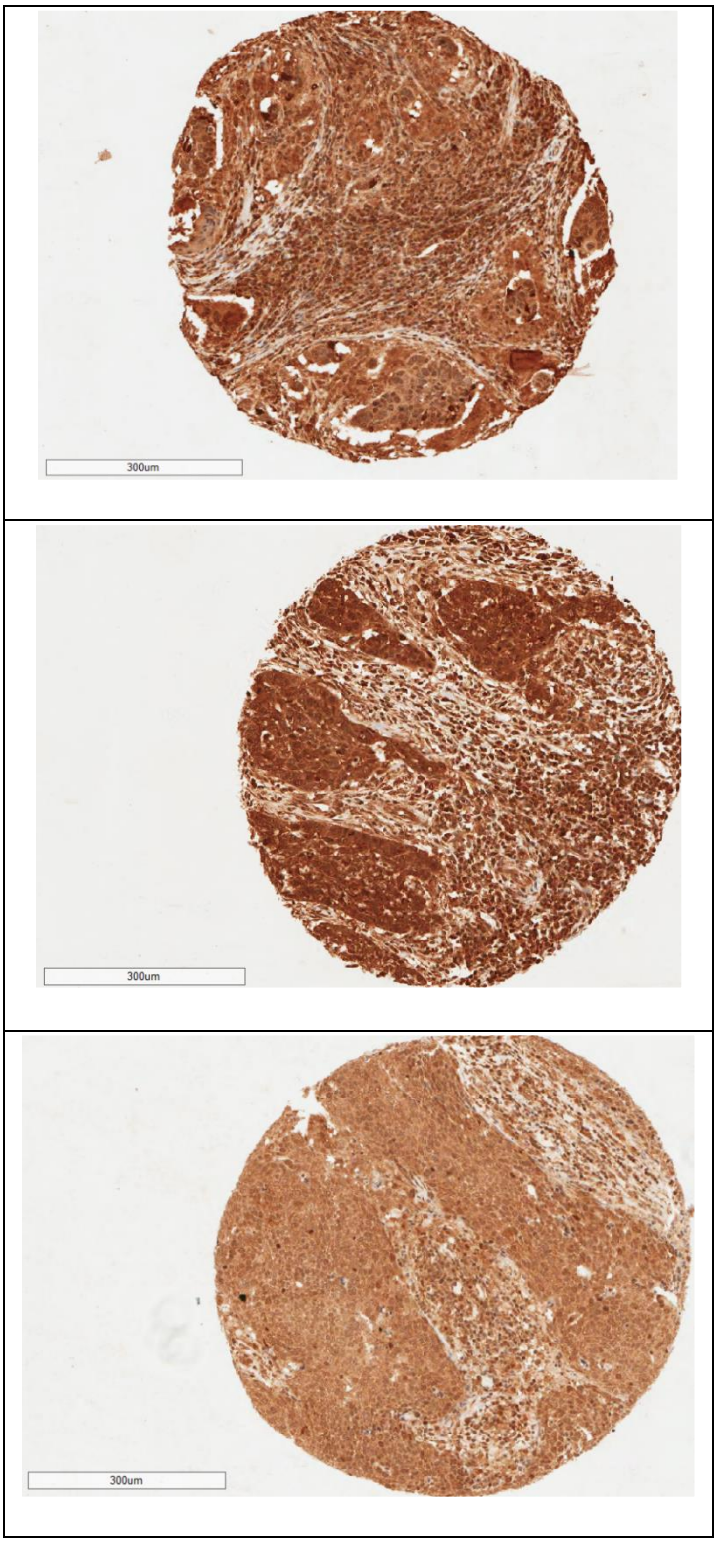

Figure 3:32 Immunohistochemical analysis of TIGAR expression TMA set 2. A tissue microarray (TMA) was stained using a purified rabbit polyclonal antibody (AB10545), as described in section 2.4.3. This figure illustrates the magnified views of representative cores from TMA set 2. Magnification is represented by the individual scale bar in the figure. (A) represents TIGAR expression in larynx primary tumour (B) represents TIGAR expression in hypopharynx primary tumour (C) represents TIGAR expression in oropharynx primary tumour

3.3.7 HK-2 expression in larynx and hypopharynx primaries

The pattern of HK-2 expression in larynx primaries is shown in figure 3.33.

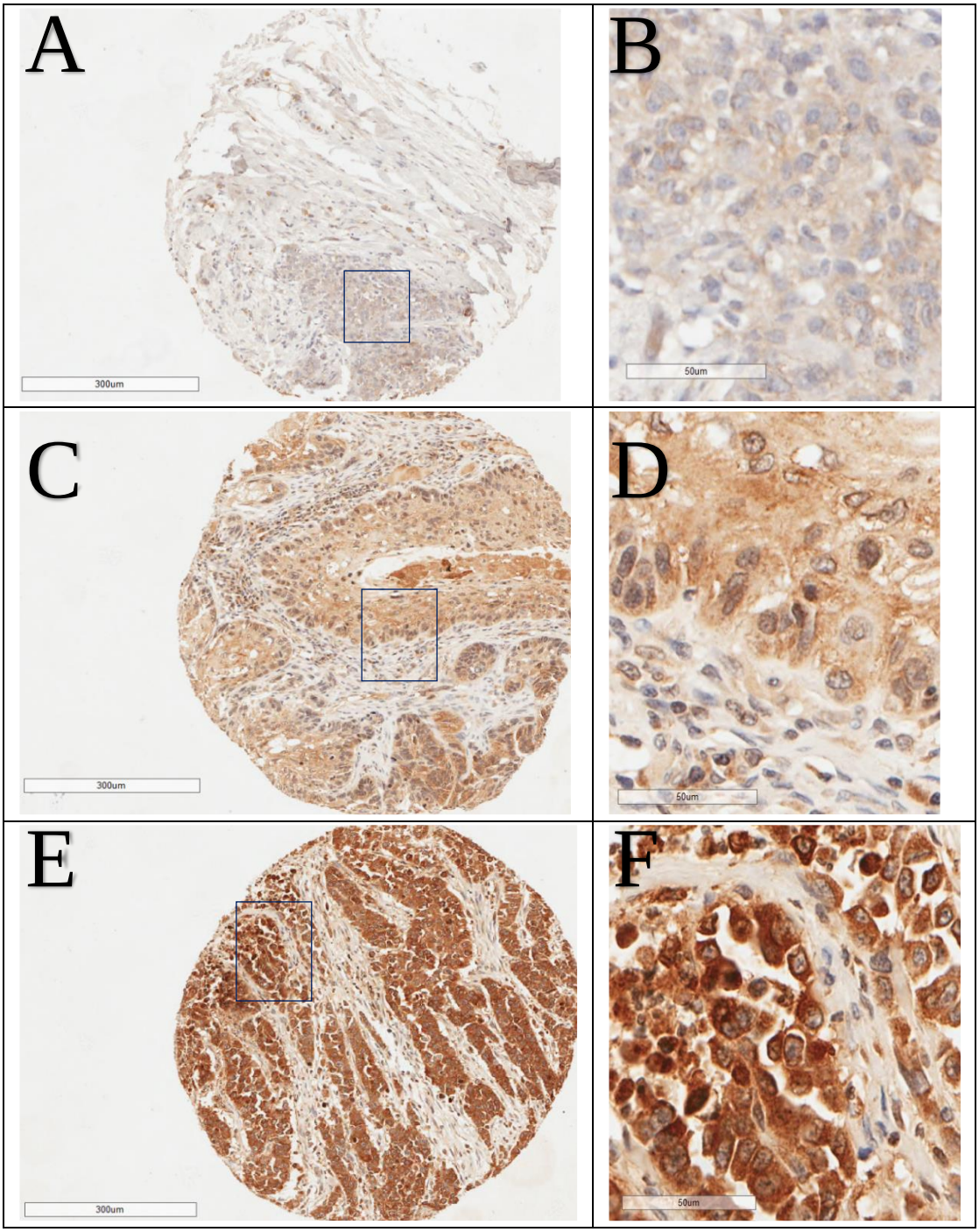

Figure 3:33 Immunohistochemical analysis of HK-2 expression in larynx primaries. A tissue microarray (TMA) was stained using a mouse monoclonal HK-2 antibody (Novus) as described in section 2.4.3. This figure illustrates the magnified views of representative cores from TMA set 2. Magnification is represented by the individual scale bar in the figure. (A) represents score 1 (weak staining) (B) detailed image of the area indicated in blue in panel A (C) represents score 2 (moderate staining) (D) detailed image of the area indicated in blue in panel C (E) represents score 3 (strong staining) (F) detailed image of the area indicated in blue in panel E

The pattern of HK-2 expression in hypopharynx primaries is shown in figure 3.34.

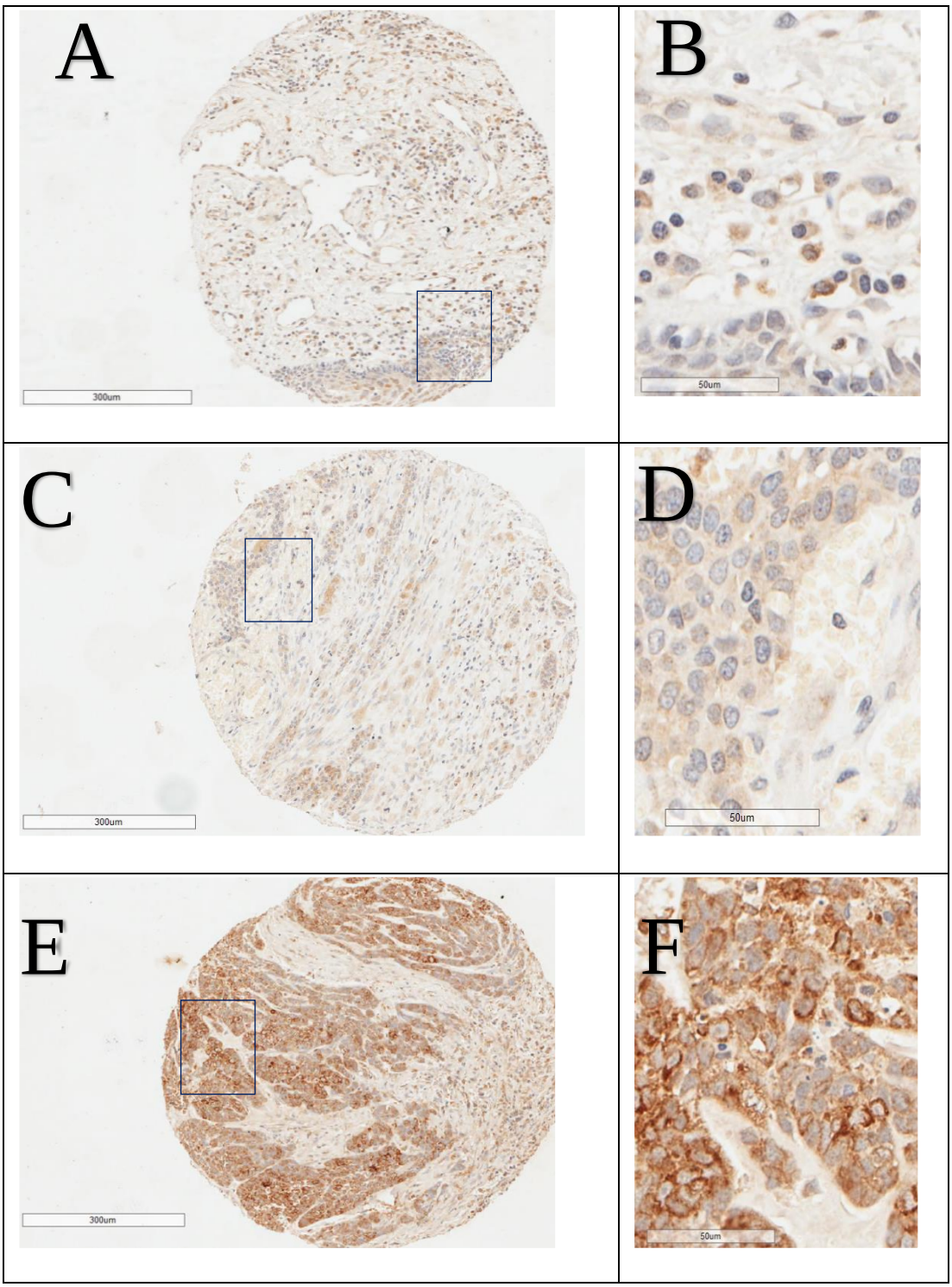

Figure 3:34 Immunohistochemical analysis of HK-2 expression in hypopharynx primaries. A tissue microarray (TMA) was stained using a mouse monoclonal HK-2 antibody (Novus) as described in section 2.4.3. This figure illustrates the magnified views of representative cores from TMA set 2. Magnification is represented by the individual scale bar in the figure. (A) represents score 1 (weak staining) (B) detailed image of the area indicated in blue in panel A (C) represents score 2 (moderate staining) (D) detailed image of the area indicated in blue in panel C (E) represents score 3 (strong staining) (F) detailed image of the area indicated in blue in panel E

3.3.7.1 Association of HK-2 expression with clinical variables in tumour core samples of larynx and hypopharynx

We have observed 42.4% of 'strong HK-2 expression' in the tumour core samples of larynx and hypopharynx primaries in TMA set 2 (see table 3.38).

Table 3-38 Frequency distribution of HK-2 expression in tumour core samples of larynx and hypopharynx

	Frequency	Percentage (%)
No tumour	4	4.0
Weak	0	0.0
Moderate	46	46.5
Strong	42	42.4
Missing	7	7.1
Total	99	100

We analysed whether any association present between HK-2 expression in tumour core samples of larynx and hypopharynx with known clinical variables (see table 3.39).

Table 3-39 Association between HK-2 expression in tumour core samples of larynx and hypopharynx and clinicopathological variables ('no tumour' samples excluded)

	HK 2 expression – tumour core		
	Moderate	**Strong**	***P*-value**
Anatomical sites			
Larynx	41 (61.2)	26 (38.8)	0.017*
Hypopharynx	4 (26.7)	11 (73.3)	
Larynx and Hypopharynx combined	1 (20.0)	4 (80.0)	
T stage			
T 1	2 (33.3)	4 (66.7)	0.276
T 2	7 (38.9)	11 (61.1)	
T 3	21 (63.6)	12 (36.4)	
T 4	16 (53.3)	14 (46.7)	
N stage			
N 0	27 (64.3)	15 (35.7)	0.023*
N 1	6 (66.7)	3 (33.3)	
N 2	13 (35.1)	24 (64.9)	
Differentiation			
Well	11 (78.6)	3 (21.4)	0.041*
Moderate	25 (53.2)	22 (46.8)	
Poor	10 (37.0)	17 (63.0)	
Invasive front			
Cohesive	11 (50.0)	11 (50.0)	0.851
Non-cohesive	34 (52.3)	31 (47.7)	
Vascular invasion			
Yes	10 (35.7)	18 (64.3)	0.034*
No	36 (60.0)	24 (40.0)	
Nerve invasion			
Yes	17 (60.7)	11 (39.3)	0.313
No	29 (49.2)	30 (50.8)	
ECS			
Yes	11 (40.7)	16 (59.3)	0.655
No	9 (47.4)	10 (52.6)	
Death			
Yes	19 (57.6)	14 (42.4)	0.393
No	26 (48.1)	28 (51.9)	

NOTE. Values are n(%). (ECS – extracapsular spread) P-value determined by Pearson Chi-Square test. (*statistically significant at 5%)

3.3.7.2 Association of HK-2 expression with clinical variables in advancing front samples of larynx and hypopharynx

We have observed 28.3% of 'strong HK-2 expression' in the advancing front samples of larynx and hypopharynx primaries in TMA set 2 (see table 3.40).

Table 3-40 Frequency distribution of HK-2 expression in the advancing front of larynx and hypopharynx

	Frequency	Percentage (%)
No tumour	19	19.2
Weak	2	2.0
Moderate	47	47.5
Strong	28	28.3
Missing	3	3.0
Total	99	100

We analysed whether any association present between HK-2 expression in advancing front samples of larynx and hypopharynx with known clinical variables (see table 3.41).

Table 3-41 Association between HK-2 expression in advancing front samples of larynx and hypopharynx and clinicopathological variables ('no tumour' samples excluded)

	HK-2 expression – advancing front			
	Weak	**Moderate**	**Strong**	***P*-value**
Anatomical sites				
Larynx	1 (1.8)	40 (70.2)	16 (28.1)	
Hypopharynx	1 (6.7)	4 (26.7)	10 (66.7)	0.041*
Larynx and hypopharynx combined	0 (0.0)	2 (50.0)	2 (50.0)	
T stage				
T 1	1 (25.0)	2 (50.0)	1 (25.0)	
T 2	0 (0.0)	6 (42.9)	8 (57.1)	0.064
T 3	1 (3.6)	18 (64.3)	9 (32.1)	
T 4	0 (0.0)	20 (66.7)	10 (33.3)	
N stage				
N 0	1 (3.1)	23 (71.9)	8 (25.0)	
N 1	0 (0.0)	6 (54.5)	5 (45.5)	0.502
N 2	1 (2.9)	18 (52.9)	15 (44.1)	
Differentiation				
Well	1 (8.3)	8 (66.7)	3 (25.0)	0.333
Moderate	0 (0.0)	27 (65.9)	14 (34.1)	
Poor	1 (4.2)	12 (50.0)	11 (45.8)	
Invasive front				
Cohesive	0 (0.0)	10 (58.8)	7 (41.2)	0.669
Non-cohesive	2 (3.4)	37 (62.7)	20 (33.9)	
Vascular invasion				
Yes	1 (3.7)	12 (44.4)	14 (51.9)	0.090
No	1 (2.0)	35 (70.0)	14 (28.0)	
Nerve invasion				
Yes	0 (0.0)	17 (73.9)	6 (26.1)	0.323
No	2 (3.8)	30 (57.7)	20 (38.5)	
ECS				
Yes	1 (4.0)	13 (52.0)	11 (44.0)	0.658
No	0 (0.0)	11 (57.9)	8 (42.1)	
Death				
Yes	1 (3.0)	21 (63.6)	11 (33.3)	0.851
No	1 (2.3)	25 (58.1)	17 (39.5)	

NOTE. Values are n(%). (ECS – extracapsular spread) P-value determined by Pearson Chi-Square test. (*statistically significant at 5%)

3.3.7.3 Disease-specific survival analysis of HK-2 expression in tumour core samples of larynx and hypopharynx

Kaplan-Meier survival analysis was conducted as described in 2.4.8 to compare the survival period between two categories of HK-2 expression in tumour core samples of larynx and hypopharynx namely, moderate and strong (see Table 3.42 for case processing summary) in TMA set 2.

Table 3-42 Case processing summary for survival analysis of HK-2 expression in tumour core samples of larynx and hypopharynx

HK-2 expression	Total No	No of deaths	No of censored	% of censored cases
Moderate	22	18	4	18.2%
Strong	25	14	11	44.0%
Overall	47	32	15	31.9%

A log-rank test was conducted to determine whether there were any differences in the survival distributions between moderate and strong categories (see figure 3.35).

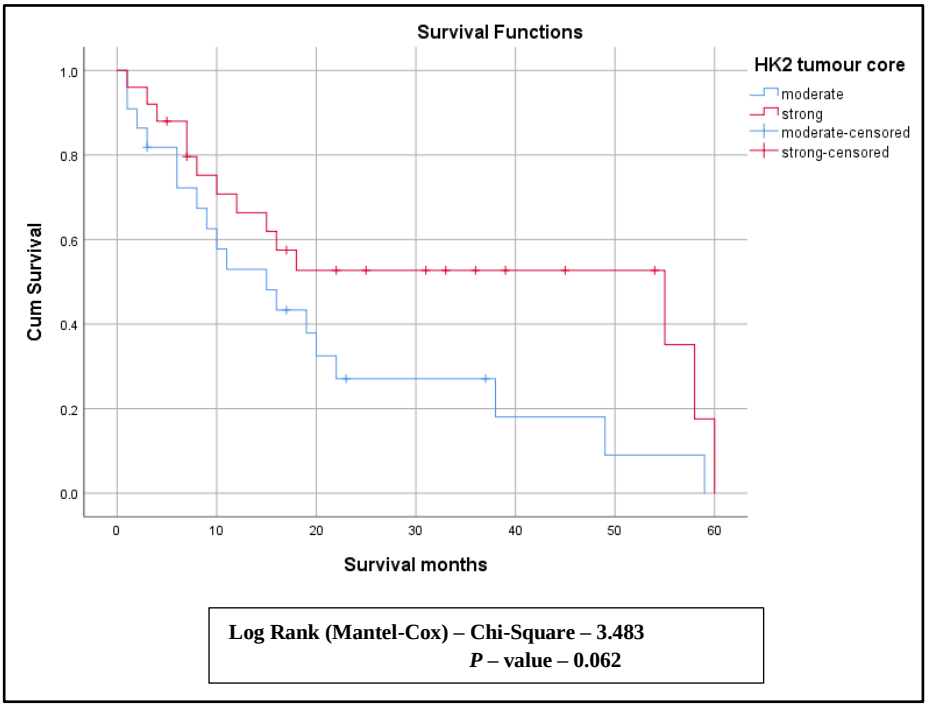

Figure 3:35 Disease-specific survival curve for moderate and strong categories of HK-2 expression in tumour core samples of larynx and hypopharynx

3.3.7.4 Disease-specific survival analysis of HK-2 expression in advancing front samples of larynx and hypopharynx

Kaplan-Meier survival analysis was conducted as described in 2.4.8 to compare the survival period among three categories of HK-2 expression (weak, moderate and strong) in advancing front samples of larynx and hypopharynx (see Table 3.43 for case processing summary) in TMA set 2.

Table 3-43 Case processing summary for survival analysis of HK-2 expression in advancing front samples of larynx and hypopharynx

HK-2 expression	Total No	No of deaths	No of censored	% of censored cases
Weak	1	1	0	0.0%
Moderate	30	21	9	30.0%
Strong	14	10	4	28.6%
Overall	45	32	13	28.9%

A log-rank test was conducted to determine whether there were any differences in the survival distributions among weak, moderate and strong categories (see figure 3.36).

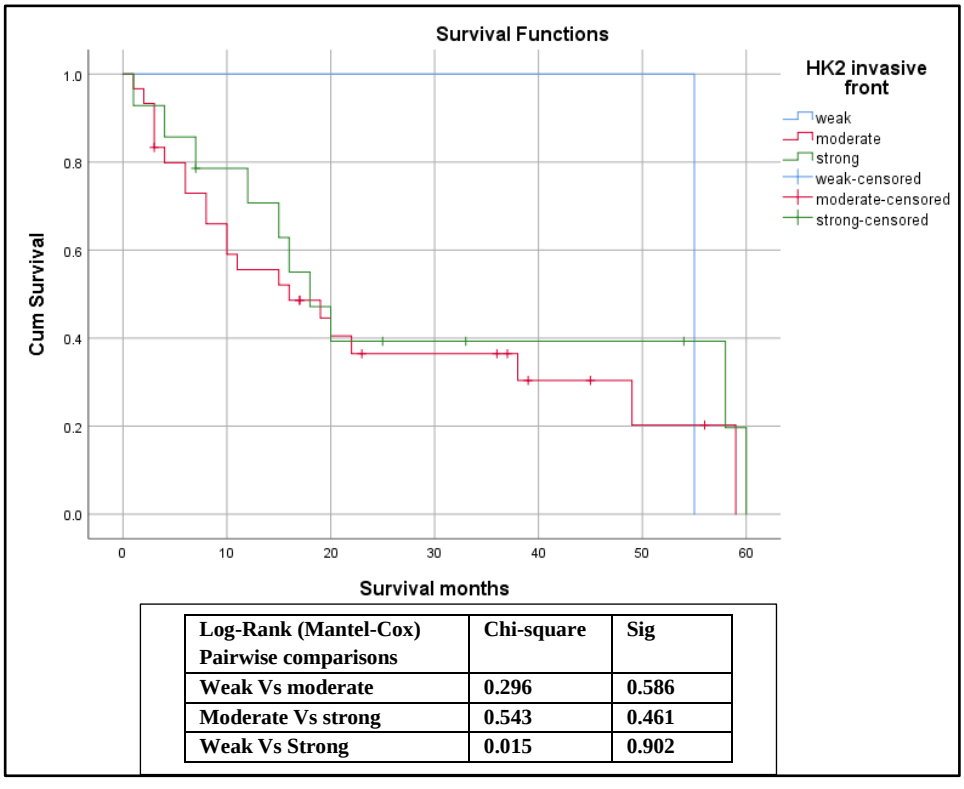

Log-Rank (Mantel-Cox) Pairwise comparisons	Chi-square	Sig
Weak Vs moderate	0.296	0.586
Moderate Vs strong	0.543	0.461
Weak Vs Strong	0.015	0.902

Figure 3:36 Disease-specific survival curve for weak, moderate, and strong categories in the advancing front samples of larynx and hypopharynx

3.3.8 HK-2 expression in larynx and hypopharynx lymph nodes

The pattern of HK-2 expression in lymph node samples of larynx and hypopharynx was represented in figures 3.37 and 3.38, respectively.

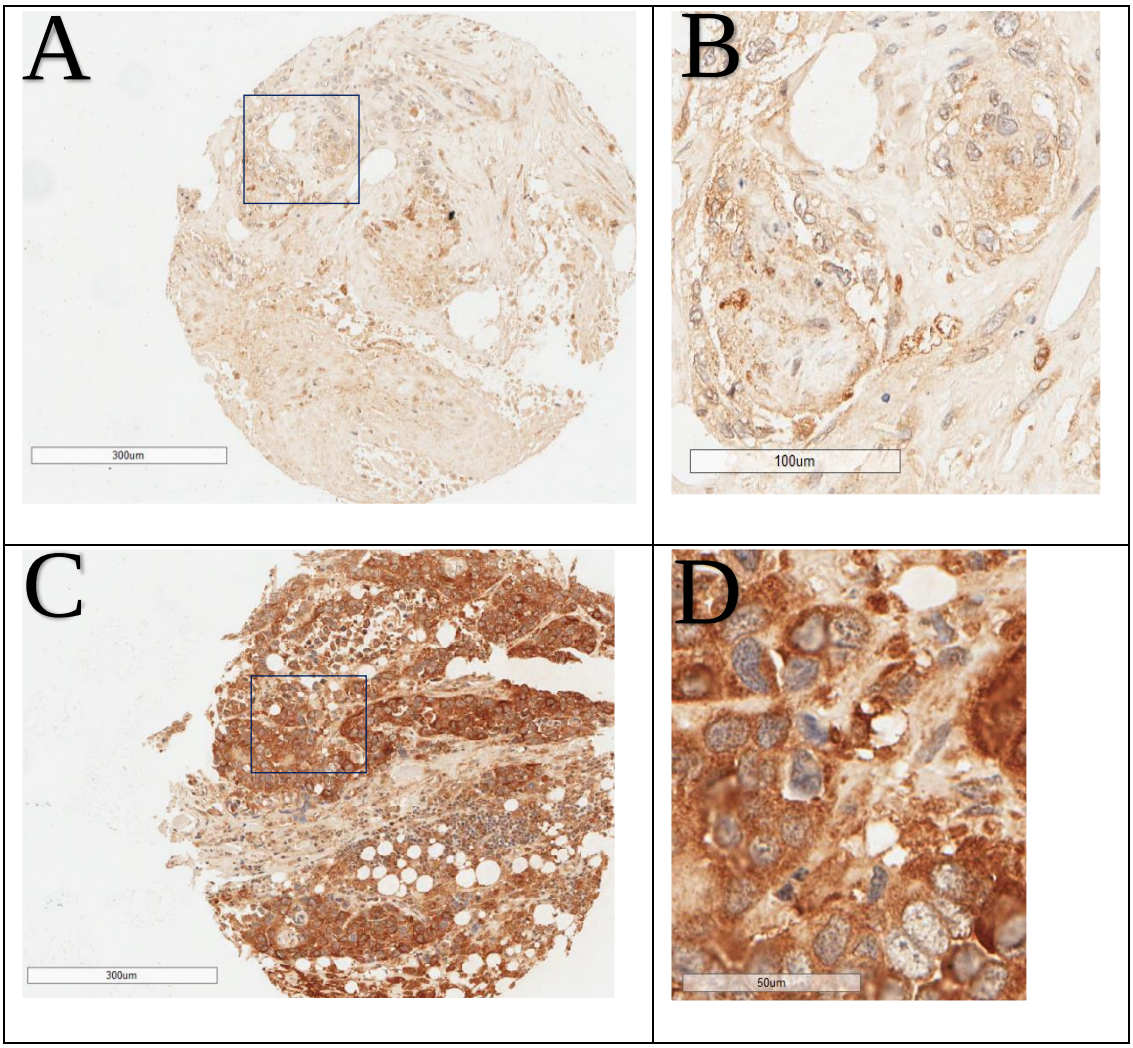

Figure 3:37 Immunohistochemical analysis of HK-2 expression in larynx lymph nodes. A tissue microarray (TMA) was stained using a mouse monoclonal HK-2 antibody (Novus) as described in section 2.4.3. This figure illustrates the magnified views of representative cores from TMA set 2. Magnification is represented by the individual scale bar in the figure. (A) represents score 2 (moderate staining) (B) detailed image of the area indicated in blue in panel A (C) represents score 3 (strong staining) (D) detailed image of the area indicated in blue in panel C

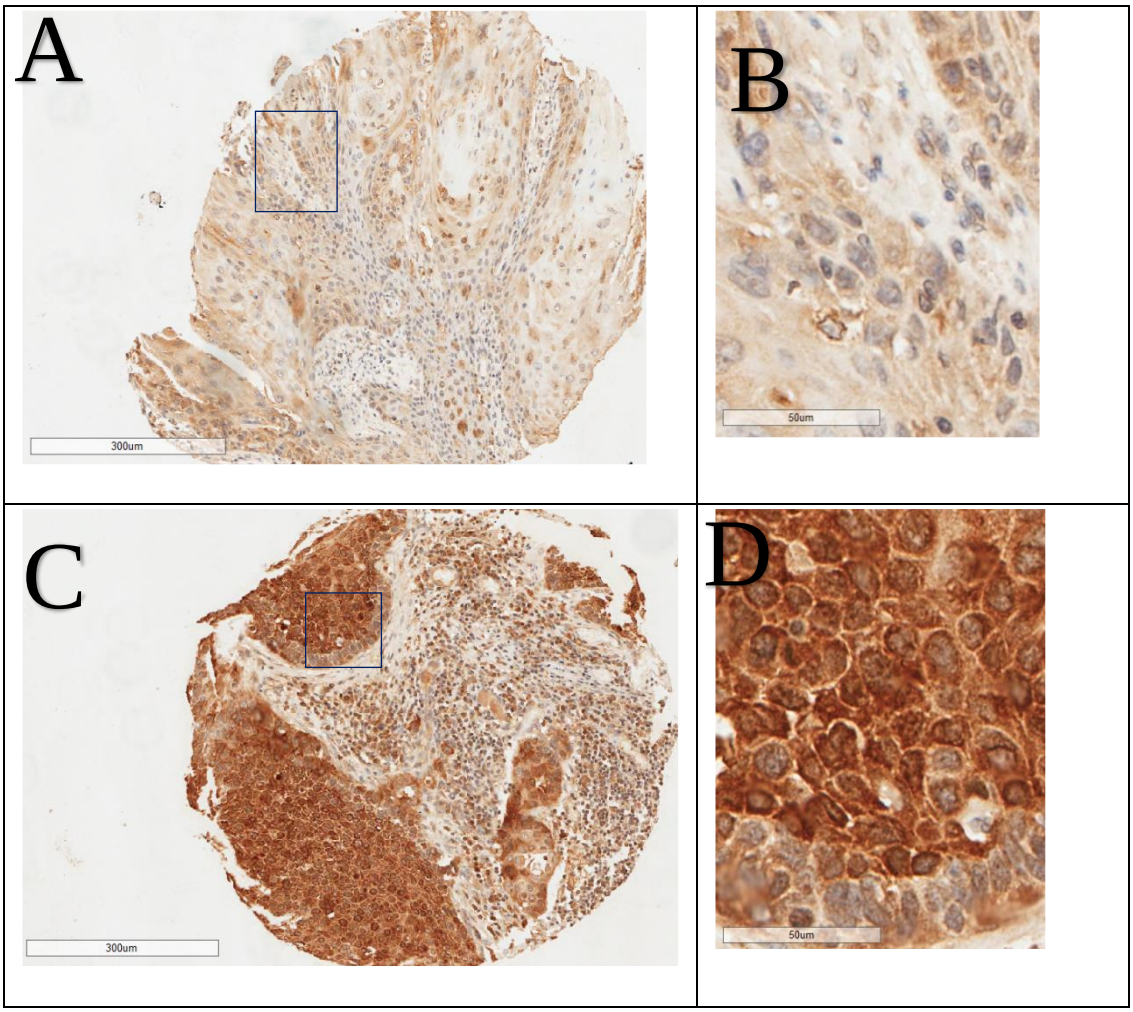

Figure 3:38 Immunohistochemical analysis of HK-2 expression in hypopharynx lymph nodes. A tissue microarray (TMA) was stained using a mouse monoclonal HK-2 antibody (Novus) as described in section 2.4.3. This figure illustrates the magnified views of representative cores from TMA set 2. Magnification is represented by the individual scale bar in the figure. (A) represents score 2 (moderate staining) (B) detailed image of the area indicated in blue in panel A (C) represents score 3 (strong staining) (D) detailed image of the area indicated in blue in panel C

3.3.8.1 Association of HK-2 expression with clinical variables in lymph nodes samples of larynx and hypopharynx

We have observed 61.3% of 'strong HK-2' expression in the lymph nodes samples of larynx and hypopharynx in TMA set 2 (see table 3.44).

Table 3-44 Frequency distribution of HK-2 expression in lymph nodes of larynx and hypopharynx

	Frequency	Percentage (%)
No tumour	3	9.7
Weak	0	0.0
Moderate	9	29.0
Strong	19	61.3
Total	31	100

We analysed whether any association present between HK-2 expression in lymph nodes samples from the larynx and hypopharynx with known clinical variables (see table 3.45).

Table 3-45 Association between HK-2 expression in lymph nodes samples of larynx and hypopharynx and clinicopathological variables ('no tumour' samples excluded)

	HK 2 expression – Lymph nodes		
	Moderate	Strong	*P*- value
Anatomical sites			
Larynx	5 (31.3)	11 (68.8)	0.852
Hypopharynx	3 (30.0)	7 (70.0)	
Larynx and Hypopharynx combined	1 (50.0)	1 (50.0)	
T stage			
T 1	0 (0.0)	1 (100.0)	0.766
T 2	2 (50.0)	2 (50.0)	
T 3	3 (33.3)	6 (66.7)	
T 4	4 (28.6)	10 (71.4)	
N stage			
N 1	1 (20.0)	4 (80.0)	0.521
N 2	8 (34.8)	15 (65.2)	
Differentiation			
Moderate	5 (35.7)	9 (64.3)	0.686
Poor	4 (28.6)	10 (71.4)	
Invasive front			
Cohesive	1 (16.7)	5 (83.3)	0.326
Non-cohesive	8 (38.1)	13 (61.9)	
Vascular invasion			
Yes	4 (30.8)	9 (69.2)	0.885
No	5 (33.3)	10 (66.7)	
Nerve invasion			
Yes	5 (50.0)	5 (50.0)	0.159
No	4 (23.5)	13 (76.5)	
ECS			
Yes	4 (26.7)	11 (73.3)	0.411
No	5 (41.7)	7 (58.3)	
Death			
Yes	6 (37.5)	10 (62.5)	0.483
No	3 (25.0)	9 (75.0)	

NOTE. Values are n(%). (ECS – extracapsular spread) P-value determined by Pearson Chi-Square test.

3.3.8.2 Disease-specific survival analysis HK-2 expression in lymph nodes samples of larynx and hypopharynx

Kaplan-Meier survival analysis was conducted as described in 2.4.8 to compare the survival period between two categories of HK-2 expression; moderate and strong in lymph node samples of larynx and hypopharynx (see Table 3.46 for case processing summary) in TMA set 2.

Table 3-46 Case processing summary for survival analysis of HK-2 expression in lymph nodes of larynx and hypopharynx

HK-2 expression	Total No	No of deaths	No of censored	% of censored cases
Moderate	8	6	2	25.0%
Strong	15	10	5	33.3%
Overall	23	16	7	30.4%

A log-rank test was conducted to determine whether there were any differences in the survival distributions between moderate and strong categories (see figure 3.39).

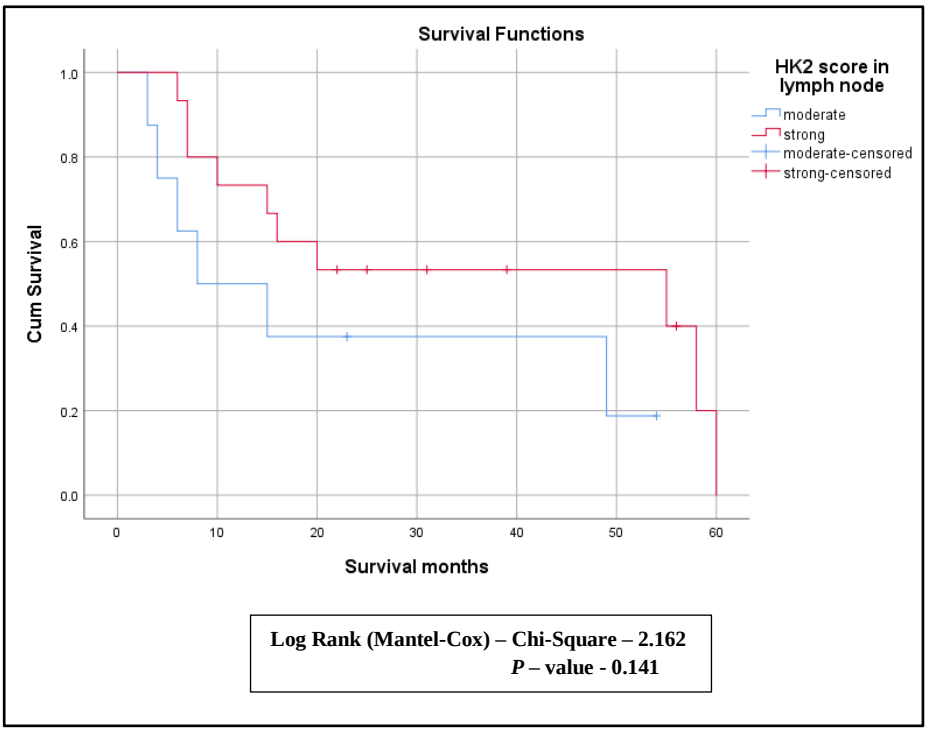

Figure 3:39 Disease-specific survival curve for moderate and strong categories of HK-2 expression in lymph nodes samples of larynx and hypopharynx

3.3.9 Analysis of association between p53 and HK-2 expression in larynx and hypopharynx samples

3.3.9.1 Association between p53 and HK-2 expression in tumour core samples of larynx and hypopharynx

The correlation between HK-2 and p53 expression in the tumour core samples of larynx and hypopharynx is given in Table 3.47 and shows that there is a significant association (*P*=0.003) which demonstrates that patients with strong HK-2 are more likely to have inferred mutant p53 status in the tumour core samples of larynx and hypopharynx.

Table 3-47 p53 tumour core * HK-2 tumour core - Chi-square statistics

		HK-2 tumour core		
		Moderate	**Strong**	
p53 expression - tumour core	Inferred wild type	17	4	*P*- value 0.003
	Inferred mutant	20	28	

3.3.9.2 Association between p53 and HK-2 expression in advancing front samples of larynx and hypopharynx

The correlation between HK-2 and p53 expression in the advancing front samples of larynx and hypopharynx is given in Table 3.48 and shows that there is a significant association (*P*=0.047), which demonstrates that patients with strong HK-2 are likely to have an inferred mutant p53 status in the advancing front samples of larynx and hypopharynx.

Table 3-48 p53 invasive front * HK-2 invasive front Chi-square statistics

		HK-2 advancing front			
		Weak	**Moderate**	**Strong**	
p53 expression - advancing front	Inferred Wild type	1	19	4	*P*-value 0.047
	Inferred Mutant	1	23	21	

3.3.10 HK-2 expression in oropharynx primaries

Figure 3.40 shows the pattern of HK-2 expression in oropharynx primaries

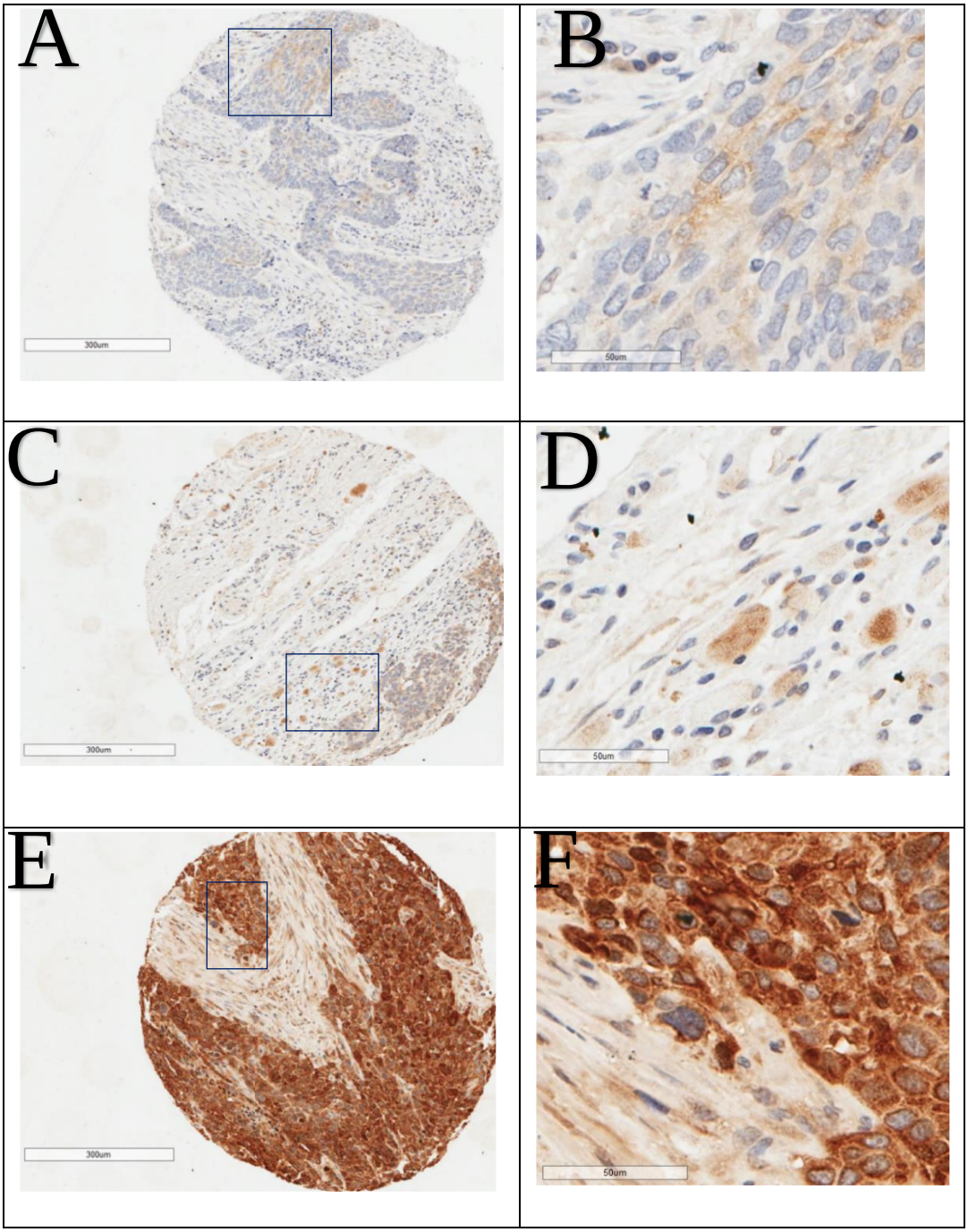

Figure 3:40 Immunohistochemical analysis of HK-2 expression in oropharynx primaries. A tissue microarray (TMA) was stained using a mouse monoclonal HK-2 antibody (Novus) as described in section 2.4.3. This figure illustrates the magnified views of representative cores from TMA set 2. Magnification is represented by the individual scale bar in the figure. (A) represents score 1 (weak staining) (B) detailed image of the area indicated in blue in panel A (C) represents score 2 (moderate staining) (D) detailed image of the area indicated in blue in panel C (E) represents score 3 (strong staining) (F) detailed image of the area indicated in blue in panel E

3.3.10.1 Association of HK-2 expression with clinical variables in the tumour core samples of the oropharynx

We have observed 54.8% of 'strong HK-2 expression' in the tumour core samples of the oropharynx in TMA set 2 (see table 3.49).

Table 3-49 Frequency distribution of HK-2 expression in tumour core samples of the oropharynx

	Frequency	Percentage (%)
No tumour	1	1.6
Weak	0	0.0
Moderate	25	40.3
Strong	**34**	**54.8**
Missing	2	3.2
Total	62	100

We analysed whether any association present between HK-2 expression in tumour cores samples of the oropharynx with known clinical variables (see table 3.50).

Table 3-50 Association between HK2 expression in tumour core samples of the oropharynx and clinicopathological variables ('no tumour' samples excluded)

	HK 2 expression – tumour core		
	Moderate	Strong	*P*-value
Anatomical sites			
Tonsil	11 (32.4)	23 (67.6)	0.257
Tongue base	11 (61.1)	7 (38.9)	
Palate	2 (40.0)	3 (60.0)	
Posterior pharyngeal wall	1 (50.0)	1 (50.0)	
T stage			
T 1	3 (33.3)	6 (66.7)	0.650
T 2	16 (47.1)	18 (52.9)	
T 3	5 (35.7)	9 (64.3)	
N stage			
N 0	3 (42.9)	4 (57.1)	0.989
N 1	4 (44.4)	5 (55.6)	
N 2	18 (41.9)	25 (58.1)	
Differentiation			
Well	2 (66.7)	1 (33.3)	0.181
Moderate	8 (61.5)	5 (38.5)	
Poor	15 (35.7)	27 (64.3)	
Invasive front			
Cohesive	10 (43.5)	13 (56.5)	0.963
Non-cohesive	15 (42.9)	20 (57.1)	
Vascular invasion			
Yes	9 (56.3)	7 (43.8)	0.188
No	16 (37.2)	27 (62.8)	
Nerve invasion			
Yes	4 (44.4)	5 (55.6)	0.891
No	21 (42.0)	29 (58.0)	
ECS			
Yes	14 (58.3)	10 (41.7)	0.030*
No	8 (28.6)	20 (71.4)	
Death			
Yes	5 (41.7)	7 (58.3)	0.956
No	20 (42.6)	27 (57.4)	

NOTE. Values are n(%). (ECS – extracapsular spread) P-value determined by Pearson Chi-Square test. (*statistically significant at 5%)

3.3.10.2 Association of HK-2 expression with clinical variables in the advancing front samples of the oropharynx

We have observed 38.7% of 'strong HK-2 expression' in the advancing front samples of the oropharynx in TMA set 2 (see table 3.51).

Table 3-51 Frequency distribution of HK-2 expression in the advancing front samples of the oropharynx

	Frequency	Percentage (%)
No tumour	12	19.4
Weak	1	1.6
Moderate	21	33.9
Strong	**24**	**38.7**
Missing	4	6.5
Total	62	100

We analysed whether any association present between HK-2 expression in advancing front samples of the oropharynx with known clinical variables (see table 3.52).

Table 3-52 Association between HK-2 expression in the advancing front samples of the oropharynx and clinicopathological variables ('no tumour' samples excluded)

	HK-2 – advancing front			
	Weak	**Moderate**	**Strong**	***P*- value**
Anatomical sites				
Tonsil	1 (4.0)	12 (48.0)	12 (48.0)	
Tongue base	0 (0.0)	7 (46.7)	8 (53.3)	0.942
Palate	0 (0.0)	1 (25.0)	3 (75.0)	
Posterior pharyngeal wall	0 (0.0)	1 (50.0)	1 (50.0)	
T stage				
T 1	0 (0.0)	5 (62.5)	3 (37.5)	
T 2	1 (4.0)	10 (40.0)	14 (56.0)	0.764
T 3	0 (0.0)	5 (45.5)	6 (54.5)	
N stage				
N 0	0 (0.0)	3 (60.0)	2 (40.0)	
N 1	0 (0.0)	3 (42.9)	4 (57.1)	0.940
N 2	1 (2.9)	15 (44.1)	18 (52.9)	
Differentiation				
Well	0 (0.0)	2 (100.0)	0 (0.0)	0.523
Moderate	0 (0.0)	5 (38.5)	8 (61.5)	
Poor	1 (3.3)	14 (46.7)	15 (50.0)	
Invasive front				
Cohesive	1 (5.6)	7 (38.9)	10 (55.6)	0.367
Non-cohesive	0 (0.0)	14 (51.9)	13 (48.1)	
Vascular invasion				
Yes	0 (0.0)	5 (41.7)	7 (58.3)	0.768
No	1 (2.9)	16 (47.1)	17 (50.0)	
Nerve invasion				
Yes	0 (0.0)	4 (66.7)	2 (33.3)	0.525
No	1 (2.5)	17 (42.5)	22 (55.0)	
ECS				
Yes	0 (0.0)	11 (57.9)	8 (42.1)	0.190
No	1 (4.5)	7 (31.8)	14 (63.6)	
Death				
Yes	0 (0.0)	4 (40.0)	6 (60.0)	0.772
No	1 (2.8)	17 (47.2)	18 (50.0)	

NOTE. Values are n(%). (ECS – extracapsular spread) P-value determined by Pearson Chi-Square test.

3.3.10.3 Disease-specific survival analysis of HK-2 expression in tumour core samples of the oropharynx

Kaplan-Meier survival analysis was conducted as described in 2.4.8 to compare the survival period between two categories of HK-2 expression; moderate and strong in tumour core samples of the oropharynx (see Table 3.53 for case processing summary) in TMA set 2.

Table 3-53 Case processing summary for survival analysis of HK-2 expression in tumour core samples of the oropharynx

HK-2 expression	Total No	No of deaths	No of censored	% of censored cases
Moderate	24	4	20	83.3%
Strong	33	6	27	81.8%
Overall	57	10	47	82.5%

A log-rank test was conducted to determine whether there were any differences in the survival distributions between moderate and strong categories (see figure 3.41).

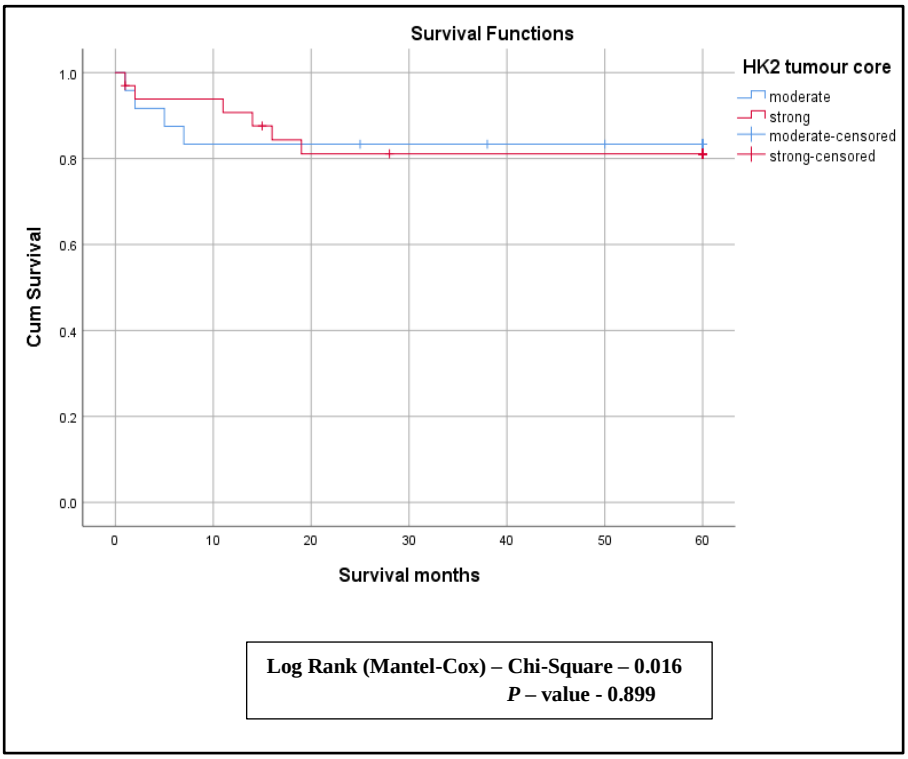

Figure 3:41 Disease-specific survival curve for moderate and strong categories of HK-2 expression in tumour core samples of the oropharynx

3.3.10.4 Disease-specific survival analysis of HK-2 expression in advancing front samples of the oropharynx

Kaplan-Meier survival analysis was conducted as described in 2.4.5 to compare the survival period among three categories of HK-2 expression (weak, moderate and strong) in advancing front samples of the oropharynx (see Table 3.54 for case processing summary) in TMA set 2.

Table 3-54 Case processing summary for survival analysis of HK-2 expression in advancing front samples of the oropharynx

HK-2 expression	Total No	No of deaths	No of censored	% of censored cases
Weak	1	0	1	100.0%
Moderate	21	4	17	81.0%
Strong	23	5	18	78.3%
Overall	45	9	36	80.0%

A log-rank test was conducted to determine whether there were any differences in the survival distributions among weak, moderate and strong categories (see figure 3.42).

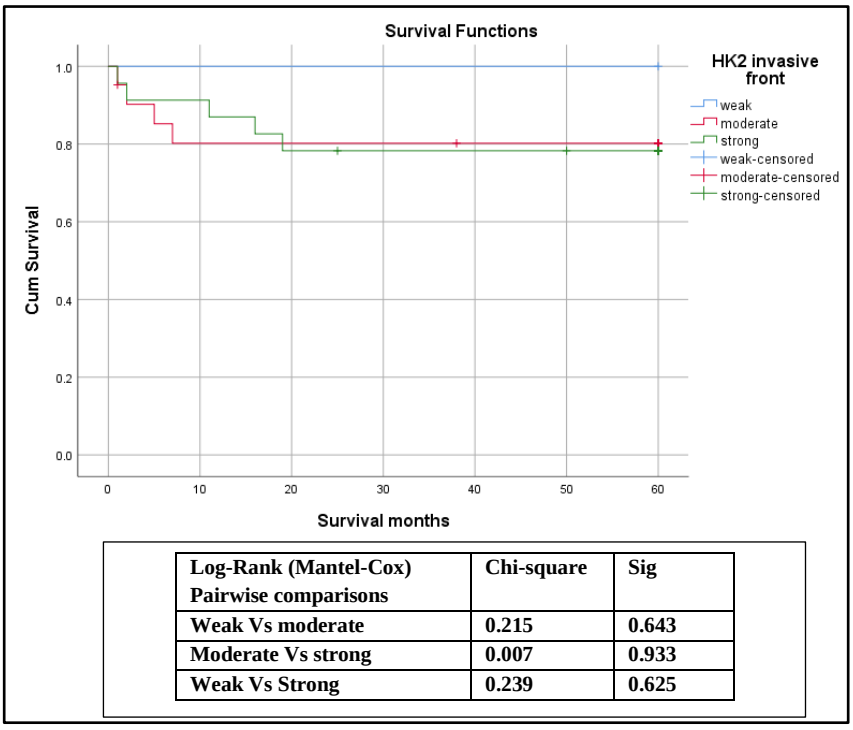

Log-Rank (Mantel-Cox) Pairwise comparisons	Chi-square	Sig
Weak Vs moderate	0.215	0.643
Moderate Vs strong	0.007	0.933
Weak Vs Strong	0.239	0.625

Figure 3:42 Disease-specific survival curve for weak, moderate, and strong categories advancing front samples of the oropharynx

3.3.11HK-2 expression in oropharynx lymph nodes

Figure 3.43 shows the pattern of HK-2 expression in oropharynx lymph nodes.

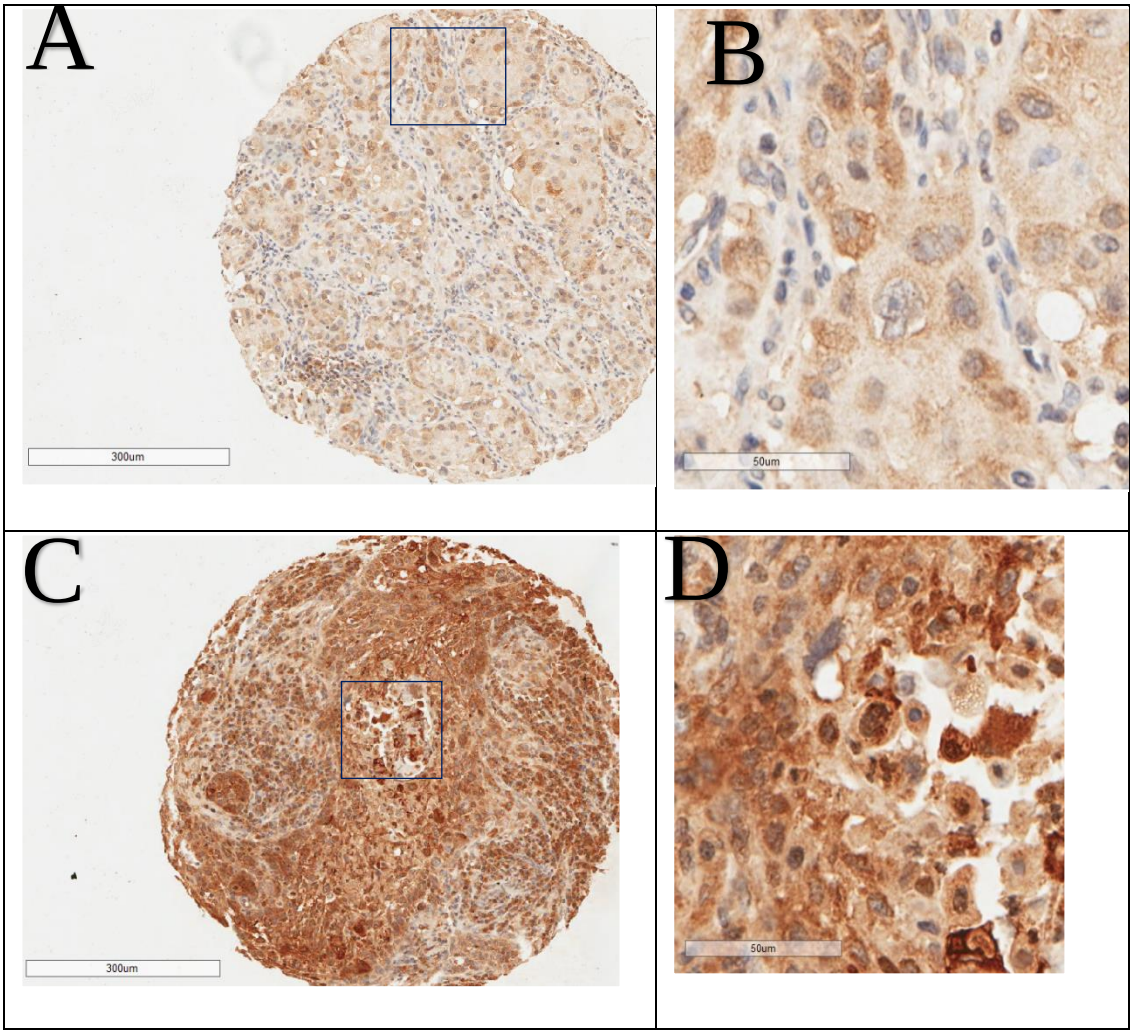

Figure 3:43 Immunohistochemical analysis of HK-2 expression in oropharynx lymph nodes. A tissue microarray (TMA) was stained using a mouse monoclonal HK-2 antibody (Novus) as described in section 2.4.3. This figure illustrates the magnified views of representative cores from TMA set 2. Magnification is represented by the individual scale bar in the figure. (A) represents score 2 (moderate staining) (B) detailed image of the area indicated in blue in panel A (C) represents score 3 (strong staining) (D) detailed image of the area indicated in blue in panel C

3.3.11.1 Association of HK-2 expression with clinical variables in oropharynx lymph nodes

We have observed 79.3% of 'strong HK-2 expression' in the lymph nodes samples of the oropharynx in TMA set 2 (see table 3.55).

Table 3-55 Frequency distribution of HK-2 expression in lymph nodes of the oropharynx

	Frequency	Percentage (%)
No tumour	1	3.4
Weak	0	0.0
Moderate	5	17.2
Strong	**23**	**79.3**
Total	29	100

We analysed whether any association present between p53 expression in samples from the lymph nodes with other clinical parameters (see table 3.56).

Table 3-56 Association between HK-2 expression in lymph nodes of the oropharynx and clinicopathological variables ('no tumour' samples excluded)

	HK 2 expression – lymph nodes		
	Moderate	**Strong**	***P*-value**
Anatomical sites			
Tonsil	2 (13.3)	13 (86.7)	0.520
Tongue base	3 (27.3)	8 (72.7)	
Palate	0 (0.0)	0 (0.0)	
Posterior pharyngeal wall	0 (0.0)	2 (100.0)	
T stage			
T 1	0 (0.0)	5 (100.0)	0.450
T 2	4 (25.0)	12 (75.0)	
T 3	1 (16.7)	5 (83.3)	
N stage			
N 1	0 (0.0)	5 (100.0)	0.250
N 2	5 (21.7)	18 (78.3)	
Differentiation			
Well	1 (100.0)	0 (0.0)	0.058
Moderate	0 (0.0)	5 (100.0)	
Poor	4 (18.2)	18 (81.8)	
Invasive front			
Cohesive	1 (8.3)	11 (91.7)	0.254
Non-cohesive	4 (25.0)	12 (75.0)	
Vascular invasion			
Yes	3 (30.0)	7 (70.0)	0.211
No	2 (11.1)	16 (88.9)	
Nerve invasion			
Yes	3 (50.0)	3 (50.0)	0.020*
No	2 (9.1)	20 (90.9)	
ECS			
Yes	2 (15.4)	11 (84.6)	0.750
No	3 (20.0)	12 (80.0)	
Death			
Yes	0 (0.0)	7 (100.0)	0.154
No	5 (23.8)	16 (76.2)	

NOTE. Values are n(%). (ECS – extracapsular spread) P-value determined by Pearson Chi-Square test. (* statistically significant at 5%)

3.3.11.2 Disease-specific survival analysis of HK-2 expression in oropharynx lymph nodes

Kaplan-Meier survival analysis was conducted as described in 2.4.8 to compare the survival period between two categories of HK-2 expression, moderate and strong, in lymph node samples of the oropharynx (see Table 3.57 for case processing summary) in TMA set 2.

Table 3-57 Case processing summary for survival analysis of HK-2 expression in lymph node samples of the oropharynx

HK-2 expression	Total No	No of deaths	No of censored	% of censored cases
Moderate	5	0	5	100.0%
Strong	22	6	16	72.7%
Overall	27	6	21	77.8%

A log-rank test was conducted to determine whether there were any differences in the survival distributions between moderate and strong categories (see figure 3.44).

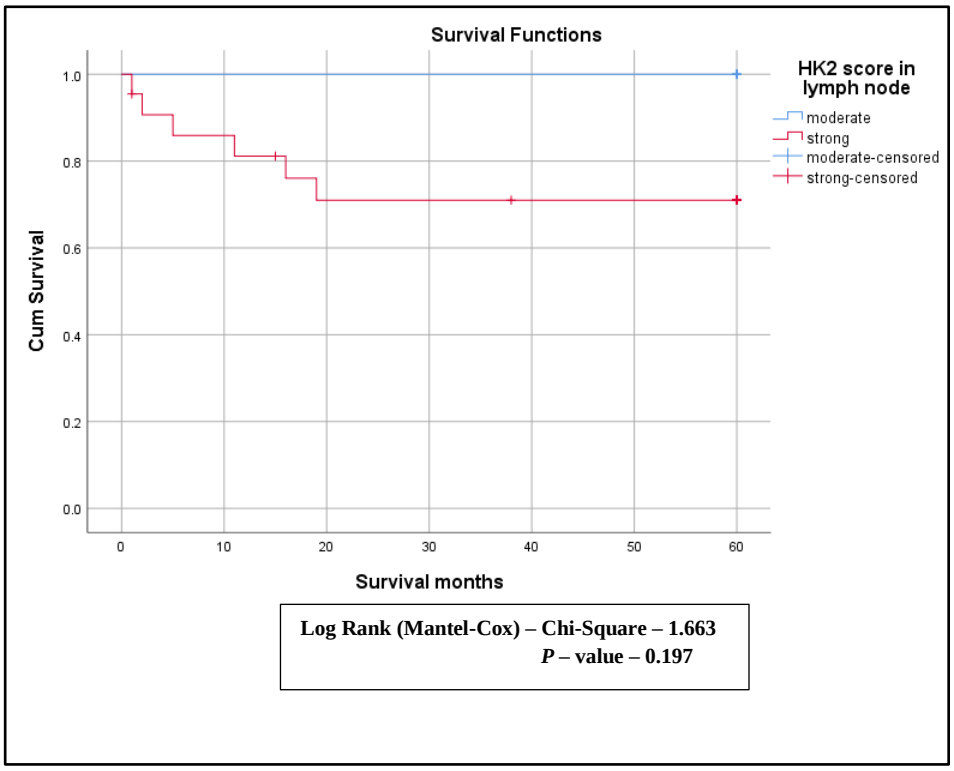

Figure 3:44 Disease-specific survival curve for moderate and strong categories of HK-2 expression in lymph nodes samples of oropharynx

3.3.12 Analysis of association between p53 and HK-2 in oropharynx samples

3.3.12.1 Association between p53 tumour core and HK-2 tumour core in oropharynx samples

The correlation between the tumour cores of HK-2 and p53 is given in Table 3.58 and shows that there is no significant association (*P*=0.076) which demonstrates that patients with high HK-2 are not likely to have inferred mutant p53 status in the tumour core samples of the oropharynx.

Table 3-58 p53 tumour core * HK-2 tumour core Chi-square statistics (normal tissues excluded)

		HK-2 tumour core		
		Moderate	**Strong**	
p53 tumour core	Inferred wild-type	7	3	*P*- value 0.076
	Inferred mutant	13	21	

3.3.12.2 Association between p53 invasive front and HK-2 invasive front in oropharynx samples

The correlation between the advancing fronts of HK-2 and p53 is given in Table 3.59 and shows that there is no significant association (*P*=0.051), which demonstrates that patients with high HK-2 are not likely to have an inferred mutant p53 status in the advancing front samples of the oropharynx.

Table 3-59 p53 invasive front * HK-2 invasive front Chi-square statistics (normal tissues excluded)

		HK-2 advancing front			
		Weak	**Moderate**	**Strong**	
p53 advancing front	Inferred Wild type	1	9	4	*P*-value 0.051
	Inferred Mutant	0	11	19	

4. Discussion

Colleagues in the p53/MDM2 research group recently published a study on the role of p53 in regulating energy metabolism in SCCHN cells, and they observed that loss of p53 function, whether through mutation or RNAi-mediated downregulation, resulted in a lack of metabolic flexibility, with cells becoming more dependent on glycolysis (112). In this context, we were interested in finding out whether any other proteins, which are connected in some functional manner to p53, might be involved in maintaining the high glycolytic status in SCCHN.

Following an analysis of the literature, two proteins came to our attention; TIGAR and HK-2, both playing crucial roles in glucose metabolism; the first one limits glycolysis and the second one initiates glycolysis by converting glucose into 6GP. Knowing the metabolic roles of each of these proteins, still, there remain unanswered questions, including the individual TIGAR and HK-2 expression patterns in head and neck cancers and the associations that might exist among the three proteins in SCCHN cells. What might this be expected to show? How might this be informative?

With the above questions in mind, the primary aim of this thesis was to analyse the expression of p53, TIGAR, and HK-2 proteins in clinical samples of SCCHN. The secondary aim was to examine whether any association might exist between the expression of these proteins and various clinical variables such as anatomical sites, T stage, N stage, differentiation, nerve invasion, vascular invasion, extracapsular spread, and also patient outcomes (survival). Also, the expression levels of these proteins were analysed in cells in culture with defined *TP53* genetic and modulated function alterations to determine whether p53 might influence the expression patterns of HK-2 and/or TIGAR in these cells.

4.1 Role of TIGAR in cancer

TIGAR *(TP*53 induced Glycolysis and Apoptosis Regulator) was identified in 2005 as a novel p53 target gene (196). To the best of our knowledge, this is the first study investigating TIGAR expression in SCCHN.

4.1.1 High TIGAR expression with wild-type p53

In our cell lines studies (described in section 3.1), we observed the highest levels of TIGAR expression were associated with wild-type p53. This pattern was observed regardless of whether p53 was expressed from a lentiviral vector in a p53 null line or comparing RNAi-mediated knock-down of p53 in a p53 wild-type line or even comparing two essentially isogenic lines from a single patient obtained at different times, with one harbouring wild-type p53 and one possessing a p53 mutation (UM-SCC-11A and 11B respectively).

Our results showing higher TIGAR expression in the cell lines with wild-type p53 compared to the mutant p53 cell lines are in accordance with the notion of p53-dependent TIGAR expression in our samples. As stated above, TIGAR is a p53 regulated gene, and we have observed that the connection between TIGAR expression and retention of wild-type p53 is potentially retained in our SCCHN cells.

Similar to our cell lines results, TIGAR expression was observed to differ in relation to the p53 status of pancreatic cancer, where it was identified that TIGAR expression in patient-derived xenografts was increased in p53 wild-type cancer and low TIGAR expression seen in p53 mutant pancreatic cancer (288).

4.1.2 Increased TIGAR expression in various cancers

Increased TIGAR expression seen in various tumour tissues and tumour cell lines (see Table 4.1).

Table 4-1 TIGAR expression in various tumours and cancer cell lines

Tumour type	Cell lines/samples	TIGAR expression and effects	Reference
Breast cancer	Invasive breast cancer	Increased expression of TIGAR. High p53 expression is associated with low TIGAR expression. TIGAR expression in breast cancer is independent of p53.	Won et al. (275)
	Epithelial breast cancer	Compared with stromal cells, increased TIGAR expression seen in epithelial breast cancer	Martinez-Outschoorn etal (289)
Gastric cancer	Gastric cancer tissues	Increased expression of TIGAR. High p53 expression is associated with low TIGAR expression	Kim et al. (274)
Colorectal tumour	Colorectal tumour tissues	Increased expression of TIGAR in stage 2 and 3 colorectal tumours.	Al-Khayal et al. (276)
Pancreatic ductal adenocarcinoma (PDAC)	PDAC mouse models	Higher TIGAR expression in premalignant lesions and lower TIGAR levels in metastasizing tumours	Cheung et al. (290)
Pancreatic cancer	Patient-derived PDAC xenografts	Higher TIGAR expression in p53 wild-type cancer and lower expression in p53 mutant pancreatic cancer	Rajeshkumar et al. (288)
Acute myeloid leukaemia	Clinical samples	Increased expression of TIGAR and positively correlated with poor prognosis	Qian et al. (291)
Chronic lymphocytic leukaemia	Clinical samples	Increased expression of TIGAR and positively correlated with poor prognosis	Hong et al. (292)
T lymphocytic leukaemia	Cell lines	Increased expression of TIGAR	Hasegawa et al. (293)
Nasopharyngeal carcinoma (NPC)	Nasopharyngeal carcinoma tissues	Higher expression of TIGAR compared to the adjacent normal tissues	Wong et al. (294)
	NPC Cell lines	Increased expression of TIGAR	Wong et al. (294), Zhao (295)
Liver cancer	HepG2 cells	Increased expression of TIGAR	Dai et al. (296)
Cervical cancer	Hela and SiHa cells	TIGAR expression seen in Hela but not in SiHa cells	Lin et al. (297)

Increased TIGAR expression in various stages of the colorectal tumour was analysed in twenty-two colorectal cancer patients, and the results identified the upregulation of TIGAR in colorectal patients with the additional finding of a noticeable increased TIGAR expression at the mRNA and protein levels in stage II and stage III colorectal cancer compared to adjacent normal tissue (276). Another interesting finding in the above study is the nuclear localisation of TIGAR in their

immunohistochemical staining (276), whereas the majority of the studies, including our study, observed cytoplasmic staining of TIGAR (see section 2.4.4).

4.1.3 TIGAR reduces ROS to promote tumour growth

The role of TIGAR in promoting tumour cell survival is based on its ability to inhibit both apoptosis and autophagy (216). It has been observed that TIGAR expression reduced the ROS levels and the cancer cells were protected from ROS-sensitive apoptotic responses, such as those induced by p53 (197).

Accumulation of ROS is one of the main sources of oxidative stress within the cells, and it has the harmful effects of arresting the cell cycle or leading to cell death (294). In mammalian cells, NADPH provides the major reducing power used to synthesize cellular antioxidant capacity and protects the cells from oxidative stress, and thus rapidly proliferating cells require NADPH for their normal function, proliferation and survival (298). In line with the pro-survival role of NADPH, TIGAR overexpression was observed in nasopharyngeal carcinoma (NPC) cell lines, and it was linked to increased cellular growth, increased NADPH production and also increased invasiveness of NPC cell lines (295). Inhibition of c-Met tyrosine kinase inhibited tumour growth in NPC cell lines, and during c-Met inhibition, it was observed a significant downregulation of TIGAR and subsequent depletion of intracellular NADPH, which suggested a link between c-Met, TIGAR and NADPH in cancer cells (298). In another study on NPC cells, knockdown of TIGAR contributed to NF-κB pathway inactivation, with an increased IκB-α expression, and an inhibited translocation of p65 into the nucleus, indicating an inhibited NF-κB pathway, thus supporting the role of TIGAR as a tumour promoter (295).

4.1.4 TIGAR expression negatively correlated with p53 expression

In a study of breast cancer patients, it was observed that high p53 expression was significantly associated with the low expression levels of SCO2 (P=0.008) and TIGAR (P=0.007), and it has been suggested that high p53 expression could promote aerobic glycolysis in breast cancer via modulation of mitochondrial enzymes (SCO2 and COX) and TIGAR (275).

A similar immunohistochemical analysis of 110 cases of primary gastric cancer identified an inverse correlation between p53 and TIGAR and suggested that high p53 expression could be associated with the promotion of glycolysis in gastric cancer via the modulation of TIGAR expression (274). Both studies on breast cancer and primary gastric tumours showed that p53 expression was negatively correlated with TIGAR expression (274, 275), and analysis of our IHC data did not reveal any significant association between inferred p53 mutant status and TIGAR expression in TMA set 1 (P=0.580) (section 3.2.3). Unfortunately, it has not been possible to address this in the TMA set 2 samples because of the overall strong staining of TIGAR in all the slides.

4.1.5 Antitumour effects of TIGAR

We have seen that increased TIGAR expression correlates with increased cellular growth and invasiveness (276, 294, 295), whereas a study on 79 patients with primary non-small cell lung cancer (NSCLC), which compared SUV_{max} (maximal standardised uptake value determined through PET imaging) with TIGAR expression identified that SUV_{max} was negatively correlated with TIGAR expression and decreased expression of TIGAR was strongly correlated with a poor clinical outcome (277). TIGAR was observed to act on cell cycle arrest, and it was proposed

that TIGAR promoted p21-independent, p53-mediated G1-phase arrest in cancer cells (299).

To summarise the effects of TIGAR on cancer;

TIGAR has two functions: (1) p53 dependent FBPase activity that is manifest in normoxic, hypoxic, and glucose-limited cells and functions to promote PPP, generate NADPH, and limit ROS (2) a non-catalytic function, independent of the FBPase, a hypoxia-induced activity that depends on HIF1α and glucose, and involves mitochondrial localisation, and binding to HK-2 stimulating HK-2 enzymatic activity (206).

In our immunohistochemical analysis, TIGAR protein expression was detected in 73% of samples in TMA set 1, whereas in TMA set 2, we observed TIGAR expression in all of the samples.

Thus, in our analysis, the majority of SCCHN samples expressed detectable levels of TIGAR. This indicates that there appear to be two distinct patterns of TIGAR expression in cancers. One in which the expression of TIGAR reduced with increased p53 expression (presumably often mutated). The second pattern of expression observed in most cancers suggests that high (possibly increased) TIGAR expression, independent of p53 expression, is a poor prognostic indicator.

At first sight, this appears to be counter-intuitive, given the commonly observed increase in aerobic glycolysis in many cancers. This can be explained in the following way. In addition to possessing activity as an FBPase, TIGAR has been shown to stimulate HK-2 activity independently of its intrinsic FBPase activity. In this way, an increase in TIGAR might promote increased glycolysis and thus contribute to tumour progression. Clearly, this mechanism is regulated by the

subcellular localisation of TIGAR, and this suggests that a more careful analysis of this might prove informative in future studies.

4.2 Immunohistochemical expression of p53

The other protein of interest in this study was p53, and our immunohistochemical analysis inferred that p53 was likely to be mutated in approximately 62% of samples from TMA set 1 and in 65% and 50% of samples from the tumour core and advancing front samples of the larynx and hypopharynx cohort of TMA set 2. In lymph node samples of larynx and hypopharynx, the inferred p53 mutant rate was 83.9%. This is similar to the estimate of 84% for p53 mutation obtained by TCGA network analyses of 279 SCCHN cases (39). Our inferred p53 mutation rate is also similar to another large series study (724 primary SCCHN patients), which identified a high p53 expression of 71.7% in their samples by immunohistochemical analysis (300).

Another important observation we have made was the pattern of p53 expression in our oropharyngeal samples. Although we would expect an inverse relationship between the presence of HPV DNA and the presence of *TP*53 mutations in oropharyngeal squamous cell carcinoma (301), in our limited number of oropharynx samples, inferred p53 mutation rate was 72.6% and 50.00% for tumour core and advancing front samples, respectively. This seems surprisingly high since we might expect p53 in these samples to frequently be wild-type as a result of HPV infection in many of this cohort.

The expression of wild-type p53 in HPV related oropharyngeal SCC (OPSCC) (39), creating a possible confounder as HPV driven tumours commonly have a favourable prognosis (192). HPV positive head and neck tumours display improved survival,

with a 60% lower risk of death, compared to the HPV negative tumours (302). We also found a significant survival difference between HPV +ve and -ve oropharyngeal cases where HPV +ve cases showed a better survival period as compared to HPV negative cases (P=<0.001) (section 3.3.5.2).

4.2.1 IHC expression of p53 as a surrogate marker for p53 mutation

Our justification for using IHC to find the inferred p53 mutation rate was based on the following facts; wild-type p53 in unstressed cells has a short half-life, and as a result, it is found at very low concentrations in all healthy cells, so wild-type p53 is almost undetectable in the routine immunohistochemical analysis (303). Compared to wild-type p53, most mutant p53 has a long half-life and tends to accumulate in the nucleus so that it can be a stable target for immunohistochemical detection (304, 305). Most p53 mutations are missense mutations, and these often compromise the p53 transcriptional activity resulting in a breakdown in the p53-MDM2 autoregulatory feedback loop and thus lead to stabilisation of the p53 protein. This can then be detected by immunohistochemical methods (303). Thus, the detection of p53 by using IHC in tumours is almost synonymous with the presence of a mutation, and immunohistochemical analysis of p53 expression is utilised as a surrogate marker for its mutation analysis (306-308).

Not all mutations in the *TP*53 gene result in protein stabilisation. For example, mutations due to gene deletion or truncation of the protein (nonsense and frameshift) do not cause protein accumulation (303). This is the reason we have considered the complete absence of p53 expression as an ‘inferred nonsense mutation’ and added it to the inferred mutant category. Based on this fact, our ‘inferred mutant’ category includes cells showing either >5% or complete absence of p53 expression.

We decided to have the cut off value as >5% for the expression of p53 in the inferred mutant category. Justification for using a 5% cut off is based on the following facts. Accumulation of p53 in the nucleus also happens after stress, but because the induction is only temporary, cells in that tissue will be in different phases of the cell cycle, and they will have different responses to stress. Corresponding immunohistochemical expression of p53 will be showing a punctate staining pattern where different cells with various staining intensity. We use a cut off value to distinguish between these occasional cells which were induced because of stress compared to tumours, where a significant percentage of cells will express detectable levels of p53 protein. We fixed a 5% cut off value based on the historical data, and we also believe that it is unusual for wild-type tissue expressing p53 protein in more than 5% of cells.

We have noted a similar cut off value (5%) in a study where they evaluated p53 response to short-term preoperative radiotherapy and patient survival in rectal cancer (309). But, various authors have used a different cut off value for the percentage of p53 nuclear staining to determine p53 mutation (189, 191, 192, 300, 310). One of the studies analysed fifty-five cases of oral squamous cell carcinomas, where the authors increased their cutoff value for p53 immunoexpression to 25%, and they observed increased overexpression of p53 (64%) in their samples (311). They suggested that 25% of p53 immunopositivity appears to be a good cut off value to predict *TP*53 mutations (311).

4.3 HK-2 expression in SCCHN

The third biomarker used in our study was HK-2, and HK-2 expression was detected in all the samples in our western blot analysis. In IHC, we observed 42.4% and 28.3% of strong HK-2 expression in the tumour core and advancing front samples of

larynx and hypopharynx, respectively, in TMA set 2. Oropharynx samples displayed a strong HK-2 expression of 54.8% in the tumour core and 38.7% in the advancing front samples. The lymph nodes displayed a strong HK-2 expression of 61.3% in the larynx and hypopharynx groups and 79.3% in the oropharynx group.

HK-2 expression is rarely observed in normal tissues, and increased levels of HK-2 expression have been reported in various solid tumours, including colorectal tumour (312), gastric cancer (313), hepatocellular carcinoma (314), ovarian cancer (315), and pancreatic cancer (316), indicating high expression of HK-2 in tumorigenesis (317).

In SCCHN, HK-2 is highly expressed, implying that SCCHNs are "glycolytic tumours" (318). Increased HK-2 expression was observed in oral squamous cell carcinoma along with other cancer metabolism-related proteins, including GLUT-1, lactate dehydrogenase A (LDHA), transketolase-like-1 (TKTL1), mitochondrial enzymes (succinate dehydrogenase SDHA, SDHB, and ATP synthase) and insulin-like growth factor receptor (IGF-1R) (319). The above study was the first evidence of the expression of glycolysis-related proteins and mitochondrial enzymes in the multi-step tumorigenesis of SCCHN (319). It was observed that squamous cell carcinoma of the tongue with higher migratory /invasive capacity had increased levels of HK-2 expression and that HK-2 overexpression promoted the proliferation, migration, and invasion of tongue cancer cells, whereas HK-2 knockdown inhibited these processes both *in vitro* and *in vivo* (320). Overexpression of HK-2 has been observed in laryngeal cancer, and it has been suggested that high HK-2 expression might be related to the progression of laryngeal cancer (321).

4.4 Interrelations between p53, TIGAR, and HK-2

We believe that our proteins of interest, p53, TIGAR and HK-2, interact in the development of cancer metabolism and influence the expression of each other proteins. This statement is further supported by the following facts; as a p53-inducible protein, TIGAR regulates mitochondrial HK-2 localisation, and this TIGAR-HK-2 complex further upregulates HK-2 and HIF1-α activity resulting in reduced ROS production, which protects the tumour cell death under hypoxic condition, implying that p53 could be an important key regulator for HK-2 mediated tumorigenesis (206, 285, 318).

Our attempts to explore the inter-relations of these proteins were based on the following observations; the association between p53 and HK-2 expression was analysed in our larynx and hypopharynx samples, and it was observed that there was a significant association in tumour core (P=0.003) and advancing front (P=0.047) samples. This observation suggested that patients with strong HK-2 are more likely to have inferred mutant p53 status in the larynx and hypopharynx samples.

An association between p53 and HK-2 in tumour cells was first reported by Mathupala et al. in 1997, who identified two functional p53 binding motifs within the HK-2 promoter and suggested that mutated p53 interacts with the HK-2 promoter in cancer cells to activate transcription of HK-2 (286). These authors were amongst the first to propose that mutation of p53 was able to induce a gain-of-function and permit transactivation of a gene (HK-2) that was essential for maintaining high glycolytic activity and therefore further support the survival of a rapidly growing tumour (286).

Following the observation of an association between p53 and HK-2 in our IHC analysis, TIGAR expression was also analysed to determine whether any association could be detected with p53 expression in TMA set 1, and no significant association between p53 and TIGAR expression was detectable (*P*=0.580). Because of the overall strong staining of TIGAR in TMA 2, we were not able to identify any correlation between TIGAR and either p53 or HK-2.

4.5 Association between p53, TIGAR, and HK-2 with the clinical variables

In our second part of the IHC analysis, the expression of TIGAR, p53 and HK-2 was analysed and compared with clinical variables to determine whether any association exists between the individual protein expression and any one of the variables. We observed a significant association between p53 expression and anatomical sites in oropharynx samples (both tumour core [*P*=0.011] and advancing front [*P*=0.015]), and similarly with HK-2 expression and anatomical sites in larynx and hypopharynx cases (both tumour core [*P*=0.017] and advancing front [*P*= 0.041]). The significance of differing anatomical sites altering prognosis is supported by evidence that shows that tumours from different anatomical sites display differing biological behaviour with responses to treatment depending on the primary anatomical sites (322). However, a systematic review and a meta-analysis failed to provide conclusive evidence about the prognostic value of p53 expression in patients with SCCHN arising from larynx, oropharynx, hypopharynx, or oral cavity (182).

There was a significant association between p53 expression in tumour core samples of the oropharynx and the event (death) status (*P*=0.017), but the subsequent disease-specific survival analysis by Kaplan- Meier did not identify any statistically

significant association between p53 expression and the survival period in our oropharynx samples.

There is good evidence from the literature suggesting accumulation of p53 can serve as a prognostic indicator of overall and disease-specific mortality in SCCHN (323). We have observed a significant association between p53 expression in the advancing front samples of larynx and hypopharynx and survival period (P=0.034), suggesting inferred p53 mutant status in the advancing front samples was associated with poorer disease-specific survival compared to the inferred wild-type category (see section 3.3.1.4).

Our analysis of the association between HK-2 expression with clinical variables identified the following findings; there was a significant association between HK-2 expression in tumour core samples of larynx and hypopharynx and N stage (P=0.023), differentiation (P=0.041), and vascular invasion (P=0.034).

In the oropharynx samples, we observed the following association between HK-2 expression and the known clinical variables; there was an association between HK-2 expression in tumour core samples of the oropharynx and ECS (extracapsular spread) (P=0.030), and in lymph nodes samples of the oropharynx with nerve invasion (P=0.020).

4.6 Targeting metabolic pathways

Targeting altered metabolic pathways related to carbohydrate metabolism is a potentially promising anti-cancer strategy (324).

4.6.1 Targeting TIGAR for anti-cancer treatment

There is emerging evidence that targeting TIGAR and its downregulation favours anti-growth properties (298, 325-327). Resveratrol (3,5,4'-trihydroxystilbene), a phytoalexin, has been identified to exhibit its anti-cancer effects through a variety of mechanisms, and one among them is downregulation of TIGAR (328). An RNA-directed nucleoside analogue, ECyd, is known to possess anti-cancer activity, and it was observed that ECyd also could induce significant downregulation of TIGAR (329).

4.6.2 Targeting p53 for anti-cancer treatment

There is convincing evidence that aerobic glycolysis constitutes the metabolic signature of SCCHN, and this metabolic adaptation is driven by the mutational loss of wild-type p53 function (330). Thus, p53 becomes the promising target, which either restores wild-type p53 activity or inhibits mutant p53 oncogenic activity, which could provide a potent strategy to treat malignant diseases (331). The approaches to activate endogenous wild-type p53 include the use of gene therapy to introduce wild-type p53 or modified adenovirus to kill tumour cells with mutant p53, the use of chemoradiation to activate endogenous wild-type p53, and the use of synthetic peptides or nongenotoxic small molecules to activate wild-type p53 (332). Nutlins are potent and selective low molecular weight inhibitors of MDM2-p53 binding, which activate the p53 pathway and suppress tumour growth *in vitro* and *in vivo* (333). Another small molecule that reactivates wild-type p53 is RITA (Reactivation of p53 and induction of tumour cell apoptosis) could suppress tumour cell growth both *in vitro* and *in vivo* by inducing massive apoptosis in a p53-dependent manner (334). Restoring p53 function in those tumours expressing mutant

p53 is even more challenging, and small molecules that refold some mutant p53 proteins and thus reactivate their wild-type functions that have been described (335).

4.6.3 Targeting HK-2 for anti-cancer treatment

Metabolic enzymes could be an attractive candidate for cancer therapy, but there must be a significant difference in the requirement for a given enzyme activity between cancer cells and normal proliferating cells; potential examples include GLUT1, HK-2 and LDH-A (336). Hexokinases, which catalyse the first committed step of glucose metabolism, are one of the promising targets for anti-cancer therapy as many cancer cells overexpress HK-2, and preclinical studies demonstrated that the inhibition of HK-2 could be an effective cancer therapy (337). As most healthy adult cells do not express HK-2, its systemic ablation could selectively target tumour cells, and there is good evidence that HK-2 acts on tumour cells without adverse physiological consequences (116). However, it is challenging to develop small-molecule inhibitors, which preferentially inhibit HK-2, as there are structural similarities between HK-1 and HK-2 (116, 218, 226, 231). The allosteric inhibition of HK-1 and HK-2 by their own product, G6P, could be utilised to target HK-2 (116). G6P could also be utilised to preferentially target HK-2, although G6P inhibits both HK-1 and HK-2, its inhibitory effect on HK-2 increases in the presence of orthophosphate, whereas HK-1 inhibition is reduced (218). Another promising agent for targeting HK-2 is 3-bromopyruvate (3-BP), whose biological function is based on the alkylation of free thiol groups on the cysteine residues of proteins (338). The small alkylating molecule, 3-BP, was discovered as a novel anticancer agent *in vitro* in the year 2000 and was published in 2001 (339). The inhibitory effects of 3-BP on the glycolytic pathway have been demonstrated in various *in-vitro* studies, which are mediated by covalent modification of HK-2 (340). 3-BP targets cancer

cell's energy metabolism, i.e., both glycolysis and mitochondrial oxidative phosphorylation to inhibit total energy (ATP) generation and depletes all energy reserves (338, 339). The action of 3-BP happens rapidly (within minutes) and with little or no effect on most normal cells or the animals as compared to the frequently used chemotherapeutic drugs which may take a longer duration of time (weeks/months) to exhibit any significant changes (338). Therefore, 3-BP, as a pyruvate mimetic, is a potent, rapid and quite specific anti-cancer agent (221, 341). 3-BP was tested in pre-clinical models, where it was shown to be effective, eradicating advanced tumours in 19/19 animals, without harming the animals and without returning of the cancer during their lifetime (342). It has been reported that 3-BP is non-toxic to all sorts of vertebrates and certain failure cases were still reported in clinical trials (343). Apart from 3-BP**,** other agents that can inhibit hexokinases are 2DG (2-deoxy-D-glucose) (344), and Lonidamine (345).

4.7 Limitations of our study

The main limitations of our study were different cohorts of patient samples, choosing IHC for evaluating p53 expression, and practical difficulties in conducting metabolic studies. Due to the delay in the construction of new head and neck TMA, we started the research by using readily available TMA, which had samples of oral cavity and oropharynx (TMA set 1). The new TMA had different patient's samples from larynx, hypopharynx, and oropharynx with different sets of clinical data (TMA 2), which made us evaluate the two TMAs separately.

Selecting immunohistochemistry to investigate p53 was based on the fact that most mutations change the conformation of p53, indirectly leading to a more stable protein which can then accumulate in tumour nuclei and subsequently can be detected

immunohistochemically (278). However, there are many problems in IHC that can result in false-negative or false-positive outcomes (306, 308, 346).

False-positive results can be due to stabilisation of wild type p53 by physiological stimuli such as hypoxia, oncogenic stresses, or DNA damage resulting from the free radicals released from the tumour-associated macrophages or following therapy, leading to positive staining in the absence of mutation (347, 348). On the other hand, false-negative results are possible because of truncating alterations, including nonsense, frameshift and splice site mutations, which result in a lack of immunolabeling due to the absence of gene product (349). Erroneous splicing produces a truncated protein, which will have a shorter half-life and escapes IHC detection (350).

The common antibodies used (DO7, DO1, and Pab 1801) for p53 detection in IHC are unable to differentiate between mutant and wild-type p53 proteins (182, 351). Presently, there is no consensus for the most appropriate antibody for evaluating mutation associated p53 expression (352).

Another issue is the selection of cutoff points to dichotomize p53 positivity versus p53 negativity, which varies from one positively stained cell to 50% positivity, and both extremes are difficult to justify from a biological perspective (182). The frequent occurrence of heterogeneous upregulation of mutant p53 has been observed (353), and thus fixing a cutoff of 50% might exclude many mutant proteins that display low levels of p53 positivity (182). In future studies, it is essential to improve the reliability of p53 IHC as a surrogate method, and one simple strategy is to combine p53 detection along with monitoring of p53 target gene expression (MDM2 and/or p21) (278). When cells expressing p53 but not expressing MDM2 and/or p21,

regardless of the relative levels, likely to have mutant p53, whereas coexpression of p53 and MDM2 would be likely to have wild-type p53 proteins (182, 278).

Targeting cancer cell metabolism seems appealing at first glance because enzymes are attractive molecular targets; however, there are some significant issues when targeting glucose metabolism for anticancer therapy (336). Apart from the tumour cells, immune and stem cells can also perform aerobic glycolysis, and it can be hard for anti-metabolic therapies to differentiate between tumour and non-tumour cells (336). Most of the metabolic reprogramming studies were performed in cancer cell lines rather than intact tumours, and it is challenging to model an accurate tumour microenvironment in culture (111). Another challenge could arise from the metabolic plasticity displayed by cancer cells as there is a possibility that cancer cells could develop resistance to inhibition of a particular pathway through the expression of alternative isoforms or up-regulation of alternate pathways, such as gluconeogenesis (336). Despite these challenges and several unanswered questions in the field of cancer metabolism, our understanding of cancer metabolism has advanced noticeably in recent years and is being used for the development of novel targeted therapeutic strategy (354).

4.8 Future work related to cancer metabolism

Our unit's recent work has confirmed the role of p53 in the metabolic regulation in SCCHN cells and suggested that when cells display loss of p53 function, they can be sensitised to ionizing radiation by pre-treatment with a glycolytic inhibitor (112). Future experiments in a pre-clinical model are required to provide further evidence for the feasibility of therapeutic strategy.

We were recently awarded an ODA Research Seed fund of £10,000 from the University of Liverpool (2020/21 round) to conduct an animal study, collaborating with Adyar Cancer Institute and Sri Ramachandra Institute of Higher Education (SRIHER) at Chennai, India. We propose to develop a preclinical model for oral cancer, and as a first step, we will test the tumorigenicity of our selected SCCHN cell lines in nude mice. With the collaboration between the University of Liverpool and Cancer Institute and SRIHER, we hope to develop local expertise at Indian Institutions in growing and manipulating SCCHN cell lines as well as generating mouse models of cancer.

4.9 Summary

In summary, this is the first study of TIGAR expression in SCCHN, and our data suggest that, unlike some other cancers, the link between p53 and TIGAR expression is retained, at least in cell lines. HK-2 is expressed in all cell lines, and the steady-state levels do vary much between cells with different p53 status. It is, therefore, perhaps surprising that we have detected some variability in HK-2 expression in tumour samples by IHC. Moreover, we have identified a strong association between HK-2 expression and p53-inferred mutant status in larynx and hypopharynx samples which suggest that loss of p53 function, which would be expected to increase glycolysis, and is associated with increased expression of a key glycolytic enzyme. This is not surprising, but it is the first time that this association has been identified in SCCHN. Importantly, this may indicate that targeting HK-2, for example, with an inhibitor, could prove particularly effective in p53 mutant tumours. These studies include the first attempt to characterise TIGAR expression in SCCHN, and it is combined with analysis of HK-2 and using IHC to infer p53 status has revealed some intriguing associations. Ultimately, it is clear that cancer cell

metabolism is a highly attractive target for therapy. More promising results have been observed in anti-HK-2 treatments, especially with 3-BP. By creating a preclinical model, we are hoping to achieve the successful bench-to-bedside translation of basic scientific findings to novel anti-cancer interventions.

5. Appendix

5.1 Initial optimisation pictures of TIGAR staining

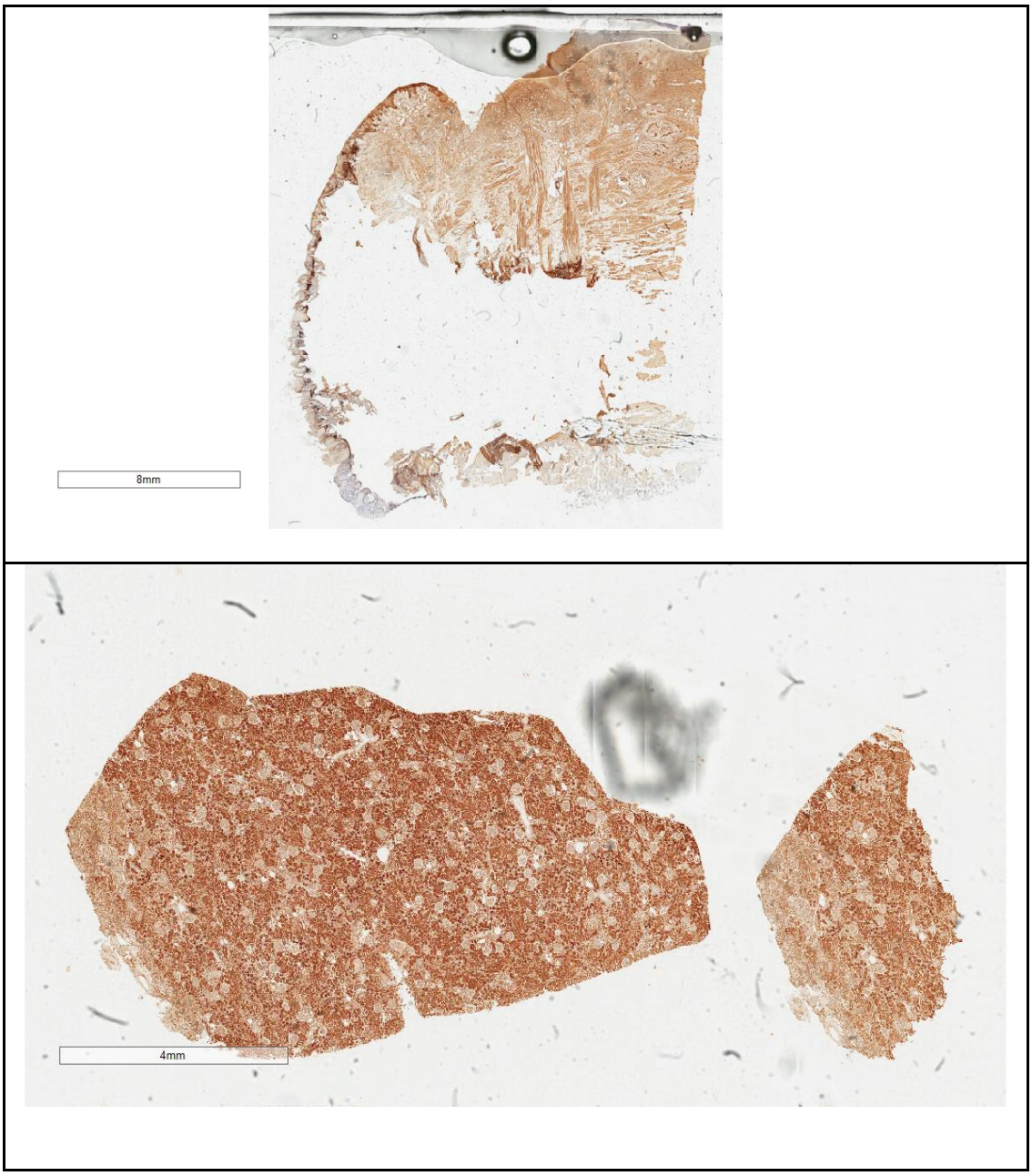

Figure 5:1 Immunohistochemical analysis of TIGAR expression. A tissue microarray (TMA) was stained using a purified rabbit polyclonal antibody (AB10545), as described in section 2.4.3. This figure illustrates the magnified views of representative slides from the initial TIGAR optimisation staining. Magnification is represented by the individual scale bar in the figure. (A) represents TIGAR expression in tonsil (B) represents TIGAR expression in kidney

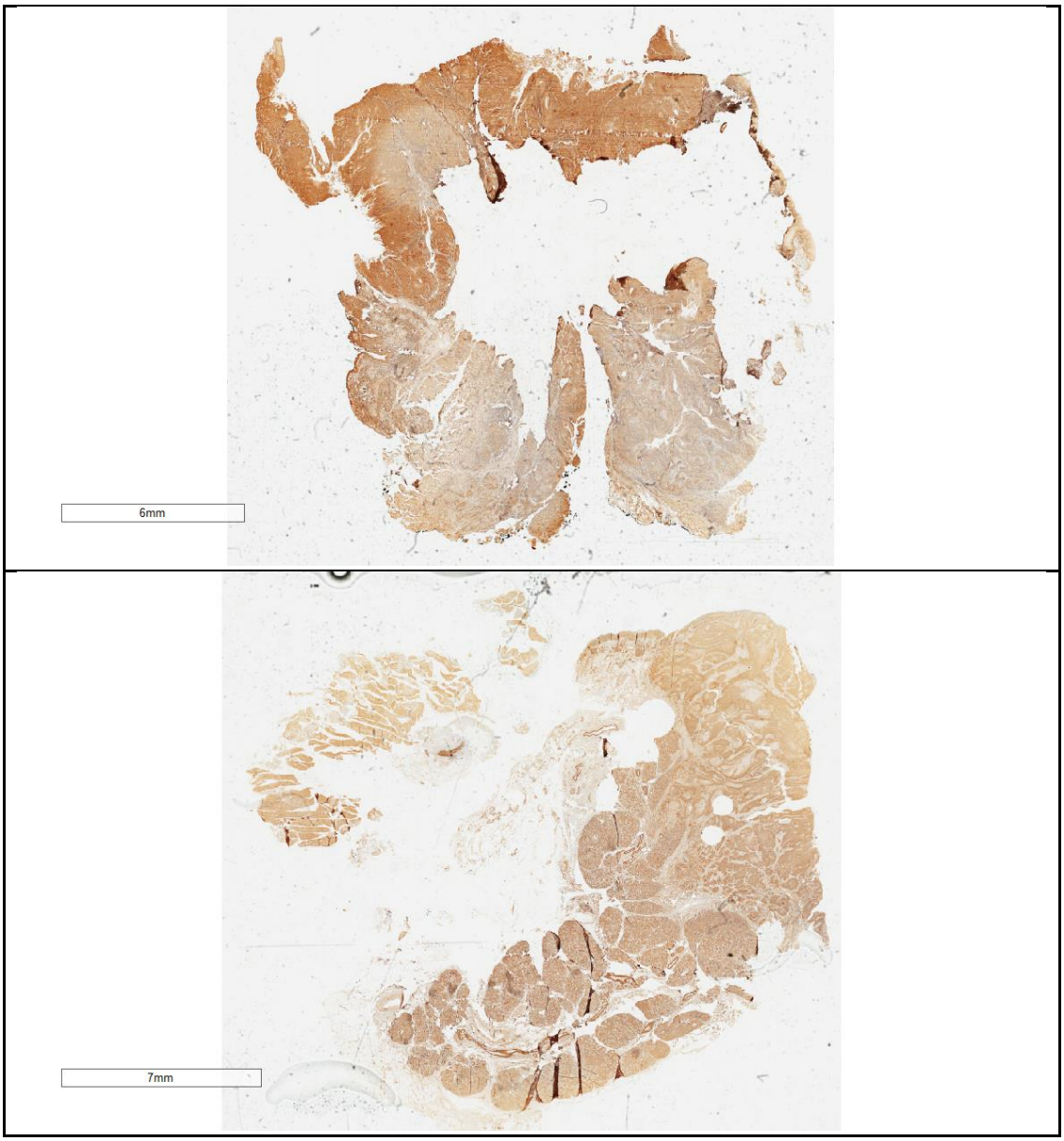

Figure 5:2 Immunohistochemical analysis of TIGAR expression. A tissue microarray (TMA) was stained using a purified rabbit polyclonal antibody (AB10545), as described in section 2.4.3. This figure illustrates the magnified views of representative slides from the initial TIGAR optimisation staining. Magnification is represented by the individual scale bar in the figure. (A) represents TIGAR expression in soft palate (B) represents TIGAR expression in the supraglottis

5.2 Initial optimisation pictures of HK-2 staining

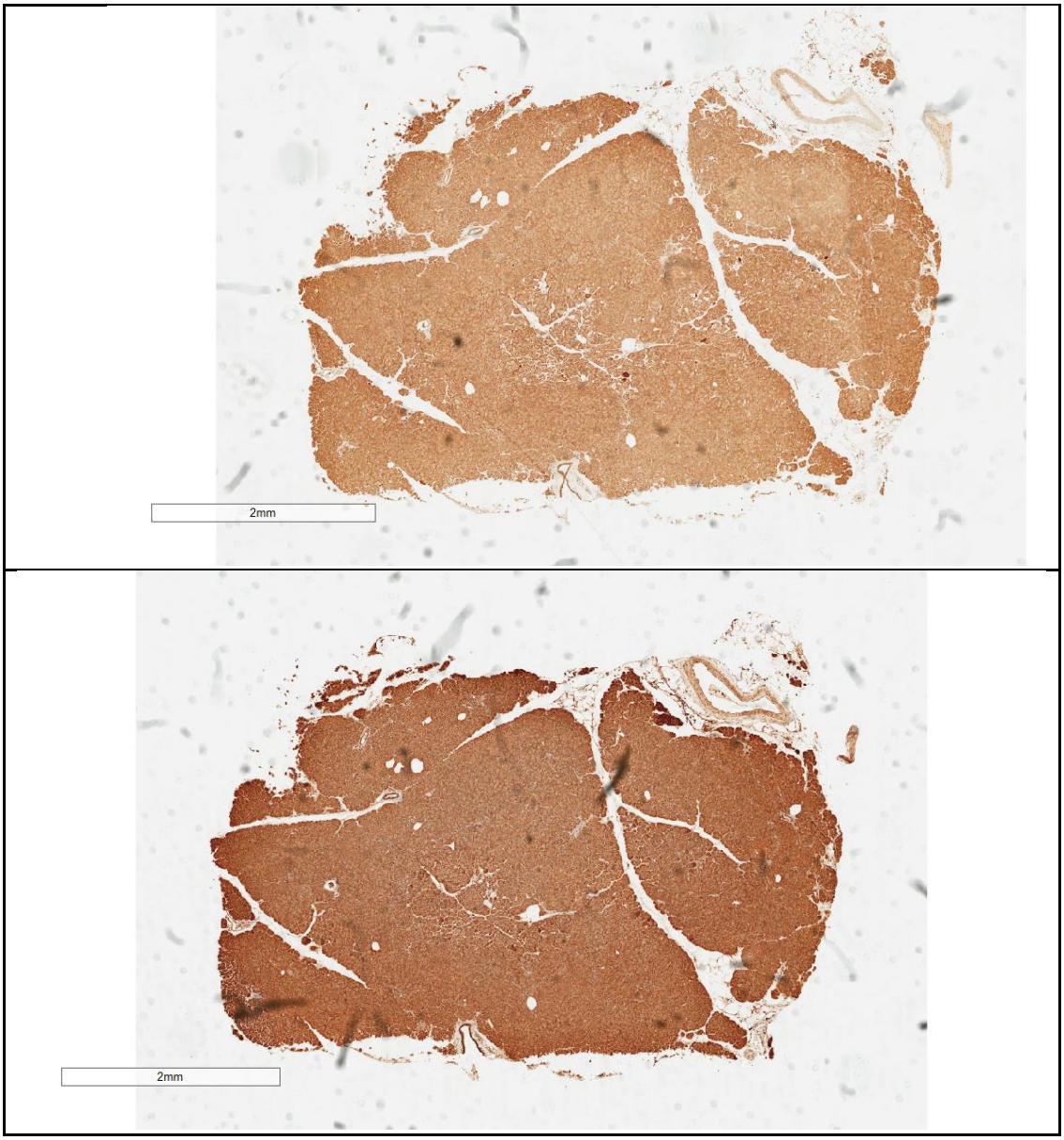

Figure 5:3 Immunohistochemical analysis of HK-2 expression. A tissue microarray (TMA) was stained using a rabbit monoclonal antibody (C64G5) from Cell Signaling (New England Biolabs), as described in section 2.4.3. This figure illustrates the magnified views of representative slides from the initial HK-2 optimisation staining. Magnification is represented by the individual scale bar in the figure. (A) represents HK-2 expression in the pancreas (1 in 50 concentration) (B) represents HK-2 expression in the pancreas (1 in 100 concentration)

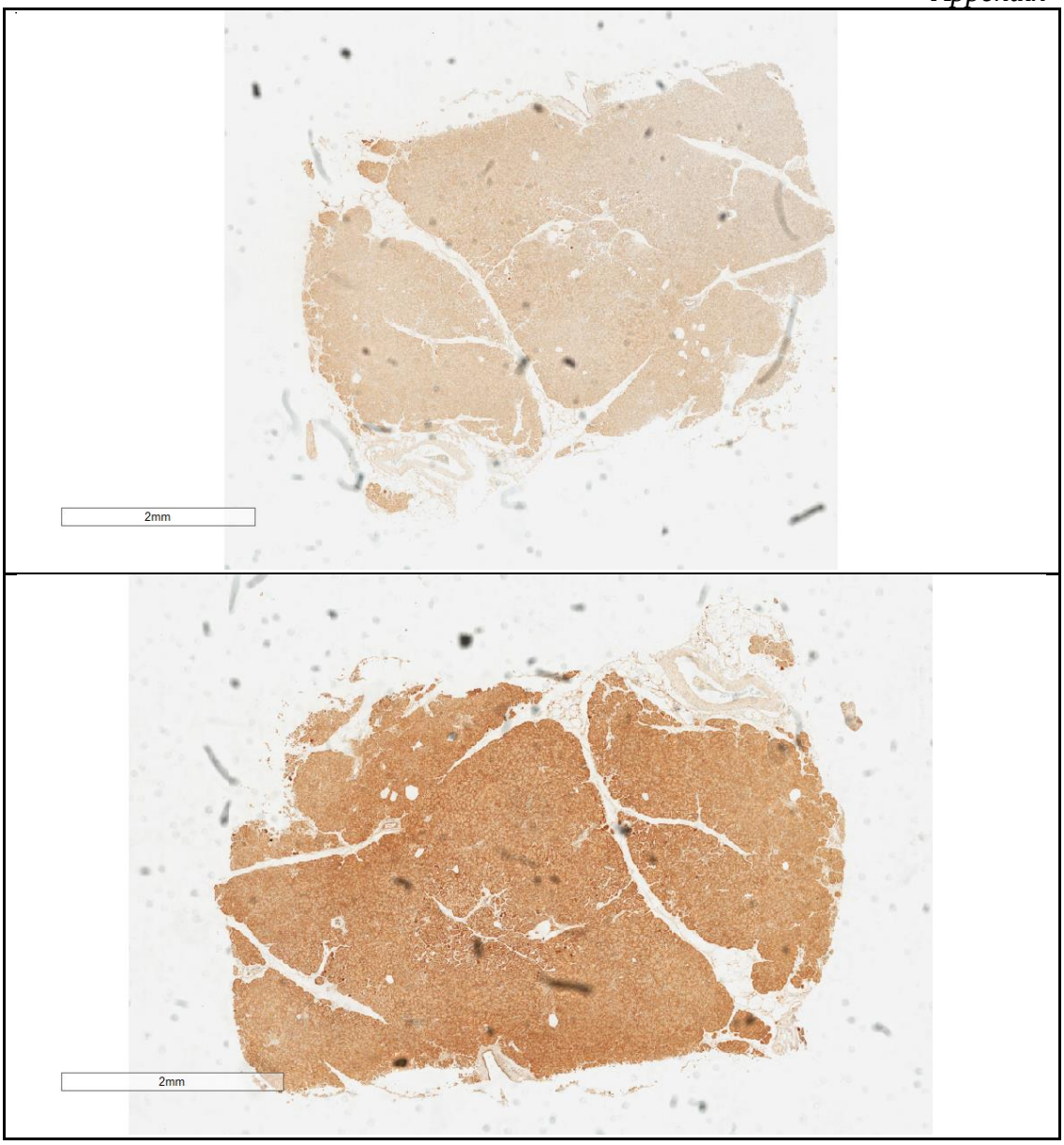

Figure 5:4 Immunohistochemical analysis of HK-2 expression. A tissue microarray (TMA) was stained using a mouse monoclonal antibody (NBP2-02272) from Novus Biologicals, as described in section 2.4.3. This figure illustrates the magnified views of representative slides from the initial HK-2 optimisation staining. Magnification is represented by the individual scale bar in the figure. (A) represents HK-2 expression in the pancreas (1 in 50 concentration) (B) represents HK-2 expression in the pancreas (1 in 100 concentration)

5.3 Distribution of cores in oropharynx

Table 5-1 Distribution of cores in oropharynx – TMA set 2

OROPHARYNX - NUMBER OF CORES				
Patient ID	**Tumour core**	**Advancing front**	**Normal tissue**	**Lymph node**
1	3	3	MISSING	
2	3	3	2	
3	3	3	MISSING	
4	2	2	MISSING	
5	MISSING	3	MISSING	
6	MISSING	MISSING	2	
7	3	3	2	
8	3	3	2	
9	3	2	3	
10	3	2	MISSING	
11	3	3	2	
12	3	3	3	
13	3	3	3	
14	3	3	MISSING	
15	3	3	3	
16	3	3	3	
17	3	2	3	
18	3	3	MISSING	
19	3	2	MISSING	
20	3	2	3	
21	3	3	3	
22	3	3	MISSING	
23	3	3	3	
24	3	3	2	
25	2	2	2	
26	3	3	3	
27	2	2	2	
28	3	2	MISSING	
29	3	MISSING	3	
30	3	3	2	
31	3	MISSING	MISSING	
32	3	MISSING	3	
33	3	2	3	
34	3	2	MISSING	
35	3	2	1	
36	2	3	3	

37	2	3	3	
38	3	3	3	
39	2	2	2	
40	1	2	3	
41	3	3	MISSING	
42	3	3	3	
43	3	3	3	
44	3	3	MISSING	
45	3	3		
46	3	3	MISSING	
47	3	3	MISSING	
48	3	3	3	
49	3	3	MISSING	
50	2	3	3	
51	3	3	MISSING	
52	3	3	MISSING	
53	2	3	MISSING	
54	3	3	MISSING	
55	3	3	MISSING	
56	3	3	3	
57	1	2	3	
58	3	3	MISSING	
59	3	3	3	
60	3	3	3	
61	2	3	MISSING	
62	2	3	MISSING	
1				3
2				3
3				3
4				2
5				3
6				3
7				3
8				3
9				3
10				3
11				3
12				2
13				3
14				3
15				3
16				3
17				3

18				2
19				3
20				3
21				3
22				3
23				3
24				3
25				3
26				3
27				3
28				3
29				3

5.4 Distribution of cores in the larynx

Table 5-2 Distribution of cores in the larynx – TMA set 2

	LARYNX - NUMBER OF CORES			
Patient ID	**Tumour core**	**Advancing front**	**Normal tissue**	**Lymph node**
1	3	3	3	
2	duplicate			
3	3	3	MISSING	
4	3	3	MISSING	
5	3	3	MISSING	
6	3	3	MISSING	
7	3	3	3	
8	3	3	MISSING	
9	3	3	MISSING	
10	3	3	MISSING	
11	3	3	MISSING	
12	3	3	MISSING	
13	3	3	3	
14	3	3	3	
15	3	3	MISSING	
16	3	3	MISSING	
17	MISSING	3	MISSING	
18	3	2	MISSING	
19	MISSING	3	MISSING	
20	3	3	MISSING	
21	3	MISSING	MISSING	
22	MISSING	3	MISSING	
23	3	3	MISSING	
24	3	3	MISSING	
25	3	3	MISSING	
26	3	3	3	
27	3	2	3	
28	3	3	3	
29	3	3	3	
30	3	3	3	
31	3	3	3	
32	3	3	3	
33	3	3	MISSING	
34	3	3	MISSING	
35	3	3	MISSING	
36	3	3	MISSING	

37	3	3	3	
38	3	3	MISSING	
39	3	3	MISSING	
40	3	3	3	
41	3	3	MISSING	
42	3	3	3	
43	1	1	2	
44	3	3	3	
45	3	3	MISSING	
46	3	3	MISSING	
47	2	3	3	
48	3	3	MISSING	
49	3	3	2	
50	3	3	MISSING	
51	3	3	3	
52	3	3	3	
53	3	3	MISSING	
54	3	3	MISSING	
55	3	3	MISSING	
56	3	3	3	
57	3	3	MISSING	
58	3	3	3	
59	3	3	3	
60	3	3	3	
61	3	3	3	
62	3	3	3	
63	3	MISSING	3	
64	3	3	MISSING	
65	3	3	3	
66	3	3	3	
67	3	3	MISSING	
68	3	3	MISSING	
69	3	MISSING	MISSING	
70	3	3	MISSING	
71	3	3	MISSING	
72	3	3	MISSING	
73	3	3	3	
74	3	3	3	
75	3	2	MISSING	
76	3	3	MISSING	
77	3	3	MISSING	
1				3

2				3
3				3
4				3
5				3
6				3
7				3
8				3
9				3
10				3
11				3
12				3
13				2
14				3
15				3
16				3
17				3
18				2
19				3

5.5 Distribution of cores in the hypopharynx

Table 5-3 Distribution of cores in hypopharynx – TMA set 2

	HYPOPHARYNX – NUMBER OF CORES			
Patient ID	**Tumour core**	**Advancing front**	**Normal tissue**	**Lymph node**
1	3	3	3	
2	3	3	2	
3	3	3	1	
4	3	3	MISSING	
5	MISSING	2	3	
6	2	3	MISSING	
7	3	3	MISSING	
8	3	3	3	
9	2	2	MISSING	
10	MISSING	3	3	
11	2	3	MISSING	
12	3	3	MISSING	
13	2	3	2	
14	3	3	2	
15	3	3	MISSING	
16	3	2	3	
17	3	3	2	
18	2	2	MISSING	
19	2	3	2	
20	3	2	2	
21	MISSING	3	MISSING	
22	2	3	3	
1				3
2				3
3				3
4				2
5				1
6				2
7				3
8				3
9				3
10				3
11				3
12				3

6. References

1. Argiris A, Karamouzis MV, Raben D, Ferris RL. Head and neck cancer. Lancet (London, England). 2008;371(9625):1695-709.
2. Lewis JS, Jr. Sinonasal Squamous Cell Carcinoma: A Review with Emphasis on Emerging Histologic Subtypes and the Role of Human Papillomavirus. Head Neck Pathol. 2016;10(1):60-7.
3. Suh Y, Amelio I, Guerrero Urbano T, Tavassoli M. Clinical update on cancer: molecular oncology of head and neck cancer. Cell Death Dis. 2014;5:e1018.
4. Psyrri E. ESMO-Essentials-for-Clinicians-Head-Neck-Cancers-Chapter-1. 2017.
5. John C Watkinson RWG. Stell & Maran's Textbook of Head and Neck Surgery and Oncology. 5th ed. London, UK: Hodder Arnold; 2012.
6. Johnson N. Oral cancer--a worldwide problem. FDI world. 1997;6(3):19-21.
7. Moore SR, Johnson NW, Pierce AM, Wilson DF. The epidemiology of mouth cancer: a review of global incidence. Oral diseases. 2000;6(2):65-74.
8. Sankaranarayanan R. Oral cancer in India: an epidemiologic and clinical review. Oral surgery, oral medicine, and oral pathology. 1990;69(3):325-30.
9. Mehanna H, Paleri V, West CM, Nutting C. Head and neck cancer--Part 1: Epidemiology, presentation, and prevention. BMJ (Clinical research ed). 2010;341:c4684.
10. Taghavi N, Yazdi I. Prognostic factors of survival rate in oral squamous cell carcinoma: clinical, histologic, genetic and molecular concepts. Archives of Iranian medicine. 2015;18(5):314-9.
11. John Andrew Ridge M, PhD, Ranee Mehra, MD, Miriam N. Lango, MD , Thomas Galloway, MD. Head and Neck Tumours. CancerNetwork. 2016.
12. Nasal and sinus cancer 2018 [cited 2018 28th September]. Available from: https://www.nhs.uk/conditions/nasal-and-sinus-cancer/.
13. Kourelis K, Stergiou T, Papadas A, Kourelis T, Petta E, Papadas T. Clinicopathologic idiosyncrasies of nasopharyngeal cancer in a moderate-risk Mediterranean region. Acta otorhinolaryngologica Italica : organo ufficiale della Societa italiana di otorinolaringologia e chirurgia cervico-facciale. 2017;37(3):180-7.
14. Shaw R, Beasley N. Aetiology and risk factors for head and neck cancer: United Kingdom National Multidisciplinary Guidelines. The Journal of laryngology and otology. 2016;130(S2):S9-s12.
15. Ragin CC, Modugno F, Gollin SM. The epidemiology and risk factors of head and neck cancer: a focus on human papillomavirus. Journal of dental research. 2007;86(2):104-14.
16. Goon PK, Stanley MA, Ebmeyer J, Steinstrasser L, Upile T, Jerjes W, et al. HPV & head and neck cancer: a descriptive update. Head Neck Oncol. 2009;1:36.
17. Marron M, Boffetta P, Zhang ZF, Zaridze D, Wunsch-Filho V, Winn DM, et al. Cessation of alcohol drinking, tobacco smoking and the reversal of head and neck cancer risk. International journal of epidemiology. 2010;39(1):182-96.
18. Mayne ST, Cartmel B, Kirsh V, Goodwin WJ, Jr. Alcohol and tobacco use prediagnosis and postdiagnosis, and survival in a cohort of patients with early stage cancers of the oral cavity, pharynx, and larynx. Cancer Epidemiol Biomarkers Prev. 2009;18(12):3368-74.
19. Potash AE, Karnell LH, Christensen AJ, Vander Weg MW, Funk GF. Continued alcohol use in patients with head and neck cancer. Head & neck. 2010;32(7):905-12.
20. Biological agents. Volume 100 B. A review of human carcinogens. IARC monographs on the evaluation of carcinogenic risks to humans. 2012;100(Pt B):1-441.

21. Chaturvedi AK, Engels EA, Pfeiffer RM, Hernandez BY, Xiao W, Kim E, et al. Human papillomavirus and rising oropharyngeal cancer incidence in the United States. Journal of clinical oncology : official journal of the American Society of Clinical Oncology. 2011;29(32):4294-301.
22. Junor EJ, Kerr GR, Brewster DH. Oropharyngeal cancer. Fastest increasing cancer in Scotland, especially in men. BMJ (Clinical research ed). 2010;340:c2512.
23. Heck JE, Berthiller J, Vaccarella S, Winn DM, Smith EM, Shan'gina O, et al. Sexual behaviours and the risk of head and neck cancers: a pooled analysis in the International Head and Neck Cancer Epidemiology (INHANCE) consortium. International journal of epidemiology. 2010;39(1):166-81.
24. Rautava J, Syrjanen S. Biology of human papillomavirus infections in head and neck carcinogenesis. Head Neck Pathol. 2012;6 Suppl 1:S3-15.
25. Burd EM. Human papillomavirus and cervical cancer. Clin Microbiol Rev. 2003;16(1):1-17.
26. de Sanjose S, Quint WG, Alemany L, Geraets DT, Klaustermeier JE, Lloveras B, et al. Human papillomavirus genotype attribution in invasive cervical cancer: a retrospective cross-sectional worldwide study. The Lancet Oncology. 2010;11(11):1048-56.
27. Wood ZC, Bain CJ, Smith DD, Whiteman DC, Antonsson A. Oral human papillomavirus infection incidence and clearance: a systematic review of the literature. The Journal of general virology. 2017;98(4):519-26.
28. Ndiaye C, Mena M, Alemany L, Arbyn M, Castellsagué X, Laporte L, et al. HPV DNA, E6/E7 mRNA, and p16INK4a detection in head and neck cancers: a systematic review and meta-analysis. The Lancet Oncology. 2014;15(12):1319-31.
29. de Martel C, Plummer M, Vignat J, Franceschi S. Worldwide burden of cancer attributable to HPV by site, country and HPV type. Int J Cancer. 2017;141(4):664-70.
30. Tumban E. A Current Update on Human Papillomavirus-Associated Head and Neck Cancers. Viruses. 2019;11(10).
31. Guha N, Warnakulasuriya S, Vlaanderen J, Straif K. Betel quid chewing and the risk of oral and oropharyngeal cancers: a meta-analysis with implications for cancer control. Int J Cancer. 2014;135(6):1433-43.
32. Control of oral cancer in developing countries. A WHO meeting. Bulletin of the World Health Organization. 1984;62(6):817-30.
33. Warnakulasuriya S. Global epidemiology of oral and oropharyngeal cancer. Oral Oncol. 2009;45(4-5):309-16.
34. Merchant A, Husain SS, Hosain M, Fikree FF, Pitiphat W, Siddiqui AR, et al. Paan without tobacco: an independent risk factor for oral cancer. Int J Cancer. 2000;86(1):128-31.
35. Javed F, Tenenbaum HC, Nogueira-Filho G, Qayyum F, Correa FO, Al-Hezaimi K, et al. Severity of periodontal disease in individuals chewing betel quid with and without tobacco. Am J Med Sci. 2013;346(4):273-8.
36. Betel-quid and areca-nut chewing. IARC monographs on the evaluation of the carcinogenic risk of chemicals to humans. 1985;37:137-202.
37. Betel-quid and areca-nut chewing and some areca-nut derived nitrosamines. IARC monographs on the evaluation of carcinogenic risks to humans. 2004;85:1-334.
38. G Price1 MR, R Wight2 and R Crowther1. Profile of head and neck cancers in England: secular and geographical trends in the incidence, mortality and survival of laryngeal and oropharyngeal cancers 2010 [Available from: http://www.ncin.org.uk/home.
39. Cancer Genome Atlas N. Comprehensive genomic characterization of head and neck squamous cell carcinomas. Nature. 2015;517(7536):576-82.
40. Rivlin N, Brosh R, Oren M, Rotter V. Mutations in the p53 Tumor Suppressor Gene: Important Milestones at the Various Steps of Tumorigenesis. Genes Cancer. 2011;2(4):466-74.

41. Hanahan D, Weinberg RA. The hallmarks of cancer. Cell. 2000;100(1):57-70.
42. Hanahan D, Weinberg RA. Hallmarks of cancer: the next generation. Cell. 2011;144(5):646-74.
43. Bernstein JM, Bernstein CR, West CM, Homer JJ. Molecular and cellular processes underlying the hallmarks of head and neck cancer. European archives of oto-rhino-laryngology : official journal of the European Federation of Oto-Rhino-Laryngological Societies (EUFOS) : affiliated with the German Society for Oto-Rhino-Laryngology - Head and Neck Surgery. 2013;270(10):2585-93.
44. Weinberg RA. The biology of Cancer. Second ed. Weinberg RA, editor: Garland Science; 2014 2014.
45. Normanno N, De Luca A, Bianco C, Strizzi L, Mancino M, Maiello MR, et al. Epidermal growth factor receptor (EGFR) signaling in cancer. Gene. 2006;366(1):2-16.
46. Salomon DS, Brandt R, Ciardiello F, Normanno N. Epidermal growth factor-related peptides and their receptors in human malignancies. Critical reviews in oncology/hematology. 1995;19(3):183-232.
47. Agarwal V, Subash A, Nayar RC, Rao V. Is EGFR really a therapeutic target in head and neck cancers? Journal of surgical oncology. 2019;119(6):685-6.
48. Rubin Grandis J, Melhem MF, Gooding WE, Day R, Holst VA, Wagener MM, et al. Levels of TGF-alpha and EGFR protein in head and neck squamous cell carcinoma and patient survival. Journal of the National Cancer Institute. 1998;90(11):824-32.
49. Bossi P, Resteghini C, Paielli N, Licitra L, Pilotti S, Perrone F. Prognostic and predictive value of EGFR in head and neck squamous cell carcinoma. Oncotarget. 2016;7(45):74362-79.
50. Vermorken JB, Trigo J, Hitt R, Koralewski P, Diaz-Rubio E, Rolland F, et al. Open-label, uncontrolled, multicenter phase II study to evaluate the efficacy and toxicity of cetuximab as a single agent in patients with recurrent and/or metastatic squamous cell carcinoma of the head and neck who failed to respond to platinum-based therapy. Journal of clinical oncology : official journal of the American Society of Clinical Oncology. 2007;25(16):2171-7.
51. Zimmermann M, Zouhair A, Azria D, Ozsahin M. The epidermal growth factor receptor (EGFR) in head and neck cancer: its role and treatment implications. Radiation oncology (London, England). 2006;1:11.
52. Lim YC, Han JH, Kang HJ, Kim YS, Lee BH, Choi EC, et al. Overexpression of c-Met promotes invasion and metastasis of small oral tongue carcinoma. Oral Oncol. 2012;48(11):1114-9.
53. Amin A, Karpowicz PA, Carey TE, Arbiser J, Nahta R, Chen ZG, et al. Evasion of anti-growth signaling: A key step in tumorigenesis and potential target for treatment and prophylaxis by natural compounds. Semin Cancer Biol. 2015;35 Suppl:S55-s77.
54. Lane DP. Cancer. p53, guardian of the genome. Nature. 1992;358(6381):15-6.
55. Zilfou JT, Lowe SW. Tumor suppressive functions of p53. Cold Spring Harb Perspect Biol. 2009;1(5):a001883.
56. Stransky N, Egloff AM, Tward AD, Kostic AD, Cibulskis K, Sivachenko A, et al. The mutational landscape of head and neck squamous cell carcinoma. Science. 2011;333(6046):1157-60.
57. Shin DM, Charuruks N, Lippman SM, Lee JJ, Ro JY, Hong WK, et al. p53 protein accumulation and genomic instability in head and neck multistep tumorigenesis. Cancer Epidemiol Biomarkers Prev. 2001;10(6):603-9.
58. Weinberg RA. The retinoblastoma protein and cell cycle control. Cell. 1995;81(3):323-30.
59. Shin MK, Pitot HC, Lambert PF. Pocket proteins suppress head and neck cancer. Cancer research. 2012;72(5):1280-9.

60. Braakhuis BJ, Snijders PJ, Keune WJ, Meijer CJ, Ruijter-Schippers HJ, Leemans CR, et al. Genetic patterns in head and neck cancers that contain or lack transcriptionally active human papillomavirus. Journal of the National Cancer Institute. 2004;96(13):998-1006.
61. Zhao J, Chi J, Gao M, Zhi J, Li Y, Zheng X. Loss of PTEN Expression Is Associated With High MicroRNA 24 Level and Poor Prognosis in Patients With Tongue Squamous Cell Carcinoma. Journal of oral and maxillofacial surgery : official journal of the American Association of Oral and Maxillofacial Surgeons. 2017;75(7):1449.e1-.e8.
62. Agrawal N, Frederick MJ, Pickering CR, Bettegowda C, Chang K, Li RJ, et al. Exome sequencing of head and neck squamous cell carcinoma reveals inactivating mutations in NOTCH1. Science. 2011;333(6046):1154-7.
63. Elmore S. Apoptosis: a review of programmed cell death. Toxicologic pathology. 2007;35(4):495-516.
64. Sasahira T, Kirita T. Hallmarks of Cancer-Related Newly Prognostic Factors of Oral Squamous Cell Carcinoma. International journal of molecular sciences. 2018;19(8).
65. Lopez J, Tait SW. Mitochondrial apoptosis: killing cancer using the enemy within. Br J Cancer. 2015;112(6):957-62.
66. Zaman S, Wang R, Gandhi V. Targeting the apoptosis pathway in hematologic malignancies. Leukemia & lymphoma. 2014;55(9):1980-92.
67. Kato K, Kawashiri S, Yoshizawa K, Kitahara H, Yamamoto E. Apoptosis-associated markers and clinical outcome in human oral squamous cell carcinomas. Journal of oral pathology & medicine : official publication of the International Association of Oral Pathologists and the American Academy of Oral Pathology. 2008;37(6):364-71.
68. Wilson GD, Saunders MI, Dische S, Richman PI, Daley FM, Bentzen SM. bcl-2 expression in head and neck cancer: an enigmatic prognostic marker. International journal of radiation oncology, biology, physics. 2001;49(2):435-41.
69. Hayflick L. The illusion of cell immortality. Br J Cancer. 2000;83(7):841-6.
70. Zhao T, Hu F, Qiao B, Chen Z, Tao Q. Telomerase reverse transcriptase potentially promotes the progression of oral squamous cell carcinoma through induction of epithelial-mesenchymal transition. International journal of oncology. 2015;46(5):2205-15.
71. Patel MM, Parekh LJ, Jha FP, Sainger RN, Patel JB, Patel DD, et al. Clinical usefulness of telomerase activation and telomere length in head and neck cancer. Head & neck. 2002;24(12):1060-7.
72. Chen HH, Yu CH, Wang JT, Liu BY, Wang YP, Sun A, et al. Expression of human telomerase reverse transcriptase (hTERT) protein is significantly associated with the progression, recurrence and prognosis of oral squamous cell carcinoma in Taiwan. Oral Oncol. 2007;43(2):122-9.
73. Benhamou Y, Picco V, Raybaud H, Sudaka A, Chamorey E, Brolih S, et al. Telomeric repeat-binding factor 2: a marker for survival and anti-EGFR efficacy in oral carcinoma. Oncotarget. 2016;7(28):44236-51.
74. Carmeliet P. Angiogenesis in life, disease and medicine. Nature. 2005;438(7070):932-6.
75. Adams RH, Alitalo K. Molecular regulation of angiogenesis and lymphangiogenesis. Nat Rev Mol Cell Biol. 2007;8(6):464-78.
76. Eisma RJ, Spiro JD, Kreutzer DL. Role of angiogenic factors: coexpression of interleukin-8 and vascular endothelial growth factor in patients with head and neck squamous carcinoma. Laryngoscope. 1999;109(5):687-93.
77. Zang J, Li C, Zhao LN, Shi M, Zhou YC, Wang JH, et al. Prognostic value of vascular endothelial growth factor in patients with head and neck cancer: A meta-analysis. Head & neck. 2013;35(10):1507-14.
78. Yanase M, Kato K, Yoshizawa K, Noguchi N, Kitahara H, Nakamura H. Prognostic value of vascular endothelial growth factors A and C in oral squamous cell carcinoma.

Journal of oral pathology & medicine : official publication of the International Association of Oral Pathologists and the American Academy of Oral Pathology. 2014;43(7):514-20.
79. Kyzas PA, Cunha IW, Ioannidis JP. Prognostic significance of vascular endothelial growth factor immunohistochemical expression in head and neck squamous cell carcinoma: a meta-analysis. Clin Cancer Res. 2005;11(4):1434-40.
80. Leber MF, Efferth T. Molecular principles of cancer invasion and metastasis (review). International journal of oncology. 2009;34(4):881-95.
81. Cavallaro U, Christofori G. Multitasking in tumor progression: signaling functions of cell adhesion molecules. Ann N Y Acad Sci. 2004;1014:58-66.
82. Jiang WG, Sanders AJ, Katoh M, Ungefroren H, Gieseler F, Prince M, et al. Tissue invasion and metastasis: Molecular, biological and clinical perspectives. Semin Cancer Biol. 2015;35 Suppl:S244-s75.
83. Luo SL, Xie YG, Li Z, Ma JH, Xu X. E-cadherin expression and prognosis of oral cancer: a meta-analysis. Tumour Biol. 2014;35(6):5533-7.
84. Tanaka N, Odajima T, Ogi K, Ikeda T, Satoh M. Expression of E-cadherin, alpha-catenin, and beta-catenin in the process of lymph node metastasis in oral squamous cell carcinoma. Br J Cancer. 2003;89(3):557-63.
85. Kessenbrock K, Plaks V, Werb Z. Matrix metalloproteinases: regulators of the tumor microenvironment. Cell. 2010;141(1):52-67.
86. Pu Y, Wang L, Wu H, Feng Z, Wang Y, Guo C. High MMP-21 expression in metastatic lymph nodes predicts unfavorable overall survival for oral squamous cell carcinoma patients with lymphatic metastasis. Oncol Rep. 2014;31(6):2644-50.
87. Roche J. The Epithelial-to-Mesenchymal Transition in Cancer. Cancers (Basel). 2018;10(2).
88. Liu S, Liu L, Ye W, Ye D, Wang T, Guo W, et al. High Vimentin Expression Associated with Lymph Node Metastasis and Predicated a Poor Prognosis in Oral Squamous Cell Carcinoma. Sci Rep. 2016;6:38834.
89. Sasahira T, Bosserhoff AK, Kirita T. The importance of melanoma inhibitory activity gene family in the tumor progression of oral cancer. Pathology international. 2018;68(5):278-86.
90. Scully C, Field JK, Tanzawa H. Genetic aberrations in oral or head and neck squamous cell carcinoma 2: chromosomal aberrations. Oral Oncol. 2000;36(4):311-27.
91. Pérez-Sayáns M, Somoza-Martín JM, Barros-Angueira F, Reboiras-López MD, Gándara Rey JM, García-García A. Genetic and molecular alterations associated with oral squamous cell cancer (Review). Oncol Rep. 2009;22(6):1277-82.
92. Lee JJ, Hong WK, Hittelman WN, Mao L, Lotan R, Shin DM, et al. Predicting cancer development in oral leukoplakia: ten years of translational research. Clin Cancer Res. 2000;6(5):1702-10.
93. Pitiyage G, Tilakaratne WM, Tavassoli M, Warnakulasuriya S. Molecular markers in oral epithelial dysplasia: review. Journal of oral pathology & medicine : official publication of the International Association of Oral Pathologists and the American Academy of Oral Pathology. 2009;38(10):737-52.
94. Califano J, van der Riet P, Westra W, Nawroz H, Clayman G, Piantadosi S, et al. Genetic progression model for head and neck cancer: implications for field cancerization. Cancer research. 1996;56(11):2488-92.
95. Chen C, Zhang Y, Loomis MM, Upton MP, Lohavanichbutr P, Houck JR, et al. Genome-Wide Loss of Heterozygosity and DNA Copy Number Aberration in HPV-Negative Oral Squamous Cell Carcinoma and Their Associations with Disease-Specific Survival. PLoS One. 2015;10(8):e0135074.
96. Grivennikov SI, Greten FR, Karin M. Immunity, inflammation, and cancer. Cell. 2010;140(6):883-99.

97. Ricciotti E, FitzGerald GA. Prostaglandins and inflammation. Arteriosclerosis, thrombosis, and vascular biology. 2011;31(5):986-1000.
98. Gallo O, Masini E, Bianchi B, Bruschini L, Paglierani M, Franchi A. Prognostic significance of cyclooxygenase-2 pathway and angiogenesis in head and neck squamous cell carcinoma. Hum Pathol. 2002;33(7):708-14.
99. Chan G, Boyle JO, Yang EK, Zhang F, Sacks PG, Shah JP, et al. Cyclooxygenase-2 expression is up-regulated in squamous cell carcinoma of the head and neck. Cancer research. 1999;59(5):991-4.
100. Faouzi M, Neupane RP, Yang J, Williams P, Penner R. Areca nut extracts mobilize calcium and release pro-inflammatory cytokines from various immune cells. Sci Rep. 2018;8(1):1075.
101. Takahashi H, Ogata H, Nishigaki R, Broide DH, Karin M. Tobacco smoke promotes lung tumorigenesis by triggering IKKbeta- and JNK1-dependent inflammation. Cancer Cell. 2010;17(1):89-97.
102. Huang X, Li X, Ma Q, Xu Q, Duan W, Lei J, et al. Chronic alcohol exposure exacerbates inflammation and triggers pancreatic acinar-to-ductal metaplasia through PI3K/Akt/IKK. International journal of molecular medicine. 2015;35(3):653-63.
103. Szczepanski MJ, Czystowska M, Szajnik M, Harasymczuk M, Boyiadzis M, Kruk-Zagajewska A, et al. Triggering of Toll-like receptor 4 expressed on human head and neck squamous cell carcinoma promotes tumor development and protects the tumor from immune attack. Cancer research. 2009;69(7):3105-13.
104. Vinay DS, Ryan EP, Pawelec G, Talib WH, Stagg J, Elkord E, et al. Immune evasion in cancer: Mechanistic basis and therapeutic strategies. Semin Cancer Biol. 2015;35 Suppl:S185-s98.
105. Grandis JR, Falkner DM, Melhem MF, Gooding WE, Drenning SD, Morel PA. Human leukocyte antigen class I allelic and haplotype loss in squamous cell carcinoma of the head and neck: clinical and immunogenetic consequences. Clin Cancer Res. 2000;6(7):2794-802.
106. Lopez-Albaitero A, Nayak JV, Ogino T, Machandia A, Gooding W, DeLeo AB, et al. Role of antigen-processing machinery in the in vitro resistance of squamous cell carcinoma of the head and neck cells to recognition by CTL. Journal of immunology (Baltimore, Md : 1950). 2006;176(6):3402-9.
107. Hoffmann TK, Dworacki G, Tsukihiro T, Meidenbauer N, Gooding W, Johnson JT, et al. Spontaneous apoptosis of circulating T lymphocytes in patients with head and neck cancer and its clinical importance. Clin Cancer Res. 2002;8(8):2553-62.
108. Maruse Y, Kawano S, Jinno T, Matsubara R, Goto Y, Kaneko N, et al. Significant association of increased PD-L1 and PD-1 expression with nodal metastasis and a poor prognosis in oral squamous cell carcinoma. International journal of oral and maxillofacial surgery. 2018;47(7):836-45.
109. Qiao XW, Jiang J, Pang X, Huang MC, Tang YJ, Liang XH, et al. The Evolving Landscape of PD-1/PD-L1 Pathway in Head and Neck Cancer. Frontiers in immunology. 2020;11:1721.
110. Warburg O, Wind F, Negelein E. THE METABOLISM OF TUMORS IN THE BODY. The Journal of general physiology. 1927;8(6):519-30.
111. DeBerardinis RJ, Chandel NS. Fundamentals of cancer metabolism. Science advances. 2016;2(5):e1600200.
112. Wilkie MD, Anaam EA, Lau AS, Rubbi CP, Jones TM, Boyd MT, et al. TP53 mutations in head and neck cancer cells determine the Warburg phenotypic switch creating metabolic vulnerabilities and therapeutic opportunities for stratified therapies. Cancer Lett. 2020;478:107-21.
113. Patra KC, Hay N. The pentose phosphate pathway and cancer. Trends Biochem Sci. 2014;39(8):347-54.
114. Warburg O. On the origin of cancer cells. Science. 1956;123(3191):309-14.

115. Crabtree HG. The carbohydrate metabolism of certain pathological overgrowths. Biochem J. 1928;22(5):1289-98.
116. Hay N. Reprogramming glucose metabolism in cancer: can it be exploited for cancer therapy? Nat Rev Cancer. 2016;16(10):635-49.
117. Leemans CR, Braakhuis BJ, Brakenhoff RH. The molecular biology of head and neck cancer. Nat Rev Cancer. 2011;11(1):9-22.
118. Klement RJ. Restricting carbohydrates to fight head and neck cancer-is this realistic? Cancer Biol Med. 2014;11(3):145-61.
119. Landor SK, Mutvei AP, Mamaeva V, Jin S, Busk M, Borra R, et al. Hypo- and hyperactivated Notch signaling induce a glycolytic switch through distinct mechanisms. Proc Natl Acad Sci U S A. 2011;108(46):18814-9.
120. Garcia-Cao I, Song MS, Hobbs RM, Laurent G, Giorgi C, de Boer VC, et al. Systemic elevation of PTEN induces a tumor-suppressive metabolic state. Cell. 2012;149(1):49-62.
121. Riaz N, Morris LG, Lee W, Chan TA. Unraveling the molecular genetics of head and neck cancer through genome-wide approaches. Genes Dis. 2014;1(1):75-86.
122. Robey RB, Hay N. Is Akt the "Warburg kinase"?-Akt-energy metabolism interactions and oncogenesis. Semin Cancer Biol. 2009;19(1):25-31.
123. Li CX, Sun JL, Gong ZC, Lin ZQ, Liu H. Prognostic value of GLUT-1 expression in oral squamous cell carcinoma: A prisma-compliant meta-analysis. Medicine. 2016;95(45):e5324.
124. Kunkel M, Reichert TE, Benz P, Lehr HA, Jeong JH, Wieand S, et al. Overexpression of Glut-1 and increased glucose metabolism in tumors are associated with a poor prognosis in patients with oral squamous cell carcinoma. Cancer. 2003;97(4):1015-24.
125. Reisser C, Eichhorn K, Herold-Mende C, Born AI, Bannasch P. Expression of facilitative glucose transport proteins during development of squamous cell carcinomas of the head and neck. Int J Cancer. 1999;80(2):194-8.
126. Nordsmark M, Bentzen SM, Rudat V, Brizel D, Lartigau E, Stadler P, et al. Prognostic value of tumor oxygenation in 397 head and neck tumors after primary radiation therapy. An international multi-center study. Radiother Oncol. 2005;77(1):18-24.
127. Zhu GQ, Tang YL, Li L, Zheng M, Jiang J, Li XY, et al. Hypoxia inducible factor 1alpha and hypoxia inducible factor 2alpha play distinct and functionally overlapping roles in oral squamous cell carcinoma. Clin Cancer Res. 2010;16(19):4732-41.
128. Ullah MS, Davies AJ, Halestrap AP. The plasma membrane lactate transporter MCT4, but not MCT1, is up-regulated by hypoxia through a HIF-1alpha-dependent mechanism. J Biol Chem. 2006;281(14):9030-7.
129. Iyer NV, Kotch LE, Agani F, Leung SW, Laughner E, Wenger RH, et al. Cellular and developmental control of O2 homeostasis by hypoxia-inducible factor 1 alpha. Genes & development. 1998;12(2):149-62.
130. Brizel DM, Schroeder T, Scher RL, Walenta S, Clough RW, Dewhirst MW, et al. Elevated tumor lactate concentrations predict for an increased risk of metastases in head-and-neck cancer. International journal of radiation oncology, biology, physics. 2001;51(2):349-53.
131. Quennet V, Yaromina A, Zips D, Rosner A, Walenta S, Baumann M, et al. Tumor lactate content predicts for response to fractionated irradiation of human squamous cell carcinomas in nude mice. Radiother Oncol. 2006;81(2):130-5.
132. Sandulache VC, Myers JN. Altered metabolism in head and neck squamous cell carcinoma: an opportunity for identification of novel biomarkers and drug targets. Head & neck. 2012;34(2):282-90.
133. Stokkel MP, ten Broek FW, van Rijk PP. The role of FDG PET in the clinical management of head and neck cancer. Oral Oncol. 1998;34(6):466-71.
134. Liang Y, Liu J, Feng Z. The regulation of cellular metabolism by tumor suppressor p53. Cell & bioscience. 2013;3(1):9.

135. Goldstein I, Marcel V, Olivier M, Oren M, Rotter V, Hainaut P. Understanding wild-type and mutant p53 activities in human cancer: new landmarks on the way to targeted therapies. Cancer Gene Ther. 2011;18(1):2-11.
136. Vousden KH, Lane DP. p53 in health and disease. Nat Rev Mol Cell Biol. 2007;8(4):275-83.
137. Vousden KH, Prives C. Blinded by the Light: The Growing Complexity of p53. Cell. 2009;137(3):413-31.
138. Guimaraes DP, Hainaut P. TP53: a key gene in human cancer. Biochimie. 2002;84(1):83-93.
139. Joerger AC, Fersht AR. Structural biology of the tumor suppressor p53. Annu Rev Biochem. 2008;77:557-82.
140. Hu W, Chen S, Thorne RF, Wu M. TP53, TP53 Target Genes (DRAM, TIGAR), and Autophagy. Advances in experimental medicine and biology. 2019;1206:127-49.
141. Laptenko O, Tong DR, Manfredi J, Prives C. The Tail That Wags the Dog: How the Disordered C-Terminal Domain Controls the Transcriptional Activities of the p53 Tumor-Suppressor Protein. Trends Biochem Sci. 2016;41(12):1022-34.
142. Levine AJ. p53, the cellular gatekeeper for growth and division. Cell. 1997;88(3):323-31.
143. Michael H.G. Kubbutat SNJ, Karen H. Vousden. Regulation of p53 stability by Mdm2. Nature. 1997;387(15):299-303.
144. Momand J, Zambetti GP, Olson DC, George D, Levine AJ. The mdm-2 oncogene product forms a complex with the p53 protein and inhibits p53-mediated transactivation. Cell. 1992;69(7):1237-45.
145. Moll UM, Petrenko O. The MDM2-p53 interaction. Molecular cancer research : MCR. 2003;1(14):1001-8.
146. Wu X, Bayle JH, Olson D, Levine AJ. The p53-mdm-2 autoregulatory feedback loop. Genes & development. 1993;7(7a):1126-32.
147. Ygal Haupt RM, Anat Kazaz, Moshe Oren. Mdm2 promotes the rapid degradation of p53. Nature. 1997;387(115):296-9.
148. Li M, Brooks CL, Wu-Baer F, Chen D, Baer R, Gu W. Mono- versus polyubiquitination: differential control of p53 fate by Mdm2. Science. 2003;302(5652):1972-5.
149. Hientz K, Mohr A, Bhakta-Guha D, Efferth T. The role of p53 in cancer drug resistance and targeted chemotherapy. Oncotarget. 2017;8(5):8921-46.
150. Lev Bar-Or R, Maya R, Segel LA, Alon U, Levine AJ, Oren M. Generation of oscillations by the p53-Mdm2 feedback loop: a theoretical and experimental study. Proc Natl Acad Sci U S A. 2000;97(21):11250-5.
151. Zhao Y, Yu H, Hu W. The regulation of MDM2 oncogene and its impact on human cancers. Acta Biochim Biophys Sin (Shanghai). 2014;46(3):180-9.
152. Madan E, Gogna R, Bhatt M, Pati U, Kuppusamy P, Mahdi AA. Regulation of glucose metabolism by p53: emerging new roles for the tumor suppressor. Oncotarget. 2011;2(12):948-57.
153. Cory U. Lago HJS, Wenzhe Ma,Ping-yuan Wang, and Paul M. Hwang. p53, aerobic metabolism, and cancer. Antioxid Redox Signal. 2011;15:1739–48.
154. Schwartzenberg-Bar-Yoseph F, Armoni M, Karnieli E. The tumor suppressor p53 down-regulates glucose transporters GLUT1 and GLUT4 gene expression. Cancer research. 2004;64(7):2627-33.
155. Kawauchi K, Araki K, Tobiume K, Tanaka N. p53 regulates glucose metabolism through an IKK-NF-kappaB pathway and inhibits cell transformation. Nat Cell Biol. 2008;10(5):611-8.
156. Kondoh H, Lleonart ME, Gil J, Wang J, Degan P, Peters G, et al. Glycolytic enzymes can modulate cellular life span. Cancer research. 2005;65(1):177-85.

157. Feng Z. p53 regulation of the IGF-1/AKT/mTOR pathways and the endosomal compartment. Cold Spring Harb Perspect Biol. 2010;2(2):a001057.
158. Stambolic V, MacPherson D, Sas D, Lin Y, Snow B, Jang Y, et al. Regulation of PTEN transcription by p53. Mol Cell. 2001;8(2):317-25.
159. Yeung SJ, Pan J, Lee MH. Roles of p53, MYC and HIF-1 in regulating glycolysis - the seventh hallmark of cancer. Cell Mol Life Sci. 2008;65(24):3981-99.
160. Gottlieb E, Vousden KH. p53 regulation of metabolic pathways. Cold Spring Harb Perspect Biol. 2010;2(4):a001040.
161. Blons H, Laurent-Puig P. TP53 and head and neck neoplasms. Hum Mutat. 2003;21(3):252-7.
162. Ko Y, Abel J, Harth V, Brode P, Antony C, Donat S, et al. Association of CYP1B1 codon 432 mutant allele in head and neck squamous cell cancer is reflected by somatic mutations of p53 in tumor tissue. Cancer research. 2001;61(11):4398-404.
163. Halvorsen AR, Silwal-Pandit L, Meza-Zepeda LA, Vodak D, Vu P, Sagerup C, et al. TP53 Mutation Spectrum in Smokers and Never Smoking Lung Cancer Patients. Frontiers in genetics. 2016;7:85.
164. Brennan JA, Boyle JO, Koch WM, Goodman SN, Hruban RH, Eby YJ, et al. Association between cigarette smoking and mutation of the p53 gene in squamous-cell carcinoma of the head and neck. The New England journal of medicine. 1995;332(11):712-7.
165. Sisk EA, Soltys SG, Zhu S, Fisher SG, Carey TE, Bradford CR. Human papillomavirus and p53 mutational status as prognostic factors in head and neck carcinoma. Head & neck. 2002;24(9):841-9.
166. Hong A, Zhang X, Jones D, Veillard AS, Zhang M, Martin A, et al. Relationships between p53 mutation, HPV status and outcome in oropharyngeal squamous cell carcinoma. Radiother Oncol. 2016;118(2):342-9.
167. Updated TCGA 2016 [Available from: http://gdac.broadinstitute.org/.
168. Gasco M, Crook T. The p53 network in head and neck cancer. Oral Oncol. 2003;39(3):222-31.
169. Westra WH, Taube JM, Poeta ML, Begum S, Sidransky D, Koch WM. Inverse relationship between human papillomavirus-16 infection and disruptive p53 gene mutations in squamous cell carcinoma of the head and neck. Clin Cancer Res. 2008;14(2):366-9.
170. Boscolo-Rizzo P, Del Mistro A, Bussu F, Lupato V, Baboci L, Almadori G, et al. New insights into human papillomavirus-associated head and neck squamous cell carcinoma. Acta otorhinolaryngologica Italica : organo ufficiale della Societa italiana di otorinolaringologia e chirurgia cervico-facciale. 2013;33(2):77-87.
171. Butz K, Whitaker N, Denk C, Ullmann A, Geisen C, Hoppe-Seyler F. Induction of the p53-target gene GADD45 in HPV-positive cancer cells. Oncogene. 1999;18(14):2381-6.
172. Huang H, Li CY, Little JB. Abrogation of P53 function by transfection of HPV16 E6 gene does not enhance resistance of human tumour cells to ionizing radiation. International journal of radiation biology. 1996;70(2):151-60.
173. Muller PA, Vousden KH. p53 mutations in cancer. Nat Cell Biol. 2013;15(1):2-8.
174. Austin F, Oyarbide U, Massey G, Grimes M, Corey SJ. Synonymous mutation in TP53 results in a cryptic splice site affecting its DNA-binding site in an adolescent with two primary sarcomas. Pediatric blood & cancer. 2017;64(11).
175. Bouaoun L, Sonkin D, Ardin M, Hollstein M, Byrnes G, Zavadil J, et al. TP53 Variations in Human Cancers: New Lessons from the IARC TP53 Database and Genomics Data. Hum Mutat. 2016;37(9):865-76.
176. Gillison ML, Koch WM, Capone RB, Spafford M, Westra WH, Wu L, et al. Evidence for a causal association between human papillomavirus and a subset of head and neck cancers. Journal of the National Cancer Institute. 2000;92(9):709-20.

177. Hafkamp HC, Speel EJ, Haesevoets A, Bot FJ, Dinjens WN, Ramaekers FC, et al. A subset of head and neck squamous cell carcinomas exhibits integration of HPV 16/18 DNA and overexpression of p16INK4A and p53 in the absence of mutations in p53 exons 5-8. Int J Cancer. 2003;107(3):394-400.
178. Scholes AG, Liloglou T, Snijders PJ, Hart CA, Jones AS, Woolgar JA, et al. p53 mutations in relation to human papillomavirus type 16 infection in squamous cell carcinomas of the head and neck. Int J Cancer. 1997;71(5):796-9.
179. Boyle JO, Hakim J, Koch W, van der Riet P, Hruban RH, Roa RA, et al. The incidence of p53 mutations increases with progression of head and neck cancer. Cancer research. 1993;53(19):4477-80.
180. G.W.A. Tjebbes a, F.G.J. Leppers vd Straat b, M.G.J. Tilanus b, G.J. Hordijk a,, b PJS. P53 tumor suppressor gene as a clonal marker in head and neck squamous cell carcinoma P53 mutations in primary tumor and matched lymph node metastases.pdf. Oral Oncol. 1999;35(4):384-9.
181. Lavieille JP, Gazzeri S, Riva C, Reyt E, Brambilla C, Brambilla E. p53 mutations and p53, Waf-1, Bax and Bcl-2 expression in field cancerization of the head and neck. Anticancer research. 1998;18(6b):4741-9.
182. Tandon S, Tudur-Smith C, Riley RD, Boyd MT, Jones TM. A systematic review of p53 as a prognostic factor of survival in squamous cell carcinoma of the four main anatomical subsites of the head and neck. Cancer Epidemiol Biomarkers Prev. 2010;19(2):574-87.
183. Narayana A, Vaughan AT, Gunaratne S, Kathuria S, Walter SA, Reddy SP. Is p53 an independent prognostic factor in patients with laryngeal carcinoma? Cancer. 1998;82(2):286-91.
184. Jin YT, Kayser S, Kemp BL, Ordonez NG, Tucker SL, Clayman GL, et al. The prognostic significance of the biomarkers p21WAF1/CIP1, p53, and bcl-2 in laryngeal squamous cell carcinoma. Cancer. 1998;82(11):2159-65.
185. Georgiou A, Gomatos IP, Ferekidis E, Syrigos K, Bistola V, Giotakis J, et al. Prognostic significance of p53, bax and bcl-2 gene expression in patients with laryngeal carcinoma. Eur J Surg Oncol. 2001;27(6):574-80.
186. Gonzalez-Moles MA, Galindo P, Gutierrez-Fernandez J, Sanchez-Fernandez E, Rodriguez-Archilla A, Ruiz-Avila I, et al. P53 protein expression in oral squamous cell carcinoma. survival analysis. Anticancer research. 2001;21(4b):2889-94.
187. Jeannon JP, Soames J, Lunec J, Awwad S, Ashton V, Wilson JA. Expression of cyclin-dependent kinase inhibitor p21(WAF1) and p53 tumour suppressor gene in laryngeal cancer. Clinical otolaryngology and allied sciences. 2000;25(1):23-7.
188. Sittel C, Eckel HE, Damm M, von Pritzbuer E, Kvasnicka HM. Ki-67 (MIB1), p53, and Lewis-X (LeuM1) as prognostic factors of recurrence in T1 and T2 laryngeal carcinoma. Laryngoscope. 2000;110(6):1012-7.
189. Cabanillas R, Rodrigo JP, Astudillo A, Dominguez F, Suarez C, Chiara MD. P53 expression in squamous cell carcinomas of the supraglottic larynx and its lymph node metastases: new results for an old question. Cancer. 2007;109(9):1791-8.
190. Bandoh N, Hayashi T, Kishibe K, Takahara M, Imada M, Nonaka S, et al. Prognostic value of p53 mutations, bax, and spontaneous apoptosis in maxillary sinus squamous cell carcinoma. Cancer. 2002;94(7):1968-80.
191. Mineta H, Borg A, Dictor M, Wahlberg P, Akervall J, Wennerberg J. p53 mutation, but not p53 overexpression, correlates with survival in head and neck squamous cell carcinoma. Br J Cancer. 1998;78(8):1084-90.
192. Omura G, Ando M, Ebihara Y, Saito Y, Kobayashi K, Fukuoka O, et al. The prognostic value of TP53 mutations in hypopharyngeal squamous cell carcinoma. BMC Cancer. 2017;17(1):898.

193. Poeta ML, Manola J, Goldwasser MA, Forastiere A, Benoit N, Califano JA, et al. TP53 mutations and survival in squamous-cell carcinoma of the head and neck. The New England journal of medicine. 2007;357(25):2552-61.
194. Riley T, Sontag E, Chen P, Levine A. Transcriptional control of human p53-regulated genes. Nat Rev Mol Cell Biol. 2008;9(5):402-12.
195. Bensaad K, Vousden KH. p53: new roles in metabolism. Trends in cell biology. 2007;17(6):286-91.
196. Jen KY, Cheung VG. Identification of novel p53 target genes in ionizing radiation response. Cancer research. 2005;65(17):7666-73.
197. Bensaad K, Tsuruta A, Selak MA, Vidal MN, Nakano K, Bartrons R, et al. TIGAR, a p53-inducible regulator of glycolysis and apoptosis. Cell. 2006;126(1):107-20.
198. UniProtKB - Q9NQ88 (TIGAR_HUMAN) [Available from: https://www.uniprot.org/uniprot/Q9NQ88#structure.
199. Li H, Jogl G. Structural and biochemical studies of TIGAR (TP53-induced glycolysis and apoptosis regulator). J Biol Chem. 2009;284(3):1748-54.
200. Lee P, Vousden KH, Cheung EC. TIGAR, TIGAR, burning bright. Cancer & metabolism. 2014;2(1):1.
201. Ray PD, Huang BW, Tsuji Y. Reactive oxygen species (ROS) homeostasis and redox regulation in cellular signaling. Cell Signal. 2012;24(5):981-90.
202. Martindale JL, Holbrook NJ. Cellular response to oxidative stress: signaling for suicide and survival. Journal of cellular physiology. 2002;192(1):1-15.
203. Balaban RS, Nemoto S, Finkel T. Mitochondria, oxidants, and aging. Cell. 2005;120(4):483-95.
204. Pinthus JH, Whelan KF, Gallino D, Lu JP, Rothschild N. Metabolic features of clear-cell renal cell carcinoma: mechanisms and clinical implications. Can Urol Assoc J. 2011;5(4):274-82.
205. Mullarky E, Cantley LC. Diverting Glycolysis to Combat Oxidative Stress. Nakao K, Minato N, Uemoto S, editors. Tokyo: Springer; 2015.
206. Cheung EC, Ludwig RL, Vousden KH. Mitochondrial localization of TIGAR under hypoxia stimulates HK2 and lowers ROS and cell death. Proc Natl Acad Sci U S A. 2012;109(50):20491-6.
207. Cheung EC, Athineos D, Lee P, Ridgway RA, Lambie W, Nixon C, et al. TIGAR is required for efficient intestinal regeneration and tumorigenesis. Dev Cell. 2013;25(5):463-77.
208. Kimata M, Matoba S, Iwai-Kanai E, Nakamura H, Hoshino A, Nakaoka M, et al. p53 and TIGAR regulate cardiac myocyte energy homeostasis under hypoxic stress. Am J Physiol Heart Circ Physiol. 2010;299(6):H1908-16.
209. Hoshino A, Matoba S, Iwai-Kanai E, Nakamura H, Kimata M, Nakaoka M, et al. p53-TIGAR axis attenuates mitophagy to exacerbate cardiac damage after ischemia. J Mol Cell Cardiol. 2012;52(1):175-84.
210. Li M, Sun M, Cao L, Gu JH, Ge J, Chen J, et al. A TIGAR-regulated metabolic pathway is critical for protection of brain ischemia. J Neurosci. 2014;34(22):7458-71.
211. Cao L, Chen J, Li M, Qin YY, Sun M, Sheng R, et al. Endogenous level of TIGAR in brain is associated with vulnerability of neurons to ischemic injury. Neurosci Bull. 2015;31(5):527-40.
212. Sun M, Li M, Huang Q, Han F, Gu JH, Xie J, et al. Ischemia/reperfusion-induced upregulation of TIGAR in brain is mediated by SP1 and modulated by ROS and hormones involved in glucose metabolism. Neurochem Int. 2015;80:99-109.
213. Maiuri MC, Zalckvar E, Kimchi A, Kroemer G. Self-eating and self-killing: crosstalk between autophagy and apoptosis. Nat Rev Mol Cell Biol. 2007;8(9):741-52.
214. Yun CW, Lee SH. The Roles of Autophagy in Cancer. International journal of molecular sciences. 2018;19(11).

215. Zhou S, Zhao L, Kuang M, Zhang B, Liang Z, Yi T, et al. Autophagy in tumorigenesis and cancer therapy: Dr. Jekyll or Mr. Hyde? Cancer Lett. 2012;323(2):115-27.
216. Xie JM, Li B, Yu HP, Gao QG, Li W, Wu HR, et al. TIGAR has a dual role in cancer cell survival through regulating apoptosis and autophagy. Cancer research. 2014;74(18):5127-38.
217. Bensaad K, Cheung EC, Vousden KH. Modulation of intracellular ROS levels by TIGAR controls autophagy. EMBO J. 2009;28(19):3015-26.
218. Wilson JE. Isozymes of mammalian hexokinase: structure, subcellular localization and metabolic function. Journal of Experimental Biology. 2003;206(12):2049-57.
219. Tsai HJ, Wilson JE. Functional organization of mammalian hexokinases: characterization of chimeric hexokinases constructed from the N- and C-terminal domains of the rat type I and type II isozymes. Archives of biochemistry and biophysics. 1995;316(1):206-14.
220. Tsai HJ, Wilson JE. Functional organization of mammalian hexokinases: characterization of the rat type III isozyme and its chimeric forms, constructed with the N- and C-terminal halves of the type I and type II isozymes. Archives of biochemistry and biophysics. 1997;338(2):183-92.
221. Mathupala SP, Ko YH, Pedersen PL. Hexokinase-2 bound to mitochondria: cancer's stygian link to the "Warburg Effect" and a pivotal target for effective therapy. Semin Cancer Biol. 2009;19(1):17-24.
222. Roberts DJ, Miyamoto S. Hexokinase II integrates energy metabolism and cellular protection: Akting on mitochondria and TORCing to autophagy. Cell Death Differ. 2015;22(2):248-57.
223. Patra KC, Wang Q, Bhaskar PT, Miller L, Wang Z, Wheaton W, et al. Hexokinase 2 is required for tumor initiation and maintenance and its systemic deletion is therapeutic in mouse models of cancer. Cancer Cell. 2013;24(2):213-28.
224. Chen Z, Zhang H, Lu W, Huang P. Role of mitochondria-associated hexokinase II in cancer cell death induced by 3-bromopyruvate. Biochimica et biophysica acta. 2009;1787(5):553-60.
225. Heikkinen S, Suppola S, Malkki M, Deeb SS, Janne J, Laakso M. Mouse hexokinase II gene: structure, cDNA, promoter analysis, and expression pattern. Mammalian genome : official journal of the International Mammalian Genome Society. 2000;11(2):91-6.
226. Robey RB, Hay N. Mitochondrial hexokinases, novel mediators of the antiapoptotic effects of growth factors and Akt. Oncogene. 2006;25(34):4683-96.
227. Mathupala SP, Ko YH, Pedersen PL. Hexokinase II: cancer's double-edged sword acting as both facilitator and gatekeeper of malignancy when bound to mitochondria. Oncogene. 2006;25(34):4777-86.
228. Tan VP, Miyamoto S. HK2/hexokinase-II integrates glycolysis and autophagy to confer cellular protection. Autophagy. 2015;11(6):963-4.
229. Pedersen PL. Warburg, me and Hexokinase 2: Multiple discoveries of key molecular events underlying one of cancers' most common phenotypes, the "Warburg Effect", i.e., elevated glycolysis in the presence of oxygen. J Bioenerg Biomembr. 2007;39(3):211-22.
230. Rose IA, Warms JV. Mitochondrial hexokinase. Release, rebinding, and location. J Biol Chem. 1967;242(7):1635-45.
231. Sui D, Wilson JE. Structural determinants for the intracellular localization of the isozymes of mammalian hexokinase: intracellular localization of fusion constructs incorporating structural elements from the hexokinase isozymes and the green fluorescent protein. Archives of biochemistry and biophysics. 1997;345(1):111-25.
232. Vyssokikh MY, Brdiczka D. The function of complexes between the outer mitochondrial membrane pore (VDAC) and the adenine nucleotide translocase in regulation of energy metabolism and apoptosis. Acta biochimica Polonica. 2003;50(2):389-404.

233. Arora KK, Pedersen PL. Functional significance of mitochondrial bound hexokinase in tumor cell metabolism. Evidence for preferential phosphorylation of glucose by intramitochondrially generated ATP. J Biol Chem. 1988;263(33):17422-8.
234. John S, Weiss JN, Ribalet B. Subcellular localization of hexokinases I and II directs the metabolic fate of glucose. PLoS One. 2011;6(3):e17674.
235. Lowry OH, Passonneau JV. THE RELATIONSHIPS BETWEEN SUBSTRATES AND ENZYMES OF GLYCOLYSIS IN BRAIN. J Biol Chem. 1964;239:31-42.
236. Mandarino LJ, Printz RL, Cusi KA, Kinchington P, O'Doherty RM, Osawa H, et al. Regulation of hexokinase II and glycogen synthase mRNA, protein, and activity in human muscle. The American journal of physiology. 1995;269(4 Pt 1):E701-8.
237. Wu R, Wyatt E, Chawla K, Tran M, Ghanefar M, Laakso M, et al. Hexokinase II knockdown results in exaggerated cardiac hypertrophy via increased ROS production. EMBO molecular medicine. 2012;4(7):633-46.
238. Colombini M. VDAC: the channel at the interface between mitochondria and the cytosol. Mol Cell Biochem. 2004;256-257(1-2):107-15.
239. Pedersen PL. Voltage dependent anion channels (VDACs): a brief introduction with a focus on the outer mitochondrial compartment's roles together with hexokinase-2 in the "Warburg effect" in cancer. J Bioenerg Biomembr. 2008;40(3):123-6.
240. De Saedeleer CJ, Porporato PE, Copetti T, Pérez-Escuredo J, Payen VL, Brisson L, et al. Glucose deprivation increases monocarboxylate transporter 1 (MCT1) expression and MCT1-dependent tumor cell migration. Oncogene. 2014;33(31):4060-8.
241. Rigo P, Paulus P, Kaschten BJ, Hustinx R, Bury T, Jerusalem G, et al. Oncological applications of positron emission tomography with fluorine-18 fluorodeoxyglucose. European journal of nuclear medicine. 1996;23(12):1641-74.
242. Di Chiro G, DeLaPaz RL, Brooks RA, Sokoloff L, Kornblith PL, Smith BH, et al. Glucose utilization of cerebral gliomas measured by [18F] fluorodeoxyglucose and positron emission tomography. Neurology. 1982;32(12):1323-9.
243. Kapoor V, McCook BM, Torok FS. An introduction to PET-CT imaging. Radiographics : a review publication of the Radiological Society of North America, Inc. 2004;24(2):523-43.
244. Katzen HM, Soderman DD, Wiley CE. Multiple forms of hexokinase. Activities associated with subcellular particulate and soluble fractions of normal and streptozotocin diabetic rat tissues. J Biol Chem. 1970;245(16):4081-96.
245. Duarte AI, Santos P, Oliveira CR, Santos MS, Rego AC. Insulin neuroprotection against oxidative stress is mediated by Akt and GSK-3beta signaling pathways and changes in protein expression. Biochimica et biophysica acta. 2008;1783(6):994-1002.
246. Mathupala SP, Rempel A, Pedersen PL. Glucose catabolism in cancer cells: identification and characterization of a marked activation response of the type II hexokinase gene to hypoxic conditions. J Biol Chem. 2001;276(46):43407-12.
247. Gwak GY, Yoon JH, Kim KM, Lee HS, Chung JW, Gores GJ. Hypoxia stimulates proliferation of human hepatoma cells through the induction of hexokinase II expression. Journal of hepatology. 2005;42(3):358-64.
248. DeBerardinis RJ, Lum JJ, Hatzivassiliou G, Thompson CB. The biology of cancer: metabolic reprogramming fuels cell growth and proliferation. Cell Metab. 2008;7(1):11-20.
249. Ahn KJ, Hwang HS, Park JH, Bang SH, Kang WJ, Yun M, et al. Evaluation of the role of hexokinase type II in cellular proliferation and apoptosis using human hepatocellular carcinoma cell lines. J Nucl Med. 2009;50(9):1525-32.
250. Gottlob K, Majewski N, Kennedy S, Kandel E, Robey RB, Hay N. Inhibition of early apoptotic events by Akt/PKB is dependent on the first committed step of glycolysis and mitochondrial hexokinase. Genes & development. 2001;15(11):1406-18.
251. Zhou H, Hou Q, Chai Y, Hsu YT. Distinct domains of Bcl-XL are involved in Bax and Bad antagonism and in apoptosis inhibition. Experimental cell research. 2005;309(2):316-28.

252. Pérez Sayáns M, Chamorro Petronacci CM, Lorenzo Pouso AI, Padín Iruegas E, Blanco Carrión A, Suárez Peñaranda JM, et al. Comprehensive Genomic Review of TCGA Head and Neck Squamous Cell Carcinomas (HNSCC). Journal of clinical medicine. 2019;8(11).
253. Mathupala SP, Rempel A, Pedersen PL. Glucose catabolism in cancer cells. Isolation, sequence, and activity of the promoter for type II hexokinase. J Biol Chem. 1995;270(28):16918-25.
254. Lee MG, Pedersen PL. Glucose metabolism in cancer: importance of transcription factor-DNA interactions within a short segment of the proximal region og the type II hexokinase promoter. J Biol Chem. 2003;278(42):41047-58.
255. Mayer D, Klimek F, Rempel A, Bannasch P. Hexokinase expression in liver preneoplasia and neoplasia. Biochemical Society transactions. 1997;25(1):122-7.
256. Lin CJ, Grandis JR, Carey TE, Gollin SM, Whiteside TL, Koch WM, et al. Head and neck squamous cell carcinoma cell lines: established models and rationale for selection. Head & neck. 2007;29(2):163-88.
257. Krause CJ, Carey TE, Ott RW, Hurbis C, McClatchey KD, Regezi JA. Human squamous cell carcinoma. Establishment and characterization of new permanent cell lines. Archives of otolaryngology (Chicago, Ill : 1960). 1981;107(11):703-10.
258. Sano D, Xie TX, Ow TJ, Zhao M, Pickering CR, Zhou G, et al. Disruptive TP53 mutation is associated with aggressive disease characteristics in an orthotopic murine model of oral tongue cancer. Clin Cancer Res. 2011;17(21):6658-70.
259. Bradford CR, Zacks SE, Androphy EJ, Gregoire L, Lancaster WD, Carey TE. Human papillomavirus DNA sequences in cell lines derived from head and neck squamous cell carcinomas. Otolaryngology--head and neck surgery : official journal of American Academy of Otolaryngology-Head and Neck Surgery. 1991;104(3):303-10.
260. Hauser U, Balz V, Carey TE, Grénman R, Van Lierop A, Scheckenbach K, et al. Reliable detection of p53 aberrations in squamous cell carcinomas of the head and neck requires transcript analysis of the entire coding region. Head & neck. 2002;24(9):868-73.
261. Brenner JC, Graham MP, Kumar B, Saunders LM, Kupfer R, Lyons RH, et al. Genotyping of 73 UM-SCC head and neck squamous cell carcinoma cell lines. Head & neck. 2010;32(4):417-26.
262. Frank CJ, McClatchey KD, Devaney KO, Carey TE. Evidence that loss of chromosome 18q is associated with tumor progression. Cancer research. 1997;57(5):824-7.
263. Mahmood T, Yang PC. Western blot: technique, theory, and trouble shooting. North American journal of medical sciences. 2012;4(9):429-34.
264. Aryal S. Western blotting - Introduction, Principle and Applications 2017 [updated Jan 6 2020. Available from: https://microbenotes.com/western-blotting-introduction-principle-and-applications/#introduction.
265. Image Lab Software Version 6.1 [Available from: https://www.bio-rad.com/webroot/web/pdf/lsr/literature/110000076953.pdf.
266. Biologicals N. Loading control handbook.
267. Ramos-Vara JA. Principles and methods of immunohistochemistry. Methods Mol Biol. 2011;691:83-96.
268. Getting started with Immunohistochemistry: Innova Biosciences; 2014 [Available from: https://bitesizebio.com/20929/getting-started-with-immunohistochemistry/.
269. Immunohistochemistry application guide: Abcam; 2019 [Available from: https://docs.abcam.com/pdf/kits/immunohistochemistry-ihc-application-guide.pdf.
270. Dhanda J, Triantafyllou A, Liloglou T, Kalirai H, Lloyd B, Hanlon R, et al. SERPINE1 and SMA expression at the invasive front predict extracapsular spread and survival in oral squamous cell carcinoma. Br J Cancer. 2014;111(11):2114-21.

271. Schache AG, Liloglou T, Risk JM, Filia A, Jones TM, Sheard J, et al. Evaluation of human papilloma virus diagnostic testing in oropharyngeal squamous cell carcinoma: sensitivity, specificity, and prognostic discrimination. Clin Cancer Res. 2011;17(19):6262-71.
272. Upile NS, Shaw RJ, Jones TM, Goodyear P, Liloglou T, Risk JM, et al. Squamous cell carcinoma of the head and neck outside the oropharynx is rarely human papillomavirus related. Laryngoscope. 2014;124(12):2739-44.
273. Abcam. Rabbit specific HRP/DAB Detection IHC Detection Kit - Micro-polymer.
274. Kim SH, Choi SI, Won KY, Lim SJ. Distinctive interrelation of p53 with SCO2, COX, and TIGAR in human gastric cancer. Pathol Res Pract. 2016;212(10):904-10.
275. Won KY, Lim SJ, Kim GY, Kim YW, Han SA, Song JY, et al. Regulatory role of p53 in cancer metabolism via SCO2 and TIGAR in human breast cancer. Hum Pathol. 2012;43(2):221-8.
276. Al-Khayal K, Abdulla M, Al-Obeed O, Al Kattan W, Zubaidi A, Vaali-Mohammed MA, et al. Identification of the TP53-induced glycolysis and apoptosis regulator in various stages of colorectal cancer patients. Oncol Rep. 2016;35(3):1281-6.
277. Zhou X, Xie W, Li Q, Zhang Y, Zhang J, Zhao X, et al. TIGAR is correlated with maximal standardized uptake value on FDG-PET and survival in non-small cell lung cancer. PLoS One. 2013;8(12):e80576.
278. Nenutil R, Smardova J, Pavlova S, Hanzelkova Z, Muller P, Fabian P, et al. Discriminating functional and non-functional p53 in human tumours by p53 and MDM2 immunohistochemistry. The Journal of pathology. 2005;207(3):251-9.
279. Palmieri D, Fitzgerald D, Shreeve SM, Hua E, Bronder JL, Weil RJ, et al. Analyses of resected human brain metastases of breast cancer reveal the association between up-regulation of hexokinase 2 and poor prognosis. Molecular cancer research : MCR. 2009;7(9):1438-45.
280. Liu H, Liu N, Cheng Y, Jin W, Zhang P, Wang X, et al. Hexokinase 2 (HK2), the tumor promoter in glioma, is downregulated by miR-218/Bmi1 pathway. PLoS One. 2017;12(12):e0189353.
281. Huang X, Liu M, Sun H, Wang F, Xie X, Chen X, et al. HK2 is a radiation resistant and independent negative prognostic factor for patients with locally advanced cervical squamous cell carcinoma. International journal of clinical and experimental pathology. 2015;8(4):4054-63.
282. Min JW, Kim KI, Kim HA, Kim EK, Noh WC, Jeon HB, et al. INPP4B-mediated tumor resistance is associated with modulation of glucose metabolism via hexokinase 2 regulation in laryngeal cancer cells. Biochem Biophys Res Commun. 2013;440(1):137-42.
283. Kwee SA, Hernandez B, Chan O, Wong L. Choline kinase alpha and hexokinase-2 protein expression in hepatocellular carcinoma: association with survival. PLoS One. 2012;7(10):e46591.
284. Landis JR, Koch GG. The measurement of observer agreement for categorical data. Biometrics. 1977;33(1):159-74.
285. Wang L, Xiong H, Wu F, Zhang Y, Wang J, Zhao L, et al. Hexokinase 2-mediated Warburg effect is required for PTEN- and p53-deficiency-driven prostate cancer growth. Cell reports. 2014;8(5):1461-74.
286. Mathupala SP, Heese C, Pedersen PL. Glucose catabolism in cancer cells. The type II hexokinase promoter contains functionally active response elements for the tumor suppressor p53. J Biol Chem. 1997;272(36):22776-80.
287. Arya AK, El-Fert A, Devling T, Eccles RM, Aslam MA, Rubbi CP, et al. Nutlin-3, the small-molecule inhibitor of MDM2, promotes senescence and radiosensitises laryngeal carcinoma cells harbouring wild-type p53. Br J Cancer. 2010;103(2):186-95.
288. Rajeshkumar NV, Dutta P, Yabuuchi S, de Wilde RF, Martinez GV, Le A, et al. Therapeutic Targeting of the Warburg Effect in Pancreatic Cancer Relies on an Absence of p53 Function. Cancer research. 2015;75(16):3355-64.

289. Martinez-Outschoorn UE, Goldberg A, Lin Z, Ko YH, Flomenberg N, Wang C, et al. Anti-estrogen resistance in breast cancer is induced by the tumor microenvironment and can be overcome by inhibiting mitochondrial function in epithelial cancer cells. Cancer Biol Ther. 2011;12(10):924-38.
290. Cheung EC, DeNicola GM, Nixon C, Blyth K, Labuschagne CF, Tuveson DA, et al. Dynamic ROS Control by TIGAR Regulates the Initiation and Progression of Pancreatic Cancer. Cancer Cell. 2020;37(2):168-82.e4.
291. Qian S, Li J, Hong M, Zhu Y, Zhao H, Xie Y, et al. TIGAR cooperated with glycolysis to inhibit the apoptosis of leukemia cells and associated with poor prognosis in patients with cytogenetically normal acute myeloid leukemia. Journal of hematology & oncology. 2016;9(1):128.
292. Hong M, Xia Y, Zhu Y, Zhao HH, Zhu H, Xie Y, et al. TP53-induced glycolysis and apoptosis regulator protects from spontaneous apoptosis and predicts poor prognosis in chronic lymphocytic leukemia. Leukemia research. 2016;50:72-7.
293. Hasegawa H, Yamada Y, Iha H, Tsukasaki K, Nagai K, Atogami S, et al. Activation of p53 by Nutlin-3a, an antagonist of MDM2, induces apoptosis and cellular senescence in adult T-cell leukemia cells. Leukemia. 2009;23(11):2090-101.
294. Wong EY, Wong SC, Chan CM, Lam EK, Ho LY, Lau CP, et al. TP53-induced glycolysis and apoptosis regulator promotes proliferation and invasiveness of nasopharyngeal carcinoma cells. Oncol Lett. 2015;9(2):569-74.
295. Zhao M, Fan J, Liu Y, Yu Y, Xu J, Wen Q, et al. Oncogenic role of the TP53-induced glycolysis and apoptosis regulator in nasopharyngeal carcinoma through NF-kappaB pathway modulation. International journal of oncology. 2016;48(2):756-64.
296. Dai Q, Yin Y, Liu W, Wei L, Zhou Y, Li Z, et al. Two p53-related metabolic regulators, TIGAR and SCO2, contribute to oroxylin A-mediated glucose metabolism in human hepatoma HepG2 cells. Int J Biochem Cell Biol. 2013;45(7):1468-78.
297. Lin CC, Cheng TL, Tsai WH, Tsai HJ, Hu KH, Chang HC, et al. Loss of the respiratory enzyme citrate synthase directly links the Warburg effect to tumor malignancy. Sci Rep. 2012;2:785.
298. Lui VW, Wong EY, Ho K, Ng PK, Lau CP, Tsui SK, et al. Inhibition of c-Met downregulates TIGAR expression and reduces NADPH production leading to cell death. Oncogene. 2011;30(9):1127-34.
299. Madan E, Gogna R, Kuppusamy P, Bhatt M, Pati U, Mahdi AA. TIGAR induces p53-mediated cell-cycle arrest by regulation of RB-E2F1 complex. Br J Cancer. 2012;107(3):516-26.
300. De Paula AM, Souza LR, Farias LC, Correa GT, Fraga CA, Eleuterio NB, et al. Analysis of 724 cases of primary head and neck squamous cell carcinoma (HNSCC) with a focus on young patients and p53 immunolocalization. Oral Oncol. 2009;45(9):777-82.
301. Zhou G, Liu Z, Myers JN. TP53 Mutations in Head and Neck Squamous Cell Carcinoma and Their Impact on Disease Progression and Treatment Response. Journal of cellular biochemistry. 2016;117(12):2682-92.
302. Dayyani F, Etzel CJ, Liu M, Ho CH, Lippman SM, Tsao AS. Meta-analysis of the impact of human papillomavirus (HPV) on cancer risk and overall survival in head and neck squamous cell carcinomas (HNSCC). Head Neck Oncol. 2010;2:15.
303. Raybaud-Diogene H, Tetu B, Morency R, Fortin A, Monteil RA. p53 overexpression in head and neck squamous cell carcinoma: review of the literature. European journal of cancer Part B, Oral oncology. 1996;32b(3):143-9.
304. Yemelyanova A, Vang R, Kshirsagar M, Lu D, Marks MA, Shih Ie M, et al. Immunohistochemical staining patterns of p53 can serve as a surrogate marker for TP53 mutations in ovarian carcinoma: an immunohistochemical and nucleotide sequencing analysis. Modern pathology : an official journal of the United States and Canadian Academy of Pathology, Inc. 2011;24(9):1248-53.

305. Finlay CA, Hinds PW, Tan TH, Eliyahu D, Oren M, Levine AJ. Activating mutations for transformation by p53 produce a gene product that forms an hsc70-p53 complex with an altered half-life. Molecular and cellular biology. 1988;8(2):531-9.
306. Wynford-Thomas D. P53 in tumour pathology: can we trust immunocytochemistry? The Journal of pathology. 1992;166(4):329-30.
307. Marks JR, Davidoff AM, Kerns BJ, Humphrey PA, Pence JC, Dodge RK, et al. Overexpression and mutation of p53 in epithelial ovarian cancer. Cancer research. 1991;51(11):2979-84.
308. Hall PA, Lane DP. p53 in tumour pathology: can we trust immunohistochemistry?--Revisited! The Journal of pathology. 1994;172(1):1-4.
309. Kandioler D, Zwrtek R, Ludwig C, Janschek E, Ploner M, Hofbauer F, et al. TP53 genotype but not p53 immunohistochemical result predicts response to preoperative short-term radiotherapy in rectal cancer. Annals of surgery. 2002;235(4):493-8.
310. Peltonen JK, Helppi HM, Paakko P, Turpeenniemi-Hujanen T, Vahakangas KH. p53 in head and neck cancer: functional consequences and environmental implications of TP53 mutations. Head Neck Oncol. 2010;2:36.
311. Cruz I, Snijders PJ, Van Houten V, Vosjan M, Van der Waal I, Meijer CJ. Specific p53 immunostaining patterns are associated with smoking habits in patients with oral squamous cell carcinomas. Journal of clinical pathology. 2002;55(11):834-40.
312. Hamabe A, Yamamoto H, Konno M, Uemura M, Nishimura J, Hata T, et al. Combined evaluation of hexokinase 2 and phosphorylated pyruvate dehydrogenase-E1α in invasive front lesions of colorectal tumors predicts cancer metabolism and patient prognosis. Cancer Sci. 2014;105(9):1100-8.
313. Rho M, Kim J, Jee CD, Lee YM, Lee HE, Kim MA, et al. Expression of type 2 hexokinase and mitochondria-related genes in gastric carcinoma tissues and cell lines. Anticancer research. 2007;27(1a):251-8.
314. Guzman G, Chennuri R, Chan A, Rea B, Quintana A, Patel R, et al. Evidence for heightened hexokinase II immunoexpression in hepatocyte dysplasia and hepatocellular carcinoma. Digestive diseases and sciences. 2015;60(2):420-6.
315. Suh DH, Kim MA, Kim H, Kim MK, Kim HS, Chung HH, et al. Association of overexpression of hexokinase II with chemoresistance in epithelial ovarian cancer. Clinical and experimental medicine. 2014;14(3):345-53.
316. Anderson M, Marayati R, Moffitt R, Yeh JJ. Hexokinase 2 promotes tumor growth and metastasis by regulating lactate production in pancreatic cancer. Oncotarget. 2017;8(34):56081-94.
317. Liu Y, Wu K, Shi L, Xiang F, Tao K, Wang G. Prognostic Significance of the Metabolic Marker Hexokinase-2 in Various Solid Tumors: A Meta-Analysis. PLoS One. 2016;11(11):e0166230.
318. Li WC, Huang CH, Hsieh YT, Chen TY, Cheng LH, Chen CY, et al. Regulatory Role of Hexokinase 2 in Modulating Head and Neck Tumorigenesis. Frontiers in oncology. 2020;10:176.
319. Grimm M, Cetindis M, Lehmann M, Biegner T, Munz A, Teriete P, et al. Association of cancer metabolism-related proteins with oral carcinogenesis - indications for chemoprevention and metabolic sensitizing of oral squamous cell carcinoma? Journal of translational medicine. 2014;12:208.
320. Wang W, Liu Z, Zhao L, Sun J, He Q, Yan W, et al. Hexokinase 2 enhances the metastatic potential of tongue squamous cell carcinoma via the SOD2-H2O2 pathway. Oncotarget. 2017;8(2):3344-54.
321. Chen J, Zhang S, Li Y, Tang Z, Kong W. Hexokinase 2 overexpression promotes the proliferation and survival of laryngeal squamous cell carcinoma. Tumour Biol. 2014;35(4):3743-53.

322. Tímár J, Csuka O, Remenár E, Répássy G, Kásler M. Progression of head and neck squamous cell cancer. Cancer metastasis reviews. 2005;24(1):107-27.
323. Geisler SA, Olshan AF, Weissler MC, Cai J, Funkhouser WK, Smith J, et al. p16 and p53 Protein expression as prognostic indicators of survival and disease recurrence from head and neck cancer. Clin Cancer Res. 2002;8(11):3445-53.
324. Lin J, Xia L, Liang J, Han Y, Wang H, Oyang L, et al. The roles of glucose metabolic reprogramming in chemo- and radio-resistance. J Exp Clin Cancer Res. 2019;38(1):218.
325. Yin L, Kosugi M, Kufe D. Inhibition of the MUC1-C oncoprotein induces multiple myeloma cell death by down-regulating TIGAR expression and depleting NADPH. Blood. 2012;119(3):810-6.
326. Ye L, Zhao X, Lu J, Qian G, Zheng JC, Ge S. Knockdown of TIGAR by RNA interference induces apoptosis and autophagy in HepG2 hepatocellular carcinoma cells. Biochem Biophys Res Commun. 2013;437(2):300-6.
327. Chen S, Li P, Li J, Wang Y, Du Y, Chen X, et al. MiR-144 inhibits proliferation and induces apoptosis and autophagy in lung cancer cells by targeting TIGAR. Cell Physiol Biochem. 2015;35(3):997-1007.
328. Kumar B, Iqbal MA, Singh RK, Bamezai RN. Resveratrol inhibits TIGAR to promote ROS induced apoptosis and autophagy. Biochimie. 2015;118:26-35.
329. Lui VW, Lau CP, Cheung CS, Ho K, Ng MH, Cheng SH, et al. An RNA-directed nucleoside anti-metabolite, 1-(3-C-ethynyl-beta-d-ribo-pentofuranosyl)cytosine (ECyd), elicits antitumor effect via TP53-induced Glycolysis and Apoptosis Regulator (TIGAR) downregulation. Biochem Pharmacol. 2010;79(12):1772-80.
330. Wilkie MD, Lau AS, Vlatkovic N, Jones TM, Boyd MT. Metabolic signature of squamous cell carcinoma of the head and neck: Consequences of TP53 mutation and therapeutic perspectives. Oral Oncol. 2018;83:1-10.
331. Blandino G, Di Agostino S. New therapeutic strategies to treat human cancers expressing mutant p53 proteins. J Exp Clin Cancer Res. 2018;37(1):30.
332. Wang Z, Sun Y. Targeting p53 for Novel Anticancer Therapy. Translational oncology. 2010;3(1):1-12.
333. Vassilev LT. Small-molecule antagonists of p53-MDM2 binding: research tools and potential therapeutics. Cell cycle (Georgetown, Tex). 2004;3(4):419-21.
334. Issaeva N, Bozko P, Enge M, Protopopova M, Verhoef LG, Masucci M, et al. Small molecule RITA binds to p53, blocks p53-HDM-2 interaction and activates p53 function in tumors. Nature medicine. 2004;10(12):1321-8.
335. Selivanova G, Wiman KG. Reactivation of mutant p53: molecular mechanisms and therapeutic potential. Oncogene. 2007;26(15):2243-54.
336. Hamanaka RB, Chandel NS. Targeting glucose metabolism for cancer therapy. J Exp Med. 2012;209(2):211-5.
337. Jae HJ, Chung JW, Park HS, Lee MJ, Lee KC, Kim HC, et al. The antitumor effect and hepatotoxicity of a hexokinase II inhibitor 3-bromopyruvate: in vivo investigation of intraarterial administration in a rabbit VX2 hepatoma model. Korean journal of radiology. 2009;10(6):596-603.
338. Ko YH, Verhoeven HA, Lee MJ, Corbin DJ, Vogl TJ, Pedersen PL. A translational study "case report" on the small molecule "energy blocker" 3-bromopyruvate (3BP) as a potent anticancer agent: from bench side to bedside. J Bioenerg Biomembr. 2012;44(1):163-70.
339. Ko YH, Pedersen PL, Geschwind JF. Glucose catabolism in the rabbit VX2 tumor model for liver cancer: characterization and targeting hexokinase. Cancer Lett. 2001;173(1):83-91.
340. Gandham SK, Talekar M, Singh A, Amiji MM. Inhibition of hexokinase-2 with targeted liposomal 3-bromopyruvate in an ovarian tumor spheroid model of aerobic glycolysis. International journal of nanomedicine. 2015;10:4405-23.

341. Shoshan MC. 3-Bromopyruvate: targets and outcomes. J Bioenerg Biomembr. 2012;44(1):7-15.
342. Ko YH, Smith BL, Wang Y, Pomper MG, Rini DA, Torbenson MS, et al. Advanced cancers: eradication in all cases using 3-bromopyruvate therapy to deplete ATP. Biochem Biophys Res Commun. 2004;324(1):269-75.
343. Lis P, Dyląg M, Niedźwiecka K, Ko YH, Pedersen PL, Goffeau A, et al. The HK2 Dependent "Warburg Effect" and Mitochondrial Oxidative Phosphorylation in Cancer: Targets for Effective Therapy with 3-Bromopyruvate. Molecules (Basel, Switzerland). 2016;21(12).
344. Zhang XD, Deslandes E, Villedieu M, Poulain L, Duval M, Gauduchon P, et al. Effect of 2-deoxy-D-glucose on various malignant cell lines in vitro. Anticancer research. 2006;26(5a):3561-6.
345. Nath K, Guo L, Nancolas B, Nelson DS, Shestov AA, Lee SC, et al. Mechanism of antineoplastic activity of lonidamine. Biochimica et biophysica acta. 2016;1866(2):151-62.
346. Munro AJ, Lain S, Lane DP. P53 abnormalities and outcomes in colorectal cancer: a systematic review. Br J Cancer. 2005;92(3):434-44.
347. Prives C, Hall PA. The p53 pathway. The Journal of pathology. 1999;187(1):112-26.
348. Vogelstein B, Lane D, Levine AJ. Surfing the p53 network. Nature. 2000;408(6810):307-10.
349. Murnyak B, Hortobagyi T. Immunohistochemical correlates of TP53 somatic mutations in cancer. Oncotarget. 2016;7(40):64910-20.
350. Eicheler W, Zips D, Dorfler A, Grenman R, Baumann M. Splicing mutations in TP53 in human squamous cell carcinoma lines influence immunohistochemical detection. The journal of histochemistry and cytochemistry : official journal of the Histochemistry Society. 2002;50(2):197-204.
351. Lee SH, Kim H, Kim WY, Han HS, Lim SD, Kim WS, et al. Genetic alteration and immunohistochemical staining patterns of ovarian high-grade serous adenocarcinoma with special emphasis on p53 immnnostaining pattern. Pathology international. 2013;63(5):252-9.
352. Shahin MS, Hughes JH, Sood AK, Buller RE. The prognostic significance of p53 tumor suppressor gene alterations in ovarian carcinoma. Cancer. 2000;89(9):2006-17.
353. Helliwell STHBTMJMBMBTR. Immunohistochemical expression of p53 and MDM2 within head and neck squamous cell carcinoma. Clinical Otolaryngology. 2006;31(3):247-.
354. Vazquez A, Kamphorst JJ, Markert EK, Schug ZT, Tardito S, Gottlieb E. Cancer metabolism at a glance. J Cell Sci. 2016;129(18):3367-73.